Interaction between impact damage and fatigue in fibre reinforced plastics

Beheshty, M. H.

Award date:
1997

Awarding institution:
University of Bath

INTERACTION BETWEEN IMPACT DAMAGE AND FATIGUE IN FIBRE REINFORCED PLASTICS

SUBMITTED BY:

MH BEHESHTY

FOR THE DEGREE OF Ph.D.

OF THE UNIVERSITY OF BATH

1997

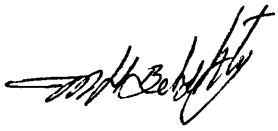

M Hosain Beheshty

ProQuest LLC
789 East Eisenhower Parkway
P.O. Box 1346
Ann Arbor, MI 48106-1346

ABSTRACT

This study has been designed to investigate the interaction between impact damage and fatigue, which is necessarily a complex one and of current interest to the aerospace industry, and to predict the fatigue response for virgin and impact-damaged materials by using a constant-life model. In order to achieve these goals, measurements have been made of the residual tensile and compressive strengths after low-velocity impacts of 1, 2, 3 and 5 Joules of two modern carbon-fibre composites, *viz.*, HTA/982A and HTA/913, and a glass-fibre laminate, E-Glass/913, all having the common lay-up $[(\pm 45,0_2)_2]_S$. The impact damage was assessed by transient thermography, ultrasonic C-scan and optical microscopy. The modes of failure under low-velocity impacts of 1-3J were found to be matrix cracking and mainly delamination. Only a 5J impact energy event caused some fibre fractures in CFRP laminates. Measurement of post-impact mechanical properties has shown that impact damage in the range 1-5J had little effect on the residual tensile strength although the compressive strength was markedly reduced.

Replicate stress/life fatigue data were obtained at different stress ratios, R, for sound and impact-damaged materials. Results show that impact energies in the range 1-3J had no effect on the tensile fatigue behaviour at R = +0.1. At R = -1.5 and +10, on the other hand, the stress/life curves are markedly affected. And as the compression component of stress increases the slope of the S/N curve decreases, which indicates less sensitivity to fatigue.

The fatigue tests results have been analysed by using a constant-life model previously developed at Bath. A new relationship between constant-life model parameters and material properties has been found. The model has been modified to predict the fatigue response of fibre composite materials in the virgin condition and after damage by low-velocity impact by using only the tensile and compressive strengths of composite in question. Results show that there is a good agreement between predicted S/N curves with experimental stress/life data for virgin and impact-damaged CFRP laminates.

ACKNOWLEDGEMENTS

The author wishes to express sincere thanks to his supervisor, Professor Bryan Harris, for his guidance, encouragement and discretion throughout this study. The many hours of discussion and fruitful exchange of ideas was greatly appreciated and has been an inspiration and a challenge for the future. My thanks also go to Professor D. P. Almond for access to the use of transient thermography and ultrasonic C-scan and for his useful advice and to Dr. M. P. Ansell for permission to use Mayes fatigue machines. I would like to thank Professor McEnaney for his kind consideration as the head of the Department of Materials Science and Engineering.

I wish to express my appreciation to Mr. N. Gathercole for his useful discussions on the field of this research and to the technician team in the Department led by Mr. P. Taylor, particularly Mr. F. Hammett for his help in laboratory work.

I wish to thank my sponsor, Ministry of Culture and Higher Education of Iran, for paying my tuition fees and living costs during this study. Last but not least, I like to thank my wife, Maryam, and my children, Zeinab and Mohammad, for their kind co-operation.

TABLE OF CONTENTS

ABSTRACT ii

ACKNOWLEDGEMENTS iii

TABLE OF CONTENTS iv

LIST OF TABLES vi

LIST OF FIGURES vii

LIST OF SYMBOLS xiv

CHAPTER ONE: INTRODUCTION 1

CHAPTER TWO: LITERATURE SURVEY 7

2.1 INTRODUCTION 8

2.2 FATIGUE BEHAVIOUR OF FRP 8

2.3 LIFE-PREDICTION METHODS 14

2.4 CONSTANT-LIFE ANALYSIS AND LIFE-PREDICTION 16

2.4.1 Data acquisition 17

2.4.2 Initial data analysis 17

2.4.3 Life prediction 18

2.5 IMPACT PERFORMANCE OF FRP 20

2.6 FATIGUE RESPONSE AFTER IMPACT 25

CHAPTER THREE: EXPERIMENTAL PROCEDURES 34

3.1 MATERIALS AND SPECIMENS 35

3.2 TESTING PROCEDURES 36

3.2.1 Monotonic tests 36

3.2.2 Fatigue tests 36

3.2.3 Impact tests 37

3.3 IMPACT DAMAGE ASSESSMENT TECHNIQUES 37

3.3.1 Transient thermography 37

3.3.2 Ultrasonic C-scan 39

3.3.3 Sectioning 40

CHAPTER FOUR: RESULTS AND DISCUSSION 47

4.1 INTRODUCTION 48

4.2 STRENGTH AND MODULUS MEASUREMENT 48

4.3 POST-IMPACT MECHANICAL PROPERTIES 50

4.4 PREDICTION OF RESIDUAL COMPRESSIVE STRENGTH 51

4.5 IMPACT DAMAGE ASSESSMENTS 52
4.5.1 Visual examination 52
4.5.2 Infrared thermography and ultrasonic testing 53
4.5.3 Sectioning 54
4.6 THE FATIGUE RESPONSE OF UNDAMAGED HTA/982A 56
4.7 THE FATIGUE RESPONSE OF UNDAMAGED E-GLASS/913 58
4.8 POST-IMPACT FATIGUE RESPONSE 59
4.8.1 Fatigue response of HTA/982A after 1J Impact 59
4.8.2 Fatigue response of HTA/982A after 2J Impact 61
4.8.3 Fatigue response of HTA/913 after 2J Impact 63
4.8.4 Fatigue response of E-Glass/913 after 2J Impact 64
4.9 DAMAGE DEVELOPMENT IN CYCLING 66
4.9.1 Compression cycling, R = +10 66
4.9.2 Tension-compression cycling, R = -0.3 67

CHAPTER FIVE: FATIGUE-LIFE PREDICTION 95

5.1 INTRODUCTION 96
5.2 CONSTANT-LIFE ANALYSIS OF FATIGUE DATA 96
5.2.1 Constant-life analysis for the undamaged materials 97
5.2.2 Constant-life analysis for the damaged materials 98
5.3 DISCUSSION 99
5.4 LIFE PREDICTION 107
5.5 CONCLUDING STATEMENT 108
5.6 APPENDIX 1 126

CHAPTER SIX: CONCLUSIONS 132

6.1 CONCLUSIONS 133
6.2 FURTHER WORK 136

REFERENCES 138

PUBLISHED PAPERS 145

LIST OF TABLES

Table 1-1. Mechanical properties of four $[(\pm 45,0_2)_2]_S$ CFRP laminates[8] 3

Table 4-1. Monotonic mechanical properties of experimental laminates together with data for three other modern $[(\pm 45,0_2)_2]_S$ CFRP laminates, 20mm wide samples (standard deviations in brackets). 49

Table 4-2. Stress/life data of 20mm and 40mm samples of HTA/982A in the virgin condition. 58

Table 4-3. Fatigue life data for $[(\pm 45,0_2)_2]_S$ HTA/982A laminate at a stress ratio of R = +0.1 for two stress levels, in the virgin condition and after damage by 1J and 2J low-velocity impacts. 64

Table 4-4. Fatigue life data for HTA/982A and HTA/913 laminates at R = +0.1 and peak stress of 1.0GPa, in the virgin condition and after damage by 3J low-velocity impacts. 64

Table 4-5. Mean and median life for E-Glass/913 in the virgin condition and after impact of 2J. 66

Table 5-1. The values of fitting parameter f for virgin and damaged materials. 100

Table 5-2. The values of the fitting parameter, f, for the virgin and damaged materials. These values were obtained by freely fitting all three parameters. 102

Table 5-3. The values of the fitting parameters, u and v , for the virgin and damaged materials. These values were obtained by freely fitting all three parameters. 102

Table 5-4. The maximum values of constant-life curves at different lives for virgin and impact-damaged materials. 104

Table 5-5. The new values of fitting f parameter at four lives for CFRP laminates in the virgin and damaged conditions. These values were obtained by free fitting the single parameter constant-life equation (5). 106

LIST OF FIGURES

Figure 1-1. Stress/median-life curves at a stress ratio R = +0.1 for seven varieties of carbon-fibre composite of lay-up $[(\pm 45,0_2)_2]_S$ (after Harris et al, 1996). 6

Figure 2-1.Schematic representation of the development of matrix and fibre damage modes and the characteristic damage state (CDS) during the fatigue life of a composite laminate (after Reifsnider KL, 1991)[11]. 31

Figure 2-2. Schematic diagram of strength change during fatigue life of an un-notched laminate (after Stinchcomb WW and Bakis CE 1991)[18]..... 31

Figure 2-3. Constant-life plots for HTA/913 composite of $[(\pm 45,0_2)_2]_S$ lay-up..... 32

Figure 2-4. σ/log median life curves for a $[(\pm 45,0_2)_2]_S$ HTA/913 laminate at various R ratios (After Harris et al, 1996)[8]. 32

Figure 2-5. Three-dimensional surface plot of the a, m, $\log N_f$ constant-life relationship defined by the first of equation 3 for the $[(\pm 45,0_2)_2]_S$ IM7/977 laminate (after Harris et al, 1995)[34]. 33

Figure 3-1. Schematic of impact test geometry..... 42

Figure 3-2. Falling dart method, impact testing instrument. 43

Figure 3-3. A close-up view to the bottom of impact tester..... 44

Figure 3-4. Impact test fixture for holding the specimen. 44

Figure 3-5. A schematic diagram of the Bath transient thermography system. 45

Figure 3-6. Block diagram of measurement and control system of through-transmission ultrasonic C-scan testing system. 46

Figure 3-7. Sectioning diagram. One specimen sectioned in longitudinal (left) and another one in transverse (right) directions relative to the fibres..... 46

Figure 4-1. Effect of low-velocity impact damage on the residual tensile and compressive strengths of $[(\pm 45,0_2)_2]_S$ HTA/982A CFRP laminate. 69

Figure 4-2. Effect of low-velocity impact damage on the residual tensile and compressive strengths of $[(\pm 45,0_2)_2]_S$ HTA/913 CFRP laminate..... 69

Figure 4-3. Effect of low-velocity impact damage on the residual tensile and compressive strengths of $[(\pm 45,0_2)_2]_S$ E-Glass/913 GRP laminate. 70

Figure 4-4. Effect of low-velocity impact damage on the residual compressive strengths of $[(\pm 45,0_2)_2]_S$ HTA/982A, HTA/913 and E-Glass/913 laminates, the residual compressive strengths are normalised with respect to the undamaged compressive strengths of each material. 70

Figure 4-5. Predicted residual compressive strength after impact for $[(\pm 45,0_2)_2]_S$ HTA/982A, HTA/913 and E-Glass/913 laminates. Symbols are experimental results. 71

Figure 4-6. Optical photos of 2J impact damage in E-Glass/913. 72

Figure 4-7. Optical photos of 5J impact damage in E-Glass/913. 72

Figure 4-8. Thermography and ultrasonic C-scan images of low-velocity impact-induced damages of 1J, 2J, 3J and 5J energy for the $[(\pm 45,0_2)_2]_S$ HTA/982A laminate, scan area was 40mm by 40mm. 73

Figure 4-9. Thermography and ultrasonic C-scan images of low-velocity impact-induced damages of 1J, 2J, 3J and 5J energy for the $[(\pm 45,0_2)_2]_S$ HTA/913 laminate, scan area was 40mm by 40mm. 74

Figure 4-10. Thermography and ultrasonic C-scan images of low-velocity impact-induced damages of 1J, 2J, 3J and 5J energy for the $[(\pm 45,0_2)_2]_S$ E-Glass/913 laminate, scan area was 40mm by 40mm. 75

Figure 4-11. Comparison of overall delamination area calculated from thermography and C-scan images for HTA/913 76

Figure 4-12. Overall impact-induced delamination area produced by 1, 2, 3 and 5 Joule impacts for the $[(\pm 45,0_2)_2]_S$ E-Glass/913, HTA/913 and HTA/982A laminates. 76

Figure 4-13. Damage map of 2J impact-damaged HTA/982A in longitudinal direction. 77

Figure 4-14. Damage map of 2J impact-damaged HTA/913 in longitudinal direction. 77

Figure 4-15. Damage map of 2J impact-damaged E-Glass/913 in longitudinal direction. 78

Figure 4-16. Damage map of 2J impact-damaged HTA/982A in transverse direction. 78

Figure 4-17. Damage map of 2J impact-damaged HTA/913 in transverse direction. 79

Figure 4-18. Damage map of 2J impact-damaged E-Glass/913 in transverse direction. 79

Figure 4-19. Damage map of 5J impact-damaged HTA/982A in longitudinal direction. 80

Figure 4-20. Damage map of 5J impact-damaged HTA/913 in longitudinal direction. 80

Figure 4-21. Damage map of 5J impact-damaged E-Glass/913 in longitudinal direction. 81

Figure 4-22. Variation of the incident energy to initiate first damage with target thickness in the $(0°_2,\pm 45°)$ and $(\pm 45°)$ XAS/914C laminates, (after Cantwell and Morton, 1989) 81

Figure 4-23. Overall impact-induced delamination area against net impact energy for the $[(\pm 45,0_2)_2]_S$ HTA/982A, HTA/913 and E-Glass/913 laminates..... 82

Figure 4-24. $\sigma/\log N_f$ curves for HTA/982A CFRP laminate of $[(\pm 45,0_2)_2]_S$ lay-up in the undamaged condition. The full curves are fitted polynomial curves of order two or three. The filled symbols are for 40mm wide samples, and the open ones are for 20mm wide samples..... 82

Figure 4-25. $\sigma/\log N_f$ curves for HTA/982A CFRP laminate of $[(\pm 45,0_2)_2]_S$ lay-up in the undamaged condition. The full curves are fitted polynomial curves of order two or three and the dashed curves represent median-stress/life curves for HTA/913 laminate, taken from reference 8. 83

Figure 4-26. Comparison of $\sigma/\log N_f$ curves for four CFRP laminates of $[(\pm 45,0_2)_2]_S$ lay-up at R ratio of +0.1. The full curves are fitted polynomial curves of order two..... 83

Figure 4-27. Comparison of $\sigma/\log N_f$ curves for four CFRP laminates of $[(\pm 45,0_2)_2]_S$ lay-up at R = +10. 84

Figure 4-28. $\sigma/\log N_f$ curves for E-Glass/913 GRP laminate of $[(\pm 45,0_2)_2]_S$ lay-up in the undamaged condition. The full curves are fitted polynomial curves of order two..... 84

Figure 4-29. $\sigma/\log N_f$ curves for HTA/982A CFRP laminate of $[(\pm 45,0_2)_2]_S$ lay-up after damage by a low-velocity impact of 1J. The full lines are polynomial curves fitted to the data for the virgin laminate. 85

Figure 4-30. Normalised $\sigma/\log N_f$ curves for HTA/982A CFRP laminate of $[(\pm 45,0_2)_2]_S$ lay-up in the undamaged condition and after damage by a low-velocity impact of 1J. Normalisation is down with respect to the compressive strength and residual compressive strength for undamaged and 1J impact-damaged materials, respectively..... 85

Figure 4-31. Residual compressive strength after fatigue cycling of samples of HTA/982A $[(\pm 45,0_2)_2]_S$ laminate with prior damage by a low-velocity impact of 1J. The cycling was at R = +10, at a peak stress (compressive) of 0.35GPa (79% of the residual compressive strength). 86

Figure 4-32. Ultrasonic C-scan images from sample of HTA/982A $[(\pm 45,0_2)_2]_S$ laminate impacted at 1J and subsequently fatigue cycled at R ratio of +10, at a peak stress (compressive) of 0.35GPa, under exactly the same conditions as Figure 4-31 (scan area was 42mm by 42mm)..... 86

Figure 4-33. Photomicrograph of impact damaged HTA/982A which shows significant delamination between 0° and -45° plies. The thickness of each lamina is about 0.125mm. 87

Figure 4-34. $\sigma/\log N_f$ *curves for HTA/982A CFRP laminate of* $[(\pm 45,0_2)_2]_S$ *lay-up after damage by a low-velocity impact of 2J. The full lines are polynomial curves fitted to the data for the virgin laminate.* *87*

Figure 4-35. Stress/log median-life curves for $[(\pm 45,0_2)_2]_S$ *HTA/982A laminate at R = –0.3, showing the effect of low-velocity impact damage.* *88*

Figure 4-36. $\sigma/\log N_f$ *curves for HTA/913 CFRP laminate of* $[(\pm 45,0_2)_2]_S$ *lay-up after damage by a low-velocity impact of 2J. The full lines are polynomial curves fitted to the data for the virgin laminate.* *88*

Figure 4-37. $\sigma/\log N_f$ *curves for E-Glass/913 GRP laminate of* $[(\pm 45,0_2)_2]_S$ *lay-up after damage by a low-velocity impact of 2J. The full lines are polynomial curves fitted to the data for the virgin laminate.* *89*

Figure 4-38. Ultrasonic C-scan images from sample of HTA/982A $[(\pm 45,0_2)_2]_S$ *laminate impacted at 1J and subsequently fatigue cycled at R ratio of +10 and a peak stress of -0.38GPa. The median life under this condition is 78,000 cycles (scan area was 42mm by 42mm).* *89*

Figure 4-39. C-scan images from sample of HTA/982A $[(\pm 45,0_2)_2]_S$ *laminate impacted at 1J and subsequently fatigue cycled at R ratio of +10 and a peak stress of -0.38GPa. The median life under this condition is 78,000 cycles, this sample failed at 36,390 cycles (scan area was 42mm by 42mm).* *90*

Figure 4-40. Ultrasonic C-scan images from sample of HTA/982A $[(\pm 45,0_2)_2]_S$ *laminate impacted at 1J and subsequently fatigue cycled at R ratio of +10 and a peak stress of -0.35GPa (scan area was 42mm by 42mm).* *91*

Figure 4-41. Ultrasonic C-scan images from sample of HTA/982A $[(\pm 45,0_2)_2]_S$ *laminate impacted at 1J and subsequently fatigue cycled at R ratio of -0.3 and a peak stress of 0.9GPa. The median life under this condition is 30,000 cycles, this sample failed at 54,280 cycles (scan area was 42mm by 42mm).* *92*

Figure 4-42. C-scan images from sample of HTA/982A $[(\pm 45,0_2)_2]_S$ *laminate impacted at 1J and subsequently fatigue cycled at R ratio of -0.3 and a peak stress of 0.73GPa. The median life under this condition is 330,000 cycles, this sample failed at 623,680 cycles (scan area: 42mm x 42mm). 93*

Figure 4-43. Ultrasonic C-scan images from samples of HTA/982A $[(\pm 45,0_2)_2]_S$ *laminate impacted at 1J and subsequently fatigue cycled at R ratio of -0.3 and a peak stress of 0.73GPa. The median life under this condition is 330,000 cycles, sample I failed at 623,680 cycles and sample II failed at 753,140 cycles (scan area was 42mm by 42mm).* *94*

Figure 5-1. Constant-life plots for HTA/982A $[(\pm 45,0_2)_2]_S$ laminate in the undamaged condition. The curves are obtained by freely fitting all three parameters. *110*

Figure 5-2. Constant-life plots for E-Glass/913 $[(\pm 45,0_2)_2]_S$ laminate in the undamaged condition. The curves are obtained by freely fitting all three parameters. *110*

Figure 5-3. Constant-life plots for HTA/982A $[(\pm 45,0_2)_2]_S$ laminate following prior damage by a 1J impact. The curve for 10^6 cycles has been artificially forced to remain close to the other two curves above R = 0.1. ..... *111*

Figure 5-4. Constant-life plots for HTA/982A $[(\pm 45,0_2)_2]_S$ laminate following prior damage by a 2J impact. Data points for R ratios of +0.5 and +0.1 are taken from the data of virgin material. The curves are obtained by freely fitting all three parameters. *111*

Figure 5-5. Constant-life plots for HTA/982A $[(\pm 45,0_2)_2]_S$ laminate in the virgin condition and after prior damage with low-velocity impacts of 1J and 2J. The curves are obtained by freely fitting all three parameters. *112*

Figure 5-6. Constant-life plots for HTA/913 $[(\pm 45,0_2)_2]_S$ laminate following prior damage by a 2J impact. Data points for R ratios of +0.5 and +0.1 are taken from the data of virgin material. The curves are obtained by freely fitting all three parameters. *112*

Figure 5-7. Constant-life plots for HTA/913 $[(\pm 45,0_2)_2]_S$ laminate in the virgin condition and after prior damage with a low-velocity impact of 2J. The curves are obtained by freely fitting all three parameters. *113*

Figure 5-8. Constant-life plots for E-Glass/913 $[(\pm 45,0_2)_2]_S$ laminate following prior damage by a 2J impact. The curves are obtained by freely fitting all three parameters. *113*

Figure 5-9. Constant-life plots for E-Glass/913 $[(\pm 45,0_2)_2]_S$ laminate in the virgin condition and after prior impact damage with a low-velocity-impact of 2J. The curves are obtained by freely fitting all three parameters. *114*

Figure 5-10. Dependence of constant-life model f *parameter on laminate tensile strength. The vertical error bars are standard deviations for the fitted values of* f, *and the horizontal bars are standard deviations for the measured tensile strengths. The plotted* f *values are the means of the values obtained by curve fitting to obtain constant-life curves for 10^4, 10^5 and 10^6 cycles (Taken from reference 8).* *114*

Figure 5-11. Dependence of constant-life model f parameter on the ratio of laminate compressive strength over tensile strength at different life. *115*

Figure 5-12. Dependence of constant-life model u parameter on the ratio of laminate compressive strength over tensile strength at different lives for virgin and

damaged materials excluding GRP. The average value of u for each material is shown in solid symbol and the line is a linear curve fit through the average values. 115

Figure 5-13. Dependence of constant-life model v parameter on the ratio of laminate compressive strength over tensile strength at different lives. The average value of v for each material is shown in solid symbol and the line is a linear curve fit through the average values. 116

Figure 5-14. Dependence of constant-life model f parameter on life for $[(\pm 45,0_2)_2]_S$ *laminates in the virgin and damaged conditions.* 116

Figure 5-15. Dependence of constant-life model u parameter on life for $[(\pm 45,0_2)_2]_S$ *laminates in the virgin and damaged conditions.* 117

Figure 5-16. Dependence of constant-life model v parameter on life for $[(\pm 45,0_2)_2]_S$ *laminates in the virgin and damaged conditions.* 117

Figure 5-17. Constant-life plots for T800/5245. The dashed curve were obtained by free fitting all three parameters while the solid curves were obtained by the constant value of u and v equal to 2. 118

Figure 5-18. Constant-life plots for T800/924. The dashed curve were obtained by free fitting all three parameters while the solid curves were obtained by the constant value of u and v equal to 2. 118

Figure 5-19. Constant-life plots for IM7/977. The dashed curve were obtained by free fitting all three parameters while the solid curves were obtained by the constant value of u and v equal to 2. 118

Figure 5-20. Constant-life plots for virgin HTA/982A. The dashed curve were obtained by free fitting all three parameters while the solid curves were obtained by the constant value of u and v equal to 2. 119

Figure 5-21 Constant-life plots for 1J impact-damaged HTA/982A. The dashed curve were obtained by free fitting all three parameters while the solid curves were obtained by the constant value of u and v equal to 2. 119

Figure 5-22. Constant-life plots for 2J impact-damaged HTA/982A. The dashed curve were obtained by free fitting all three parameters while the solid curves were obtained by the constant value of u and v equal to 2. 119

Figure 5-23. Constant-life plots for virgin HTA/913. The dashed curve were obtained by free fitting all three parameters while the solid curves were obtained by the constant value of u and v equal to 2. 120

Figure 5-24. Constant-life plots for 2J impact-damaged HTA/913. The dashed curve were obtained by free fitting all three parameters while the solid curves were obtained by the constant value of u and v equal to 2. 120

Figure 5-25. Variation of constant-life new f parameter on life for $[(\pm 45,0_2)_2]_S$ laminates in the virgin and damaged conditions. These values were obtained while u and v were considered equal to 2. 121

Figure 5-26. Dependence of constant-life new f parameter on c at four lives for $[(\pm 45,0_2)_2]_S$ laminates in the virgin and damaged conditions. These values were obtained while u and v were considered equal to 2. 121

Figure 5-27. Dependence of constant-life new f parameter on c at 10^5 cycles for $[(\pm 45,0_2)_2]_S$ laminates in the virgin and damaged conditions. These values were obtained while u and v were considered equal to 2. The vertical error bars are the average standard deviations for the fitted values of f *for four lives, and the horizontal bars are obtained from the standard deviations for the measured tensile strengths and compressive strengths [sdc = $(sd\sigma_t + sd\sigma_c)^{1/2}$].* 122

Figure 5-28. Stress/life data for the $[(\pm 45,0_2)_2]_S$ HTA/982A CFRP laminate in the undamaged condition. The full lines are predicted curves by the modified constant-life model. 122

Figure 5-29. Stress/life data for the $[(\pm 45,0_2)_2]_S$ HTA/982A CFRP laminate after damage by a 2J impact event. The full lines are predicted curves by the modified constant-life model. 123

Figure 5-30. Stress/life data for the $[(\pm 45,0_2)_2]_S$ HTA/913 CFRP laminate after damage by a 2J impact event. The full lines are predicted curves by the modified constant-life model. 123

Figure 5-31. Three-dimensional surface plot of the a, m, $\log N_f$ constant-life relationship defined by the equation 5 for the $[(\pm 45,0_2)_2]_S$ HTA/982A laminate in the virgin condition. 124

Figure 5-32. Three-dimensional surface plot of the a, m, $\log N_f$ constant-life relationship defined by the equation 5 for the $[(\pm 45,0_2)_2]_S$ HTA/982A laminate after a 1J impact event. 124

Figure 5-33. Three-dimensional surface plot of the a, m, $\log N_f$ constant-life relationship defined by the equation 5 for the $[(\pm 45,0_2)_2]_S$ HTA/982A laminate after a 2J impact event. 125

LIST OF SYMBOLS

a	Normalised alternating stress component, σ_{alt}/σ_t
σ_t	Monotonic tensile strength
σ_c	Monotonic compressive strength
σ_{alt}	Alternating stress component, equal to $\frac{1}{2}(\sigma_{max} - \sigma_{min})$
σ_{min}	Minimum Stress
σ_{max}	Maximum or Peak Stress
m	Normalised mean stress component, σ_m/σ_t
c	Normalised compression strength, σ_c/σ_t
σ_m	Mean stress, equal to $\frac{1}{2}(\sigma_{max} + \sigma_{min})$
f, u and v	Constant-life model parameters
CFRP	Carbon-Fibre Reinforced Plastics
FRP	Fibre-Reinforced Plastics
KFRP	Kevlar-Fibre Reinforced Plastics
N_f	Number of Cycles to Failure
PEEK	Poly (ether ether ketone)
R	Stress ratio, defined as $\sigma_{min}/\sigma_{max}$
S/N	Stress/life

CHAPTER ONE:

INTRODUCTION

Composite materials such as carbon-, Kevlar- and glass-fibre-reinforced plastics have played a significant role in engineering. They have led to tremendous advances in design, fabrication and application. Much of the progress in this field relates to the development of high-performance advanced fibre-reinforced composites[1,2] which include boron, glass, Kevlar, and carbon, in addition to hybrid fibre reinforced plastics. Advanced carbon-fibre-reinforced composites are finding increasing application in aerospace structures as a consequence of their high specific stiffness and strength. They offer an attractive potential for reducing the weight of high-performance structures and overall production cost as the main commercially important factor. Today, carbon fibres are widely used in high-performance sports equipment and in the aviation industry and glass fibres are increasingly important in industrial applications, such as for automotive components. By contrast with the extensive use of these various fibre-reinforced composites, the prediction of some of their more important engineering properties, such as toughness, fatigue response and time-dependent behaviour, is still far from satisfactory[2,3].

The fatigue behaviour of composites in general and of carbon-fibre composites in particular has long been a subject of serious study since, in service, fatigue loads are usually unavoidable. For load-bearing applications where variable stresses are present, fatigue is a factor that must be taken into consideration. The demand for improved performance of structural materials in transportation industries, particularly in aircraft,

makes fatigue analysis an important consideration. Although in the aerospace application of composite materials at current low design strains, it is assumed[4] that fatigue is not a problem, newer tougher materials are now available that will hopefully permit increase in design strains. In addition, it has been shown[5] that many of these tougher materials are more fatigue sensitive than standard materials and their fatigue behaviour should perhaps be considered even at the strain levels currently adopted. Fatigue behaviour could therefore become an important design issue. So that, to design appropriately with composites, we cannot ignore the fact that fatigue is a factor that must be taken into consideration. We also need to understand the mechanisms by which damage occurs in composites as well as having access to procedures for assessing the development and accumulation of this damage[6]. These kinds of information are necessary for reliable fatigue-life predictions for composite materials.

Fatigue experiments are expensive of time and resources. When a newly developed composite material is being considered for a given application, fatigue data are ideally required at an early stage of the design process and yet, in general, a detailed fatigue profile is rarely available until late in the development of project. And, while it is true that fatigue studies have been carried out on composites since these materials first began to be studied as serious engineering materials, it is still by no means possible[7] to make safe predictions for materials which have not previously been the subject of extensive investigation. In other words, although many important aspects of the fatigue of composites are now well understood, clear design criteria have not yet been established.

There is a familiar postulate, referred to as the strength-life equal-rank assumption, which supposes that if a series of composite materials are ranked according to their tensile strengths, then their fatigue responses will be similarly ranked. The danger of this were shown by Harris *et al*[8] as can be seen in Figure 1-1. This figure shows the stress/median-life curves for a range of carbon-fibre composites of $[(\pm 45,0_2)_2]_S$ lay-up, consisting of various combination of fibres and resins. It can be seen that the $\sigma/\log N_f$ curves are of different shapes; that there is no obvious pattern of responses that can be linked to specific fibre types; and that the resin matrix exerts stronger effects, in

modifying the apparent performance of a given variety of fibre, than might have been expected. The individual curves also sometimes cross and recross, which means that the strength/life assumption cannot be valid. While there is a general trend that higher strength laminates have longer fatigue lives, in detail it would be unsafe to rely on such a crude ranking procedure. Another defect in this ranking model is that[8] it attempts to relate only tensile strength to fatigue life: it gives no clues as to how a given material might behave under compression or combined tension-compression fatigue. It is known that the compressive strength of a composite laminate will usually be much lower than its tensile strength, but it is by no means clear that there is a simple relationship between the two, as illustrated in Table 1-1 for some of the composites represented in Figure 1-1.

Table 1-1. Mechanical properties of four $[(\pm 45, 0_2)_2]_S$ CFRP laminates[8].

Material	Tensile strength, σ_t GPa	Compressive strength, σ_c GPa	σ_c / σ_t
T800/5245	1.67 (0.09)	0.88 (0.10)	0.53
IM7/977	1.43 (0.07)	0.90 (0.07)	0.64
T800/924	1.42 (0.09)	0.90 (0.09)	0.63
HTA/913	1.27 (0.05)	0.97 (0.08)	0.77

One of the major factors limiting the design of fibre composite structures is their relative weakness under impact. These structures suffer from localised impact loading and may contain barely visible impact damage (BVID) which severely reduces the structural integrity of the component. Low-velocity impact damage is inevitable and may be caused during manufacturing, by careless handling, for example, or in service, by hailstones, bird strike, *etc.* It may also occur during maintenance, perhaps by accidentally dropped tools. These low-velocity impacts produce significant internal damage in composite materials that cannot be seen by the naked eye. A significant effect of this damage is to reduce the strength of the laminate, particularly in compression; however, owing to the complexity of the damage the precise mechanisms controlling the strength reduction are unclear[9]. Thus, impact damage is a critical design consideration.

In recent years many research programmes have been undertaken in an attempt better to understand the impact response of composite materials[10]. The majority of

this work has been undertaken on continuous fibre, high-performance composites since these materials are finding increasing use in the design of a large number of civil and military aircraft. The responses of composite materials to impact loading and the manner in which they dissipate the incident kinetic energy of the projectile is very different from that of metals. For low and intermediate incident energies, metals absorb energy through elastic and plastic deformation. Although the latter may cause some permanent structural deformation, its consequences on the load carrying capability of the component are usually small. In composites, however, the ability to undergo plastic deformation is extremely limited. The energy is frequently absorbed in creating large areas of fracture, resulting in reductions in both strength and stiffness. Furthermore, the prediction of the post-impact load-bearing capability of a damaged composite structure is more difficult than for metals since the damage zone is generally complex in nature and consequently very difficult to characterise[10].

The control of this unavoidable damage necessitates a knowledge of the influence of the damage on lifetime and reliability of the affected structure. In other words, an understanding of the factors that affect the long-term behaviour of laminates must be achieved in order to satisfy damage requirements for structural performance. In addition, there is concern that damage resulting from minor impact could grow to large size under cyclic loading. Post-impact fatigue behaviour, even for a material of which the fatigue response has been extensively studied, is still unlikely to be understood. Conservative predictions of the lives of damaged composites cannot therefore be made with certainty. This study, therefore, has been designed to investigate the interaction between impact damage and fatigue which is necessarily a complex one and of current interest to the aerospace industry, and to predict the fatigue response for virgin and impact-damaged materials. There has been a great deal of research on methods of fatigue life prediction for composites and the major recent work will be reviewed in the following chapter. But few existing models are readily applicable to a wide range of materials and realistic applications. Any generally useful model should have the capability for conservative prediction, with appropriate statistical safeguards, from as small an experimental data base as possible, and with the ability to upgrade its predictions smoothly as new fatigue data become available.

In a series of studies over a number of years at Bath on fatigue behaviour of fibre reinforced plastics, FRP, Harris and co-workers have established an empirical model, called a constant-life model, for fatigue-life prediction which appears to be applicable to a variety of different kinds of composite laminates. A wide range of composites has been studied with a view to assessing the potential usefulness of the model and the likely level of confidence in using it to make preliminary predictions of life from limited data sets. As a sequel to the earlier work, it was planned for this study to verify the generality of this model by using other materials of the same group which had been used before and one different one, in the virgin condition and after low-velocity low-energy impacts. It was intended to study the effects of low-velocity impacts on the subsequent applicability of the constant-life prediction model. The goal of our efforts was to study the effect of damage caused by dropped weights or something similar and its effect on the residual strength and the fatigue response of FRP. The main objective was to ascertain whether the effect of prior impact damage changes the response of material as predicted by the constant-life model and to assess the sensitivity of this model for impact-damaged specimens.

The three materials studied in this work were HTA/982A and HTA/913 both carbon-fibre/epoxy-resin composites and a glass-fibre/epoxy-resin composite, E-Glass/913. These were chosen because of their widespread use in the aerospace and industrial applications. The main lay-up sequence of $[(\pm 45,0_2)_2]_S$ was selected as being representative of major elements of lay-up sequences in industrial applications.

The following thesis is divided into five chapters. The next chapter is a literature survey in which some of the major achievements on fatigue, fatigue-life prediction, impact and fatigue after impact will be reviewed. The third chapter describes the material and experimental methods used in the work. The main experimental results are presented in chapter four and this is followed by a constant-life analysis of fatigue data and life-prediction in chapter five. Chapter six gives conclusions of the whole work.

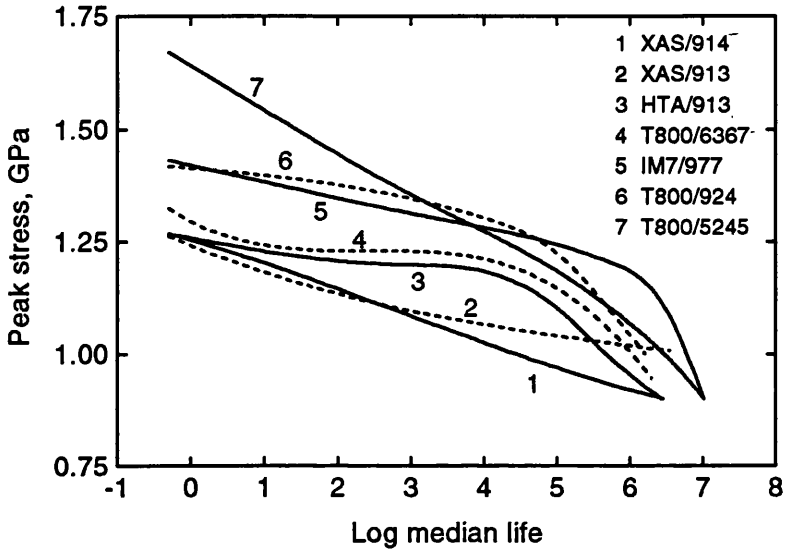

Figure 1-1. Stress/median-life curves at a stress ratio R = +0.1 for seven varieties of carbon-fibre composite of lay-up $[(\pm 45, 0_2)_2]_S$ (after Harris et al, 1996)[8].

CHAPTER TWO:

LITERATURE SURVEY

CHAPTER TWO: LITERATURE SURVEY 7

2.1 INTRODUCTION 8

2.2 FATIGUE BEHAVIOUR OF FRP 8

2.3 LIFE-PREDICTION METHODS 14

2.4 CONSTANT-LIFE ANALYSIS AND LIFE-PREDICTION 16

2.4.1 Data acquisition 17

2.4.2 Initial data analysis 17

2.4.3 Life prediction 18

2.5 IMPACT PERFORMANCE OF FRP 20

2.6 FATIGUE RESPONSE AFTER IMPACT 25

2.1 INTRODUCTION

In structures subjected to fatigue loading, composite materials offer substantial advantages over metallic materials for engineering applications. The fatigue response and impact resistance of composite materials, however, are completely different from those of metals. Most composites are brittle and so can only absorb energy in elastic deformation and through damage mechanisms, and not via plastic deformation. On the other hand, in metal structures owing to the ductile nature of the material, large amounts of energy may be absorbed. The purpose of this chapter is to review significant recent work dealing with fatigue, fatigue-life prediction methods, impact and the post-impact fatigue response of fibre-reinforced plastics (FRP).

2.2 FATIGUE BEHAVIOUR OF FRP

In general, fatigue is concerned with the loss of properties and performance caused by internal processes driven by the continued application and variation of external influences such as mechanical loading, thermal loading and the chemical environment[11]. Usually, the term fatigue indicates the behaviour of materials under cyclic loading. Results of fatigue tests are typically presented as a plot of applied stress (S) against number of cycles to failure (N_f). This graph is called an S/N or $\sigma/\log N_f$ curve. The ordinate is generally the stress or strain amplitude or the maximum/peak stress or strain in a cycle and is plotted on a linear scale. The abscissa is the number of cycles to failure for a fixed stress cycle and is plotted on a logarithmic scale.

Initiation and propagation of fatigue damage, strength and stiffness degradation during cycling, influence of material variables (such as matrix material, ply orientation, fibre content), testing variables (such as loading conditions, frequency and environmental effects (*eg.* humidity and temperature)), statistical considerations and finally, predicting fatigue damage and fatigue life are the important subjects that have been discussed in the literature. The major achievements can be summarised as follows.

Since the monotonic loading of a fibre composite induces a variety of micro-structural damage mechanisms, including fibre breakage, matrix cracking, interfacial debonding and so forth, it is self-evident that repeated loading is likely to continue

developing this damage, even when the overall stress level is well below the normal failure stress[6]. The progressive accumulation of local damage leads to a deterioration in the strength and stiffness of the material. If the damage continues until the residual strength of the composite falls to about the same level as the externally applied load, the material will fail.

Chen and Harris investigated[12] the fatigue-induced damage mechanisms in two high-performance CFRP composites. Several damage mechanisms, including matrix cracking, fibre fracture, delamination and fibre end drop-out from the edges of the 0° plies (or in isolation inside the plies as a combination of fibre fracture and inter-fibre splitting) was observed during fatigue. These modes of damage appeared in a distinctive manner and order in the two composite materials. All of the damage mechanisms occurred in a specific sequence at different numbers of cycles according to the fatigue stress levels, and this sequence may be changed in composite systems which have different structural properties, such as fibre/matrix interfacial bond strength. The damage maps, which combine all fatigue-induced damage information, can be recognised as characteristic of different composite material systems.

Haque *et al*[13], investigated damage development under fatigue and static loading for $[0,0,90]_{3S}$ graphite/epoxy laminates. The results showed that the fatigue damage primarily initiates as matrix cracking in the transverse plies, which is mostly evident up to 0.5 N_f applied cycles, and the residual strength and stiffness reduction appears to be insignificant during this stage. The damage mode gradually extends in the form of delamination, debonding and fibre breakage with an increase in the number of applied cycles. The extent of such damage modes are most critical beyond $0.75N_f$ fatigue cycles. The fatigue cycle stage between 0.5 to $0.75N_f$ appears to be the initiation period of damage modes which are mostly responsible for the final fatigue failure of the laminate structure. Weibull analysis also showed a significant change in characteristic lives of the number of cycles to failure at stress levels 70, 80 and 90% of ultimate strength.

The degradation of a plain-weave carbon-fibre/epoxy composite under tension-tension fatigue loading was studied by Takemura and Fujii[14]. For low-cycle fatigue,

fibre breaks occur from the beginning of fatigue testing, but specimens fail without stiffness reduction or with no damage in weft bundles. Such fibre breaks lead to the breakage of the fibre bundle. Fibre bundle breakage forms a crack which is regarded as a 'metacrack'. After the growth of the metacrack, the specimen fails. For high-cycle fatigue, the fatigue failure process is divided into four stages. Cracks do not occur and no significant stiffness reduction is detected in the first stage. Transverse cracks occur in the middle stage. The stiffness decreases owing to the occurrence of multiple cracks in the weft after which the observed stiffness becomes constant because the distance between cracks becomes so short that few cracks initiate in the last period of this middle stage. Cracks in the weft bundles progressed toward the interfaces between warp and weft bundles, and then progressed along the interface. This results in the formation of quasi-delamination.

Fatigue damage mechanisms, as indicated by residual strength data have been examined[15] for a range of 0°/90° composite laminates. It was observed that Kevlar-49 and glass-fibre composites exhibit similar behaviour resulting in a continuous and increasing loss in strength with cyclic loading, whereas a carbon-fibre composite retains its original static strength throughout most of its life.

Harris *et al*[16] investigated the fatigue behaviour of several varieties of CFRP. It was shown that the fatigue response of these materials follows a relatively simple pattern which implies that the shape of the stress (or strain) *vs.* life curve is determined largely by the tensile failure strain of the composite in question. The tensile response of a range of conventional carbon-fibre/epoxy composites with various resin matrices and lay-ups conforms to a single pattern of behaviour when the stress/loglife data are normalised with respect to the monotonic tensile strength.

Fatigue damage growth in a T800/5245 CFRP laminate was studied[8] recently in Bath at three stress ratios, R (defined as $\sigma_{min}/\sigma_{max}$), pure tension (R = +0.1), pure compression (R = +10) and fully reversed loading (R = -1.0). It has been shown that in pure tension, damage growth behaviour has typical characteristics for each sample independent of the peak stress. These patterns could allow estimation of the stage of life associated with the damage profile analysed from a sample after an interrupted

test. The results from tests at R = +10 and R = -1.0, both with fatigue behaviour dominated by compression, showed very low densities of damage which was concentrated locally so that fatigue appeared catastrophic and prevented evaluation of the results in the same way as for R = +0.1. However, several general characteristics of the damage behaviour could be determined, describing the dominating types of damage and their local concentration. Because samples fatigued at R = -1.0 showed an overlaid damage pattern induced by the tension component, samples fatigued at R = +10 or R = -1.0 could easily be distinguished.

The progressive development of damage during fatigue life can be overviewed[11] with the aid of Figure 2-1, which traces the damage process as a function of percentage of life of composite laminates which contain 0° plies and off loading axis (θ) plies subjected to cyclic loading. This schematic diagram shows some combination of damage modes to occur under fatigue cycling.

The effect of prior damage introduced by tension fatigue cycling on the tensile strength and toughness of a number of carbon and glass-fibre-reinforced plastics materials was studied by Harris *et al*[17]. They concluded that tensile fatigue cycling of a $[(\pm 45,0_2)_2]_S$ CFRP laminate results in fibre and matrix damage that led to reductions in both the notched and un-notched strength and an overall reduction of some 11% in the ratio of toughness to tensile strength.

The fatigue-induced damage results in the lowering of the stiffness and strength of composite materials. In general, the tensile and compressive residual strengths of un-notched composite laminates decreases through the fatigue life, as described by Stinchcomb and Bakis[18]: their model is reproduced here in Figure 2-2. The ordinate is applied cyclic stress (S_a) or residual strength (S_r), each normalised with respect to initial strength (S_u). The S/N curve is also represented to define fatigue life as the coincidence of residual strength and maximum cyclic stress. The shape of the residual strength curve can be related to fatigue damage mechanisms. Fatigue damage, such as matrix cracks and early fibre fracture, which develop during the first 10-15% of fatigue life and are widely scattered throughout the laminate, have a small, but measurable, effect on stiffness and strength, particularly the tensile strength. After the

first (stage I) characteristic damage state (CDS) of regularly spaced matrix cracks forms and as stage II damage develops, the residual strength decreases at an increasing rate. Residual strength continues to decrease throughout stage II and into stage III where delamination and fibre fracture greatly influence response. It is worth while indicating that the actual shape of the residual strength versus cycles curve will vary with material, stacking sequence, loading history and environment.

A brief explanation of the effect of materials variables such as the kind of matrix, fibres, fibre content and lay-up on the fatigue behaviour of composite materials can be seen in the literature[19]. Among the test variable parameters, the effect of fatigue loading frequency and environment on fatigue properties of composite materials have been much studied.

Tsai *et al*[20] investigated the effect of frequency on fatigue life by performing fatigue tests at different frequency and stress levels. Their results showed that tests on $(\pm 45)_{2S}$ laminates at a constant stress level but different frequencies gave the same results as those at a constant frequency but at different stress levels which produced the same strains.

In a program of fatigue testing of multi-angle laminates of carbon-fibre/poly (ether ether ketone) (PEEK), Curtis *et al*[21] pointed out that loading frequency effects can significantly complicate the generation of S/N curves. The higher the test frequency, the lower the fatigue strength for any given number of cycles. Furthermore, the greater the matrix influence in the laminate then the greater the influence of the test frequency was the conclusion drawn from the observation that the effect of frequency is considerably more pronounced for $(\pm 45)_{ns}$ specimens than for $(-45/0/+45/90)_{ns}$ specimens.

A different opinion of the effect of frequency on the fatigue behaviour of fibre composites is given by Adam et al[22]. According to the results of an experimental investigation of the mechanical response of unidirectional CFRP, KFRP and carbon-Kevlar hybrid composites at different strain rates and cycling frequencies, they observed that there was no effect of frequency on the fatigue behaviour of these fibre-reinforced composites.

It has been shown by Sims and Gladman[23] that the dependence of the ultimate tensile strength of a glass-fibre-fabric-reinforced epoxy laminate on the rate of stress application (RSA) transposes directly to the fatigue strength, so that tests at different rates can be normalised with respect to the ultimate tensile strength (UTS) obtained at the same RSA to give a single fatigue behaviour. In other words data collected at two frequencies should be normalised with respect to the appropriate UTS. They also reported that a constant RSA allows easier analysis of S/N data. However, the difference between results obtained at a single RSA and at a constant intermediate frequency is small and may be acceptable. A constant RSA allows increased test frequencies at low stresses, provided that autogenous hysteretic heating is absent and should enable more data at 10^6 cycles and above to be collected.

It has been shown by Harris[24] that the $\sigma/\log N_f$ curves for many GRP materials are not linear and there are two factors which complicate the appearance of their S/N curves. Firstly, the tensile strengths of GRP materials are strain-rate and temperature sensitive, and secondly, during cycling at large strains there is usually a significant rise in temperature as a result of hysteretic heating which is not easily dissipated by the non-conducting constituents of the GRP. These effects are due to the high failure strain of the glass fibres and their sensitivity to the moisture.

It can be concluded that carbon-fibre composites are largely rate insensitive and, because they deform less than GRP under working loads and they have reasonably high thermal conductivities, hysteretic heating effects are usually insignificant. But glass-fibre composites are rate sensitive and it is better for all $\sigma/\log N_f$ curves for GRP materials to be determined at a fixed rate of load application, for the material strength to be measured at the same rate, and for hysteretic effects to be either eliminated or accounted for.

A series of investigation programs, in which the effect of hygrothermal conditions on the mechanical properties and fatigue behaviour of epoxy-based composites reinforced with carbon, glass and aromatic polyamide fibres, as well as of carbon-PEEK laminates were studied by Jones *et al*[25] and Dickson *et al*[26] in Bath. They concluded that in CFRP there is no effect of conditioning on the fatigue behaviour of

0°/90° samples, and in GRP only drastic boiling-water treatment seriously affects the results. The fatigue resistance of KFRP composites is reduced more by drying than by boiling in water, and in all conditions the material shows very good fatigue resistance at high stresses, but behaves poorly at low and intermediate stress levels with downward sloping $S/Log N_f$ curves. This appears to be because of the occurrence of fibre damage resulting from complete unloading of the composite on each cycle.

2.3 LIFE-PREDICTION METHODS

There has been a great deal of research on methods of life prediction for composites and recent reviews of various models can be found, for example, in the 1991 volume of fatigue of composite materials edited by Reifsnider[11]. But few existing models are readily applicable to a wide range of materials and realistic applications and components. Any generally useful model should have the capability for conservative prediction, with appropriate statistical safeguards, from as small an experimental data base as possible, and with the ability to upgrade its predictions smoothly as new fatigue data become available.

Available methods for predicting fatigue lives of polymer-matrix composite materials can be classified as follows[27]:

(1) Empirical fatigue theories
(2) Residual strength degradation based fatigue theories.
(3) Stiffness change based fatigue theories.
(4) Actual damage mechanisms based fatigue theories.

Empirical fatigue theories are used to characterise S/N curves for the material. The choice of a particular empirical fatigue theory depends on the nature of the S/N data and the experience of the user. As a result, many empirical equations have been used to characterise the S/N data for polymer-matrix composite materials. The empirical fatigue equations that have been mentioned are limited to uniaxial cyclic loading, which seldom occurs in service. Extension of the empirical fatigue theories to the multi-axial loading case have been proposed. These extensions involve the generalisation of static strength criteria to the case of residual strength after cyclic loading, thereby introducing the effect of cyclic loading. In principle, the empirical multi-axial fatigue theories can be used to predict the life of any laminate, subjected to

constant-amplitude fatigue loading, from lamina constant-amplitude fatigue data by using laminate theory.

Most of the currently accepted life prediction methods for composite materials are based on the residual strength as the damage metric. It is based on the assumption that the rate of residual strength degradation is a power function of applied cyclic stress. Moreover, the implicit assumption is made that the parameters defining the residual strength degradation rate are material constants. As a result, all of the scatter in the fatigue data is attributed to scatter in the initial static strength of the material. This is not necessarily correct. Since the residual-strength degradation rate cannot be experimentally determined for a given specimen under test, it is not possible to assess the degree of variability of the parameters defining the residual-strength degradation rate. It has been shown[27] that the residual-strength degradation based fatigue models may not be valid for composite materials.

Since measurement of the residual strengths of composites involves the destruction of the test specimens, a fatigue-damage model based on the residual strength may not be suitable for predicting and tracking the fatigue damage. On the other hand, measurement of the residual stiffness can be made non-destructively. Lee, Fu and Yang[28] recently reviewed different stiffness-degradation models that have been proposed in the literature. They characterised the fatigue damage in a T300/976 $[0°/90°/\pm45]_{2S}$ graphite/epoxy laminate under block-type spectrum loading to simulate service loadings on aircraft structures by measuring the degradation of residual stiffness. They suggested a stiffness-degradation model under this kind of loading for predicting the statistical distribution of the residual stiffness and fatigue life. They proposed an empirical fatigue failure strain criterion and derived theoretically the statistical distributions of failure stiffness and fatigue life for composite laminates subjected to service loading spectra. They have shown that the theoretical predictions and experimental results correlate reasonably well. Adam[29] and Harris[30] and co-workers have recently studied fatigue response of CFRP laminates under block-loading conditions. They found that different CFRP laminates appear to behave in a similar manner and the most significant feature of the behaviour is that combinations

of tension and compression loading are more damaging than purely tensile or purely compressive stress cycling régimes.

In the last few years artificial neural networks have appeared as a new branch of computing suitable for applications in a wide range of fields. It is worthwhile indicating that the application of neural network analysis for prediction of the fatigue lives of fibre-composite materials is one of the on-going research projects in the Department of Materials Science at Bath[31,32].

2.4 CONSTANT-LIFE ANALYSIS AND LIFE-PREDICTION

In recent years[7,31,33,34] Harris and co-workers have given descriptions of a constant-life model for fatigue-life prediction which appears to be applicable to a variety of different kinds of composite laminates. They have discussed the fatigue response of four modern carbon-fibre-reinforced plastics materials, *viz.* T800/5245, T800/924, HTA/913, and IM7/977, all with a $[(\pm 45,0_2)_2]_S$ lay-up, after preliminary work in establishing the constant-life model for XAS-carbon/epoxy, Kevlar-49/epoxy, and hybrids of those two materials, in unidirectional lay-up[15,35,36,37]. They have shown that there is a general relationship between the alternating and mean components of stress of the form:

$$a = f(1-m)^u(c+m)^v \quad \text{.....(1)}$$

where a is the normalised alternating stress component, σ_{alt}/σ_t, m is the normalised mean stress component, σ_m/σ_t, and c is the normalised compressive strength, σ_c/σ_t. The alternating component of stress, σ_{alt}, is equal to $\frac{1}{2}(\sigma_{max} - \sigma_{min})$, the mean stress, σ_m, is $\frac{1}{2}(\sigma_{max} + \sigma_{min})$, and σ_t and σ_c are the monotonic tensile and compressive strengths, respectively. For the purpose of this parametric analysis, the sign of σ_c is kept positive, so that the parameter c is also positive. From previous observations on these carbon-fibre composites, it appeared that f may be a function of the laminate tensile strength. The exponents u and v separately characterise the shapes of the right (predominantly tensile) and left (predominantly compressive) wings of a bell-shaped curve represented by equation (1), as can be seen for example in Figure 2-3, and allow for different degrees of asymmetry in the curve: f, u and v have all been found to be linear functions of loglife. The use of equation (1) to analyse stress/life data allows

interpolation and a limited amount of extrapolation for the prediction, from only a modest data-base if necessary, of median fatigue lives representative of conditions (stress range and R ratio) for which experimental data may not yet be available. The extreme values of m for $a = 0$ are 1 on the tensile side of the ordinate and -c on the compression side, the mean stress range is thus (1+c). The setting up of this parametric form of the constant life curve is in fact a double normalisation with respect to the monotonic tensile strength of the hybrid material. In order to apply this analysis, the following stages have been used[7].

2.4.1 Data acquisition

In addition to determining the tensile and compressive strengths of any new material, it is necessary to obtain stress/life data for a series of stress levels that cover to an adequate extent the whole working range from the monotonic strength level down to any notional 'endurance limit'. Initially, five or so replicate tests at each of four or five stress levels will define a reasonable stress/life curve for a particular R ratio, and data for several R ratios from repeated tension to repeated compression will be required.

2.4.2 Initial data analysis

For the plotting of constant-life diagrams, a suitable method of interpolation of data such as those in Figure 2-4 is required. In this figure the curves are plotted in terms of peak stress as a function of lives. The plotted points are the median life, and the curves are second-order polynomial fits to the data. There are several possibilities, including linear interpolation between the median data points and non-linear interpolation, either between the median data points or along a curve fitted to the whole data set for a given R value. Previously, only non-linear fitting of polynomials, usually of second/third order have been used, but it is not certain that this is the most appropriate method. It has been observed, however, that for a reasonably well-arranged set of data, polynomial fits to the median points and to the full data sets are indistinguishable. One advantage of fitting a curve to the full data set is that the extent to which the fitted curves may be safely extrapolated is somewhat greater than when only the median points are used. After an acceptable level of goodness-of-fit is

established, the resulting polynomial coefficients are entered into a spreadsheet (Microsoft Excel), together with the values for the monotonic tensile and compressive strengths of the laminate. The spread sheet calculates the data pairs, (m,a), as defined by equation (1), for each R value at predetermined values of life, N_f. It includes the end points $(c,0)$ and (1,0) representing the monotonic failure conditions. These data sets, for given lives (*eg.* 10^4, 10^5 and 10^6 cycles) are then exported back to Origin software for plotting in the form of constant-life diagrams.

2.4.3 Life prediction

In order to use the constant-life model of equation (1) for life prediction, it is first necessary to explore the variation of the fitting parameters with fatigue life. This is done by fitting equation (1) to the data sets. In a preliminary fitting session, all three parameters, f, u, and v, are allowed to vary freely. The parameter f controls the overall height of the bell-shaped curve, whereas u and v determine the shapes of the left and right wings of the curve, and therefore allow for any asymmetry in the material's fatigue response. Usually, the values of f are reasonably close to each other for different lives and the goodness-of-fit does not change significantly if equation (1) is refitted to the (m,a) curves with the value of f fixed at the mean value from the previous unconstrained fitting operations.

With the value of f fixed, the variation of u and v with life is then established in the form of the pair of functions:

$$u, v = A + B\log N_f \quad \text{.....(2)}$$

Having established the parameters of the relationships in equation (2), it is now possible to predict $\sigma/\log N_f$ curves for any desired R ratio. This is done by solving the pair of simultaneous equations:

$$a = f(\log N_f).(1-m)^{u(\log N_f)}(c+m)^{v(\log N_f)} \quad \text{.....(3)}$$
$$a = m\left(\frac{1-R}{1+R}\right)$$

The first of these is the constant-life equation, equation (1), modified to include information about the life-dependence of the two exponents, $u(N_f)$ and $v(N_f)$, as established from the form of equation (2). The second equation is derived from the

conventional definition of the stress ratio. Solution of these two equations is easily carried out in a package like the MathSoft MathCAD programme which will graph or tabulate $\sigma/\log N_f$ curves for a chosen range of R values. The output can be in the form of a surface plot showing the full variation of $(a,m,\log N_f)$, as illustrated for an IM7/977 laminate in Figure 2-5 or in a simple form as can be seen for an HTA/913 in Figure 2-3. It follows from the derivation of the constant-life plots that the higher the values of *f*, the better the fatigue performance at any given life, since *f*, overall, determines the relative height of the curve, the alternating stress that can be tolerated for a given mean stress at a given life. The parameters of *u* and *v* both depend on the fatigue life. Likewise, the higher values of *u* and *v*, the poorer the fatigue performance because the further *u* and *v* rise above unity (the parabolic 'special case' of the generalised constant-life relationship) the more the 'wings' of the curve are pulled downwards and the more bell-shaped the curve becomes, so reducing the level of alternating stress that can be tolerated for a given mean stress at a given life. And, finally, the greater the slopes, $du/d\log N_f$ and $dv/d\log N_f$ (B in equation 2), the poorer the fatigue performance because the higher the slope, the greater the downward deviation of the $\sigma/\log N_f$ curve at long lives. It is mentioned[6] that the greater the difference in the values of the *u* and *v*, for a particular material, the greater the degree of asymmetry of the constant-life curve. This may influence the choice of material if it is known in advance that for a given application a relative degree of compression or tension loading will predominate.

Alternatively, a family of stress/life curves of conventional form can be produced for ranges of lives that are consistent within the original experimental data window. It is a simple matter to obtain curves for any life within the original experimental window and for any required R value. The proviso is that although some extrapolation to longer or shorter lives is acceptable if there is some indication from the $\sigma/\log N_f$ original data as to the direction that a particular stress/life curve may take, the extrapolation is only as good as the fit of the original polynomial curve to the data set.

This model appears to be applicable to a wide variety of types of CFRP and other kinds of composite. The apparently similar patterns of behaviour for different

materials suggest that preliminary predictions of life for specific R ratios can be made on the basis of relatively small amounts of information, and that these preliminary predictions can be gradually improved as more fatigue experiments are carried out[7].

2.5 IMPACT PERFORMANCE OF FRP

In many of the engineering applications of composite materials, high strain rate or impact loads may be expected. Impact or energy-absorbing properties of composite materials indicates their suitability for such applications. It is generally accepted that composite materials suffer from localised impact loading. Low-velocity impact damage, such as that imparted by a dropped tool or runway debris, is also inevitable and often undetectable by the naked eye. As a result, in recent years many research programs have been undertaken in an attempt better to understand the impact response of composite materials and recent reviews of various aspects of impact properties of composite materials can be seen in the literature[10,38]. Different aspects of this subject that have been studied can be classified as follows.

1. Definition of low-velocity and high-velocity impacts
2. Impact test techniques for composite materials
3. Modes of failure in low-velocity impact
   - 3.1 Matrix damage
     - 3.1.1 Shear cracks
     - 3.1.2 Bending cracks
   - 3.2 Delamination
   - 3.3 Interaction between matrix cracking and delamination
   - 3.4 Fibre fracture
   - 3.5 Penetration
4. Impact-damage assessment techniques
5. Influence of constituents on the impact response
   - 5.1 Fibres
   - 5.2 Fibre stacking sequence
   - 5.3 Matrix
   - 5.4 Interface region
6. Effect of testing variables on impact properties
   - 6.1 Geometry of specimen
   - 6.2 Rate of test
   - 6.3 Impactor characteristics
7. Post-impact Residual strength

7.1 Effect of fibres
7.2 Effect of fibre stacking sequence
7.3 Effect of matrix
7.4 Effect of interface region
8. Prediction of impact-induced damage
9. Prediction of post-impact residual strength

Summaries of the major achievements for each part are as follows.

It is useful to mention that the discussion of impact performance is divided into two categories; impact performance under impacts of relatively low energy, where the composite is damaged but still capable of performing its primary function; and impact performance under impacts of higher energy, where the composite is completely ruptured or penetrated by the striker. Low-velocity impact refers to impacts in the range 1 to 10m/s which are ordinarily introduced in the laboratory. In this kind of impact, the contact period is such that the whole structure has time to respond to the loading. High-velocity impact response is dominated by stress-wave propagation through the material, in which the structure does not have time to respond, leading to very localised damage[38] or perforation. The influence of material variables on performance was found by Hogg[39] to be different in these two categories. When a composite plate is subjected to a low-energy impact, the plate deformation absorbs the energy of the striker elastically at first and subsequently by a combination of micro-fracture processes and further elastic deformation. If the matrix is a thermoplastic, a degree of plastic deformation may also occur, particularly at the point of contact between striker and specimen, although this is usually restricted to a small indentation.

At present, no acceptable standard testing procedures are available for impact testing of composite materials[10]. Consequently a wide variety of testing procedures, specimen geometry are presently being employed. Pendulum techniques such as the Charpy and Izod tests often require specimen geometries that are not representative of component dimensions and so are essentially suitable only for ranking the impact response of composites. Drop-weight rigs and gas guns offer more representative approaches for assessing the impact response of these materials. Greater use of

instrumented impactors has led to a deeper understanding of the processes of energy absorption and dissipation in these materials.

The modes of impact damage induced range from matrix cracking and delamination through to fibre failure and penetration[38]. It is very important to identify the modes of failure because this will yield information not only about the impact event, but also regarding the structure's residual strength. Interaction between damage modes is also very important in understanding damage-mode initiation and propagation. The impact performance of a structure is usually associated with the effects of being struck by an impacting object (foreign-object impact) or the effects of high-strain-rate loading. The resulting damage depends on the impacting object (density, mass, hardness, velocity, shape, attitude, etc.), on the dynamic response of the target structure (skin thickness, support conditions, etc.) and on the target material properties (modulus, strength, toughness, etc.)[40]. In isotropic, homogeneous materials, impact damage is determined mainly by the loading; in composite materials impact damage is influenced significantly by the relatively weak interface between the reinforcement and the matrix. In typical CFRP, the fracture energy parallel to the fibres (splitting and delamination) is usually less than 1 kJ/m^2, whereas the fracture energy perpendicular to the fibres is 50-100 kJ/m^2. Composite materials will therefore tend to fracture parallel to the fibres unless constrained not to[40].

A fibre-reinforced composite consists of two major constituents, fibre and matrix, and the interphase region, which is the area of bond between fibre and matrix. The properties of each of these constituents affect the threshold energies or stresses required to initiate the different failure modes induced by impact.

For low-velocity impact loading, the ability of fibres to store energy elastically appears to be the fundamental parameter in determining impact resistance. Kevlar fibres, which have large areas under their stress/strain curves, offer excellent impact resistance. The role of fibre diameter is not entirely clear[10]. A simple pull-out model suggests that composites with larger-diameter fibres should be inherently tougher. However, current trends are towards smaller-diameter fibres offering higher strains to

failure. Any reduction in toughness is thereby hidden by the increased energy-absorbing capacity of the fibres[10].

It is clear that matrix properties play a significant role in determining the impact resistance and subsequent load-bearing capability of a fibre-reinforced plastic. The damage associated with the impact of a quasi-isotropic epoxy-matrix/carbon-fibre composite was studied by Boll *et al*[41] for resins of low and high fracture energy. Damage in the low-toughness matrix laminate was characterised by a network of interlaminar and transverse cracking that extended some distance beyond the centre of impact. A similar network of transverse and interlaminar cracking developed in the impacted tough-matrix laminate, but was largely confined to a region immediately below the impact centre. The area of damage through the entire thickness of the laminate was much greater (4 to 5 times) for the low fracture-energy matrix resin.

The effect of matrix on the post-impact compressive behaviour of woven-carbon-fibre laminates was studied by Kinsey *et al*[42]. They examined three new low-temperature-cure epoxy resins, an unmodified, a rubber-modified and a thermoplastic-toughened epoxy resin and concluded that toughening composites by using elastomeric particles results in higher interlaminar shear strength and flexural strength, and reduces the level of delamination and matrix cracking considerably during impact and therefore enhances residual compressive properties. However, the presence of such inclusions may reduce the glass transition temperature of the matrix material, which in turn reduces the hot-wet properties of the composite.

The impact resistance is strongly dependent upon the stacking sequence. Unidirectional laminates should be avoided since they split and fail at low energies. The mismatch in bending stiffness between two plies appears to have a significant effect upon the level of damage incurred at that interface[43]. Damage appears to be greatest where ply orientation changes of 90° occur. This suggest that changes in fibre direction should be avoided. It has been shown also by Cantwell et al[44] that the impact resistance of a composite is sensitive to the stacking sequence. Replacing individual ±45° prepreg plies with a woven fabric resulted in panels displaying an improved impact performance. The residual compressive strengths showed a marked

reduction with increasing impact energy, the effect being greater in the case of the non-woven laminates.

The effect of stacking sequence on impact damage and compression-after-impact (CAI) was evaluated on 16-ply panels of carbon-fibre/toughened epoxy T800H/924C composites by Hitchen and Kemp[45]. They found that the major form of damage was delamination, which initiated at almost every interface through the panel. The energy absorbed in delamination initiation was influenced by the stacking sequence, being increased by placing 45° fibres in the surface plies and by increasing the number of dissimilar interfaces. The compression-after-impact strength was determined by the maximum delamination area, which decreased as the delamination area increased.

A significant effect of impact damage is to reduce the strength of the laminate, particularly in compression; however, owing to the complexity of the damage the precise mechanisms controlling the strength reduction are unclear. Pavier and Clark[9] investigated the effect of impact damage on the residual strengths of two CFRP laminates, T300/913C and T800/5245C of $[\pm 45,0_3,\pm 45,0_2]_S$ construction. They concluded that strength reduction in tension of impact-damaged laminates is attributable to fibre cracks: delamination does not play a significant role. Tensile strength after impact may be approximated satisfactorily by a calculation of the net-section of unbroken plies. On the other hand, under compression loading, delamination has a significant role and strength reduction is largely caused by redistribution of stress resulting from buckling of delaminated plies. They found some growth of the delamination lateral to the loading direction and a limited amount of compressive fibre crack growth prior to failure. Residual compressive strength may be predicted by calculating stresses in the un-delaminated part of the laminate.

Since the low-velocity impact event has been recognised as a real threat for many years in fibre-reinforced laminates, many research programs have been carried out to predict the impact-induced damage and residual strength after impact. Following the work of Choi and Chang[46] and Edlund[47] for predicting the initiation of damage and its extent as a function of material properties by using a finite-element model for stress analysis, Davies *et al*[48,49,50] proposed a theoretical method to predict the impact

damage by numerical modelling. Guild *et al*[51] also proposed a finite-element model for the reduction in compressive strength of continuous fibre composites after impact damage.

Caprino[52] developed a linear elastic fracture mechanics model to predict residual tensile and compressive strengths as a function of impacting kinetic energy which gave good correlation to experimental results. The mismatching of bending stiffness between two adjacent laminae was proposed by Liu[43] as an indicator of delamination in the composite laminates subjected to sub-perforation impact. Following their work, Papanicolaou[53] proposed a semi-experimental model based upon bending stiffness mismatching which took into account parameters such as stacking sequence and material properties. He found good agreement between experimental findings and theoretical predictions.

In a series of pieces of work, Soutis and Fleck[54,55,56] studied the static compression failure of carbon-fibre composite plates with a single hole and developed a fracture toughness model[57] to estimate the notched compressive strength of composite plates with an open circular hole. Following these studies, Soutis and Curtis[58] employed that model to predict the post-impact compressive strength of CFRP laminated composites. Their results show that from independently measured laminate parameters of plain (unnotched) compressive strength and fracture toughness, the model successfully predicts the CAI strength for a wide range of lay-ups of standard and toughened CFRP systems. They mentioned that if delamination occurs in only a few interfaces through the thickness then the proposed model is less appropriate and a modified or alternative fracture model may be needed.

2.6 FATIGUE RESPONSE AFTER IMPACT

The sensitivity of carbon-fibre-composite materials to low-level impact damage leads to some concern about possible long-term degradation of these materials by fatigue, particularly under compression-dominated loading. While it is true that fatigue studies have been carried out on composite materials since they first began to be studied as serious engineering materials, their fatigue response after low-velocity

impact events, particularly under a wide range of loading conditions to include from pure tension to pure compression cycling, has not been extensively studied.

The influence of low-velocity impact on the fatigue behaviour, R = -1.0, of various multidirectionally orientated T300 CFRP laminates (1.8-2.7mm thick) was investigated by Stellbrink[59]. It has been found that in some laminates there was an apparent sudden death only and no damage propagation could be noticed visually or by ultrasonic scanning until just before the failure of the specimen. But in some laminates visible damage propagation at higher stress levels could be observed. His results showed that the S/N curves for damaged materials are almost flat.

Impact and subsequent fatigue performance of carbon-fibre laminates with non-woven and mixed-woven layers were studied by Cantwell *et al*[44,60]. They found that both the non-woven and the mixed woven laminates exhibited a reduction in strength as a result of low-velocity impact loading. The residual tensile strengths of the mixed-woven laminates were significantly greater than those of the non-woven laminates. In both laminates, 0-tension fatigue cycles improved the residual strengths for a given incident impact energy. In the case of the mixed-woven composites, the post-fatigue residual tensile strengths showed little dependence on the incident impact energy. Cycling the non-woven composites led to improvements in static strength of up to 30%. Fatiguing the mixed woven laminates resulted in improvements up to 40% in the residual strengths and by 10^6 cycles the residual strengths showed little dependence on the incident impact energy. It was concluded that mixed-woven composites offer both improved impact resistance and improved post-impact fatigue performance, coupled with the ease of manufacture. It was also concluded that mixed-woven laminates offer clear advantages over their non-woven counterparts. This conclusion was also approved by Aoki and Heyduck[61], *ie.* that laminates made of fabric CFRP are more damage tolerant than those made of unidirectional CFRP tapes.

Ramkumar[62] investigated the effect of low-velocity impact damage on the fatigue behaviour of AS/3501-6 graphite/epoxy laminates. The behaviour of impact damaged specimens was investigated under tension-tension ($R \approx 0$), tension-compression ($R = -1$), and compression-compression ($R \rightarrow -\infty$) fatigue loads. It has been concluded

that compression-compression fatigue tests result in the lowest threshold strain levels. The threshold stress (or strain) is defined as the stress for which fatigue failure will be averted for a million cycles at the test load ratio (R). Tension-compression fatigue tests yield marginally higher threshold strain levels than those at R = - ∞, Impact-induced delaminations exhibited a stable growth with cycling with one kind of damage as revealed by ultrasonic pulse-echo scanning, but in a laminate with a different kind of low-velocity impact damage no delamination growth under cycling was recorded.

Clark and Blaricum[63] studied the fatigue behaviour of impact-damaged carbon-fibre composites consisting of XAS/914C with a lay-up of $[\pm 45,0_2]_{7S}$ representative of an aircraft wing skin. Low-level impact damage, as they pointed out, can propagate to failure by compression-dominated fatigue under severe aircraft wing-skin loading conditions. Damage growth normal to the 0° fibre direction was pronounced; little growth rate was observed in the 0° fibre direction, and the damage growth rate was controlled by damage width, apparently independently of initial damage area. The authors also mentioned that by careful control of impact-damage conditions and test methods, the scatter observed in fatigue life may be reduced to a value similar to that seen in metal testing.

Jones *et al* discussed[64] the necessity of fatigue testing of impact damaged composite laminates. They reported that tension-tension fatigue loading is considered to be less critical than compression-compression and tension-compression loading. It had been found that the S/N curves generated from experimental data, for impact damaged specimens, are often flat over a large range of cycles which indicates the large order of magnitude of differences in fatigue lives at a constant stress level. The maximum residual compressive load divided by the static failure load (S) typically decreases from 1.0 to 0.6 in the range 1 to 10^6 cycles (N), depending on the initial damage size. The rate of degradation is at its highest up to N = 100 cycles, and after 10^6 cycles no further degradation occurs; so S = 0.6 may be assumed to be the fatigue threshold. Therefore, it is believed that fatigue loading is not a good way of characterising residual properties.

The measurement of the ratio of the enlarged impact damage area at the corresponding load cycle to the impact damage area before fatigue loading, as a function of number of cycles under compression-compression cycling, R = +10, showed[61] a gradually growing damage area up to a steep increase at the last loading stage before failure.

Post-impact fatigue response for thermoplastic AS4/APC-2 composite and T300/976 thermoset composite, both with a lay-up of $[(0,45,90,-45)_2]_S$, has been studied by Ong *et al*[65]. After compressive fatigue, improvements in residual compressive strength were recorded for T300/976, which coincided with the observation of micro-cracks around the delamination edges. But regarding the thermoplastic composite, after compressive fatigue, the residual compressive strength was reduced. Delamination was the main mechanism of impact fracture for the thermoset composite, however, the transverse shear cracking in the resin matrix was the main impact damage mechanism for the thermoplastic AS4/APC-2 composite.

Griffin and Becht investigated[66] the static and fatigue behaviour of impact-damaged IM7/5250-4 and IM8/HTA (thermoplastic) composite materials. Results showed that the thermoplastic composite system has superior compressive strength retention and damage-tolerance characteristics as compared to the thermoset material. Typically the thermoplastic material sustained less damage during impact event than did the thermosetting material. Also the damage growth during fatigue loading for thermoplastic stiffened panel was negligible, whereas damage in the thermoset material tended to grow until arrested by the fastener line.

Morphology of impact damage growth by fatigue in a 56-ply XAS/914C laminate of $[\pm 45,0_2]_{7S}$ construction was studied by Clark and Saunders[67]. They pointed out several factors which are significant in damage growth, including interactions between overlapping delaminations and the termination and interlocking of delaminations by intra-ply cracking. Delaminations are also believed to form in fatigue at the crossover points of intra-ply cracks, although most of the delamination growth which occurred was associated with delaminations formed at impact. Clark and Saunders pointed out

the complex nature of the damage growth process and the inherent difficulties in modelling the process for predictive purposes.

Curtis *et al*[4] studied the impact damage growth under tension-tension, R = 0.1, and compression-compression cycling, R = +10, in five carbon fibre composites of $[(\pm 45,0,90)_2]_S$ construction. Fatigue tests were performed on 7J impact-damaged materials and fatigue limit strains were determined for no damage growth up to one million fatigue cycles. Results showed that at low stresses damage did not grow at all. At intermediate stress levels, all the materials showed an incubation period when no damage growth was visible. At increasing numbers of fatigue cycles damage was then observed to grow. This incubation period may be due to the fact that impact damage was initially blunted by the fatigue loading and it required large numbers of fatigue cycles to degrade the matrix material and fibre/matrix interface before damage would grow. The work has shown that if working strains reach 0.4% strain in compression, damage growth in fatigue will have to be a serious design consideration. It will be very important, therefore, to develop damage growth predictive methodology and fatigue life prediction capability for composite materials if the advantages of new tough materials are to be fully exploited through designs at higher strains and stresses.

It can be concluded that although many important aspects of the fatigue of composites are now well understood, clear design criteria have not yet been established. Since the nature of fatigue-induced damage is complicated, this needs more research to explore the modes of fatigue failure, especially under pure-compression and tension-compression cycling or under block-loading, in order to simulate real service conditions.

It is generally accepted that fibre-reinforced plastics may be subjected to low-velocity impact damage that reduces their mechanical properties, particularly under compression loadings. A combination of tension and compression residual testing is therefore required to characterise the composite laminates and the precise mechanisms controlling the strength reduction. In this respect, the effect of the geometry of test samples is still unclear and needs to be understood for scaling-up-of laboratory results to practical applications. Although many research programs have been carried out to

predict the impact-induced damage and residual strengths after impact, this remains a challenging area for researchers.

Fatigue-life prediction methods for composite materials in the virgin condition and specifically after low-velocity impact events are still far from satisfactory. Damage-mechanisms-based models are not of interest to designers since these methods include some complicated laboratory work. A model should have the capability for conservative prediction, with appropriate statistical safeguards, from as small an experimental data base as possible, and with the ability to upgrade its predictions smoothly as new fatigue data become available.

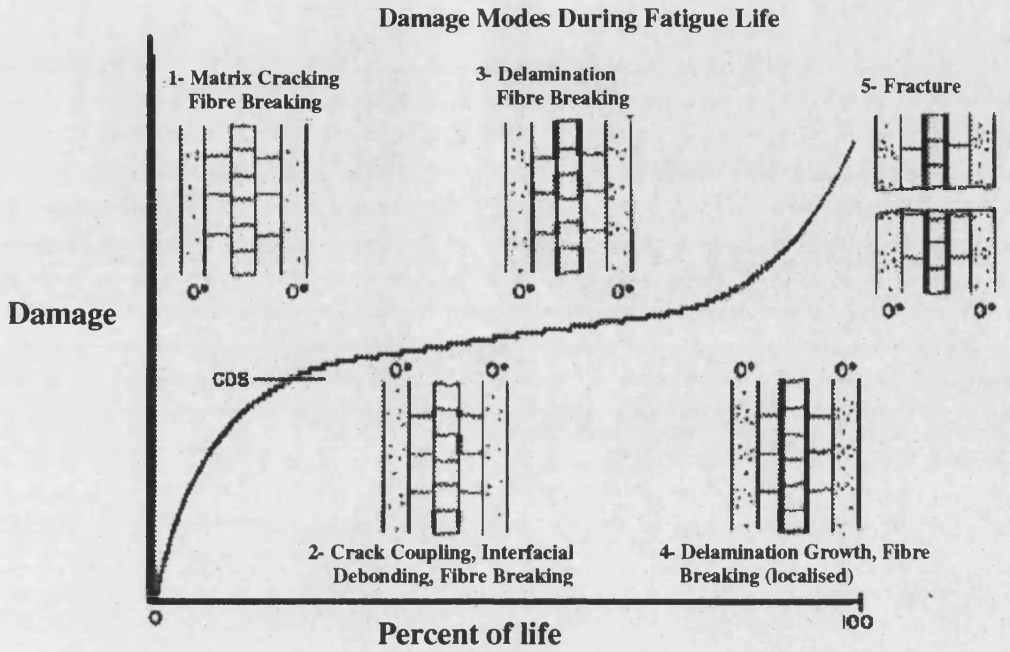

Figure 2-1.Schematic representation of the development of matrix and fibre damage modes and the characteristic damage state (CDS) during the fatigue life of a composite laminate. (after Reifsnider KL, 1991)[11].

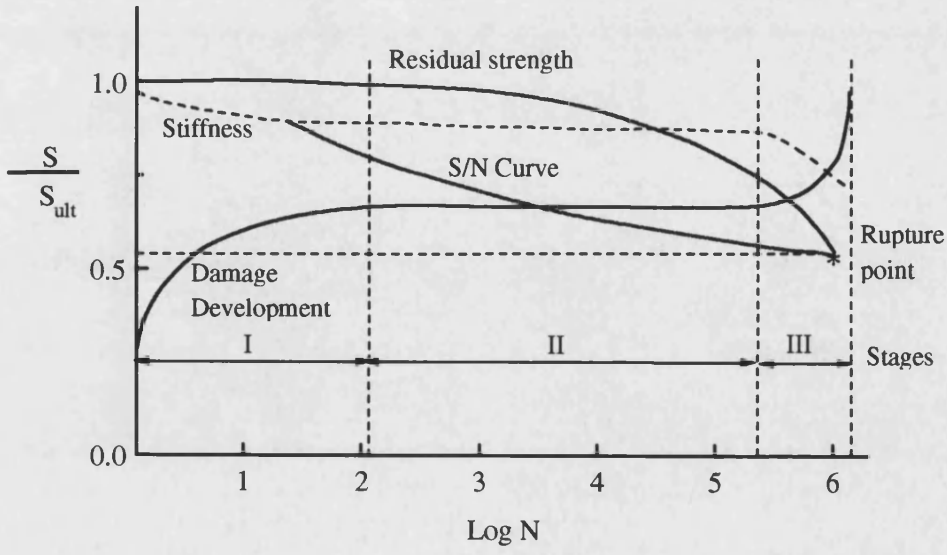

Figure 2-2. Schematic diagram of strength change during fatigue life of an un-notched laminate (after Stinchcomb WW and Bakis CE 1991)[18].

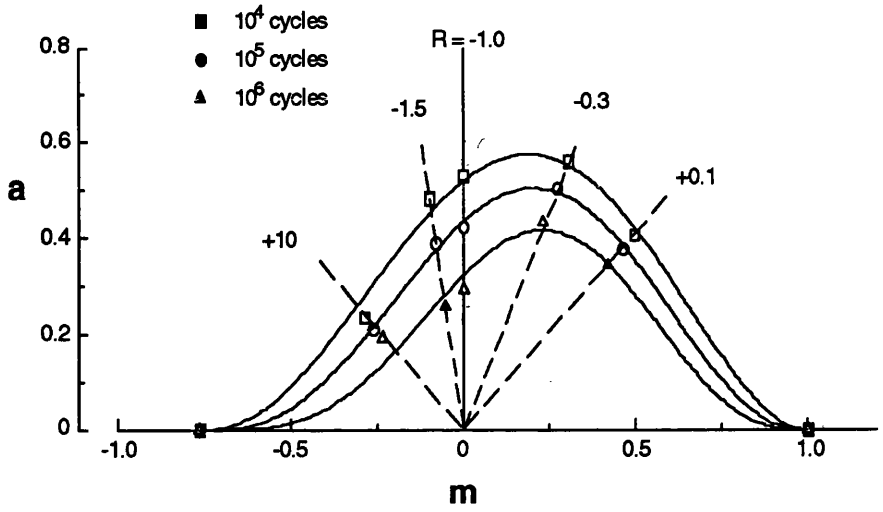

Figure 2-3. Constant-life plots for HTA/913 composite of $[(\pm 45,0_2)_2]_S$ lay-up. (after Harris et al, 1995)[34].

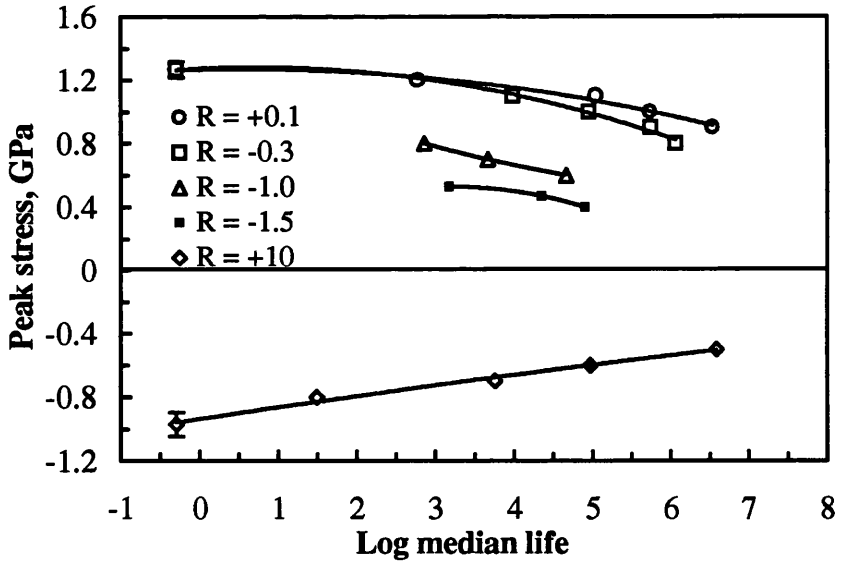

Figure 2-4. σ/log median life curves for a $[(\pm 45,0_2)_2]_S$ HTA/913 laminate at various R ratios (After Harris et al, 1996)[8].

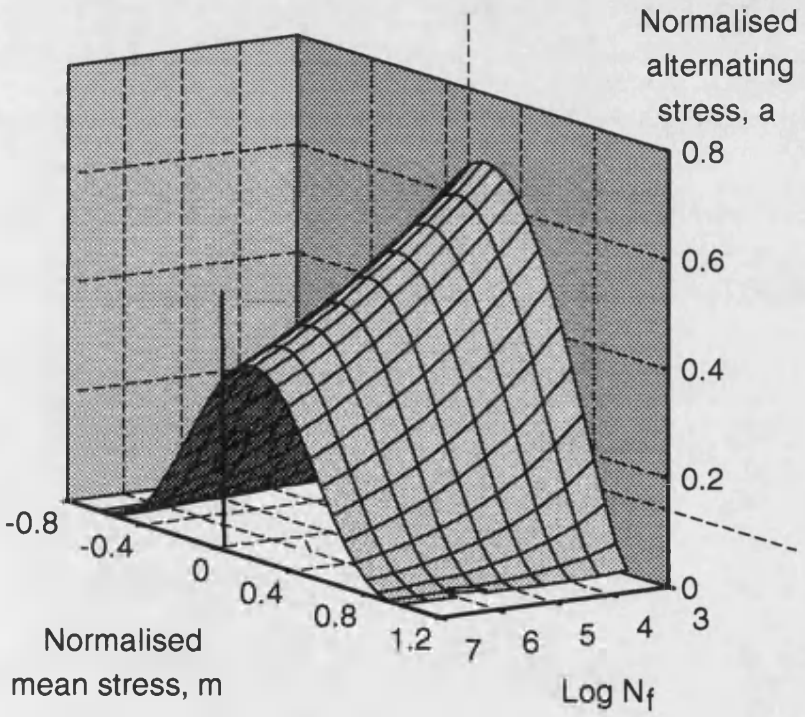

Figure 2-5. Three-dimensional surface plot of the a, m, logN_f constant-life relationship defined by the first of equation 3 for the $[(\pm 45,0_2)_2]_s$ IM7/977 laminate (after Harris et al, 1995)[34].

CHAPTER THREE:

EXPERIMENTAL PROCEDURES

CHAPTER THREE: EXPERIMENTAL PROCEDURES 34

3.1 MATERIALS AND SPECIMENS 35

3.2 TESTING PROCEDURES 36

3.2.1 Monotonic tests 36

3.2.2 Fatigue tests 36

3.2.3 Impact tests 37

3.3 IMPACT DAMAGE ASSESSMENT TECHNIQUES 37

3.3.1 Transient thermography 37

3.3.2 Ultrasonic C-scan 39

3.3.3 Sectioning 40

3.1 MATERIALS AND SPECIMENS

The materials used in the program were two carbon-epoxy composites and a glass-epoxy composite. The main material was HTA/982A manufactured by ICI Fiberite (Europe). This consists of the high-strength, standard-modulus, continuous Tenax HTA 12k carbon fibre in Fiberite 982A, a modified epoxy resin with good hot-wet characteristics, coded Fiberite HyE 3982AH. The second material was HTA/913 which consisted of the same kind of carbon fibre as in the HTA/982A but in BSL 913 standard epoxy resin. This material, which was supplied by Ciba-Geigy (UK) is a representative of the older-established variety of carbon-fibre composites which is similar in many respects to the T300/913 composite that has been the subject of many research programmes. The third material was a glass-epoxy composite Fibredux 913 manufactured by Ciba-Geigy which consisted of E-glass fibre in 913 epoxy resin. This will be referred in the following sections as E-Glass/913. All three materials were supplied in zero-bleed prepreg form with a low cure temperature of 120°C. Among these three composites, therefore, there is the opportunity to investigate the effects of fibre and resin characteristics on the fatigue and impact performance of the composite and on the capability of the life-prediction model.

The main 16-ply lay-up sequence of $[(\pm 45, 0_2)_2]_S$ was selected to represent a lay-up of major importance in the aerospace industry. It is worthwhile indicating that this lay-up was the major one which had been used in previous MoD contract research programs at Bath[8,68,69].

All of the composites were laid up by hand and hot pressed in a Mackey Bowley press as 300mm by 450mm plates (only the HTA/913 laminates were autoclaved) according to the suppliers' recommendations. The curing condition, following supplier specification, was 90 minutes for HTA/982A and 6o minutes for HTA/913 and E-Glass/913 at 120°C and 630kPa (90psi). After curing, the hot-pressed laminates had a nominal thickness of 2mm.

All test samples were cut to dimensions of 200mm long by 20mm or 40mm wide straight-sided (unwaisted) on a water-cooled circular saw with a diamond wheel. Samples, 40mm wide, were used for impact and post-impact fatigue tests and 20mm

wide samples were used for fatigue and fatigue damage studies. The cut edges of all test coupons were wet polished with 220 grade abrasive paper by using a polishing jig of the kind developed and described by Chen[68], and a Buehler Metaserv Motopol 12 polishing machine.

Soft 16SWG aluminium end-tabs, approximately 50mm by 21 mm or 41mm, were attached to both ends of each test coupon to prevent grip damage and give approximately a 100mm test gauge length during testing. These end-tabs were glued to the abraded surfaces of the ends of the specimen, following shot-blasting of the aluminium, with Ciba-Geigy Redux 403 epoxy-resin paste. The cure procedure, 48 hours under light pressure, was done at room temperature. The Redux 403 epoxy-resin paste has been found to be the adhesive system that is best suited to the requirements of fatigue testing.[68]

3.2 TESTING PROCEDURES

3.2.1 Monotonic tests

The measurements of monotonic tensile properties on the 20mm wide samples were carried out in a universal Instron Model 1195 testing machine at a cross-head speed of 2 mm/min. Extension measurements were made by means of a Wallace optical extensometer at a magnification of 200:1, in which 0.002 mm absolute accuracy is guaranteed and with a 50 mm gauge length the accuracy of the strain measurement is better than ±0.004%. Compression tests of virgin samples and post-impact compression tests were carried out in a 100kN servo-hydraulic Instron Model 1342 testing machine at a fixed loading rate of 20 kN/min with anti-buckling fixtures of the kind described by Curtis[70], to support the coupon during loading to prevent macro-buckling. The monotonic tensile tests on 40mm wide samples were carried out under load control in a 200kN servo-hydraulic Mayes test machine model DH 200, again at a rate of 20 kN/min.

3.2.2 Fatigue tests

Fatigue tests were carried out in 100kN servo-hydraulic Instron series 1300 machines under load control and anti-buckling fixtures were again used for compression-compression or tension-compression fatigue tests. Post-impact fatigue

tests at stress ratio, R, of +0.1 were carried out under load control in the 200kN servo-hydraulic Mayes machine. All fatigue tests were run at frequencies between 2.5 and 6Hz with a constant-amplitude sine-wave load, under ambient laboratory conditions.

3.2.3 Impact tests

Impact damage was introduced into the test samples by means of a purpose-built, falling-weight test instrument with a 12.7mm diameter hemispherical tup (Figure 3-1 to Figure 3-3) based on BS 2782 part 3 method 353A. The mass of the impacter was 0.248kg for 1J and 2J impacts, the impact energy being varied by changing the drop height. Impact events at 3J and 5J were made from a constant height of 1m by changing the mass of the impacter. During the impact event the specimen was clamped between two steel rings (Figure 3-4) of internal diameter 30mm and the impact head was captured on rebound after impact to prevent secondary strikes.

3.3 IMPACT DAMAGE ASSESSMENT TECHNIQUES

A number of non-destructive testing, NDT, or non-destructive evaluation, NDE, techniques for the detection of impact damage have been described in the literature[71,72], all of which are suitable for different circumstances. A review of these techniques for detection of low energy impacts in CFRP including their advantages and limitations can be seen in reference[73]. Among them, infrared thermography and radiography are commonly used in aerospace industry, but visual and ultrasonic testing are the reference techniques for inspections[73]. In this program, therefore, transient thermography and ultrasonic C-scanning were used for the assessment of impact-induced damage. In addition, an optical microscopy study following sectioning through the damage zone was used to determine the type and the extent of damage.

3.3.1 Transient thermography

Thermography is a technique of obtaining an image of the heat distribution over the surface of an object. Thermography techniques are classified into the two categories of passive and active[74]. Passive thermography is the monitoring of the heat already present in the system component whereas active thermography needs an external heat source to produce a heat distribution in the component. For NDE, active

thermography has been developed as a transient thermography technique for defect detection and characterisation of a material. In this technique a uniform heat flux (i.e. flash lamp, hot air, laser) is applied to the surface of the component. Consequently the heat-flow pattern through the component is altered by a defect that may be present and this produces local temperature differences on the surface of the component. If the component has homogeneous thermal properties, a uniform response will be obtained. These variations can be collected by an infrared camera and the output can be stored or viewed in real time. This technique has several advantages:

- It is a totally non-contacting method.
- It can be used to inspect relatively large areas in a single shot.
- It provides readily interpreted images.
- The data are easily stored and retrieved.
- Access to the component front face only is necessary.

However, there are some disadvantages:

- It is suitable only for near-surface defect inspection.
- It has low resolution in depth.
- It has poor sensitivity to porosity.
- It is sensitive to surroundings and surface conditions.

There are three main components in the set-up for transient thermography as an NDE technique, *i.e.* the detecting system, the thermal excitation and the recording and image analysis system. In Bath the experimental set-up and apparatus were established as shown in Figure 3-5. The detection system used in this study was an infra-red, Thermovision 750 camera, manufactured by BG Agema Infrared System AB, Sweden. This has a special liquid nitrogen cooled indium antimonide (InSb) photovoltaic detector which provides a resolution of 0.2°C at 30°C object temperature. The heat sources were two floodlight lamps of 500 Watt each mounted horizontally left and right of the centre-line of the sample as shown in Figure 3-5. These flood lamps were controlled by a PC and linked to the thermographic system. Since these flood lamps produced 'after glow' from the hot lamp filaments when switched off, two mechanical shutters were built and located in front of the lamps. These shutters were synchronised to the flash system to prevent any heat flow to the sample after the lamps were switched off. The IR images were recorded and digitised by an Modular Frame Grabber (MFG) electronic card installed in a 486-PC computer.

This card is a TMS34020 graphics system processor (GSP) that controls the image display and accelerates image processing and graphics operation. The commercial software called MFGIRC (Modular Frame Grabber of Infrared Camera) was used to control this card. Details of this system can be found in reference[74]. This system was used for the evaluation of impact-induced damage.

3.3.2 Ultrasonic C-scan

The basic principle of the ultrasonic technique is to use a piezoelectric transducer to fire a pulse of ultrasound (*i.e.* normally a short pulse of frequency 500kHz-10MHz) in a narrow beam into the specimen and to detect any echoes coming from a defect with the same transducer. The echoes are normally displayed on a modified oscilloscope, called a flaw detector. Coupling methods such as gel, water immersion or a water jet are needed between transducer and specimen. There are several display options when using ultrasonic techniques, but many industries prefer to use the C-scan type for a controlled scanning technique. It displays the size and position of a defect in the plane parallel to the surface of the component. Additionally, defect depth may be indicated by different shades of grey or colours. The advantage and limitation of this technique can be seen in reference[74]. This procedure will involve a great deal of manual skill or sophisticated control of scanning, signal acquisition and processing.

Ultrasonic studies of impact-damaged specimens were carried out by using the through-transmission C-scan technique. A computer-controlled system which was explained in detail by Moghisi[75] was used. Its block diagram is shown in Figure 3-6.

Short, regular radio-frequency electrical pulses were generated by a Pulse Modulator/Receiver to excite the transmitting transducer to fire ultrasonic sound into the specimen to be tested. The transmitting transducer was a focused 5MHz PZT5 one, with focal length of 50mm. An identical transducer was used to receive the attenuated ultrasonic wave after it had passed through the specimen and convert it back to electrical signal. This signal was received by the Modulator/Receiver unit and the amplitude of the signal was converted to a DC voltage. This was relayed to the y-plate of the oscilloscope, causing a peak in the trace. A square pulse was generated on the second trace of the oscilloscope by a Scan Delay Generator. The width and

position of the pulse on the time base could be adjusted so that the pulse coincided with the peak signal of the attenuated ultrasonic wave, and thus any other signals (such as secondary echoes) were ignored. The signal from the receiver transducer was also fed into a Linear Gate to be amplified and integrated and then was relayed to the computer via an analogue-to-digital converter. A Trigger Pulse Generator allowed the synchronisation of the system of signals. The computer at the same time directed the stepping motors on the "x" and "y" cross-slides of the C-scan system, which moved the specimen perpendicular to the ultrasonic beam.

As high-frequency ultrasonic waves do not propagate well in air, some means of coupling from transducer into specimen and vice versa is essential. Both transducers and specimen were immersed in water, which is transparent, cheap and easy to handle. To enable accurate and quick alignment of the two transducers, which is the basic requirement of the ultrasonic C-scan technique, a specially designed optical bench was used to hold the transducers. The readings were displayed one by one on the monitor of computer, while scanning was going on, and then stored on hard disk as a matrix. The sophisticated visual displays, such as contour image or surface image, of this matrix data could be easily done by using any commercial software, such as Mathcad Plus, Excel or Microcal Origin, with high resolution (in pixels, in colour or grey scales) for subsequent analysis

3.3.3 Sectioning

The damage associated with the impact was also studied by sectioning through the impact area and photographing the polished sections. For each level of impact energy two specimens were sectioned, one in the longitudinal direction and another in the transverse direction relative to the fibres, as can be seen in Figure 3-7. A cut was made slightly off-centre of the damage zone. One of the halves was mounted in an epoxy resin and wet polished to the centre of the damage zone with 320 grit paper followed by fine polishing. For polishing three different Buehler wheels were used starting with Metlap 4, a polymer composite with soft metal particles and a 9 micron oil-based diamond suspension. For the next stage a hard non-woven chemotextil cloth, called Texmet, with 0.3 μm alpha alumina water-based suspension was used. Final polishing was achieved with a mat made of Neoprene, called Mastermet,

together with a colloidal silica diluted 1:1 with distilled water, offering a 0.05 μm particle size. The cutting edges were so polished to a degree suitable for metallographic examination. The polished surfaces were examined by using reflected-light microscopy for the type and extent of damage in each ply.

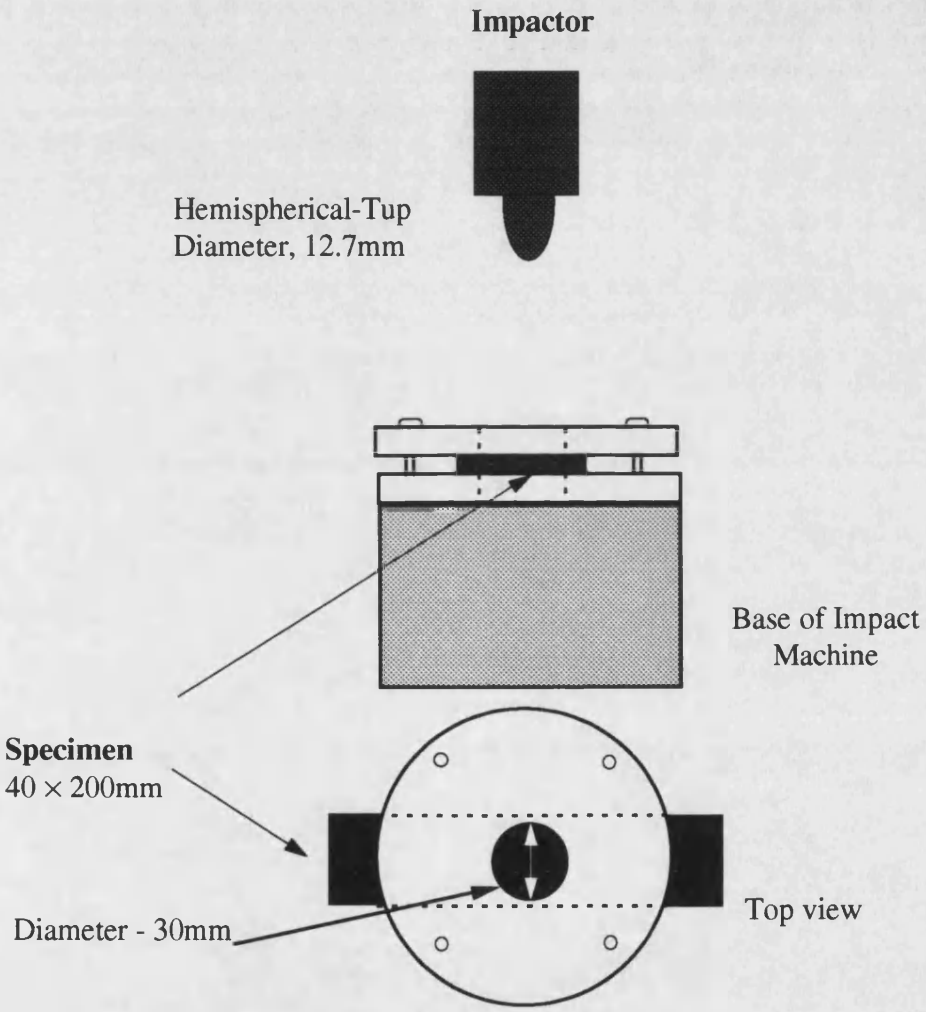

Figure 3-1. Schematic of impact test geometry.

Figure 3-2. Falling dart method, impact testing instrument.

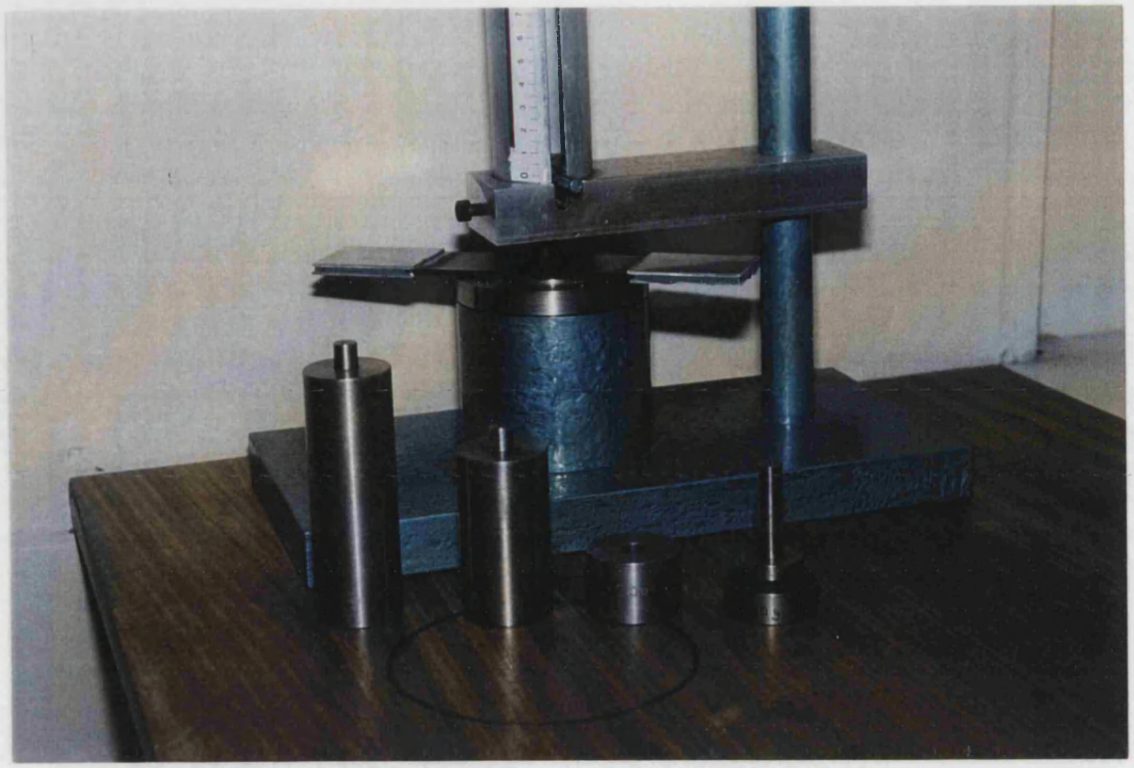

Figure 3-3. A close-up view to the bottom of impact tester.

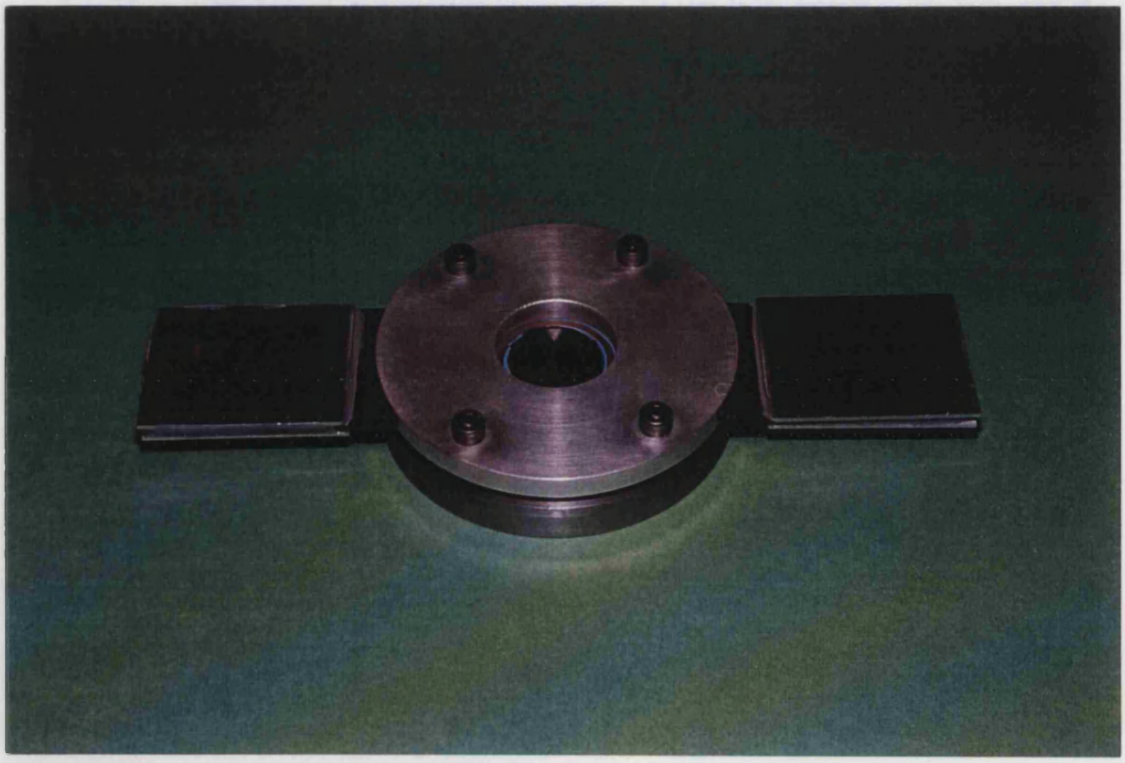

Figure 3-4. Impact test fixture for holding the specimen.

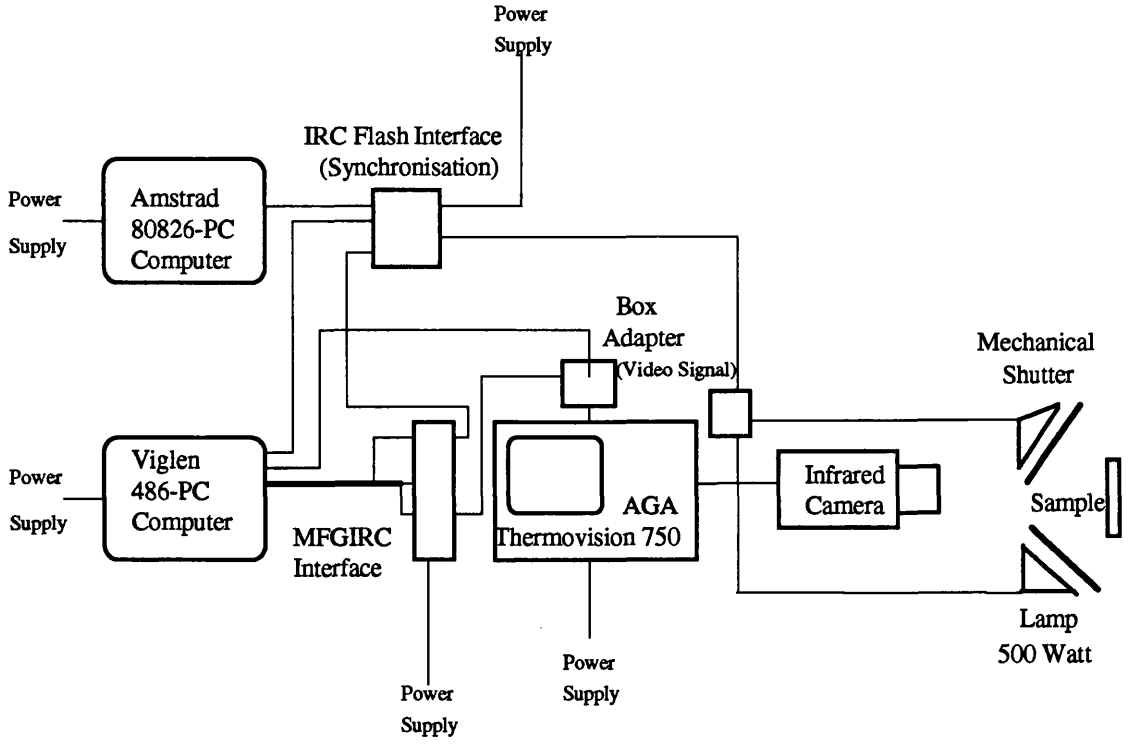

Figure 3-5. A schematic diagram of the Bath transient thermography system.

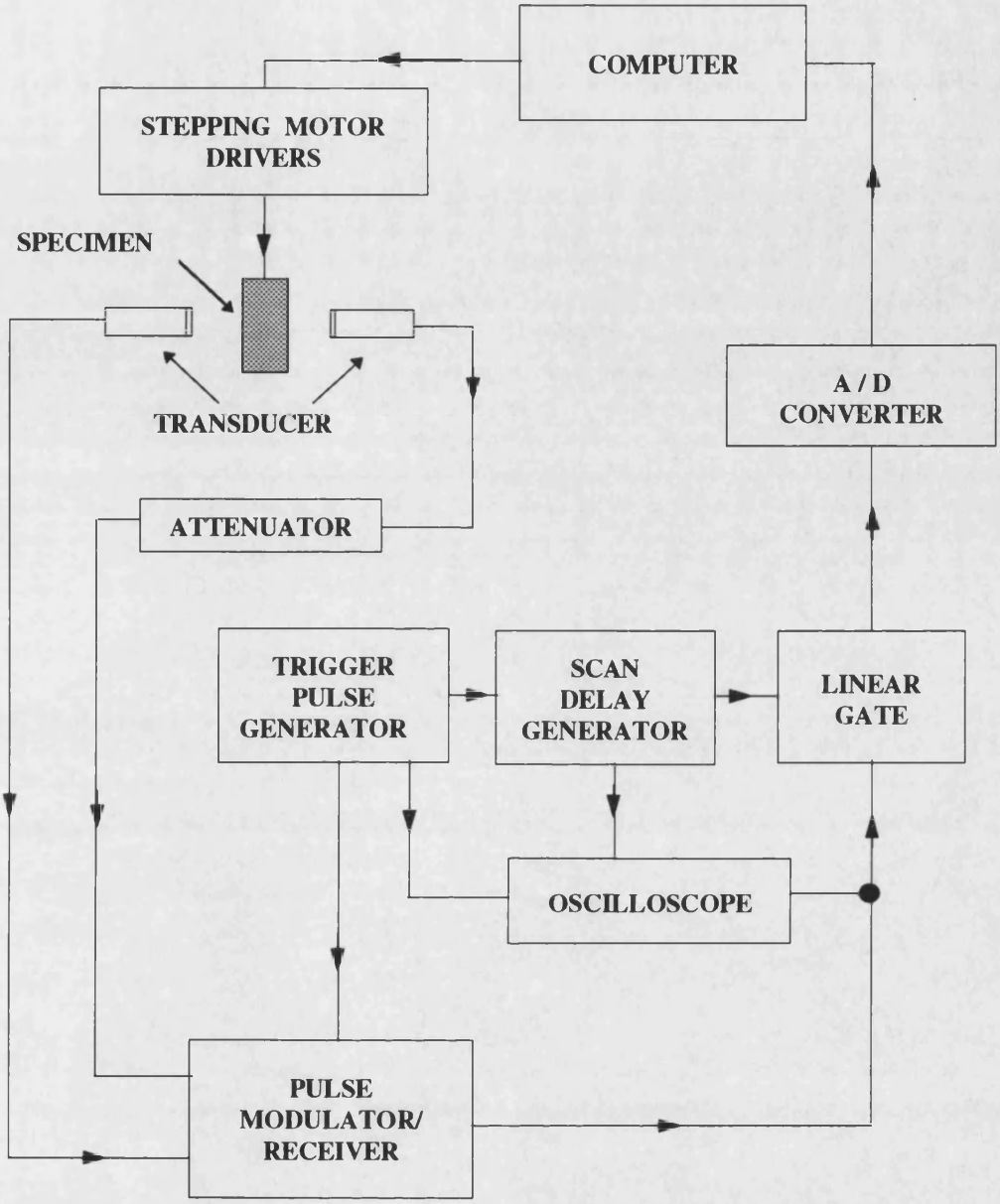

Figure 3-6. Block diagram of measurement and control system of through-transmission ultrasonic C-scan testing system.

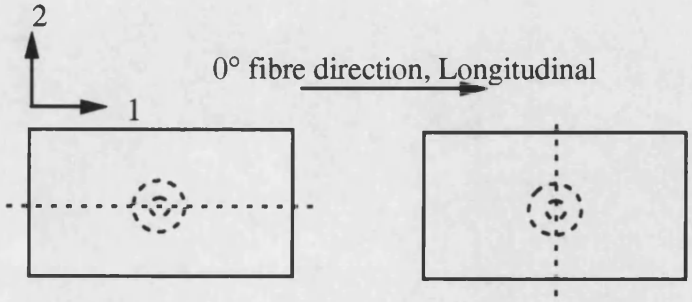

Figure 3-7. Sectioning diagram. One specimen sectioned in longitudinal (left) and another one in transverse (right) directions relative to the fibres.

CHAPTER FOUR:

RESULTS AND DISCUSSION

CHAPTER FOUR: RESULTS AND DISCUSSION 47

4.1 INTRODUCTION 48

4.2 STRENGTH AND MODULUS MEASUREMENT 48

4.3 POST-IMPACT MECHANICAL PROPERTIES 50

4.4 PREDICTION OF RESIDUAL COMPRESSIVE STRENGTH 51

4.5 IMPACT DAMAGE ASSESSMENTS 52

4.5.1 Visual examination 52

4.5.2 Infrared thermography and ultrasonic testing 53

4.5.3 Sectioning 54

4.6 THE FATIGUE RESPONSE OF UNDAMAGED HTA/982A 57

4.7 THE FATIGUE RESPONSE OF UNDAMAGED E-GLASS/913 58

4.8 POST-IMPACT FATIGUE RESPONSE 59

4.8.1 Fatigue response of HTA/982A after 1J Impact 60

4.8.2 Fatigue response of HTA/982A after 2J Impact 61

4.8.3 Fatigue response of HTA/913 after 2J Impact 63

4.8.4 Fatigue response of E-Glass/913 after 2J Impact 64

4.9 DAMAGE DEVELOPMENT IN CYCLING 66

4.9.1 Compression cycling, R = +10 66

4.9.2 Tension-compression cycling, R = -0.3 67

4.1 INTRODUCTION

The experimental program outlined in chapter three provided a considerable amount of test data. This chapter, therefore, intends to describe and discuss these results in order to contribute to the aims of this research program. The monotonic mechanical properties of materials under investigation in the virgin condition and after damage by low-velocity impact will first be discussed and this will be followed by the results of thermography, ultrasonic C-scan and sectioning of impact-induced damages. In the next sections, fatigue test results for materials before and after impact at different stress ratios will be presented. Finally, the development of the impact damage zone in compression- compression and tension-compression cycling will be explained. Constant-life analysis of fatigue data and its application in life-prediction will be discussed in the following chapter.

4.2 STRENGTH AND MODULUS MEASUREMENT

The mechanical properties of the experimental laminates are given in Table 4-1. The basic properties of the other three CFRP composites, *viz.*, T800/5245 and T800/924 and IM7/977, have been added from reference 8 for comparison. Since the fibre types and fibre contents are nominally identical in the two HTA laminates the differences between the properties shown in this table must reflect either the effects of the different matrix resins or differences in the processing procedures (or the two together). But since no detailed information for the 982A resin is available, no useful comparison of the matrices can be made. The HTA/913 laminate was autoclaved rather than hot-pressed, for 60 minutes at 120°C, slightly less than the pressing time, 90 minutes, for the HTA/982A, but the resulting fibre content is only marginally lower, as shown in Table 4-1. For a laminate of $[(\pm 45,0_2)_2]_S$ construction, the Krenchel factor[76], η_θ ($= \sum a_n \cos^4\theta$), has the value 0.625. Thus for a laminate with V_f = 0.54 of HTA fibres of Young's modulus E_f = 238GPa (manufacturer's data) and an epoxy resin of modulus E_m = 2GPa, the expected laminate stiffness ($E_c = \eta_\theta E_f V_f + E_m(1-V_f)$), should be about 81GPa, close to the experimental value given in Table 4-1. The small difference in V_f and quite large changes in resin properties, either intrinsic or as a result of processing differences, will have almost no effect on this calculation, and it is difficult, therefore, to see why the experimental stiffness of the

HTA/913 composite should be as low as 72GPa. Processing and/or interfacial characteristics are likely to be responsible for the fact that the two strengths of the HTA/913 laminate are both somewhat greater than those of the HTA/982A. The compressive strength of the HTA/982A is also rather lower relative to the material's tensile strength than that of the HTA/913. T800 and IM7 are the higher-performance carbon fibres and it can be seen that the tensile modulus of their laminates are all alike, the average value being about 92GPa, about 25% higher than that of the HTA/913 composite. It is interesting that despite the major differences in fibre tensile properties and matrix characteristics in CFRP laminates, these have almost no influence on the compression resistance of these laminates.

Table 4-1. Monotonic mechanical properties of experimental laminates together with data for three other modern $[(\pm 45, 0_2)_2]_S$ CFRP laminates, 20mm wide samples (standard deviations in brackets).

Material	V_f	Tensile modulus, GPa	Tensile strength, GPa	Tensile failure strain, %	Compressive strength, GPa	Ratio of compressive strength to tensile strength
HTA/982A	0.54	80.1 (8.5)	1.20 (0.05)	1.50 (0.12)	0.84 (0.08)	0.70
HTA/913	0.53	72.4 (4.8)	1.25 (0.02)	1.67 (0.06)	0.97 (0.08)	0.77
E-Glass/913	0.55	26.0 (2.2)	0.79 (0.03)	3.41 (0.51)	0.603 (0.09)	0.76
T800/5245	0.65-0.69	94.0 (3.1)	1.66 (0.09)	1.69 (0.10)	0.883 (0.09)	0.53
T800/924	"	92.0 (7.9)	1.42 (0.09)	1.49 (0.12)	0.897 (0.09)	0.63
IM7/977	"	90.2 (11.3)	1.43 (0.07)	1.52 (0.15)	0.903 (0.08)	0.63

For a laminate with $V_f = 0.55$ of E-glass fibres of Young's modulus $E_f = 72$GPa and an epoxy resin of modulus $E_m = 2$GPa, the expected laminate stiffness should be about 25.7GPa, again close to the experimental value. Comparison between the two 913 composites shows the significant role of the fibres. As expected, high tensile strength and stiffness have been achieved in the HTA/913, but it suffer from low failure strain, while the E-Glass/913 is very tough with a failure strain of ≈3.5%. It is, therefore, more damage tolerant than CFRP laminates.

4.3 POST-IMPACT MECHANICAL PROPERTIES

The effects of impact on the monotonic tensile and compressive strengths of the HTA/982A, HTA/913 and E-Glass/913 laminates are shown in Figure 4-1 to Figure 4-3. It can be seen that in both CFRP materials, despite major visible signs of surface and sub-surface damage at the higher energy levels, the tensile strength is not affected up to impact energies of 3J and is only slightly reduced by a 5J impact in the free-back mode. By contrast, the compressive strength is markedly affected, even by a 1J impact, the effects of which are almost undetectable by eye. It is interesting that the scatter of residual compressive strengths at each level of impact energy is significantly less than that for the residual tensile strengths. In the solid-back mode of impact test, both tensile and compressive strengths were slightly reduced. This may be due to the fact that this kind of impact event does not produce delamination and the mode of impact damage is mainly matrix cracking, interlaminar cracking and fibre fracture. A better comparison between the three experimental materials can be made from Figure 4-4. In this figure the residual compressive strengths in the free-back mode are normalised with respect to the initial compressive strength of each material. It can be seen that the mean compressive strength for HTA/982A was reduced by 45, 60, 64 and 68% after 1, 2, 3 and 5J incident energy, respectively. It can be concluded that the impact-induced damage is mainly delamination (as revealed by sectioning) because delamination reduces the shear and compressive strengths but has little effect on tensile strength, whereas broken fibres have more effect on tensile strength. Similar behaviour in reduction in compressive strength can be seen for HTA/913. It is interesting that although their initial compressive strengths are remarkably different (0.84GPa for HTA/982A in comparison to 0.97GPa for HTA/913), and their resins are also different, the percentage losses in their compressive strengths after impact are rather similar. Figure 4-4 shows that GRP is more damage tolerant than CFRP. It is interesting that after 5J incident energy, the mean compressive strength of GRP was reduced by 48%. Although glass-fibre composites are superior in this respect to carbon since they have a low modulus, a comparable strength, and a weaker interface between fibre and matrix, unfortunately their absolute performance in compression is poor anyway because of their flexibility.

4.4 PREDICTION OF RESIDUAL COMPRESSIVE STRENGTH

Since low-energy impacts reduce the compressive strength of composite materials significantly, a great amount of work has been devoted to the prediction of residual compressive strength after impact. Among them, it is worthwhile referring to a semi-empirical model developed by Papanicolaou[53] that is based on bending stiffness mismatching. A unique feature of this model is that this model has a parameter which is a linear function of the percentage, x, of ±45° plies of laminates and hence it is interesting to examine the application of this model to our materials.

The proposed model refers to linear-elastic materials where no plastic deformation is present. It is based on the assumption that the degradation in flexural stiffness is related to the residual compressive strength as follows:

$$\frac{\sigma_r}{\sigma_0} = \frac{[D_{ij}]_r}{[D_{ij}]_0} \quad \text{.....(1)}$$

where σ_r represents the residual compressive strength of the impacted material; σ_0 is the compressive strength of virgin material; $[D_{ij}]_0$ is the flexural stiffness matrix of the un-impacted laminate (already known from classical laminate theory); and finally $[D_{ij}]_r$ is the flexural stiffness matrix of the impacted material. This analysis finally gives the simple form:

$$\frac{\sigma_r}{\sigma_0} = \frac{md}{U^{\alpha}} \quad \text{.....(2)}$$

where: d is a parameter which depends on the material properties and test conditions; U is the impact energy; α is an energy absorption capacity factor which depends on the fraction of ±45° layers in the laminate and m is the following ratio:

$$m = \frac{\sum_{k=1}^{n} (\overline{M}_k)_0 [Q_{xx,k}(Z_k^3 - Z_{k-1}^3)]}{\sum_{k=1}^{n} [Q_{xx,k}(Z_k^3 - Z_{k-1}^3)]} \quad \text{.....(3)}$$

In this equation $(\overline{M}_k)_0$, $Q_{xx,k}$ and Z_k are respectively the mean value of the bending stiffness mismatching coefficient, stiffness matrix of the k-lamina and the distance of the k-lamina from the middle plane of the laminate and n is the total number of lamina. A linear relationship between α-x and d-x was observed[53] for a group of

experimental test results. These results were obtained for an HTA/6376 composite with stacking sequence of [(90-x)%0°/x%±45°/10%90°], where x = 20, 40, 60 and 80, consisting of 40 layers. These relationships were written in the following forms:

$$d = \frac{63}{4} + \frac{2}{15}x \quad \text{and} \quad \alpha = \frac{1}{300}x + \frac{1}{4} \qquad \text{.....(4)}$$

Combination of the above relationships gives:

$$d = 4(10\alpha + 1) \qquad \text{.....(5)}$$

Hence, the proposed model becomes a one-parameter model and equation (2) becomes:

$$\frac{\sigma_r}{\sigma_0} = 4m\frac{10\alpha + 1}{U^{\alpha}} \qquad \text{.....(6)}$$

To apply this model to our materials two parameters, m and α, must be calculated. For composites of $[(\pm 45, 0_2)_2]_S$ construction, the fraction of ±45° plies is x = 50%. Thus, equation (4) gives the value of α = 0.42. The m value must be calculated by using the ratio of the summation in equation (3) and depends on the material properties. To eliminate these calculations, which require many parameters to be determined, the measured residual compressive strength of materials after 2J impact was used and empirical m values of 0.0251, 0.0255 and 0.4 were obtained for HTA/982A, HTA/913 and E-Glass/913, respectively. The predicted residual compressive strength for three investigated materials are shown in Figure 4-5. In this figure the experimental results are shown as symbols and the curves represent the predicted results. It can be seen that there is good agreement between the predicted and experimental results. The differences at 5J may be due to the fact that at this level of impact energy, the impact induced damage is not pure delamination (which is the only failure mode considered in the above model) and some fibre fracture was in fact observed, as will be explained in the next section.

4.5 IMPACT DAMAGE ASSESSMENTS

4.5.1 Visual examination

Visual inspection was performed on each material before using more sophisticated techniques. There was no visible sign of damage on either front or back faces of the

laminates after 1J and 2J impacts, the higher energies, 3J and 5J, nevertheless caused serious spalling off of the outer 45° plies from the back face in HTA/982A. This kind of surface damage in HTA/913 could be seen only after a 5J impact and could not be seen in E-Glass/913. This may be related to the bending strain of material. A laminate with higher bending strain shows less back-surface damage or fibre splitting due to back-face tension forces. On the other hand, no significant dent could be seen on HTA/982A whereas dents could be detected by the naked eye on HTA/913.

Since glass-fibre-reinforced epoxy materials are transparent, sub-surface damage and the distribution of impact-induced delaminations through the thickness could easily be seen by visual examination. No significant damage could be seen after a 1J impact in this material, but the higher energies produce serious damage. Figure 4-6 and Figure 4-7 show the low-velocity impact damage after 2J and 5J impact events, respectively, taken by optical photography from the front and back faces of E-Glass/913 laminates. It can be seen from these figures that there is no delamination in the region of the centre line of the impactor. Davies and Zhang[49] explained that the region on the centre line of the impactor is a low-shear region, and in a state of through-thickness compression, so delamination will not start here. It can be also seen that the shape of the overall damage zone is approximately elliptical or peanut-shaped and elongated in the direction of the 0° fibres. This peanut shape developed with different orientations at the various interfaces. It seems from differences between the front and back face pictures that the damage zone is narrowing towards the top surface and the delamination looks rather like a spiralling surface.

4.5.2 Infrared thermography and ultrasonic testing

To explore the nature and distribution of impact damage, some specimens of each material after low-velocity impacts of 1J, 2J, 3J and 5J on free-back specimens and 4J and 6J on solid-back specimens were inspected by transient thermography and 5MHz ultrasonic C-scanning. These results are shown in Figure 4-8 to Figure 4-10. It can be seen from Figure 4-8 that an impact event of 1J produced significant delamination in HTA/982A. Thermographic images for HTA/913 and E-Glass/913 were taken from both the surface that was impacted and the back face of each sample. It is clear that

images taken from the front face (impact side) of specimens are different from those taken from the back face. Although the nominal thickness of the specimens was about 2mm, this technique is sensitive to the depths of the defects. The differences between the thermographic results reflect the nature of impact damage which comprises delaminations that increase in extent between plies towards the back face. It can be seen from Figure 4-9 or Figure 4-10 that there are differences between the results of C-scanning and thermography. These differences can be seen very clearly from Figure 4-11 which shows the overall impact-induced delaminations calculated from images taken from both techniques for HTA/913 material after 2, 3, and 5 Joule impacts. This is due to the fact that the thermal contrast depends on the depths of the damage being imaged whilst the ultrasonic C-scan images are produced by the total attenuation caused by all the delaminations to the ultrasonic waves passing through the sample.

In order to compare the impact resistance of these three materials, the overall delamination induced by 1, 2, 3 and 5 Joule impacts have been calculated from the C-scan images and are depicted in Figure 4-12. It can be seen from this figure that HTA/982A showed the weakest resistance, even a 1J impact event producing significant delamination. This may be related to their toughness: of the materials, E-Glass/913 showed the highest resistance to impact. It is expected to see this behaviour for a material like GRP with high strain to failure, but at 5J impact both CFRP laminates and GRP showed similar delaminations. This is due to the fact that the modes of failure in low-velocity impacts are matrix damage, delamination and fibre fracture. Matrix damage is the first type of failure induced by the transverse forces and usually takes the form of matrix cracking but also debonding between fibre and matrix. Delamination is the major damage mode in the thin composite plates and is mainly due to the bending. Fibre fracture occurs at higher impact energies and hence, if impact energy increases it will produce more fibre fracture and finally perforation will occur. For this reason, therefore, at 5J impact energy all three materials showed similar delamination area.

4.5.3 Sectioning

After inspection of the impact-induced damage by thermography and ultrasonic C-scanning, samples were sectioned in the longitudinal and transverse directions relative

to the fibres and after polishing they were inspected by optical microscopy. This study revealed that the damage modes of these laminates subjected to 1J, 2J and 3J low-velocity impacts are matrix cracking and delamination as can be seen, for instance, from the damage maps and photomicrographs for 2J impact events in Figure 4-13 to Figure 4-18. Matrix cracking can be seen in each lamina, mainly in the inter 45° plies and 0° plies as well and their density is higher in the transverse direction relative to the fibre. It can be seen that these matrix cracks started under the edges of the impactor and inclined at approximately 45°. These cracks are formed by the very high transverse shear stress through the material and, hence, they are also called shear cracks. There is another kind of matrix failure which is called bending cracking because it is induced by high bending stresses and is characteristically vertical and occurs in the bottom layers. This kind of bending crack is rarely seen in HTA/982A and HTA/913, but it can be seen in E-Glass/913 as shown in Figure 4-18. This may be due to the higher bending strain in E-Glass/913.

It can be seen from the damage maps that most of delaminations are between 45° plies and 0° plies and delamination is the major damage mode. This may be due to the higher value of bending stiffness mismatching between these plies. The stresses that cause the delaminations in the impacted composite plates are mainly bending stresses. Bending stiffness can then be correlated with the impact-induced delamination. The delamination area in an interface is proportional to the mismatch of bending stiffness between the lamina on each side of the interface. In other words, the delamination area in the interface increases as the mismatch of the bending stiffness between the lamina increases. This criterion was used for prediction of residual compressive strength as mentioned before. It can be seen from the damage maps that damage is distributed in the upper surfaces (layers above the mid plain) and lower surfaces. This is a unique feature of 2mm-thick laminates, as explained by Cantwell and Morton[77]. They showed that for a family of (±45°) and ($0°_2$, ±45°) laminates of XAS/914C, as can be seen in Figure 4-22, the damage threshold increases with increasing target thickness and subsequently falls. In terms of damage initiation, the optimum thickness was found to be a 2mm thick laminate where damage initiated simultaneously at the

upper surfaces owing to the locally high contact stress field and at the lower surfaces of the target as a result of the flexural stress field within the beam.

Fibre failure generally occurs much latter in the fracture process than matrix cracking and delamination. Only a 5J impact event produced fibre fracture in HTA/982A laminates under the impactor, as can be seen in Figure 4-19. This is due to locally high stresses and indentation effects. On the non-impacted faces of samples of HTA/982A and HTA/913 fibre failure can be detected by the naked eye in the 45°direction.

It has been recognised that, in an impact event, part of the impact energy is converted into elastic deformation and vibration and is then dissipated in the form of heat. However, the remaining part of the impact energy is absorbed by the specimen and results in permanent deformation and damage. The results of sectioning showed that the damage modes are matrix cracking and mainly delamination. Fibre fracture can be seen only at 5J in HTA/982A. The difference between the impact-induced energy introduced into and rebounded from the specimen was called the net impact energy and the overall delamination area is depicted against this energy in Figure 4-23. For this analysis a 5J impact energy is omitted from calculations for CFRP laminates because of fibre fracture. It can be seen that there is a linear relationship between delamination area and the net impact energy. This kind of linear relationship between delamination area and impact energy has been verified by Hong and Liu[78] for a group of thin glass/epoxy plates with different fibre orientations subjected to low-velocity impact. It can be seen from Figure 4-23 that the slopes of fitted lines, which represent the incremental delamination area per unit impact energy, are about the same. Back-extrapolation of these lines gives the minimum energy (J_0) for delamination initiation. These minimum energies are 0.12, 0.54 and 0.56 joule for HTA/982A, HTA/913 and E-Glass/913, respectively. It can be concluded that the 913 resin is more damage tolerant than the 982A resin and the role of resin is more important than the role of fibre.

4.6 THE FATIGUE RESPONSE OF UNDAMAGED HTA/982A

Replicate stress/life data were obtained at four stress ratios, R, of +0.1, -0.3, -1.5 and +10 and the results are shown in Figure 4-24. The diagram shows the actual data points and the fitted curves are third-order and second-order polynomials fitted to full data sets at R = 0.1 and -0.3, -1.5 and +10, respectively. This form of curve-fit is chosen simply for convenience: it is not intended to suggest that there is any mechanistic argument for such a fit. Fatigue tests were carried out on 20mm and 40mm wide samples to discover whether the change in width would affect the fatigue response, since comparison with earlier work on other materials would be one of the objectives of this work. The solid and open symbols in Figure 4-24 refer to the wider and narrower samples, respectively. It can be seen that the width of sample has no significant effect and there is no obvious separation of the points on the graphs. The individual $\sigma/\log N_f$ data points are also shown in Table 4-2. It can be seen that wider samples showed less scatter of results and have higher values of mean and median life. But the results of 40mm wide samples lie within the scatter bands of data for the 20mm wide samples. The slight increase in mean and median life might be due to the fact that fatigue damage begins from the free edges of sample and grows to the centre-line and hence the wider sample might have the higher life, but the difference between 20mm and 40mm sample wide is not so great as to suggest a significant effect. Although more experiments are needed to study the size effect, it was not feasible to do that because of limitation of availability of fatigue testing time and materials.

Figure 4-25 shows the actual data points and the fitted curves for HTA/982A in addition to the stress/median-life curves (dashed lines) for the comparator HTA/913 laminate taken from reference 7. It can be seen that, for the most part, these curves lie within the scatter bands of data for the HTA/982A, although there is an indication that for R ratios other than –0.3, the slopes of the curves for HTA/913 are slightly steeper and hence the fatigue resistance of the older material is marginally poorer than that of the HTA/982A composite.

Stress/median-life curves for tension-tension cycling at R = +0.1 for four CFRP including high strength T800 composites are shown in Figure 4-26. It can be seen

although there are significant differences in their monotonic tensile strengths, after three decades they all show rather similar behaviour. The stress/life (S/N or $\sigma/\log N_f$) curve for a material with higher monotonic strength is steeper than that for the material with lower monotonic strength.

Table 4-2. Stress/life data of 20mm and 40mm samples of HTA/982A in the virgin condition.

Stress ratio	σ_{max} GPa	Sample Number	Width of samples	
			20mm	40mm
R = +0.1	1.1	1	42,191	61,177
		2	52,137	107,101
		3	78,239	159,687
		4	79,904	227,577
		5	277,228	236,081
Mean life			105,940	158,325
Median life			78,239	159,687
R = +0.1	1.0	1	137,087	216,068
		2	292,620	282,724
		3	332,466	483,602
		4	370,480	864,000
		5	644,517	940,648
		6	1,669,350	1,176,871
Mean life			574,420	660,652
Median life			351,473	673,801
R = -1.5	0.4	1	62,446	140,249
		2	83,994	146,567
		3	92,709	161,719
		4	243,896	256,544
Mean life			120,761	176,270
Median life			88,352	154,143

The S/N curve for HTA/982A, with the lowest monotonic strength, is very flat and this material may have better fatigue resistance under low-stress/high-cycle conditions. Similar comparison for these materials in compression cycling at R = +10 can be seen in Figure 4-27. Again, although there are significant differences in their monotonic compressive strengths, they all showed similar fatigue responses.

4.7 THE FATIGUE RESPONSE OF UNDAMAGED E-GLASS/913

Replicate stress/life data were obtained at five stress ratios, R, of +0.5, +0.1, -0.3, -1.0 and +10 and the results are shown in Figure 4-28. The diagram shows the actual data points and the fitted curves are second-order polynomials and linear fitted to full data sets at stress ratio of +0.5, +0.1, -0.3 and -1.0 and +10, respectively. Tension cycling at R ratio of +0.5 and +0.1 was carried out at a constant frequency of 5Hz. All other tests were carried out at a constant frequency of 3Hz because of the large displacement of specimens and limitations of the fatigue machine. As the GRP materials are rate sensitive the monotonic tensile strength of E-Glass/913 was measured at testing rate equal to the rate used in the fatigue tests (5Hz equal to 900kN/min). A value of 0.86GPa was measured for this material which is about 8% higher than the monotonic tensile strength measured at the lower rate (see Table 4.1). In Figure 4-28, therefore, the fitting curves were extrapolated back to the value of 0.86GPa. In comparison to the CFRP materials the slopes of S/N curves at R ratio of +0.5, +0.1, -0.3 and also +10 for E-Glass/913 are steeper and hence the fatigue resistance of the E-Glass/913 material is significantly poorer than that of the CFRP composites. At R= -1.0 the compression and tension components of stress are equal, and since the compressive strength of modern composite systems is typically 60-75% of their tensile strength (see Table 4-1 and reference [79]), it is expected that fatigue failure of the composites would be due to the compression component of stress. The fatigue response of CFRP laminates at R=-1.0 support this expectation, but for E-Glass/913 different behaviour can be seen in Figure 4-28, namely a steeper S/N curve is expected. This may be due to the low tensile strength of E-Glass/913 (0.86GPa in comparison to the over 1.2GPa for CFRP laminates).

4.8 POST-IMPACT FATIGUE RESPONSE

Since barely-visible impact damage has become the hidden menace, and by considering the results of previous section, it was decided to study the effect of damage on fatigue response by using 1J and 2J impacts on HTA/982A and only 2J impacts on HTA/913 and E-Glass/913 laminates. The results of these studies are as follows.

4.8.1 Fatigue response of HTA/982A after 1J Impact

Replicate stress/life data were obtained for HTA/982A after a 1J impact at four stress ratios, R, of +0.1, -0.3, -1.5 and +10 and the results are shown in Figure 4-29. In this figure the individual $\sigma/\log N_f$ data points are plotted together with the curves fitted to the data for the virgin material from Figure 4-24. It appears that a 1J impact has had no effect on the tensile fatigue behaviour at R = +0.1, presumably because the tensile strength is itself unaffected by this level of damage. At R = –1.5 and +10, on the other hand, the $\sigma/\log N_f$ curves are markedly affected. It can be seen that the slopes have been considerably reduced, roughly in the same proportion as the compressive strength itself has fallen, and the relatively straight lines through the failure points are now very flat, almost horizontal. It can be seen that a slight reduction in the magnitude of applied peak compressive stress, for example 5%, can lead to a hundred-fold difference in fatigue life. On the other hand, the considerable scatter of data indicates the large order-of-magnitude of differences in fatigue lives at a constant stress level. This kind of flat S/N curve over a large range of cycles, generated from experimental data of impact-damaged materials, has been mentioned in the literature[64], but it has not been explained. At R = –0.3, however, which is a tension-compression mode in which the compression component of stress is low, the $\sigma/\log N_f$ curve has also shifted downward but to a less marked extent than those for R = –1.5 and R = +10. The flatness of these last two curves suggests that although the intrinsic compressive strength of the laminate has been materially diminished by the small amount of prior damage, the relative sensitivity to subsequent fatigue is less at these two R ratios than in the virgin material, as can clearly be seen in Figure 4-30 where the peak stresses are normalised with respect to the compressive strength and residual compressive strength of virgin and impact-damaged materials, respectively. By contrast, during cycling in the mainly tensile –0.3 régime, the $\sigma/\log N_f$ curve is slightly steeper than that for the undamaged material, suggesting increased sensitivity to fatigue.

One possible explanation for the marked reductions in the slopes of the $\sigma/\log N_f$ curves or flat S/N curves over a large range of cycles, for high-compression R ratios may be found in the results of a series of experiments to determine the residual

strength after cycling of the damaged laminate. It is a common feature of the fatigue behaviour of fibre composites that the residual strength of the material falls as a consequence of cycling. Examples may be found in references 12 and 25, among many others. It is this behaviour which forms the basis of the familiar 'wear-out' model of fatigue failure. By contrast, the effect of the impact damage in the HTA/982A in impairing the load-bearing ability of the laminate actually appears to be reduced when the damage laminate is cycled in repeated compression, as illustrated in Figure 4-31. The 5% or so increase in the compressive strength after 10^6 cycles is well-defined and could reasonably explain why the $\sigma/\log N_f$ curve for R = +10 is very flat and why many of the individual fatigue experiments become run-outs. Figure 4-32 shows C-scan images of a sample of 1J impact-damaged HTA/982A before fatigue cycling and after 10^6 cycles in compression, under exactly the same conditions as Figure 4-31. This suggests not only that the type of damage caused by the impact does not grow during subsequent fatigue cycling, but also that the effect of that damage may be reduced to some extent by the compressive fatigue loading. This kind of increase in post-impact residual properties in non-woven and mixed woven laminates was also mentioned by Cantwell *et al*[60] who reported that cycling led to improvements in static strength of up to 30% in non-woven and up to 40% in mixed woven composites. The reason for this improvement is not clear, although it could be associated with a notch blunting mechanism similar to that noted by Bishop and Morton[80] during tests on notched laminates. It may be due to the fact that after an impact event the severity of delamination in the damaged zone in each interface is not equal. In some part of damaged zone, very wide delaminations can be observed as shown in the photomicrograph in Figure 4-33. This kind of severe delamination causes a catastrophic failure in monotonic compression test, but cycling makes it uniform and results in increases in post-impact fatigue compressive strengths.

4.8.2 Fatigue response of HTA/982A after 2J Impact

Replicate stress/life data were obtained for 2J impact-damaged HTA/982A at three stress ratios of +0.1, -0.3 and +10 and the results are shown in Figure 4-34. In this figure the individual $\sigma/\log N_f$ data points are plotted together with the curves fitted to the data for the virgin material from Figure 4-24. It can be seen that the overall

appearance of the curves is similar to those of 1J impact-damaged HTA/982A mentioned above, but the deviation of the stress/life points for the damaged material from the undamaged polynomial curves is greater at 2J impact energy than at 1J, as would be expected. This deviation at an R ratio of -0.3 is significantly greater, suggesting increased sensitivity to fatigue. It can be seen that a 2J impact has had no effect on the tensile fatigue behaviour at R = +0.1.

A direct comparison of the effects of different levels of impact energy may be seen from Figure 4-35 which is a plot of the stress/median-life data at R = –0.3 for the virgin laminate and the laminate damaged by impacts of 1J and 2J. The curves in this figure are again polynomials (this form of curve-fit is chosen simply for convenience: it is not intended to suggest that there is any mechanistic argument for such a fit). For R = –0.3, the cycle is dominated by the tensile component of stress, and as we have seen, the tensile properties are unaffected by the impact damage. Nevertheless, even the relatively small compression component at this R ratio is sufficiently great to interact with the impact damage and cause a marked and progressive change in the position of the $\sigma/\log N_f$ curve. It can be seen from Figure 4-35 that at low stress levels (*eg.* 0.7GPa, 57% of the monotonic tensile strength) undamaged and damaged laminates had similar lives. At low stress levels and an R ratio of –0.3, the compressive component of stress is not significant. And although for a peak stress of 0.7GPa, for instance, the minimum stress, –0.21GPa, is about 66% of the compressive strength of a sample with 2J impact damage this still has no effect on the fatigue life of the material. It can be concluded, therefore, that as long as the nature of the impact damage is matrix cracking and delamination, it has no effect on pure tension and tension-dominated tension-compression cycling.

It is worthwhile indicating that it is difficult to say whether impact-induced matrix cracking and delamination has no effect on pure tension cycling for all stress levels. Table 4-3 shows the original fatigue life data for $[(\pm 45,0_2)_2]_S$ HTA/982A laminate at a stress ratio of R = +0.1 for two stress levels, in the virgin condition and after damage by 1J and 2J low-velocity impacts. To make a reasonable comparison (omitting the size effect) the data for virgin condition are from 40mm wide samples. In this table σ_{max} and σ_t are peak stress and monotonic tensile strength, respectively. It can be seen

that at σ_{max} = 1.1GPa which is equal to 91% of σ_t the fatigue lives are shifted to the lower lives. On the other hand, impact-induced damage accelerates the process of accumulation of fatigue damage. This may be due to the high applied strain tolerated by the material at high peak stress. From the design point of view since design strains are not usually set so high, this reduction of fatigue lives for damaged materials is not of great importance.

4.8.3 Fatigue response of HTA/913 after 2J Impact

Replicate stress/life data were obtained at four stress ratios of +0.1, -0.3, -1.0 and +10 for HTA/913 laminate after a 2J impact and the results are shown in Figure 4-36. In this figure the individual $\sigma/\log N_f$ data points are plotted again together with the curves fitted to the data for the virgin material taken from reference 7. The overall appearance of the curves is similar to those of impact-damaged HTA/982A mentioned above. Again it appears that a 2J impact has had no effect on the tensile fatigue behaviour at R = +0.1.

To make clear whether or not the prior impact-induced delamination affects tension-tension fatigue cycling, some tests were carried out on 3J-impact-damaged HTA/913 and HTA/982A at R = +0.1 at a peak stress of 1.0GPa. These results can be seen in Table 4-4. From Figure 4-12 can be seen that a 3J impact event produces huge delaminations in these materials, 473mm^2 and 592mm^2 in HTA/913 and HTA/982A, respectively. Sectioning also showed that the mode of impact damage after 3J is mainly delamination and matrix cracking. Despite this extensive damage, there were no significant changes in their tension cycling response after 3J impact at a peak stress of 1.0GPa. Because of the large scatter of fatigue test results it is difficult to say whether or not the prior damage affected the fatigue life. But it can be said that as long as the nature of the impact damage is matrix cracking and delamination, it has no effect on pure-tension cycling of FRP at rather low applied peak stresses.

Table 4-3. Fatigue life data for $[(\pm 45,0_2)_2]_S$ HTA/982A laminate at a stress ratio of R = +0.1 for two stress levels, in the virgin condition and after damage by 1J and 2J low-velocity impacts.

Sample Number	σ_{max} = 1.1GPa, 91% of σ_t			σ_{max} = 1.0GPa, 83% of σ_t		
	Virgin*	1J impact	2J impact	Virgin*	1J impact	2J impact
1	61,177	470	204	216,068	384,320	196,900
2	107,101	3,307	1,920	253,454	543,000	584,240
3	159,687	10,446	1,950	282,724	843,220	596,640
4	227,577	44,259	3,760	483,602		642,380
5	236,081	95,321	185,830	864,000	-	853,940
6	-	212,986	351,200	940,648	-	-
Mean life	158,325	61,131	71,807	506,749	590,320	574,820
Median life	159,687	27,352	1,950	383,163	543,00	596,640

* For 40mm sample wide.

Table 4-4. Fatigue life data for HTA/982A and HTA/913 laminates at R = +0.1 and peak stress of 1.0GPa, in the virgin condition and after damage by 3J low-velocity impacts.

Sample Number	HTA/982A		HTA/913	
	Virgin [a]	3J impact	Virgin [b]	3J impact
1	216,068	80,930	449,997	471,070
2	253,454	85,190	456,028	783,070
3	282,724	156,380	469,462	1,847,320
4	483,602	966,760	604,625	3,181,490+ [c]
5	864,000	-	700,277	-
6	940,648	-	-	-
Mean life	506,749	322,315	536,078	1,033,820
Median life	383,163	120,785	469,462	783,070

a) For 40mm sample wide.

b) For 20mm sample wide

c) Test interrupted due to the high number of cycle.

4.8.4 Fatigue response of E-Glass/913 after 2J Impact

Replicate stress/life data were obtained at five stress ratios, R, of +0.5, +0.1, -0.3, -1.0 and +10 for 2J impact-damaged E-Glass/913 and the results are shown in Figure 4-37. In this figure the individual $\sigma/\log N_f$ data points are plotted together with the curves fitted to the data for the virgin material from Figure 4-28. It can be seen that in

tension-tension and also at an R ratio of -0.3 there is no clear difference between the response of the virgin material and after 2J impact damaged, and for the most part, the curves lie within the scatter bands of data for the material with prior damage from a 2J impact. But individual stress/life data show some deviations as can be seen in Table 4-5. This table shows that in most cases the mean and median lives for the material with prior impact of 2J shifted by about half a decade to lower lives. This may be due to the fact that this material tolerates a large displacement in each cycle because of its high strain to failure. There might be an interaction, therefore, between prior matrix cracking and delamination from a 2J low-velocity impact and fatigue-induced damage and this slightly reduces the fatigue life of materials with prior damage. It can be seen from Figure 4-37 that at R = -1.0 damaged material showed a weaker response in the high-stress/low-cycle part of the stress/life curve, but in the low-stress/high-cycle region, the virgin and damaged materials behaved alike. This confirms again that in tension-compression cycling, as long as the compression component of stress is low, it has no effect on the fatigue response of damaged material.

Another important point can be seen in repeated-compression cycling (R= +10). Again an extremely flat curve can be seen for the damaged laminate, but the deviation of stress/life points for the damaged material and from the undamaged polynomial curve decreases significantly at high numbers of cycles to failure and it seems that they will merge together at about 10^7 cycles. Similar behaviour can be seen at R = -1.5 for virgin and impact damaged HTA/982A (see Figure 4-29). This may represent a significant finding that if the working peak stresses or strains were low (for example for E-Glass/913, peak compression stress of -0.2 about 0.77% strain) the damaged and virgin materials will have similar fatigue lives. Therefore, although the low-velocity impact damage in laminated composite structures has been recognised as a debilitating threat for many years as a result of high loss in compressive load-bearing ability resulting from the impact, it will not threaten the fatigue response of these structures if the design strains are kept low.

Table 4-5. Mean and median life for E-Glass/913 in the virgin condition and after impact of 2J.

R ratio	Peak stress GPa	Number of data points*	Mean life		Median life	
			Virgin	2J impact	Virgin	2J impact
+0.5	0.6	5(4)	3,022	1,158	3,127	1,150
	0.5	5(4)	21,971	16,515	22,429	15,395
	0.4	5(4)	2,204,831	515,560	1,451,290	486,700
+0.1	0.5	3(3)	2,633	3,237	3,080	3,080
	0.4	3(3)	92,676	93,063	82,910	87,210
	0.35	5(5)	808,950	549,526	970,940	565,080
-0.3	0.5	5(3)	7,340	3,010	7,330	3,230
	0.4	5(3)	33,788	29,363	25,650	25,620
	0.3	5(4)	428,078	366,103	442,470	359,085

* Number of data points for 2J impact-damaged material are shown in brackets.

4.9 DAMAGE DEVELOPMENT IN CYCLING

To study the effect of fatigue cycling on damage development some interrupted fatigue tests were carried out at two R-ratios, +10 and -0.3, on 1J impact-damaged HTA/982A, and in each R-ratio two stress levels were studied. Information on the changes in the size of the damaged region during fatigue cycling was obtained by ultrasonic C-scanning.

4.9.1 Compression cycling, R = +10

Some interrupted fatigue tests were carried out at an R ratio of +10 at peak stresses of -0.38GPa (86% of residual compressive strength) and -0.35GPa (79% of residual compressive strength) on 1J impact-damaged HTA/982A. The specimens were C-scanned to see whether the damage zone had grown during fatigue. At the peak stress level of -0.38GPa the median life is 78000 cycles, and Figure 4-38 shows that after 10,000, 25,000 and 60,000 cycles there have been no significant changes in the size of the delamination zone. Figure 4-39 shows C-scan images of another sample for the same conditions. The number of cycles to failure, N_f, for this sample is 36,390. It can be seen that after 25,000 cycles (69% of its life) no significant changes in the size of damage zone can be found although there appears to be some reduction in the severity of damage zone. This may be a reduction or blunting of the sharpness of the damage area boundaries or a reduction of the severity of delamination between two

interfaces, as mentioned before. This observation is in accord with the comments made earlier on the stress/life and residual strength results. The results for peak stress of -0.35GPa are shown in Figure 4-40. It is difficult to say whether or not the damage area has grown during fatigue since the difference in extent of the initial damage area and the damage area at the time of failure is not sufficiently great to permit it to be detected by the ultrasonic C-scan. Again some minor changes in the area of the zone of sever damage can be detected.

4.9.2 Tension-compression cycling, R = -0.3

Some interrupted fatigue tests were carried out at R = -0.3 at peak stresses of 0.9GPa and 0.7GPa on 1J impact-damaged HTA/982A. These results are shown in Figure 4-41 and Figure 4-42. At the peak stress level of 0.9GPa the median life is 30,000 cycles, and Figure 4-41 shows the damage which had occurred after 10,000, 20,000 and 35,000 cycles. This sample failed at 54,280 cycles. It can be seen that fatigue-induced damage began from the free edges of specimen owing to the high interlaminar shear stresses and grew towards the middle of the specimen. It appears that the impact damage began to grow in the direction of 45° plies and interacted with the fatigue-induced delamination. This interaction reduces fatigue life at this high stress level, as mentioned earlier with reference to the stress/life results at R = -0.3.

The ultrasonic C-scan images for a low stress level of 0.73GPa, 61% of σ_t, are shown in Figure 4-42. At this stress level the median life is 330,000 cycles, and images were taken after 100,000, 200,000 and 300,000 cycles. It can be seen that fatigue-induced damage began from the free edges of the specimen and grew towards the middle of the specimen, as for to the previous results. Since this sample failed at 623,680 cycles, significant damage can be seen after 300,000 cycles, namely 48% of its life. Although it seems that damage began to grow from the damage area boundaries as well, this has had no effect on the number of cycles to failure of the specimen at this stress level as for the stress/life results mentioned earlier for damaged materials at R = -0.3. The amount of damage that can be seen after each intervals is not directly proportional to the absolute number of cycles, as the numbers of cycles to failure vary over a wide range from one sample to another one. The detected damage

or the accumulated damage is more related to the ratio of numbers of cycles over the fatigue life of the sample. This can be seen from Figure 4-43 which shows the ultrasonic C-scan images of two samples after specific number of cycles. Sample II, which had a higher life than sample I, showed less damage after each interval.

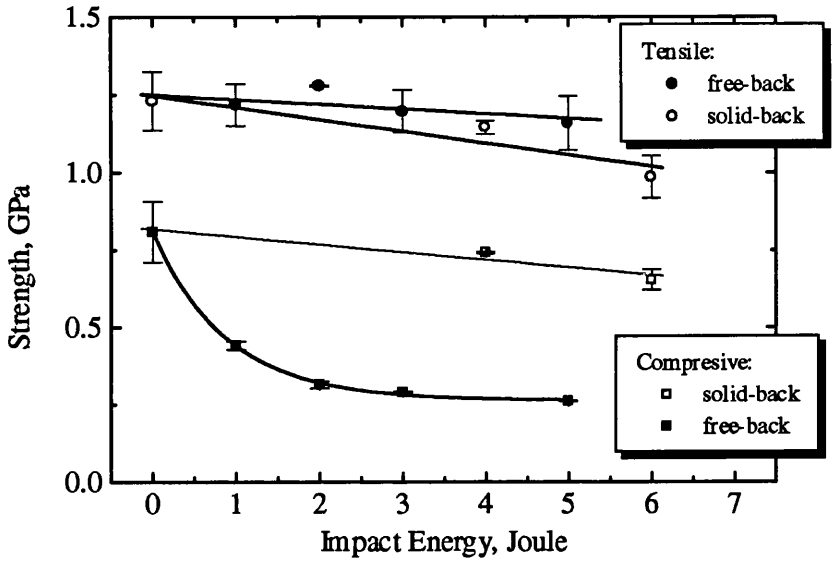

Figure 4-1. Effect of low-velocity impact damage on the residual tensile and compressive strengths of $[(\pm 45, 0_2)_2]_S$ HTA/982A CFRP laminate.

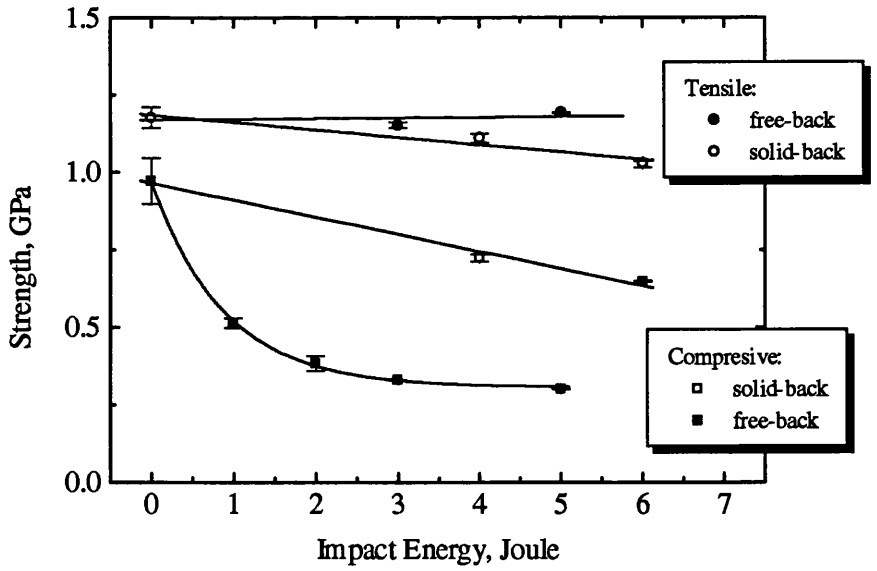

Figure 4-2. Effect of low-velocity impact damage on the residual tensile and compressive strengths of $[(\pm 45, 0_2)_2]_S$ HTA/913 CFRP laminate.

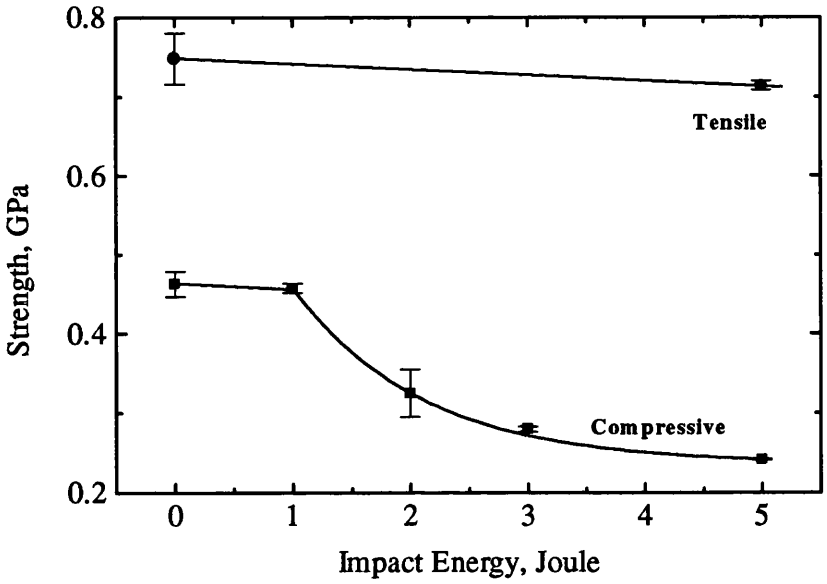

Figure 4-3. Effect of low-velocity impact damage on the residual tensile and compressive strengths of $[(\pm 45, 0_2)_2]_S$ E-Glass/913 GRP laminate.

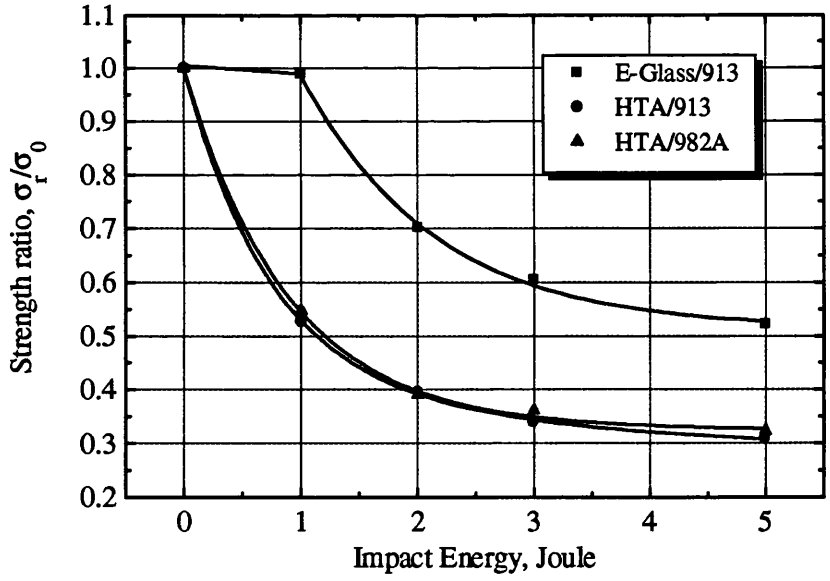

Figure 4-4. Effect of low-velocity impact damage on the residual compressive strengths of $[(\pm 45, 0_2)_2]_S$ HTA/982A, HTA/913 and E-Glass/913 laminates, the residual compressive strengths are normalised with respect to the undamaged compressive strengths of each material.

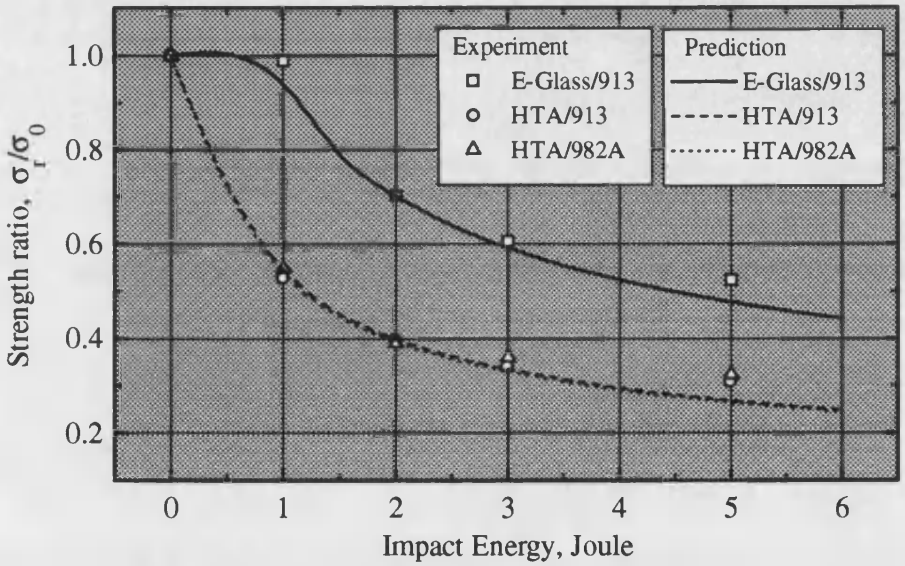

Figure 4-5. Predicted residual compressive strength after impact for $[(\pm 45, 0_2)_2]_S$ HTA/982A, HTA/913 and E-Glass/913 laminates. Symbols are experimental results.

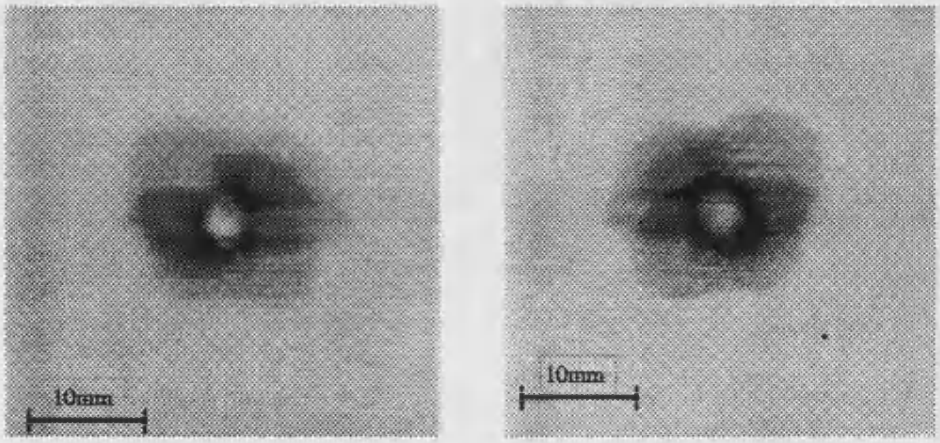

a) Front face *b) Back face*

Figure 4-6. Optical photos of 2J impact damage in E-Glass/913.

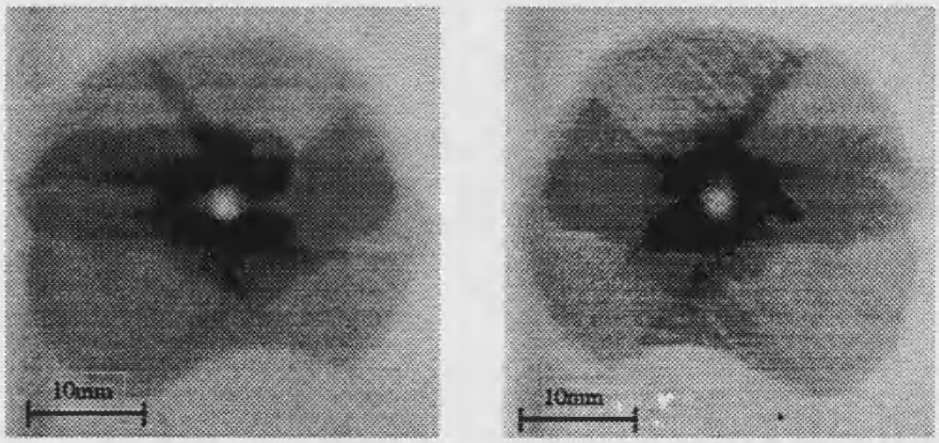

a) Front face *b) Back face*

Figure 4-7. Optical photos of 5J impact damage in E-Glass/913.

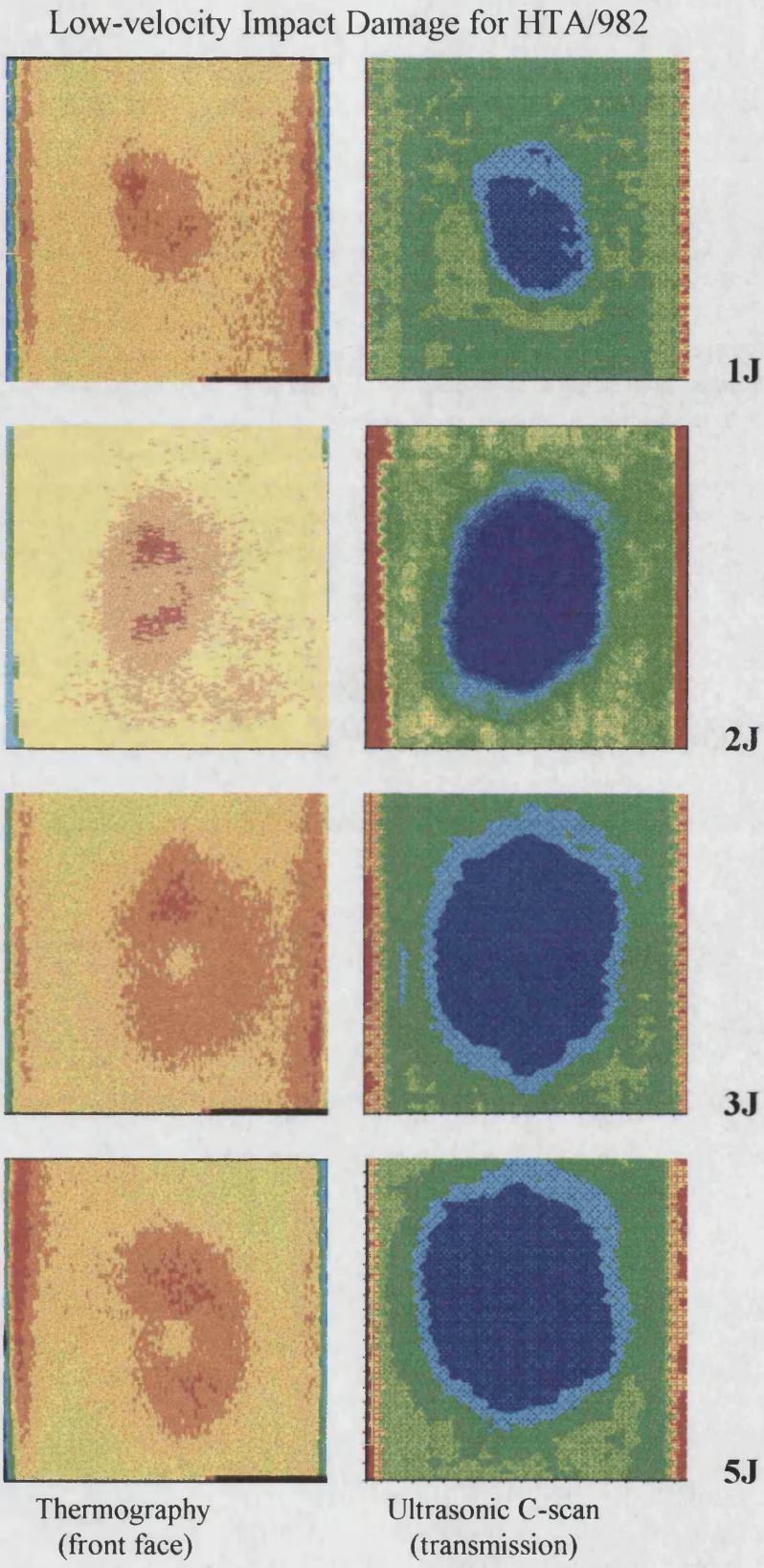

Figure 4-8. Thermography and ultrasonic C-scan images of low-velocity impact-induced damages of 1J, 2J, 3J and 5J energy for the $[(\pm 45, 0_2)_2]_S$ HTA/982A laminate, scan area was 40mm by 40mm.

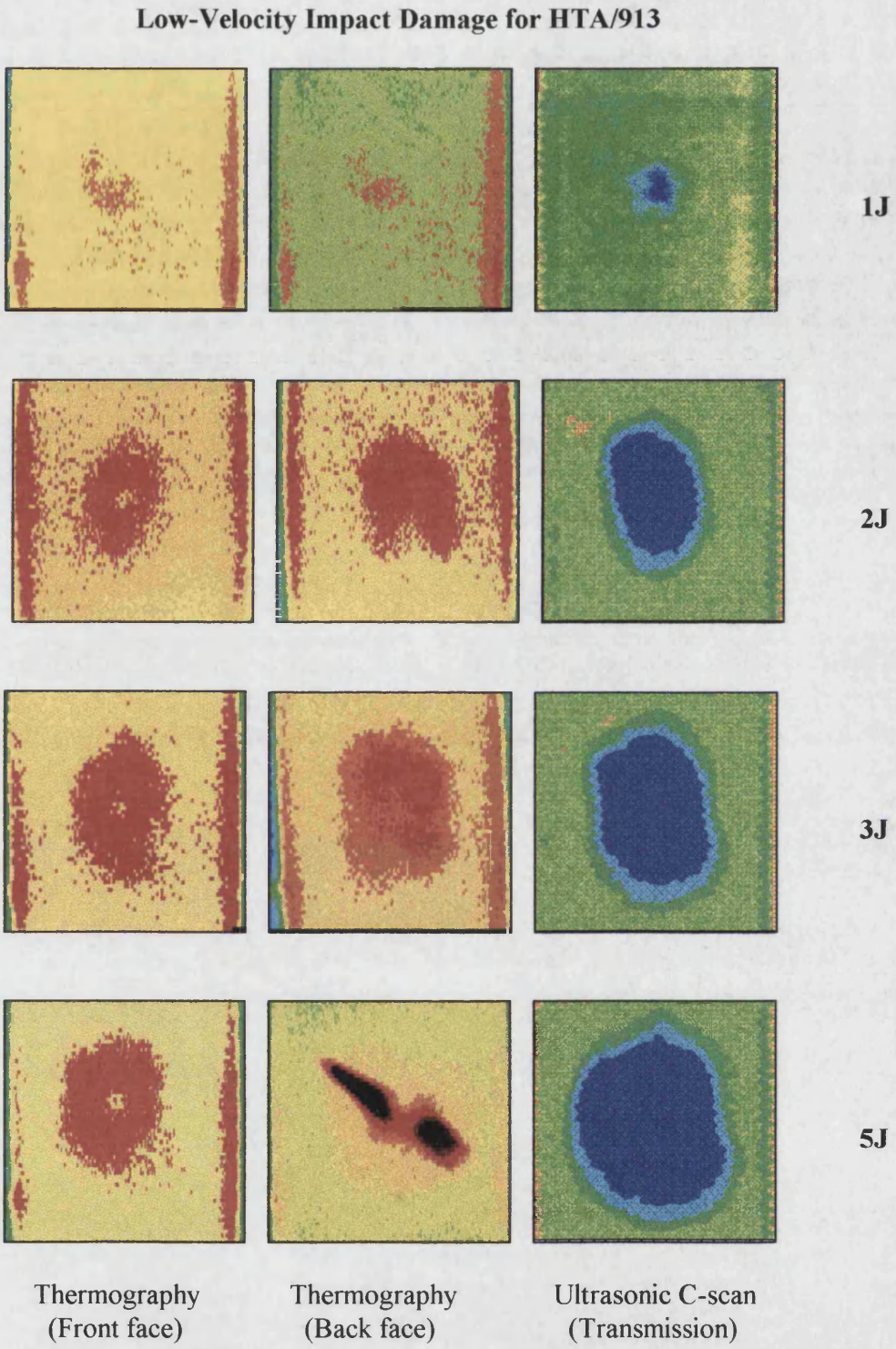

Figure 4-9. Thermography and ultrasonic C-scan images of low-velocity impact-induced damages of 1J, 2J, 3J and 5J energy for the $[(\pm 45, 0_2)_2]_S$ HTA/913 laminate, scan area was 40mm by 40mm.

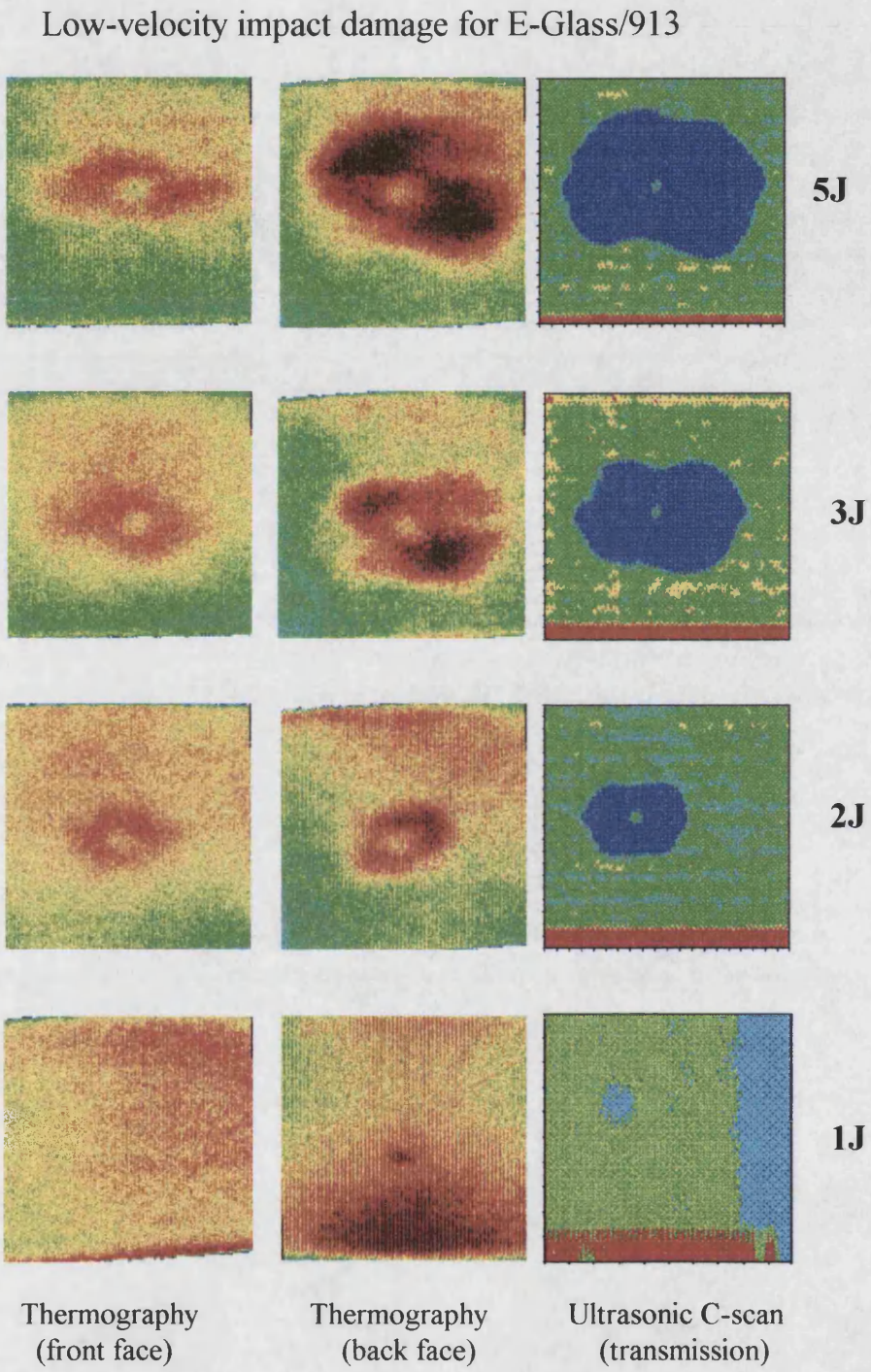

Figure 4-10. Thermography and ultrasonic C-scan images of low-velocity impact-induced damages of 1J, 2J, 3J and 5J energy for the $[(\pm 45, 0_2)_2]_S$ E-Glass/913 laminate, scan area was 40mm by 40mm.

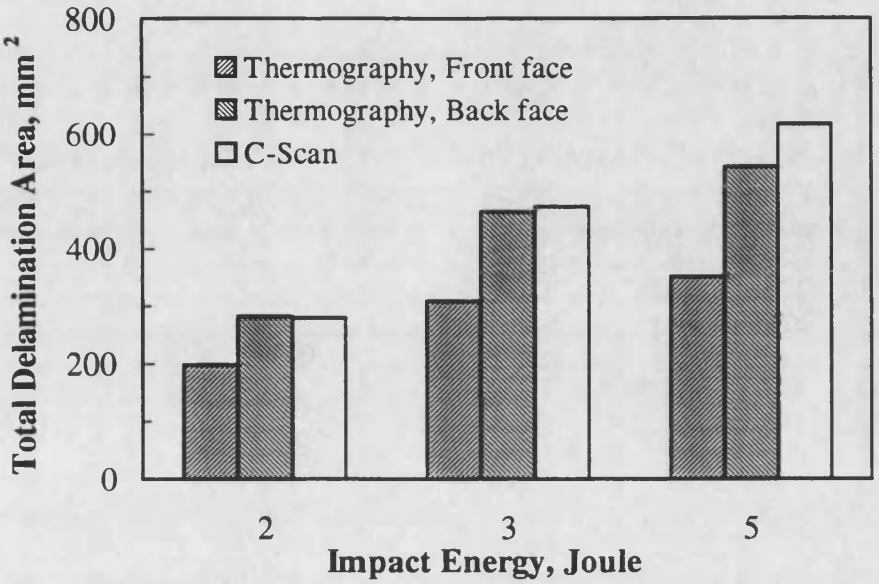

Figure 4-11. Comparison of overall delamination area calculated from thermography and C-scan images for HTA/913.

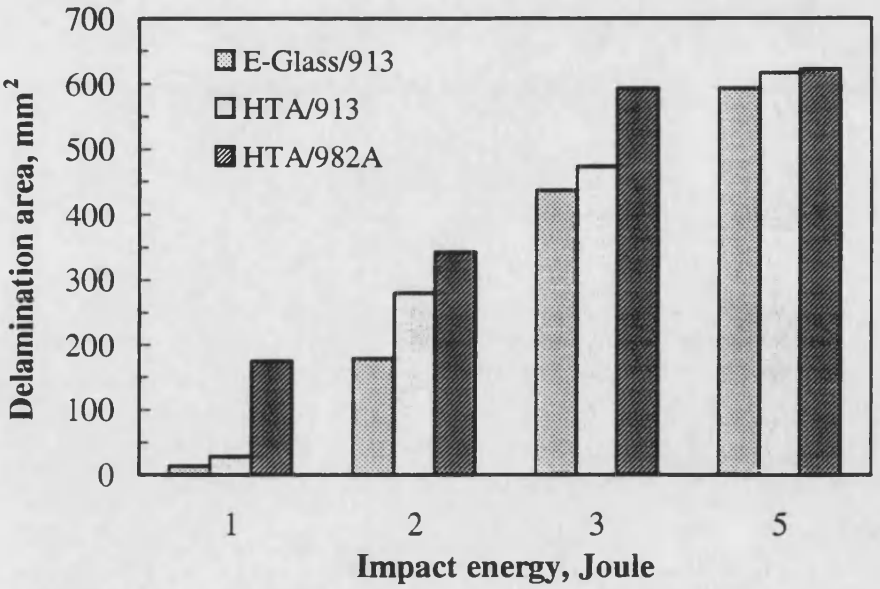

Figure 4-12. Overall impact-induced delamination area produced by 1, 2, 3 and 5 Joule impacts for the $[(\pm 45, 0_2)_2]_S$ E-Glass/913, HTA/913 and HTA/982A laminates.

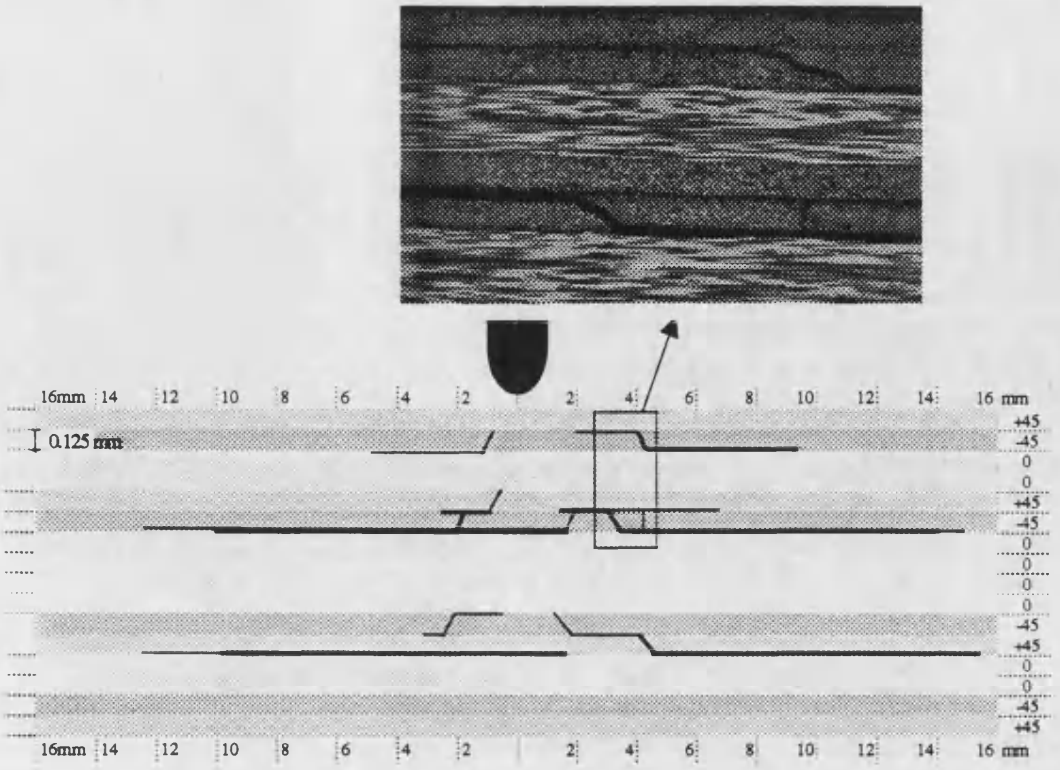

Figure 4-13. Damage map of 2J impact-damaged HTA/982A in longitudinal direction.

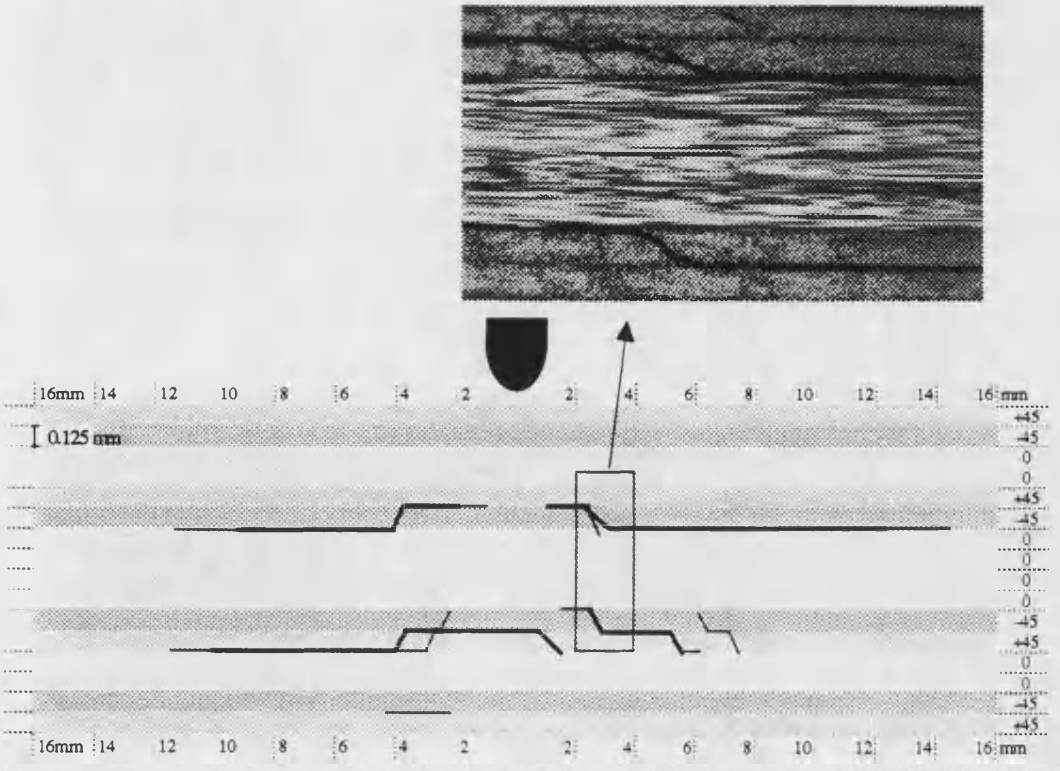

Figure 4-14. Damage map of 2J impact-damaged HTA/913 in longitudinal direction.

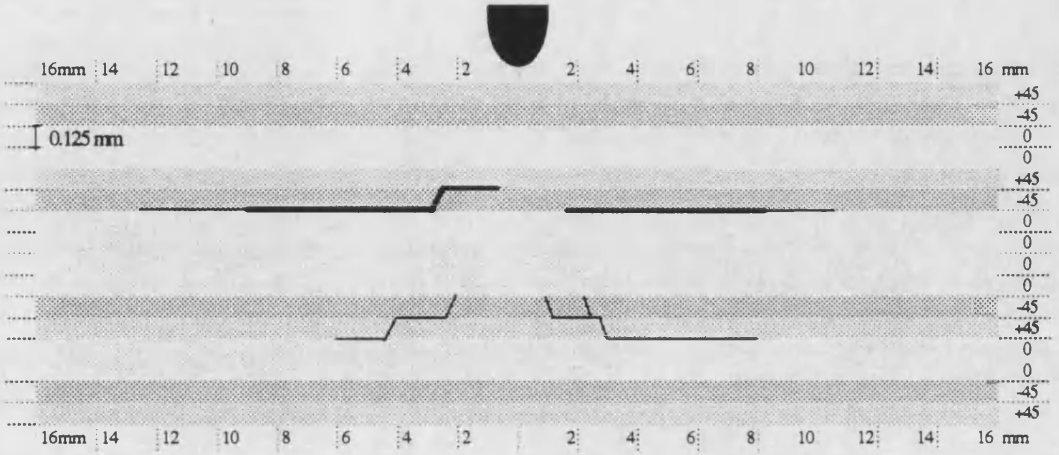

Figure 4-15. Damage map of 2J impact-damaged E-Glass/913 in longitudinal direction.

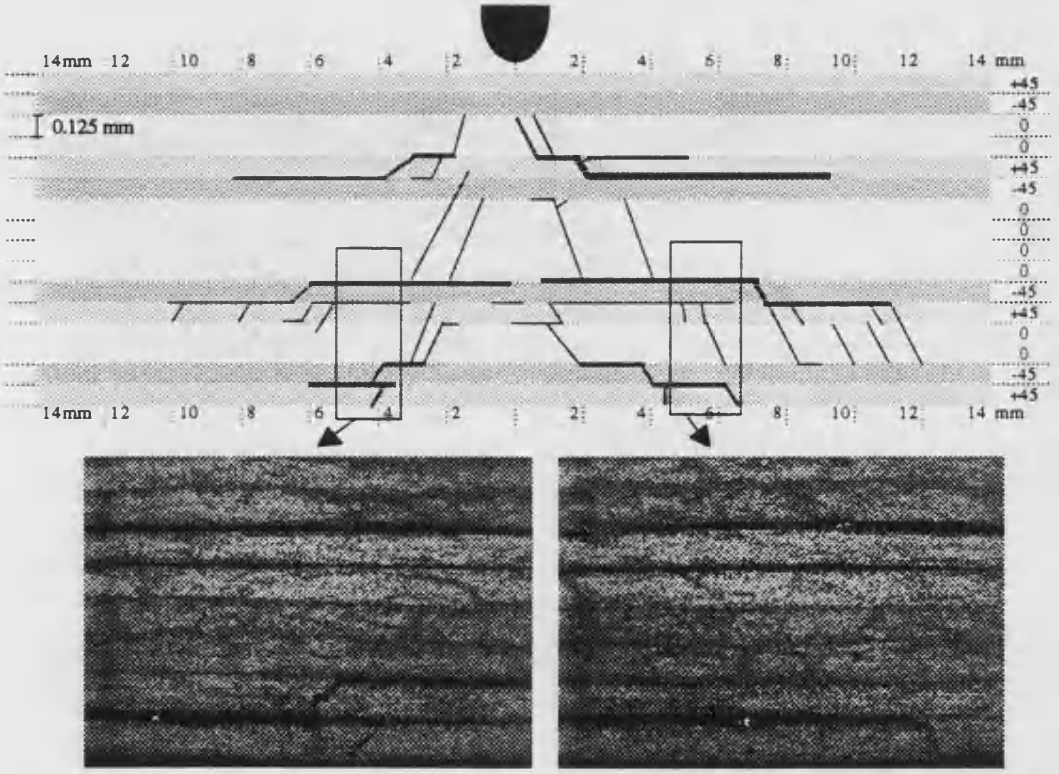

Figure 4-16. Damage map of 2J impact-damaged HTA/982A in transverse direction.

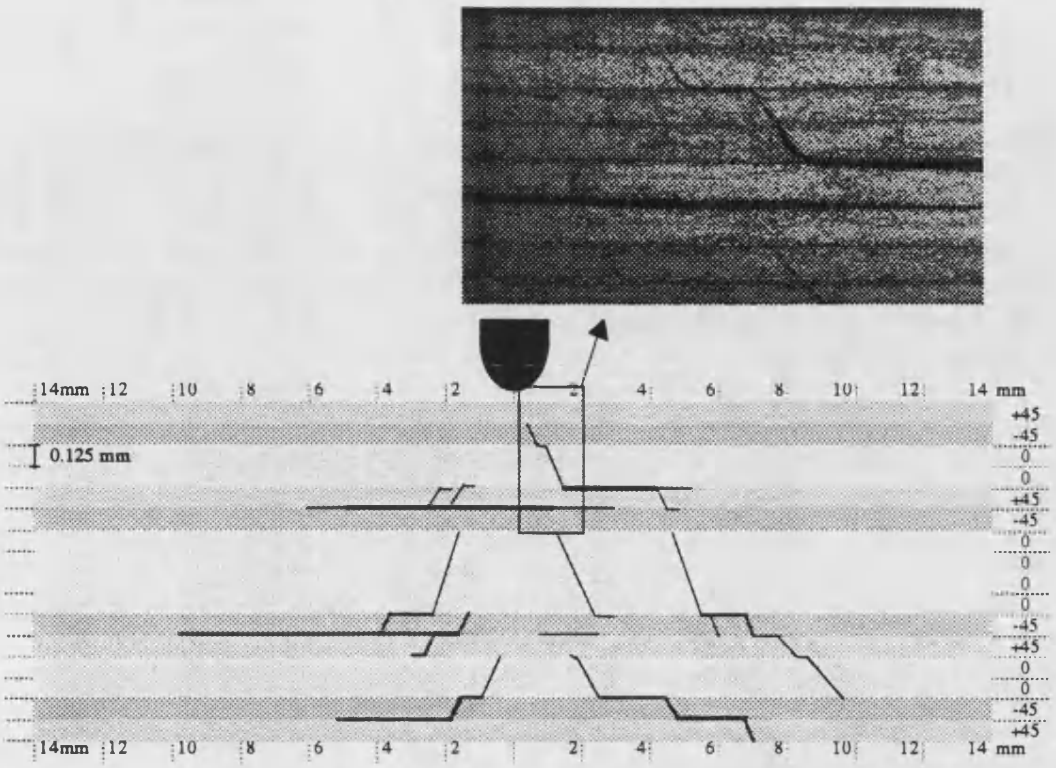

Figure 4-17. Damage map of 2J impact-damaged HTA/913 in transverse direction.

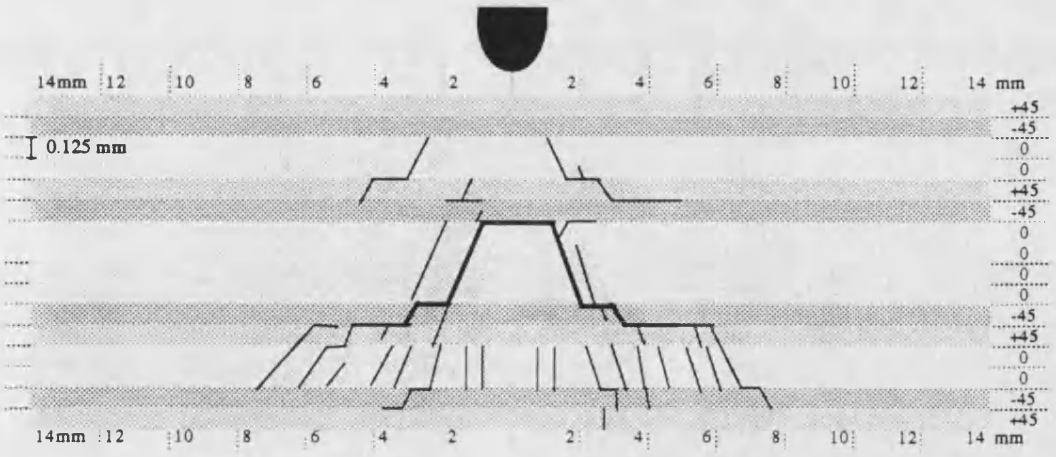

Figure 4-18. Damage map of 2J impact-damaged E-Glass/913 in transverse direction.

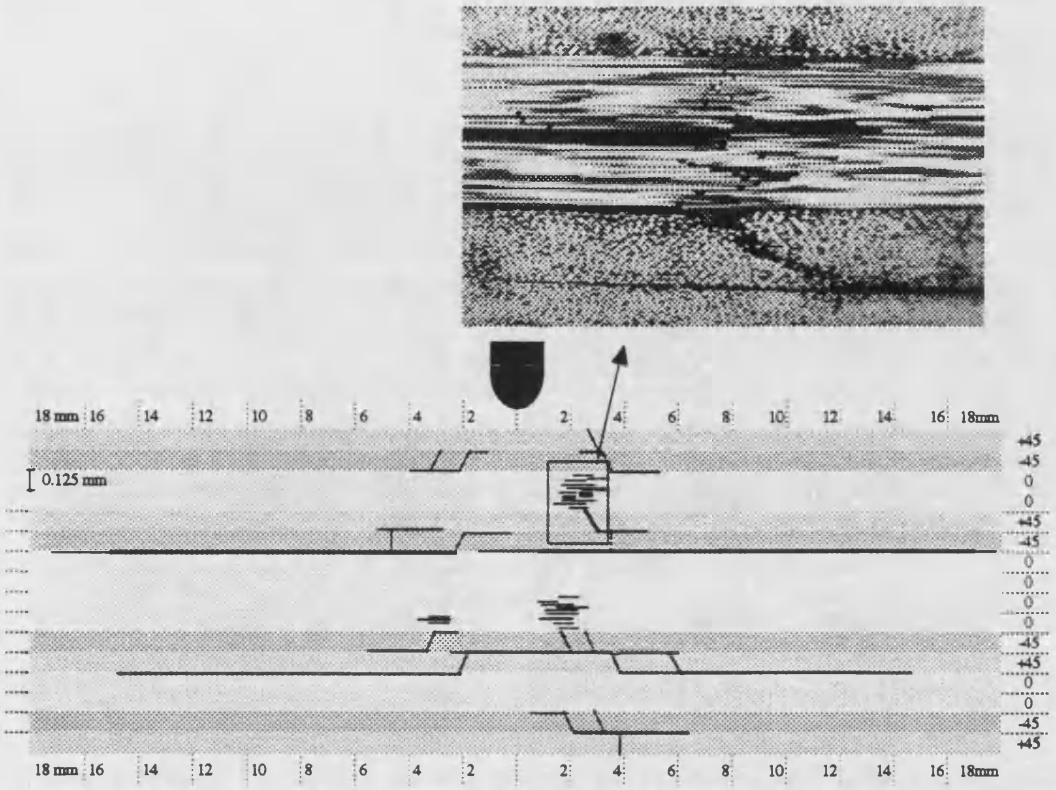

Figure 4-19. Damage map of 5J impact-damaged HTA/982A in longitudinal direction.

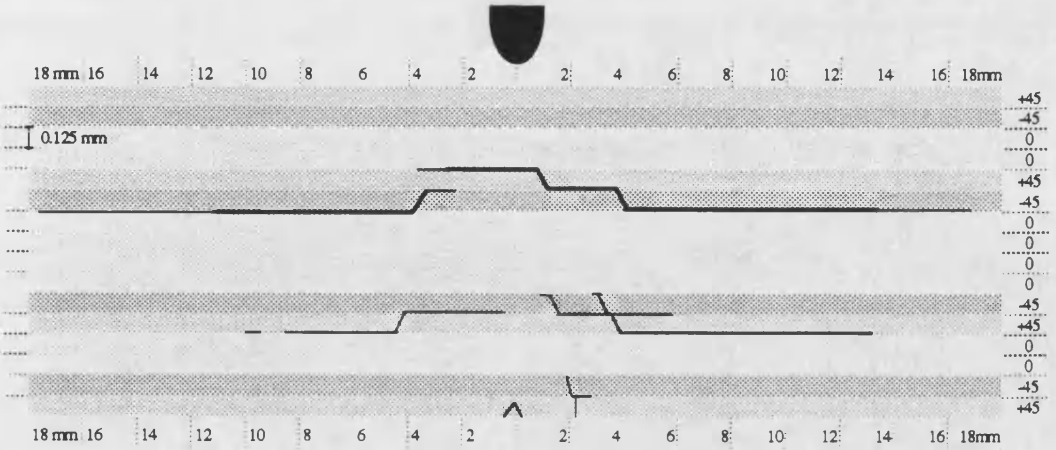

Figure 4-20. Damage map of 5J impact-damaged HTA/913 in longitudinal direction.

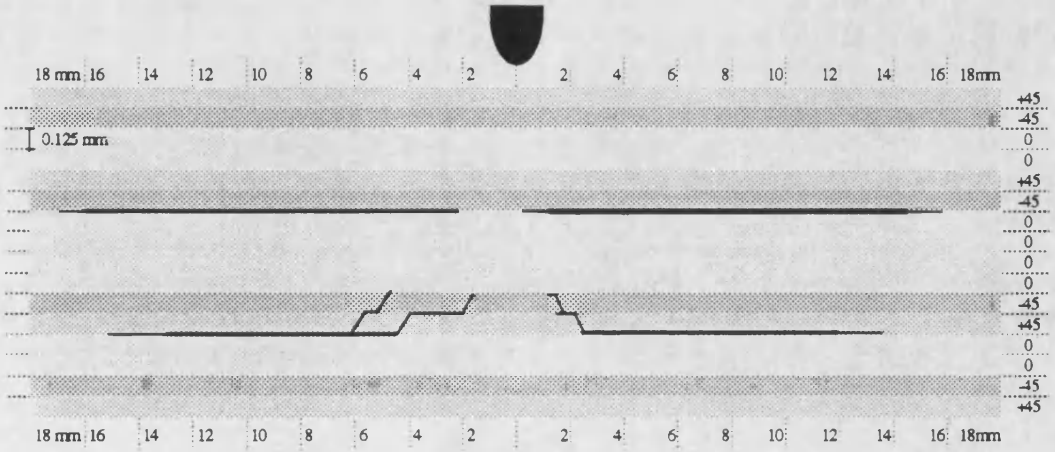

Figure 4-21. Damage map of 5J impact-damaged E-Glass/913 in longitudinal direction.

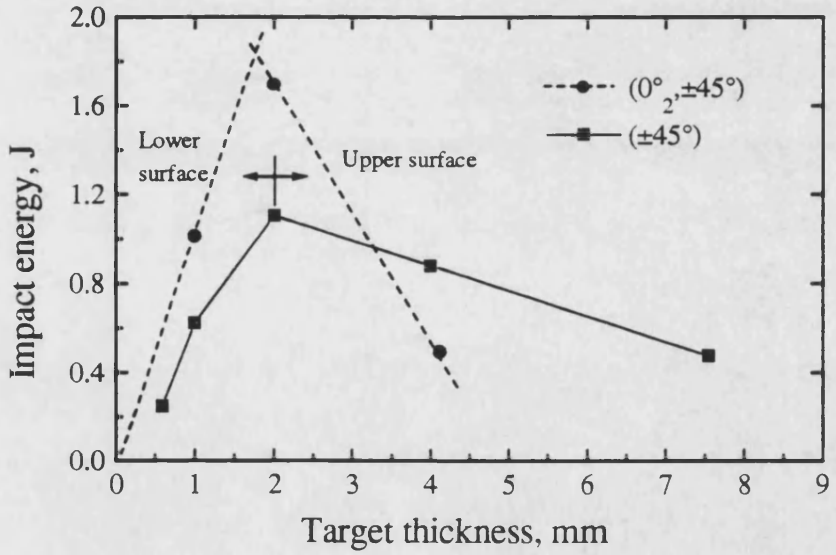

Figure 4-22. Variation of the incident energy to initiate first damage with target thickness in the ($0°_2$,±45°) and (±45°) XAS/914C laminates, (after Cantwell and Morton, 1989).

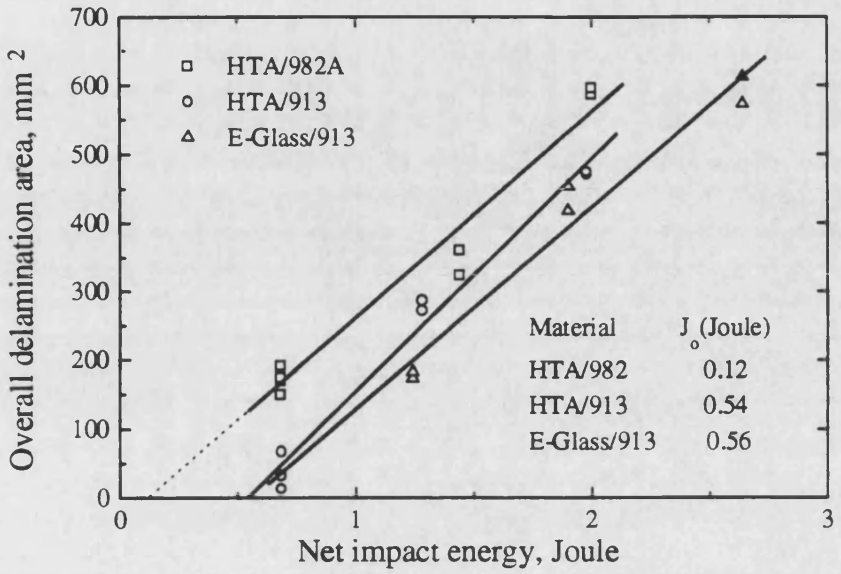

Figure 4-23. Overall impact-induced delamination area against net impact energy for the $[(\pm 45,0_2)_2]_S$ HTA/982A, HTA/913 and E-Glass/913 laminates.

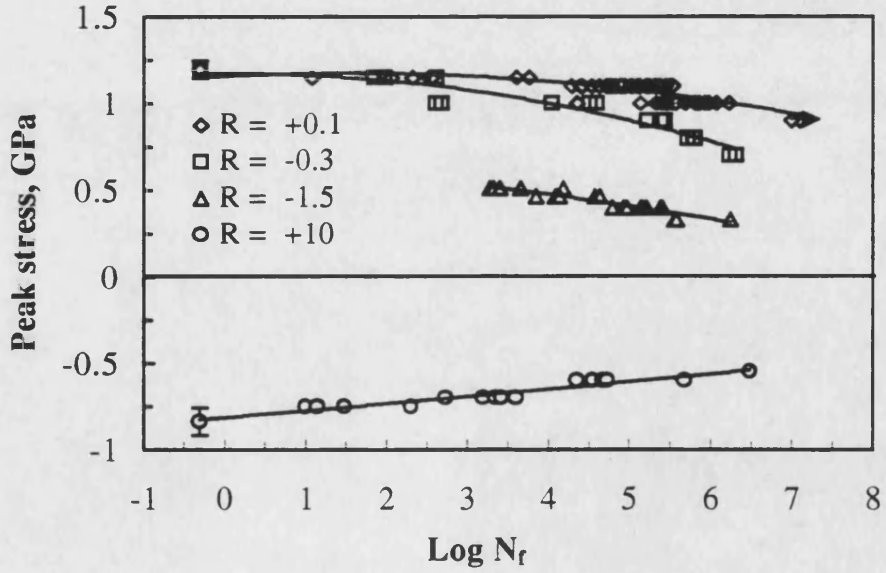

Figure 4-24. $\sigma/\log N_f$ curves for HTA/982A CFRP laminate of $[(\pm 45,0_2)_2]_S$ lay-up in the undamaged condition. The full curves are fitted polynomial curves of order two or three. The filled symbols are for 40mm wide samples, and the open ones are for 20mm wide samples.

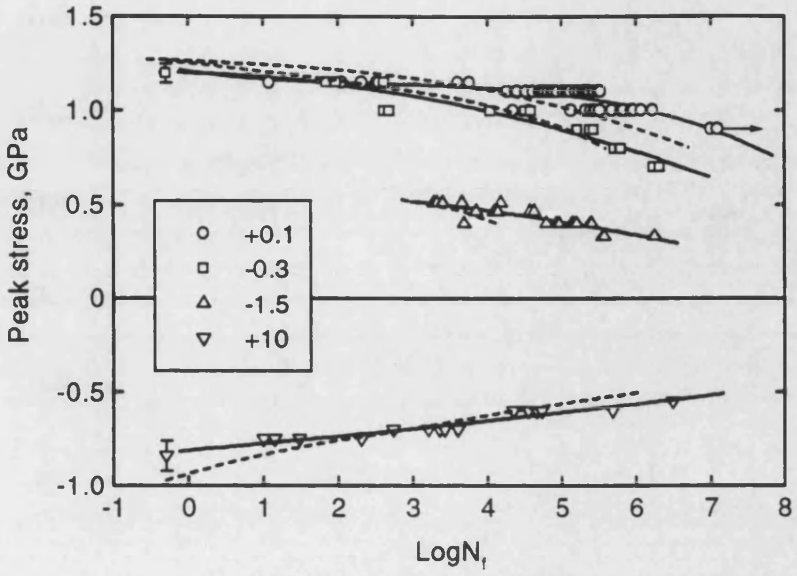

Figure 4-25. σ/logN$_f$ curves for HTA/982A CFRP laminate of [(±45,0$_2$)$_2$]$_S$ lay-up in the undamaged condition. The full curves are fitted polynomial curves of order two or three and the dashed curves represent median-stress/life curves for HTA/913 laminate, taken from reference 8.

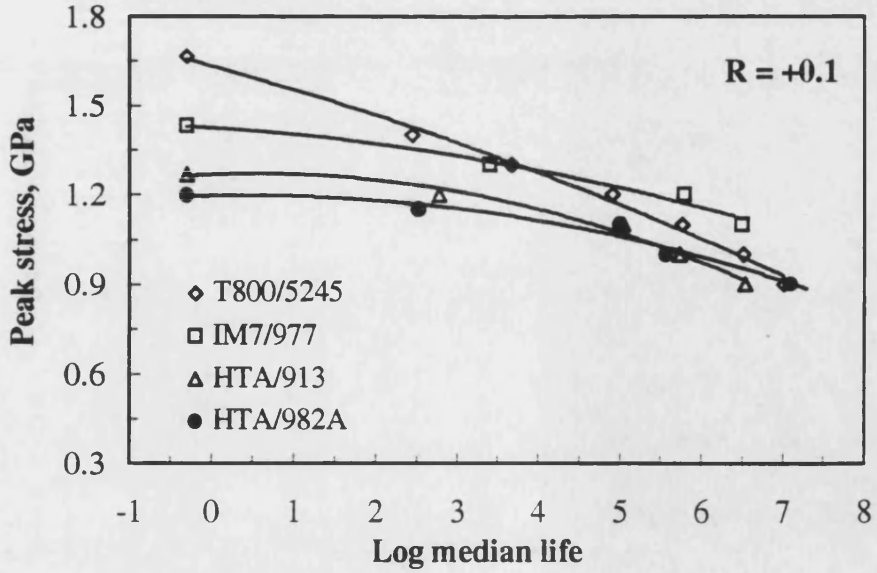

Figure 4-26. Comparison of σ/logN$_f$ curves for four CFRP laminates of [(±45,0$_2$)$_2$]$_S$ lay-up at R ratio of +0.1. The full curves are fitted polynomial curves of order two.

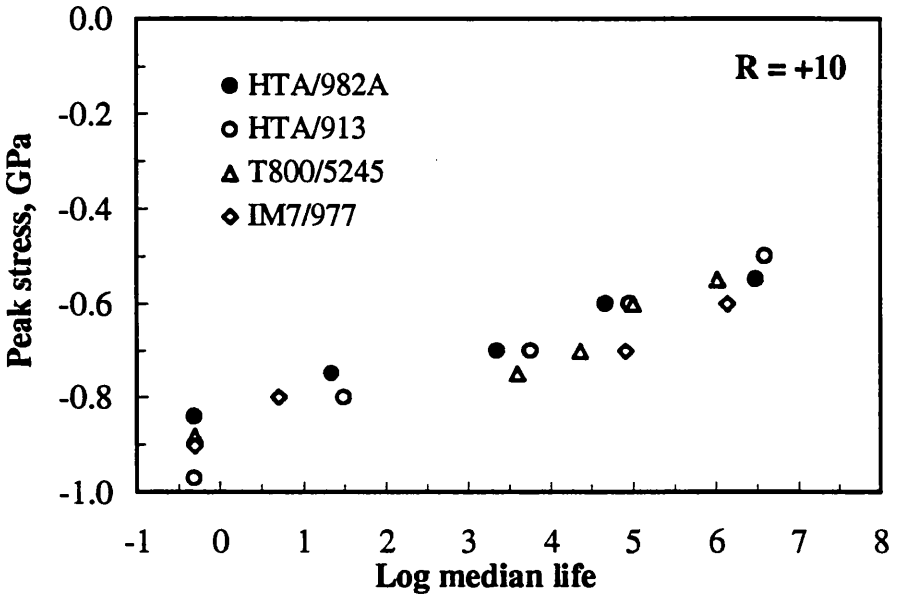

Figure 4-27. Comparison of σ/logN$_f$ curves for four CFRP laminates of [(±45,0$_2$)$_2$]$_S$ lay-up at R = +10.

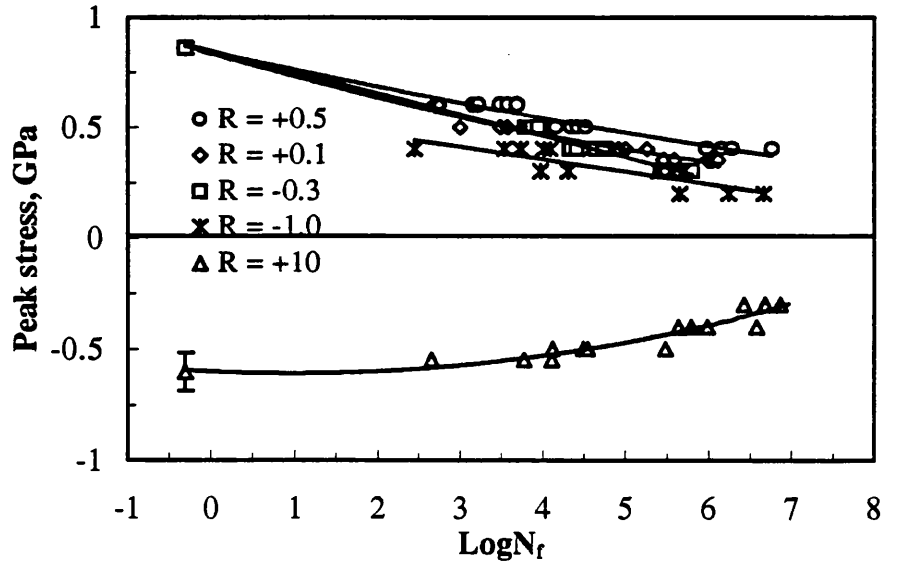

Figure 4-28. σ/logN$_f$ curves for E-Glass/913 GRP laminate of [(±45,0$_2$)$_2$]$_S$ lay-up in the undamaged condition. The full curves are fitted polynomial curves of order two.

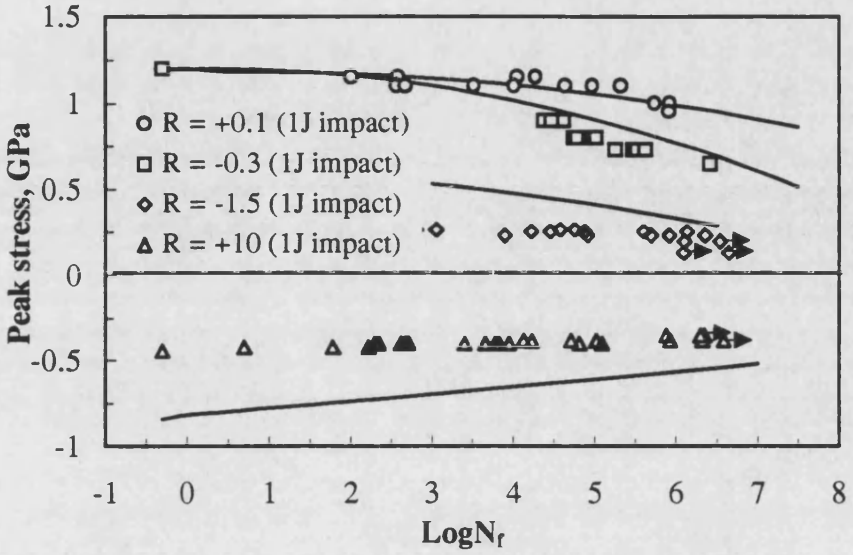

Figure 4-29. σ/logN$_f$ curves for HTA/982A CFRP laminate of [(±45,0$_2$)$_2$]$_S$ lay-up after damage by a low-velocity impact of 1J. The full lines are polynomial curves fitted to the data for the virgin laminate.

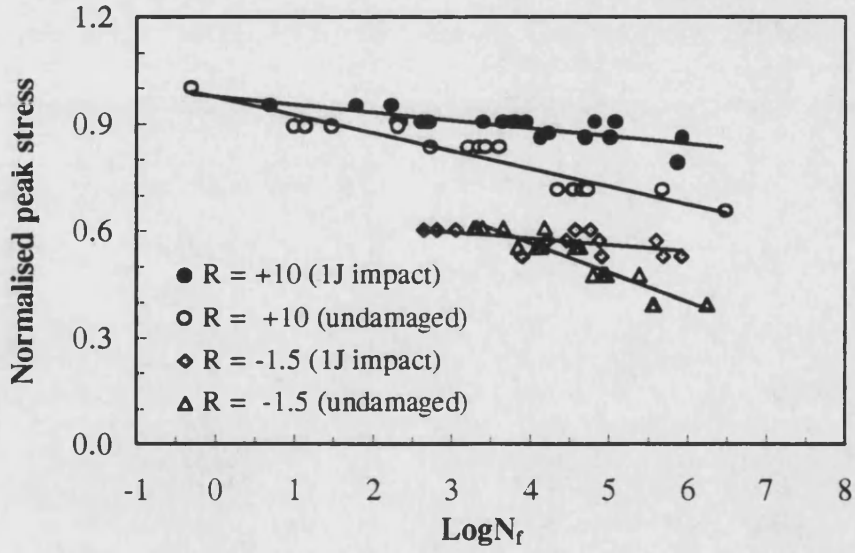

Figure 4-30. Normalised σ/logN$_f$ curves for HTA/982A CFRP laminate of [(±45,0$_2$)$_2$]$_S$ lay-up in the undamaged condition and after damage by a low-velocity impact of 1J. Normalisation is down with respect to the compressive strength and residual compressive strength for undamaged and 1J impact-damaged materials, respectively.

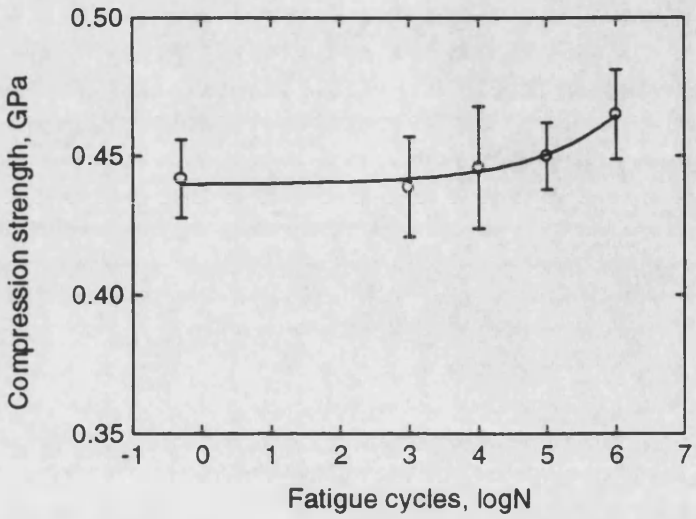

Figure 4-31. Residual compressive strength after fatigue cycling of samples of HTA/982A $[(\pm 45,0_2)_2]_S$ laminate with prior damage by a low-velocity impact of 1J. The cycling was at R = +10, at a peak stress (compressive) of 0.35GPa (79% of the residual compressive strength).

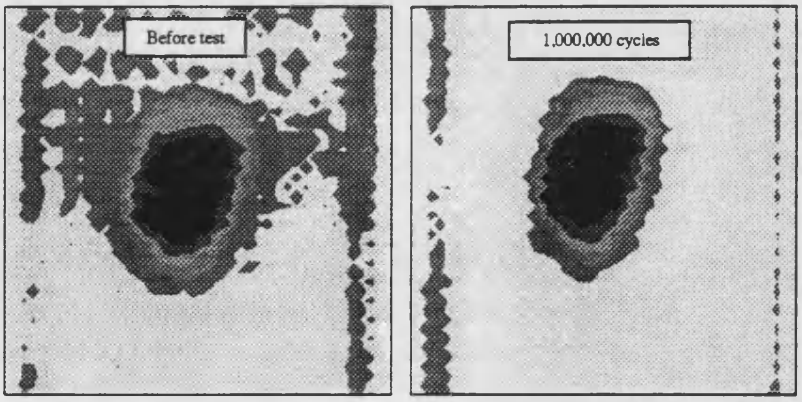

Figure 4-32. Ultrasonic C-scan images from sample of HTA/982A $[(\pm 45,0_2)_2]_S$ laminate impacted at 1J and subsequently fatigue cycled at R ratio of +10, at a peak stress (compressive) of 0.35GPa, under exactly the same conditions as Figure 4-31 (scan area was 42mm by 42mm).

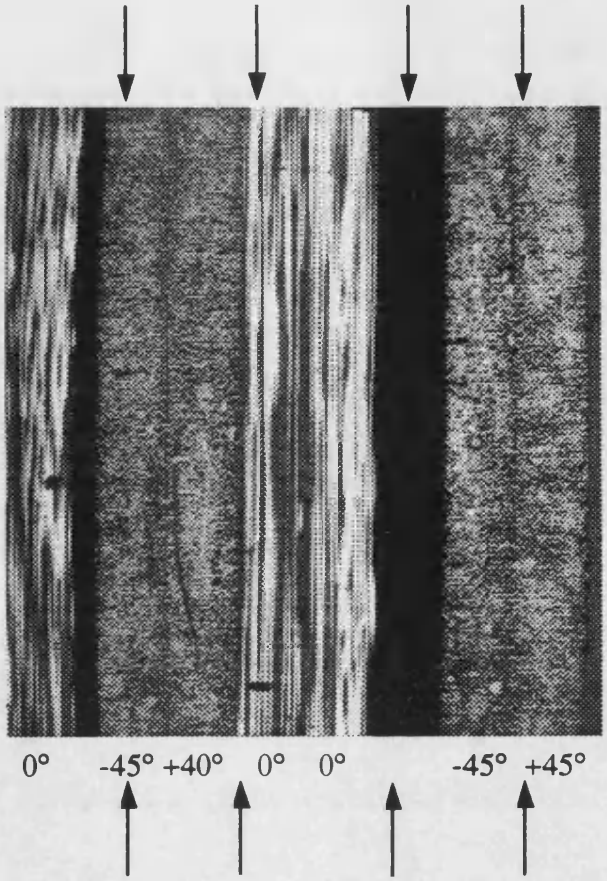

Figure 4-33. Photomicrograph of impact damaged HTA/982A which shows significant delamination between 0° and -45° plies. The thickness of each lamina is about 0.125mm.

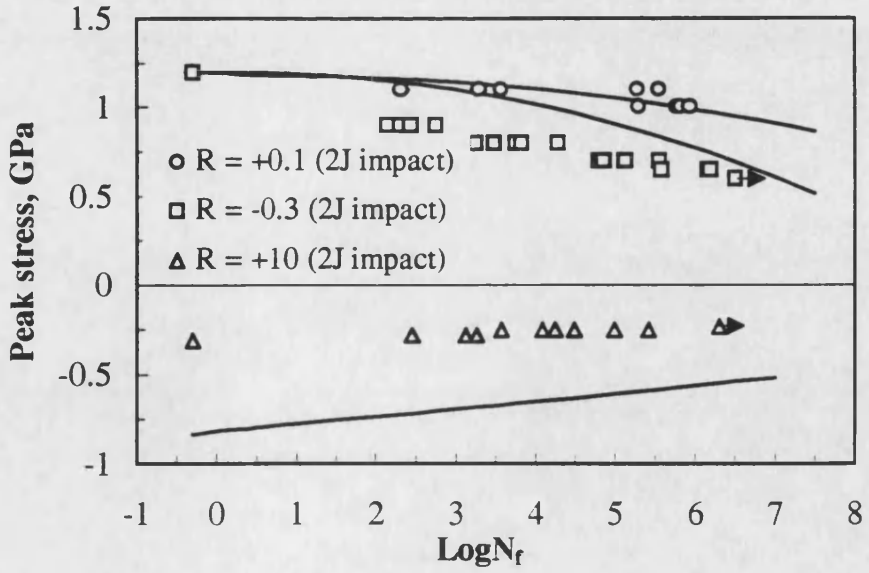

Figure 4-34. σ/logN$_f$ curves for HTA/982A CFRP laminate of [(±45,0$_2$)$_2$]$_S$ lay-up after damage by a low-velocity impact of 2J. The full lines are polynomial curves fitted to the data for the virgin laminate.

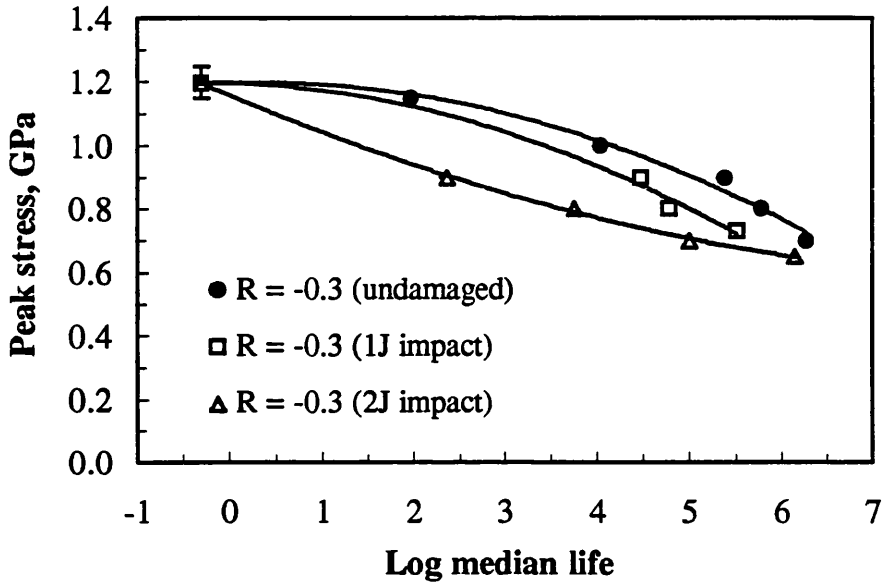

Figure 4-35. Stress/log median-life curves for $[(\pm 45,0_2)_2]_S$ HTA/982A laminate at R = –0.3, showing the effect of low-velocity impact damage.

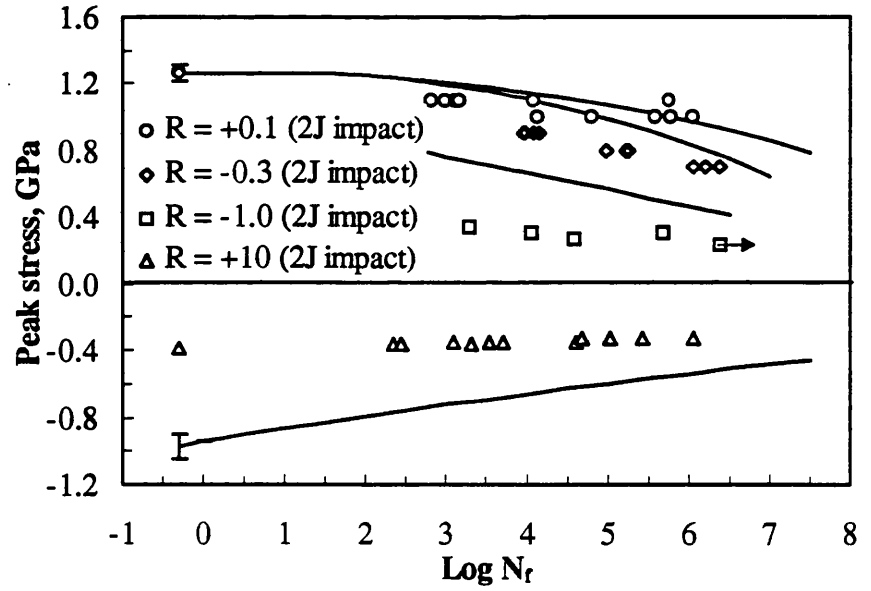

Figure 4-36. σ/logN_f curves for HTA/913 CFRP laminate of $[(\pm 45,0_2)_2]_S$ lay-up after damage by a low-velocity impact of 2J. The full lines are polynomial curves fitted to the data for the virgin laminate.

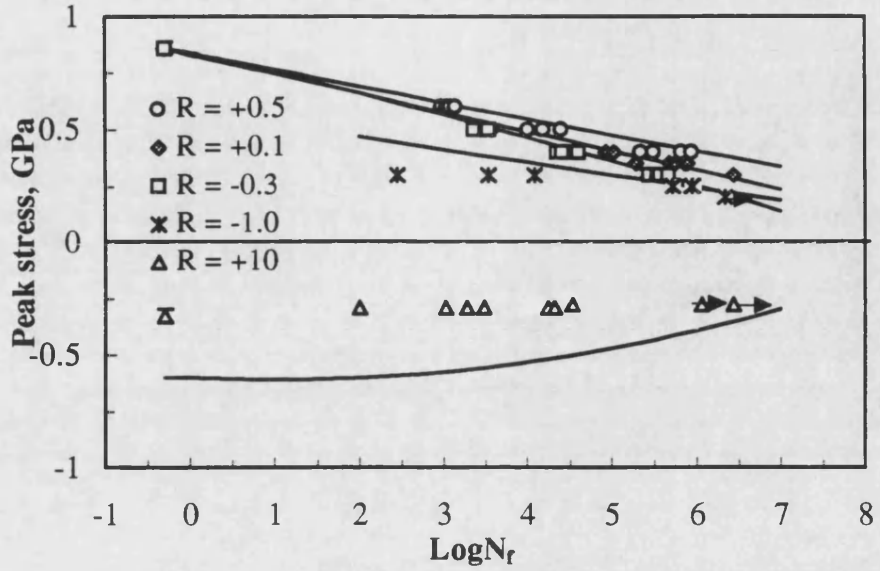

Figure 4-37. σ/logN$_f$ curves for E-Glass/913 GRP laminate of [(±45,0$_2$)$_2$]$_S$ lay-up after damage by a low-velocity impact of 2J. The full lines are polynomial curves fitted to the data for the virgin laminate.

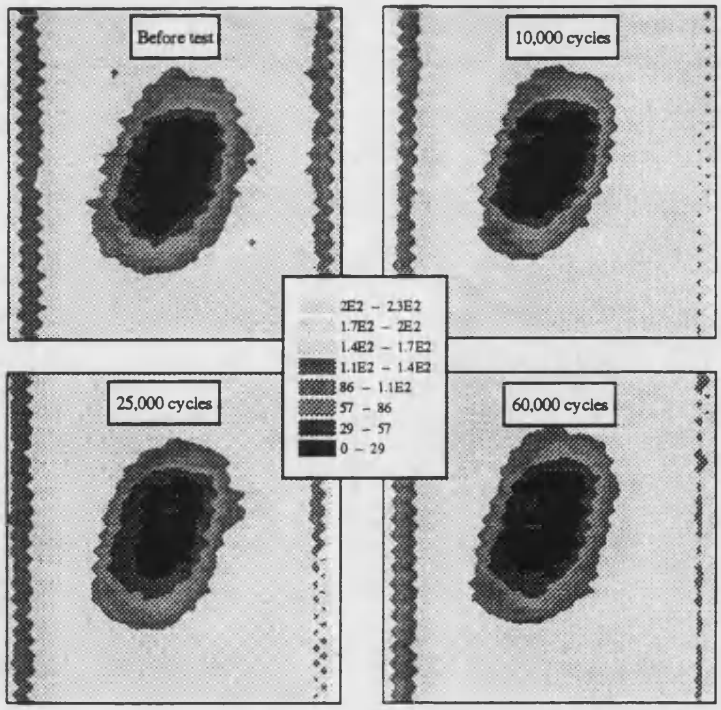

Figure 4-38. Ultrasonic C-scan images from sample of HTA/982A [(±45,0$_2$)$_2$]$_S$ laminate impacted at 1J and subsequently fatigue cycled at R ratio of +10 and a peak stress of -0.38GPa. The median life under this condition is 78,000 cycles (scan area was 42mm by 42mm).

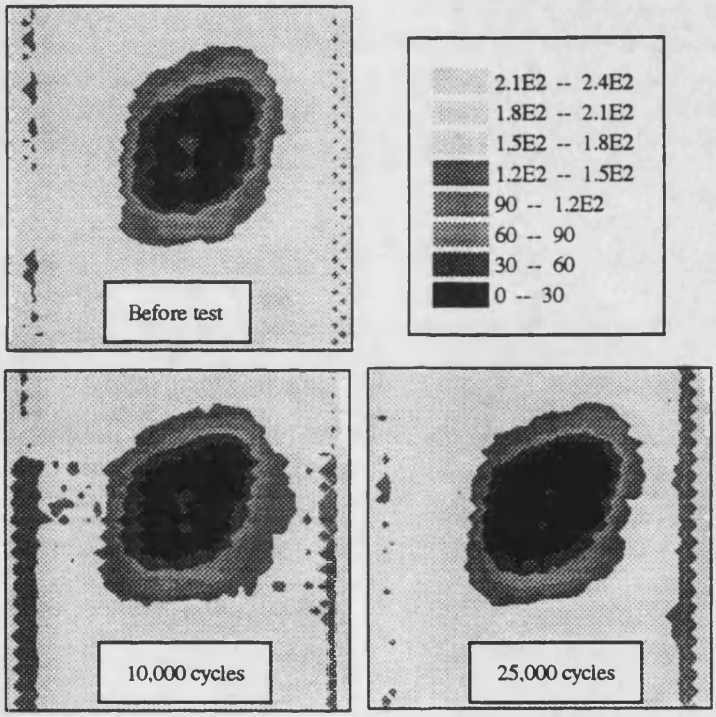

Figure 4-39. C-scan images from sample of HTA/982A $[(\pm 45,0_2)_2]_S$ laminate impacted at 1J and subsequently fatigue cycled at R ratio of +10 and a peak stress of -0.38GPa. The median life under this condition is 78,000 cycles, this sample failed at 36,390 cycles (scan area was 42mm by 42mm).

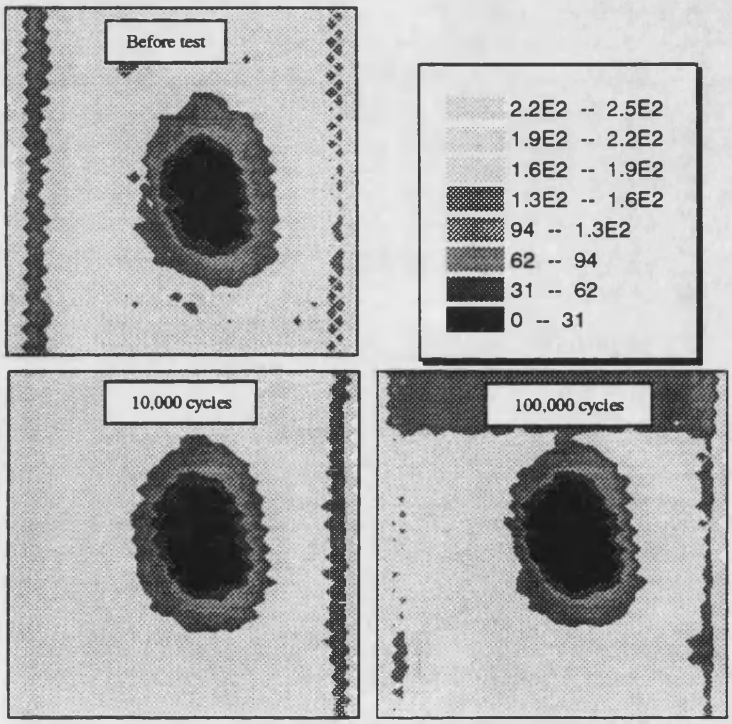

Figure 4-40. Ultrasonic C-scan images from sample of HTA/982A $[(\pm 45, 0_2)_2]_S$ laminate impacted at 1J and subsequently fatigue cycled at R ratio of +10 and a peak stress of -0.35GPa (scan area was 42mm by 42mm).

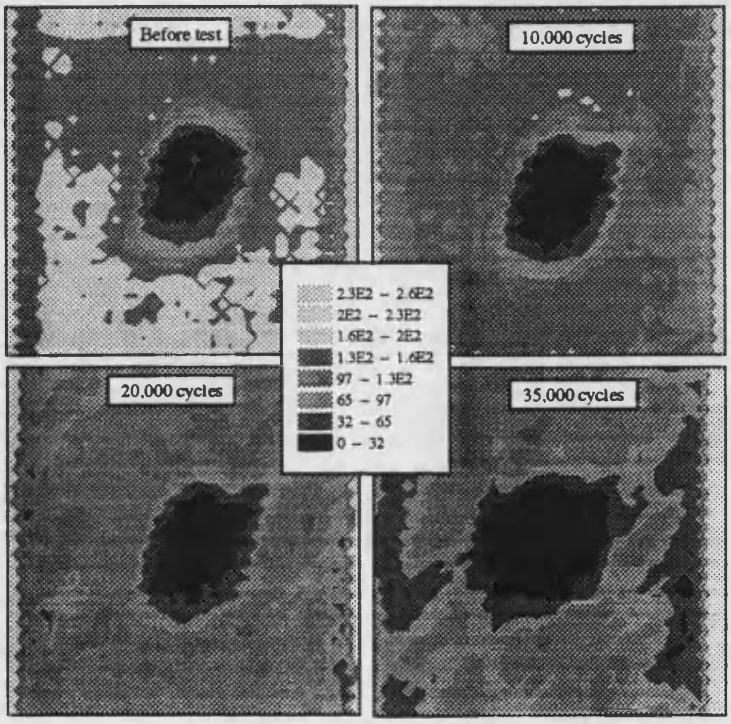

Figure 4-41. Ultrasonic C-scan images from sample of HTA/982A $[(\pm 45,0_2)_2]_S$ laminate impacted at 1J and subsequently fatigue cycled at R ratio of -0.3 and a peak stress of 0.9GPa. The median life under this condition is 30,000 cycles, this sample failed at 54,280 cycles (scan area was 42mm by 42mm).

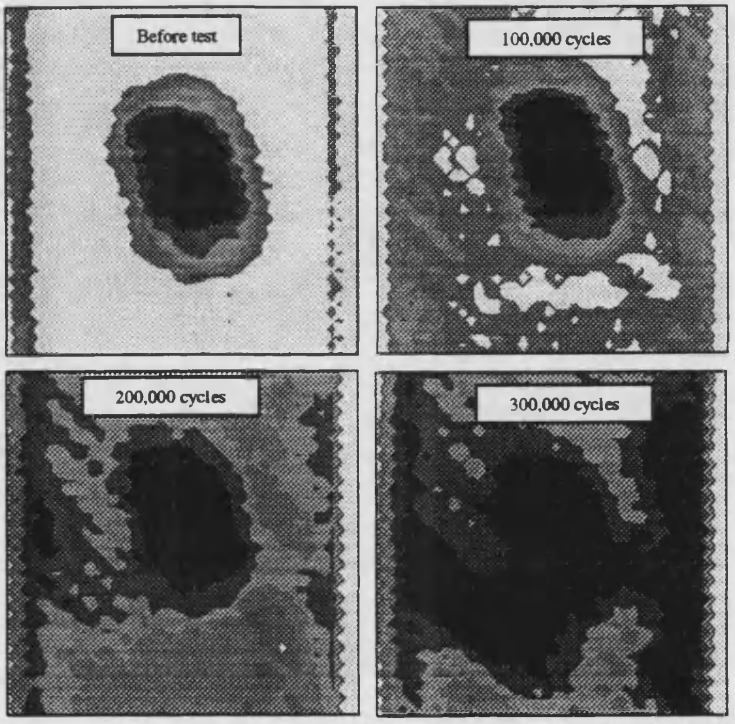

Figure 4-42. C-scan images from sample of HTA/982A $[(\pm 45,0_2)_2]_S$ laminate impacted at 1J and subsequently fatigue cycled at R ratio of -0.3 and a peak stress of 0.73GPa. The median life under this condition is 330,000 cycles, this sample failed at 623,680 cycles (scan area: 42mm x 42mm).

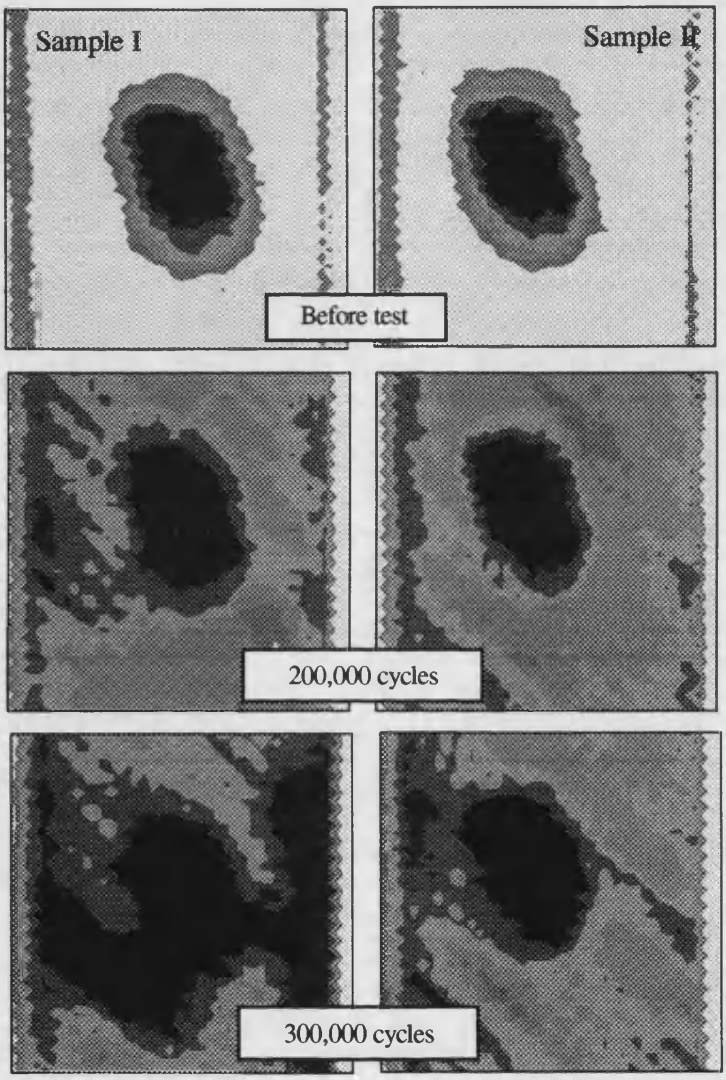

Figure 4-43. Ultrasonic C-scan images from samples of HTA/982A $[(\pm 45,0_2)_2]_S$ laminate impacted at 1J and subsequently fatigue cycled at R ratio of -0.3 and a peak stress of 0.73GPa. The median life under this condition is 330,000 cycles, sample I failed at 623,680 cycles and sample II failed at 753,140 cycles (scan area was 42mm by 42mm).

CHAPTER FIVE:

CONSTANT-LIFE ANALYSIS AND FATIGUE-LIFE PREDICTION

CHAPTER FIVE: CONSTANT-LIFE ANALYSIS 95

5.1 INTRODUCTION 96

5.2 CONSTANT-LIFE ANALYSIS OF FATIGUE DATA 96

5.2.1 Constant-life analysis for the undamaged materials 97

5.2.2 Constant-life analysis for the damaged materials 98

5.3 DISCUSSION 99

5.4 LIFE PREDICTION 107

5.5 CONCLUDING STATEMENT 108

5.6 APPENDIX 1 126

5.1 INTRODUCTION

The use of a constant-life model that can be used for fatigue-life prediction was explained in detail in chapter two. The experimental results mentioned in the previous chapter provided a considerable amount of data that can be analysed to give some general criteria for fatigue response and fatigue-life prediction for fibre-reinforced plastics. This chapter, therefore, intends to analyse the fatigue test results for virgin and impact-damaged materials in terms of the constant-life model in order to contribute to the aims of this investigation. To study the wider validity of the constant-life model, the results of constant-life analysis in recent work at Bath University on four modern aerospace CFRP laminates in the virgin condition, *viz.* T800/5245, T800/924, IM7/977 and HTA/913, all with a $[(\pm 45,0_2)_2]_S$ lay-up, have been included in this discussion.

5.2 CONSTANT-LIFE ANALYSIS OF FATIGUE DATA

It has been shown, as outlined in chapter two, that there is a general relationship between the alternating and mean components of stress of the form:

$$a = f(1 - m)^u(c + m)^v \quad \text{.....(1)}$$

where a is the normalised alternating stress component, σ_{alt}/σ_t, m is the normalised mean stress component, σ_m/σ_t, and c is the normalised compression strength, σ_c/σ_t. The alternating component of stress, σ_{alt}, is equal to $\frac{1}{2}(\sigma_{max} - \sigma_{min})$, the mean stress, σ_m, is $\frac{1}{2}(\sigma_{max} + \sigma_{min})$, and σ_t and σ_c are the monotonic tensile and compressive strengths, respectively. From previous observations on carbon-fibre composites, it appeared that f may be a function of the laminate strength. The exponents u and v separately characterise the shapes of the right (predominantly tensile) and left (predominantly compressive) wings of a bell-shaped curve represented by equation (1), and allow for different degrees of asymmetry in the curve: The use of equation (1) to analyse stress/life data allows interpolation and a limited amount of extrapolation for the prediction, from only a modest data-base if necessary, of median fatigue lives representative of conditions (stress range and R ratio, defined as $\sigma_{min}/\sigma_{max}$) for which experimental data may not yet be available. This analysis has been carried out on stress/life data obtained on virgin HTA/982A and E-Glass/913 and after low-

velocity impact of 1J on HTA/982A and 2J on HTA/982A, HTA/913 and E-Glass/913. The results of these analysis are as follows.

5.2.1 Constant-life analysis for the undamaged materials

Following the procedure described in detail in chapter two, the conventional stress/median-life fatigue curves are plotted for each experimental R ratio, and from these plots, the coefficients of fitted polynomial curves are extracted for the purpose of interpolation. Note that the choice of median-life is not appropriate for an unreasonably arranged set of data. In these cases, the polynomial or linear curves were fitted to the full data sets. The coefficients are then inserted into a spread sheet set up to calculate pairs of co-ordinates (m,a) for constant-life plots as given by equation (1). These spread sheets for virgin HTA/982A and virgin E-Glass/913 are given in table A1 of appendix 1. These (m,a) data pairs were then plotted, together with the normalised tensile and compressive strengths, to construct constant-life curves for given lives, e.g. 10^3, 10^4, 10^5, and 10^6 cycles, the curves being produced by non-linear regression fits to the data points by Microcal *Origin* software. Note that the choice of lives for this purpose must depend on the spread of data. In previous analysis of the carbon-fibre composites so far tested in the course of this work, only 10^4, 10^5, and 10^6 cycles were used, but better predictions can be obtained, provided there is a sufficiently wide spread of lives at different R ratios, if the shortest life chosen is somewhat nearer to the left-hand axis of the $\sigma/\log N_f$ curve than 10^4 cycles. A constant-life plot for HTA/982A in the undamaged condition showing the (m,a) data pairs for the five R ratios studied at the four lives referred to above, together with the extreme data pairs representing the monotonic tensile and compressive strengths, is shown in Figure 5-1. The curves were fitted through the data sets by means of the non-linear least-squares routine referred to earlier. The overall appearance of the curves is similar to those previously reported for the other CFRP laminates mentioned above, particularly that for the HTA/913 laminate.

Figure 5-2 shows constant-life plots for E-Glass/913 in the virgin condition for the five R ratios studied at the four lives. The overall shape of the constant-life plot is apparently unchanged by using a completely new material, and the constant-life

equation, equation 1, remains a valid descriptor of the constant-life surface. But the appearance of the curves is different from those of CFRP laminates, especially in that the right (predominantly tensile) wing of the curve is pulled downwards. It shows the poorer the fatigue performance for GRP since it reduces the level of alternating stress, a, that can be tolerated for a given mean stress at a given life. All four curves are shifted to the left-hand side and the positions of the maxima in the constant-life curves are on the left hand side of R ratio -1.0, (negative m values) while in CFRP laminates the positions of the maxima in the constant-life curves are between the R ratios of -0.6 and -0.3. Large separation of data points at each R ratio especially at R = +0.1 and R = -0.3 is a specific feature of GRP laminates owing to their steep stress/life curves.

5.2.2 Constant-life analysis for the damaged materials

Constant-life plots for the HTA/982A laminate after incurring damage by a 1J low-velocity impact events are shown in Figure 5-3. The four curves for 10^3, 10^4, 10^5 and 10^6 cycles have been fitted by allowing the three parameters f, u and v freedom to take any values, but because of the closeness of the four points for R = +0.1, it was necessary to force the curve for 10^6 cycles to remain close to the other three in order to avoid an unacceptable shape for this curve. The flattening of the $\sigma/\log N_f$ curve for R = +10 causes a squeezing together of the three points lying on the line for R = 10.

To build up a reasonable constant-life curve, in addition to the extreme data points representing the monotonic tensile and compressive strengths, at least three stress/life (S/N) curves are necessary to permit free fitting of equation (1) by allowing the three parameters f, u and v to take any values. Otherwise different curves can be fitted satisfactorily depending the initial values of f, u and v. These three S/N curves must be chosen properly to restrict the fitting operation at the left and at the right hands and at the peak value of the bell-shaped constant-life plots. It seems that stress ratios of +0.5, -0.6 and +10 for the undamaged materials and +0.5, -0.3 and +10 for damaged materials are the appropriate ones to determine for fitting purposes.

Figure 5-4 shows the constant-life plots for the 2J impact-damaged HTA/982A laminate. Although a complete set of stress/life data points was not available at R = +0.1 for the 2J impact-damaged HTA/982A, the available experimental results at this

R ratio did not show any deviation from the undamaged S/N curve, as explained in the previous chapter. In Figure 5-5, therefore, the data points at R ratios of +0.1 and +0.5 were taken from the data for virgin material for the purpose of reasonable curve fitting as explained above.

A more useful and direct comparison between the damaged and undamaged laminates can be made by plotting the families of constant-life curves for the two conditions on a single plot, as in Figure 5-5. In this figure, the constant-life curves of 1J and 2J impact-damaged HTA/982A have been added to the undamaged ones and the curves are obtained by freely fitting all three parameters. The overall shape of the constant-life plot is apparently unchanged by the prior damage, and the constant-life equation, equation 1, remains a valid descriptor of the constant-life surface. The two sets of curves for damaged materials lie in the same sequence as those for the undamaged material. The reduction in the compressive strength due to the prior impact damage is seen to result in a shift to the right of the left-hand tail of the curve, and the positions of the maxima in the constant-life curves are also shifted to the right.

Constant-life plots for the HTA/913 laminate after incurring damage by 2J low-velocity impact events are shown in Figure 5-6. In this figure the data points at R ratios of +0.1 and +0.5 were taken from the data for virgin material for the purpose of reasonable cure fitting. A family of constant-life plots in the virgin condition and after damage by 2J impact events can be seen in Figure 5-7. The overall appearance of the curves is similar to those for the HTA/982A laminate.

Figure 5-8 shows the constant-life plots for 2J impact damaged E-Glass/913, and the differences from the constant-life curves for the virgin laminate can be seen in Figure 5-9. This figure shows that the left-hand tail of the curve and the positions of the maxima in the constant-life curves are shifted to the right, but there was still no effect at R = -0.3.

5.3 DISCUSSION

The values of the fitting parameter f for the damaged composites are shown, together with those for virgin materials in Table 5-1. An unexpected aspect of these results, however, is the fact that the f values for the damaged laminates are much

higher than those for the virgin materials, and do not fit the pattern of relationship with the laminate tensile strength that has so far covered the behaviour of all undamaged CFRP $[(\pm 45,0_2)_2]_S$ laminates so far tested in the course of this work as shown in Figure 5-10. This is perhaps not surprising if we reflect that the area enclosed within the constant-life curves for the damaged material is markedly reduced as a consequence of the effect of the damage on the laminate compressive strength. But an important consequence of this is that, although the constant-life model appears to work just as well with damaged as with undamaged material, a simple knowledge of the fatigue response of an undamaged laminate (the *f*, *u* and *v* parameters), together with the results of measurements of the compressive strength after impact (CAI), could not be used to predict the fatigue response of that damaged laminate without the need for further fatigue data.

Table 5-1. The values of fitting parameter f for virgin and damaged materials.

Material	σ_t GPa	σ_c GPa	*f*			
			10^3 cycle	10^4 cycle	10^5 cycle	10^6 cycle
Virgin HTA/982A	1.20	0.84	1.279	1.133	0.956	0.764
1J impact HTA/982A	1.20	0.44	2.440	2.024	2.024	1.190
2J impact HTA/982A	1.20	0.32	2.438	2.447	2.382	2.206
Virgin HTA/913	1.27	0.97	1.259	1.099	0.854	0.620
2J impact HTA/913	1.27	0.38	2.541	2.248	1.854	1.376
Virgin E-Glass/913	0.86	0.60	0.910	0.840	0.780	0.689
2J impact E-Glass/913	0.86	0.33	3.009	2.895	2.638	2.260

Attempts to fit constant-life curves to the data points for the damaged laminate shown in Figure 5-3 or Figure 5-4 by fixing the value of the *f* parameter at 0.87, as indicated by the relationship in Figure 5-10, is simply not feasible. This suggests that other relationships between material properties and the constant-life model parameters should be sought.

In order to find other relationships between material properties and the constant-life model parameters, this analysis was repeated for the all CFRP laminates together with GRP composites in the virgin condition and after damage by impact events so far tested in the course of this work. In this analysis four lives, 10^3, 10^4, 10^5 and 10^6

cycles, were used at different R ratios. The values of the fitting parameters, f, u and v for the damaged composites are shown, together with those for the virgin materials, in Table 5-2 and Table 5-3 in addition to the results of four CFRP laminates, *viz.* T800/5245, T800/924, HTA/913, and IM7/977, in the virgin condition. These values were obtained by free fitting all three parameters in equation (1). To correlate the fitting parameters with materials properties different combinations (σ_t-σ_c, σ_t+σ_c, σ_t/σ_c, *etc.*) were used and finally it has been found that there is a relationship between the ratio of compressive strength over the tensile strength, σ_c/σ_t, (c parameter in equation 1) with the constant-life model parameters, and these results have been ordered in this sequence in Table 5-2 and Table 5-3.

The variation of f, u and v with the c values, σ_c/σ_t, for damaged laminates together with those for the virgin materials are show in Figure 5-11 to Figure 5-13. The lines in Figure 5-11 are the best-fit linear curves through the individual data sets for each number of cycles. It is important to point out that a linear relationship can be used to correlate the f parameter with the c values for each constant-life and the slope of fitted lines are about the same for 10^3, 10^4 and 10^5 cycles. In Figure 5-12 and Figure 5-13 the average value of u and v for all four lives for each material is shown as solid symbols and the line is a linear-fit through these data.

Table 5-2. The values of the fitting parameter, f, for the virgin and damaged materials. These values were obtained by freely fitting all three parameters.

Material	σ_c/σ_t (c)	f				f average
		10^3 cycle	10^4 cycle	10^5 cycle	10^6 cycle	
2J impact HTA/982A	0.263	2.438	2.447	2.382	2.206	2.380
2J impact HTA/913	0.303	2.541	2.248	1.854	1.376	2.005
1J impact HTA/982A	0.369	2.440	2.024	2.024	1.190	1.920
2J impact E-Glass/913	0.378	3.009	2.895	2.638	2.260	2.701
T800/5245	0.530	1.337	1.223	1.130	1.086	1.194
IM7/977	0.631	1.519	1.431	1.291	1.073	1.329
T800/924	0.633	1.405	1.364	1.378	1.360	1.377
E-Glass/913	0.701	0.910	0.840	0.780	0.689	0.805
HTA/982A	0.702	1.279	1.133	0.956	0.764	1.033
HTA/913	0.766	1.259	1.099	0.854	0.620	0.958

Table 5-3. The values of the fitting parameters, u and v , for the virgin and damaged materials. These values were obtained by freely fitting all three parameters.

Material	σ_c/σ_t (c)	u				u Average	v				v Average
		10^3 cycle	10^4 cycle	10^5 cycle	10^6 cycle		10^3 cycle	10^4 cycle	10^5 cycle	10^6 cycle	
2J impact HTA/982A	0.263	1.810	1.810	1.840	1.890	1.859	1.680	1.710	1.750	1.820	1.783
2J impact HTA/913	0.303	1.997	1.944	1.840	1.690	1.841	1.720	1.695	1.647	1.570	1.630
1J impact HTA/982A	0.369	1.970	1.860	1.860	1.500	1.798	1.930	1.810	1.810	1.500	1.763
2J impact E-Glass/913	0.378	3.680	4.340	5.090	5.960	4.768	2.190	2.240	2.250	2.220	2.225
T800/5245	0.530	1.830	1.890	2.000	2.190	1.978	1.750	1.790	1.920	2.220	1.920
IM7/977	0.631	2.085	2.160	2.230	2.210	2.171	2.320	2.400	2.430	2.340	2.373
T800/924	0.633	1.920	2.090	2.450	2.890	2.338	1.960	2.230	2.630	3.031	2.463
E-Glass/913	0.701	2.580	3.130	3.89	4.75	3.588	1.760	1.990	2.370	2.820	2.235
HTA/982A	0.702	2.010	1.940	1.820	1.640	1.853	2.110	2.130	2.120	2.090	2.113
HTA/913	0.766	2.340	2.320	2.090	1.850	2.150	2.640	2.720	2.660	2.570	2.648
Average, excluding GRP laminates	-	2.00	2.01	2.02	1.97	2.00	2.02	2.07	2.13	2.13	2.09

Since the values of u for virgin and damaged E-Glass/913 are much higher than those of CFRP laminates, these values are not included in Figure 5-12. This is due to the different behaviour of GRP laminates in mainly tension-dominated cycling as explained before. The dependence of constant-life parameters, f, u and v on life, N_f, are illustrated in Figure 5-14 to Figure 5-16. It can be seen from these figures that u and v have less sensitivity to life in comparison to the f parameter. Table 5-3 also shows an interesting new feature that the average value of u and v for each life and for all materials except the GRP laminates are about 2. This implies the symmetric nature of constant-life plots. This symmetric nature of bell-shaped constant-life plots and some other features can be revealed by calculating the maximum value of a for each life and its corresponding m value.

The maximum value of alternating stress, a_{max}, can be calculated from equation (1) by derivation with respect to m as follows:

$$\frac{da}{dm} = \frac{d\{f.[(1-m)^u.(c+m)^v]\}}{dm}$$
$$\frac{da}{dm} = -(1-m)^{(u-1)}.u.(c+m)^v + (1-m)^u.(c+m)^{(v-1)}.v \quad \text{.....(2)}$$

by setting the derivative to zero to find a_{max} and solving for m, it is found that:

$$m = \frac{-(u.c-v)}{(u+v)} \quad \text{.....(3)}$$

Therefore, by substituting in equation (1) and simplification, a_{max} can be defined as:

$$a_{max} = f.u^u.v^v.\left(\frac{1+c}{u+v}\right)^{(u+v)} \quad \text{.....(4)}$$

By using the data of Table 5-2 and Table 5-3 , the maximum value of a for each life and its corresponding m values, m_{max}, can be calculated from equations (3) and (4), respectively. These results are summarised in Table 5-4.

Table 5-4. The maximum values of constant-life curves at different lives for virgin and impact-damaged materials.

Material	σ_c/σ_t (c)	a_{max}				a_{max}	m_{max}			
		10^3 cycles	10^4 cycles	10^5 cycles	10^6 cycles	average	10^3 cycles	10^4 cycles	10^5 cycles	10^6 cycles
2J HTA/982A	0.263	0.489	0.461	0.434	0.404	0.447	0.350	0.356	0.358	0.356
2J HTA/913	0.303	0.518	0.474	0.425	0.374	0.448	0.307	0.304	0.308	0.318
1J HTA/982A	0.369	0.598	0.734	0.504	0.435	0.568	0.272	0.116	0.273	0.283
2J E-Glass/913	0.378	0.409	0.350	0.301	0.261	0.330	0.136	0.091	0.044	-0.004
T800/5245	0.530	0.513	0.457	0.396	0.333	0.425	0.218	0.214	0.219	0.240
IM7/977	0.631	0.622	0.568	0.501	0.425	0.529	0.228	0.227	0.220	0.208
T800/924	0.633	0.640	0.569	0.494	0.410	0.528	0.192	0.210	0.212	0.203
E-Glass/913	0.701	0.487	0.416	0.341	0.259	0.376	-0.011	-0.040	-0.057	-0.067
HTA/982A	0.702	0.659	0.590	0.512	0.430	0.548	0.170	0.189	0.214	0.252
HTA/913	0.766	0.684	0.596	0.489	0.379	0.537	0.170	0.187	0.223	0.261

It is important to note that the higher value of a_{max}, the better the fatigue response since it reduces the level of alternating stress that can be tolerated for a given mean stress at a given life. It can be seen from Table 5-4 that virgin HTA/982A has the highest average value of a_{max} and hence the fatigue resistance of the older material, HTA/913 and also new modern CFRP laminates, *viz.* T800/5245, T800/924 and IM7/977, are poorer than that of the HTA/982A composite. GRP laminates showed the poorest performance of all. Negative values of m_{max} for E-Glass/913 indicate the shift of the maxima to the left-hand side of constant-life plots for this material. It is interesting to see that for most of these materials m_{max} is independent of life, indicating the symmetric nature of constant-life plots for these materials.

Since the average values of u and v for all materials and all lives is equal to 2 as shown in Table 5-3, we could consider these parameters constant and, therefore, equation (1) can be modified to contain one variable parameter and is given by the relationship:

$$a = f(1-m)^2 \cdot (c+m)^2 \quad \text{.....(5)}$$

If the relationship of f with life is recognised, this equation can be used for fatigue-life prediction by measuring the monotonic tensile and compressive strength of material. To find this relationship, the equation (5) was re-fitted to the data points for

four lives, 10^3, 10^4, 10^5 and 10^6 cycles by allowing the f parameter freedom to take any values for all above-mentioned CFRP materials.

Figure 5-17 to Figure 5-24 show the constant-life plots for all CFRP laminates in the virgin condition and after damage by low-velocity impact events. In these figures, to compare the goodness of fit of equation (5) with equation (1), the constant-life plots produced by free fitting three parameters in equation (1) are shown in dashed curves. It can be seen that in most cases there is a good agreement between these two curves. The worst case can be seen for HTA/913. The new values for fitting the f parameter returned from the program are summarised in Table 5-5 for all CFRP laminates in the virgin condition and after sustained damage from low-velocity impact events.

The dependence of the f parameter on life can be seen in Figure 5-25. This figure shows that there is a decreasing linear relationship between f and $\log N_f$ and the important point is that the slopes of these curves for all materials are fairly similar. These relationships for all investigated materials are as follows:

2J impact HTA/982A $f = 3.66 - 0.181 \log N_f$ .....(6)

2J impact HTA/913 $f = 3.49 - 0.223 \log N_f$ .....(7)

1J impact HTA/982A $f = 3.31 - 0.245 \log N_f$ .....(8)

T800/5245 $f = 2.13 - 0.193 \log N_f$ .....(9)

T800/924 $f = 2.05 - 0.198 \log N_f$ .....(10)

IM7/977 $f = 1.79 - 0.142 \log N_f$ .....(11)

HTA/982 $f = 1.69 - 0.144 \log N_f$ .....(12)

HTA/913 $f = 1.55 - 0.160 \log N_f$ .....(13)

Table 5-5. The new values of fitting f parameter at four lives for CFRP laminates in the virgin and damaged conditions. These values were obtained by free fitting the single parameter constant-life equation (5).

Material	σ_c/σ_t (c)	f			
		10^3 cycles	10^4 cycles	10^5 cycles	10^6 cycles
2J HTA/982A	0.263	3.116	2.9430	2.764	2.573
2J HTA/913	0.303	2.819	2.6010	2.377	2.151
1J HTA/982A	0.369	2.559	2.3446	2.095	1.824
T800/5245	0.530	1.534	1.3624	1.168	0.954
IM7/977	0.631	1.356	1.2288	1.085	0.930
T800/924	0.633	1.464	1.2637	1.063	0.866
HTA/982A	0.702	1.254	1.1274	0.982	0.823
HTA/913	0.766	1.057	0.9187	0.757	0.578

Figure 5-26 shows the variation of f with σ_c/σ_t. It can be seen that f decreases as σ_c/σ_t increases and it seems that an exponential relationship can be considered for prediction purposes of the form:

$$f = A \cdot e^{-B \cdot c} \quad \text{.....(14)}$$

where A and B are constant values that can be calculated from Figure 5-26 for each life and c is equal to the ratio of compressive strength over tensile strength, σ_c/σ_t. The relationships for four lives are as follows:

10^3 cycles $f = 5.527 \cdot e^{-2.19 \cdot c}$ .....(15)

10^4 cycles $f = 5.383 \cdot e^{-2.34 \cdot c}$ .....(16)

10^5 cycles $f = 5.307 \cdot e^{-2.57 \cdot c}$ .....(17)

10^6 cycles $f = 5.331 \cdot e^{-2.90 \cdot c}$ .....(18)

Equation (15) to equation (18) can be used for prediction of f values for a new material or for an impact-damaged one by the prior knowledge of tensile strength and compressive strength of that material. By calculating the f parameter from these equations and using equation (5) the fatigue response of a new material can be predicted in the first instance without the need for any fatigue data.

Figure 5-27 shows the variation of f with σ_c/σ_t at 10^5 cycles. In this figure the vertical error bars are the average standard deviations for the fitted values of f for four lives, and the horizontal bars are standard deviations for the measured tensile strengths and compressive strengths. The latter values are calculated from [sdc = $(sd\sigma_t + sd\sigma_c)^{1/2}$] the square root of standard deviations for tensile strengths and compressive strengths. It can be seen that errors for the fitted values of f are very low.

5.4 LIFE PREDICTION

The next stage of the constant-life analysis is to solve the pair of simultaneous equations which describe the entire stress/R-ratio/life surface of the material. These equations, are:

$$a = f(\log N_f)\cdot(1-m)^2\cdot(c+m)^2$$

$$a = m\left(\frac{1-R}{1+R}\right) \qquad \text{.....(19)}$$

The first of these is the modified constant-life equation, equation (5), including information about the life-dependence of the f parameter. The second is derived from the conventional definition of the stress ratio, R.

The life-dependence of the f parameter, $f(\log N_f)$, can be established either from Figure 5-25 (or the equivalent information in equations 6-13) or Figure 5-26 (or the equivalent information in equations 15-18). The former one is valid only for the investigated materials mentioned earlier, but the latter one can be used for any similar material by using the ratio of compressive strength to tensile strength for that material.

Solution of these two equations is easily carried out with a package like MathCad which will graph or tabulate $\sigma/\log N_f$ curves for a chosen range of R values. A sample of a MathCad program for 2J impact-damaged HTA/982A is given in Table A2 in appendix 1. The output can be in one of two forms, depending on requirements, *viz.* a three-dimensional constant-life surface plot, showing the full variation of $(a,m,\log N_f)$, or a family of $\sigma/\log N_f$ curves at desired R ratios. An example of this analysis, for the virgin HTA/982A laminate, is shown in Figure 5-28 which includes the original

stress/life data for the four R ratios +0.1, –0.3, –1.5 and +10, the back-predicted curves for the same R ratios, and predicted curves for R ratios –0.6 and -1 for which no data have been obtained. The agreement between the data points and the predicted curves is good, as would be expected. Similar predictions for 2J impact damaged HTA/982A and HTA/913 can be seen in Figure 5-29 and Figure 5-30, respectively. In these figures the predicted results are shown as solid curves and the original stress/life data are shown in symbol. It can be seen that the agreement between the data points and the predicted curves is satisfactory. It is worthwhile indicating that in Figure 5-30 the few experimental results at R = -1.0 were obtained after this analysis had been carried out and they have not been used in the constant-life analysis.

The predicted three-dimensional constant-life surface plots for HTA/982A laminates in the virgin condition and after low-velocity impact damage by 1J and 2J impact events are shown in Figure 5-31, Figure 5-32 and Figure 5-33, respectively. It can be seen that the overall shape of these surface plots is apparently unchanged by the prior damage. The reduction in compressive strength is seen to result in a shift to the right of the left-hand tail of the plots. The positions of maxima are also shifted to the right and pulled down, but as the life increases, the amount of the reduction of the maxima is reduced. It means that for the high life, *eg.* 10^7 cycles, the virgin and damaged materials will behave alike and hence low-velocity impact will not be a threat for long-term fatigue response of composite materials.

5.5 CONCLUDING STATEMENT

It can be concluded that the constant-life model described here, is capable of conservative fatigue-life prediction for undamaged CFRP laminates by using only the tensile and compressive strengths of composite in question. By predicting the residual strengths of a composite after low-velocity impact, this model also can be used for fatigue-life prediction of impact-damaged materials. The capability of this model, however, must be evaluated against other prediction methods (an artificial neural network procedure for instance) to explore the level of safety for life-prediction made by this model before serious use. The statistical validity of the procedure and its efficacy for different kinds of lay-up would be open to question, but as further data

were obtained, the validity would improve as well as the level of confidence of true predictive capability.

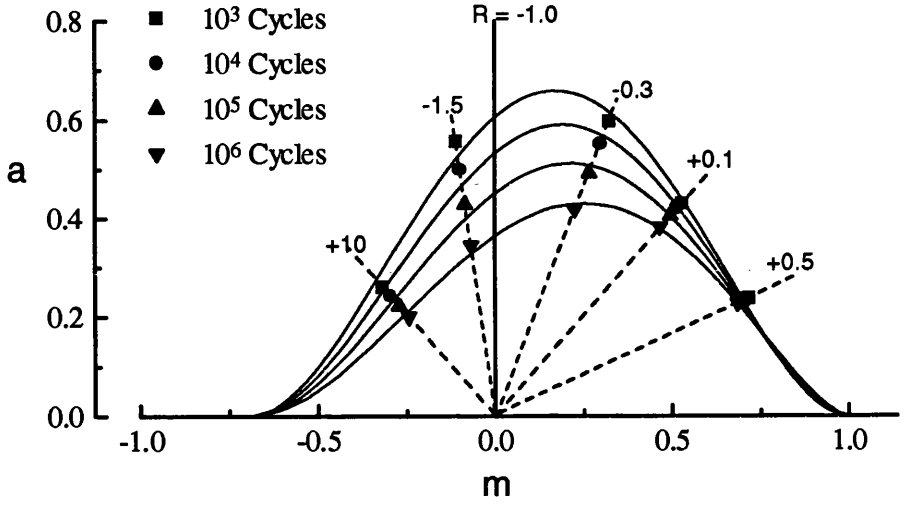

Figure 5-1. Constant-life plots for HTA/982A $[(\pm 45,0_2)_2]_S$ laminate in the undamaged condition. The curves are obtained by freely fitting all three parameters.

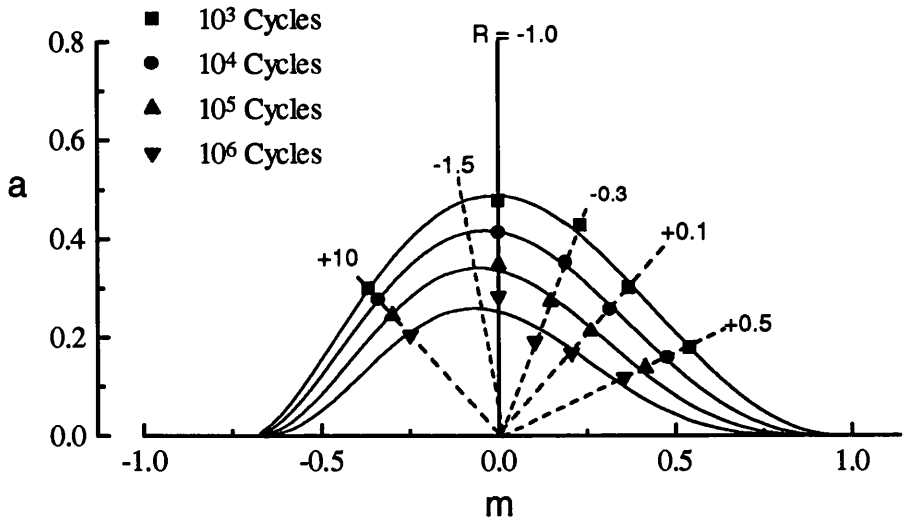

Figure 5-2. Constant-life plots for E-Glass/913 $[(\pm 45,0_2)_2]_S$ laminate in the undamaged condition. The curves are obtained by freely fitting all three parameters.

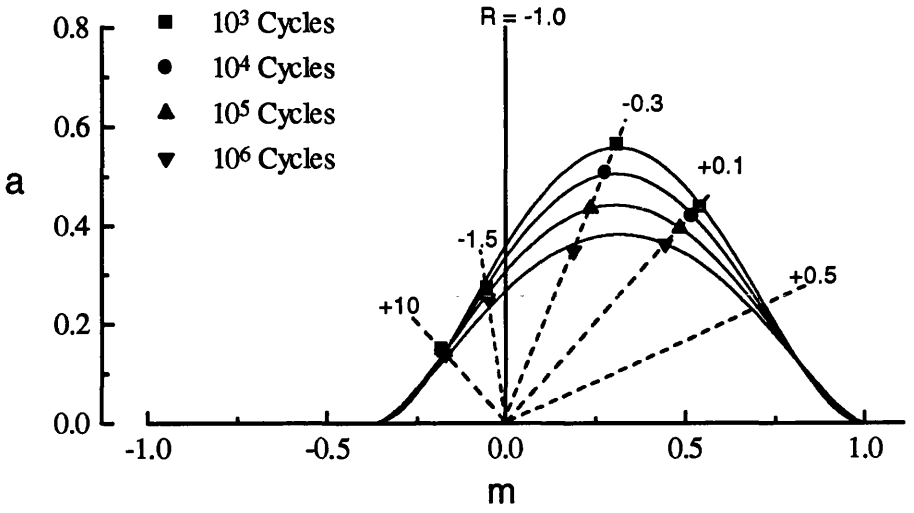

Figure 5-3. Constant-life plots for HTA/982A $[(\pm 45,0_2)_2]_S$ laminate following prior damage by a 1J impact. The curve for 10^6 cycles has been artificially forced to remain close to the other two curves above R = 0.1.

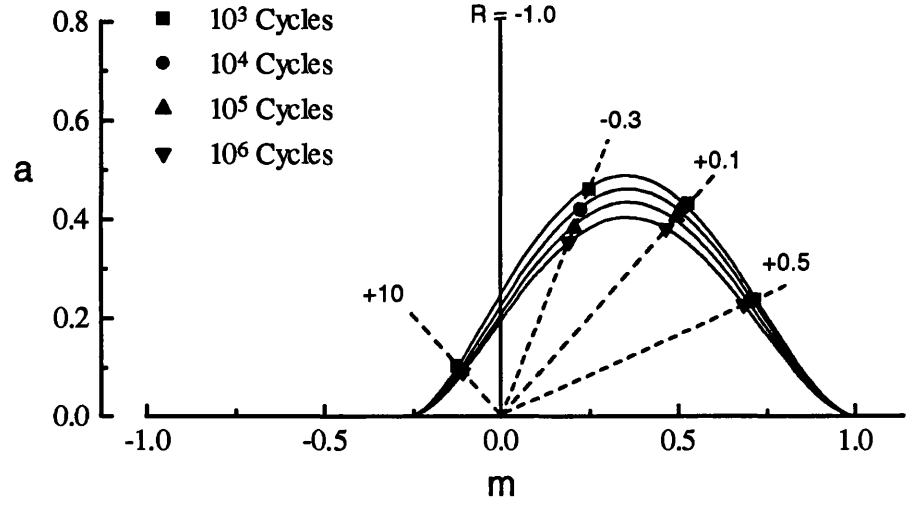

Figure 5-4. . Constant-life plots for HTA/982A $[(\pm 45,0_2)_2]_S$ laminate following prior damage by a 2J impact. Data points for R ratios of +0.5 and +0.1 are taken from the data of virgin material. The curves are obtained by freely fitting all three parameters.

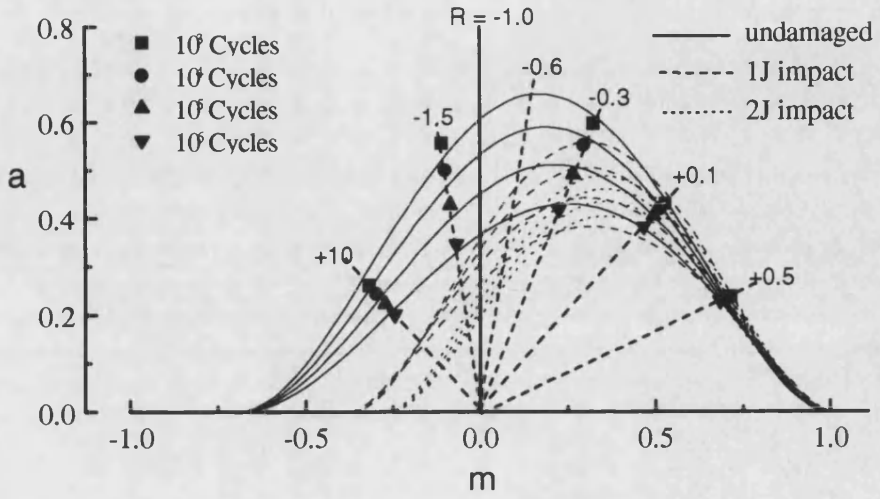

Figure 5-5. Constant-life plots for HTA/982A $[(\pm 45, 0_2)_2]_S$ laminate in the virgin condition and after prior damage with low-velocity impacts of 1J and 2J. The curves are obtained by freely fitting all three parameters.

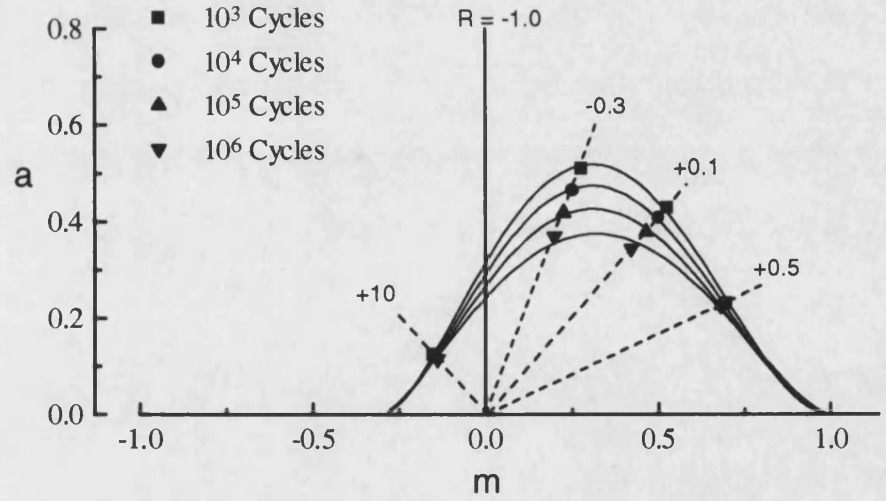

Figure 5-6. Constant-life plots for HTA/913 $[(\pm 45, 0_2)_2]_S$ laminate following prior damage by a 2J impact. Data points for R ratios of +0.5 and +0.1 are taken from the data of virgin material. The curves are obtained by freely fitting all three parameters.

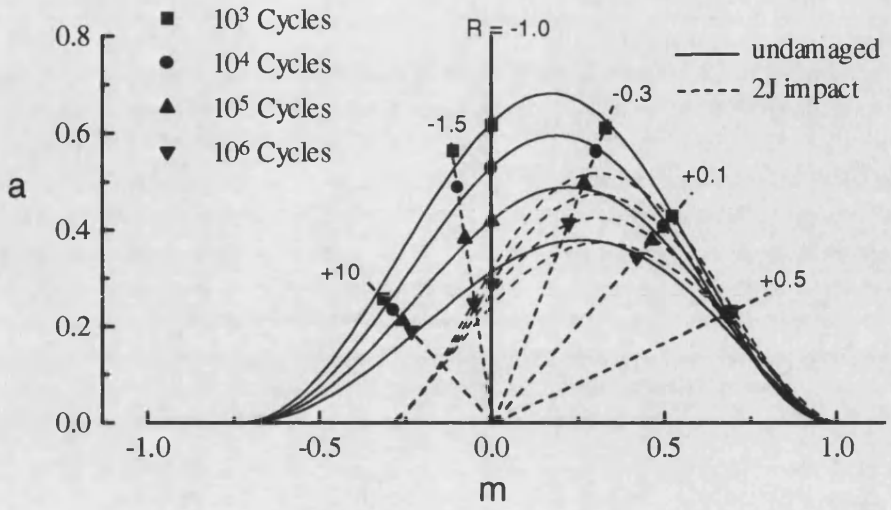

Figure 5-7. Constant-life plots for HTA/913 $[(\pm 45,0_2)_2]_S$ laminate in the virgin condition and after prior damage with a low-velocity impact of 2J. The curves are obtained by freely fitting all three parameters.

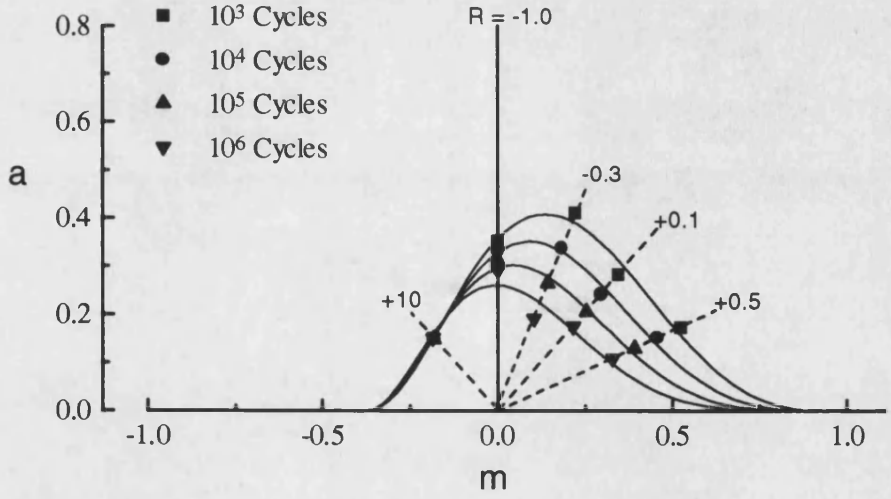

Figure 5-8. Constant-life plots for E-Glass/913 $[(\pm 45,0_2)_2]_S$ laminate following prior damage by a 2J impact. The curves are obtained by freely fitting all three parameters.

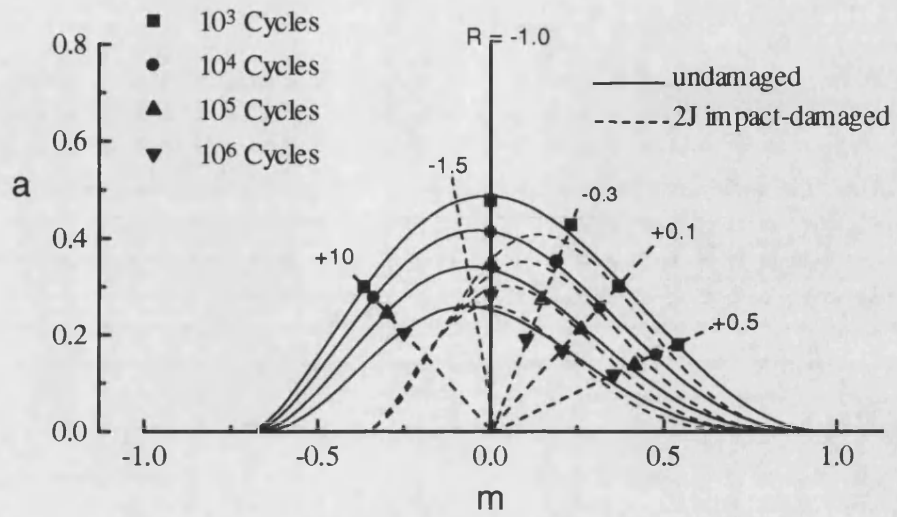

Figure 5-9. Constant-life plots for E-Glass/913 $[(\pm 45,0_2)_2]_S$ laminate in the virgin condition and after prior impact damage with a low-velocity-impact of 2J. The curves are obtained by freely fitting all three parameters.

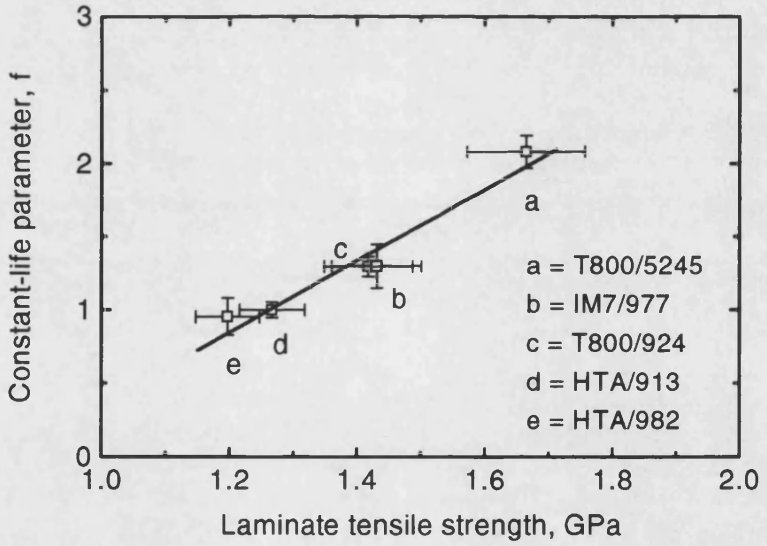

Figure 5-10. Dependence of constant-life model f parameter on laminate tensile strength. The vertical error bars are standard deviations for the fitted values of f, and the horizontal bars are standard deviations for the measured tensile strengths. The plotted f values are the means of the values obtained by curve fitting to obtain constant-life curves for 10^4, 10^5 and 10^6 cycles (Taken from reference 8).

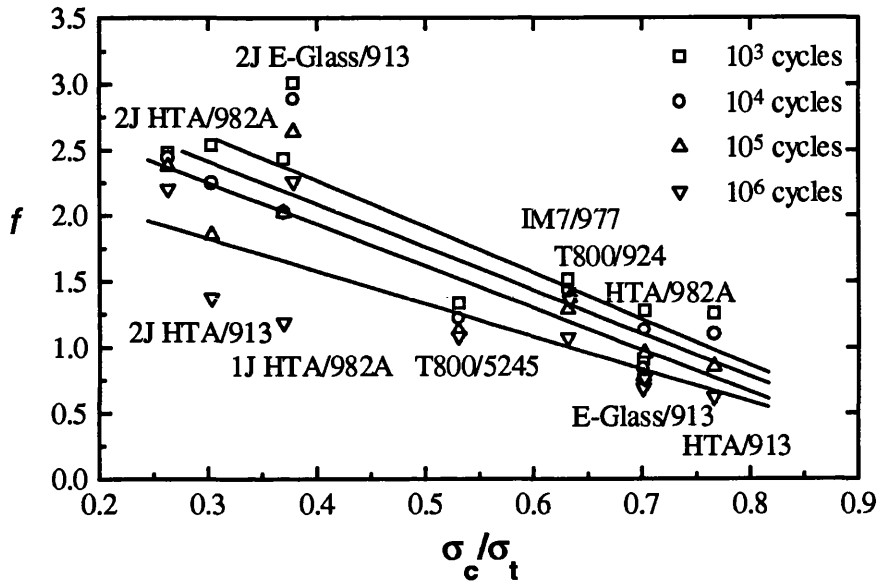

Figure 5-11.Dependence of constant-life model f parameter on the ratio of laminate compressive strength over tensile strength at different life.

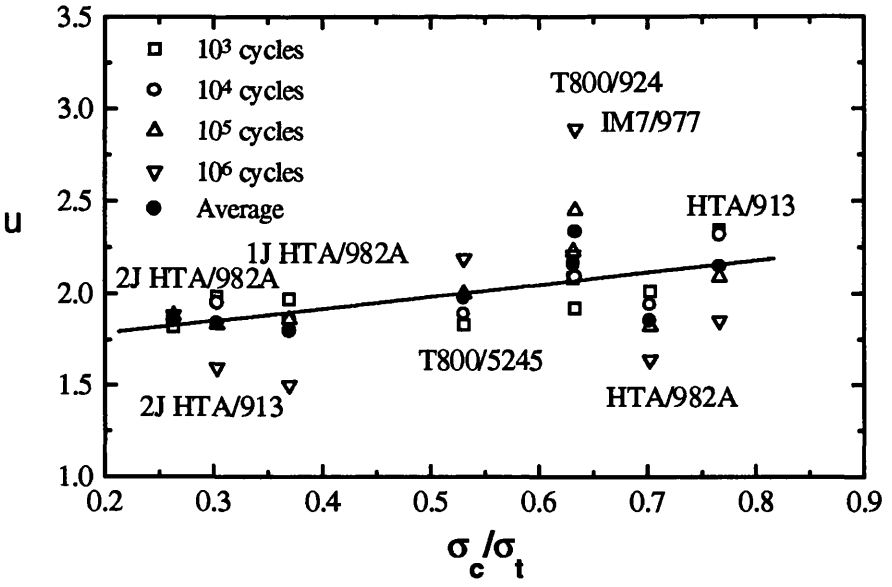

Figure 5-12. Dependence of constant-life model u parameter on the ratio of laminate compressive strength over tensile strength at different lives for virgin and damaged materials excluding GRP. The average value of u for each material is shown in solid symbol and the line is a linear curve fit through the average values.

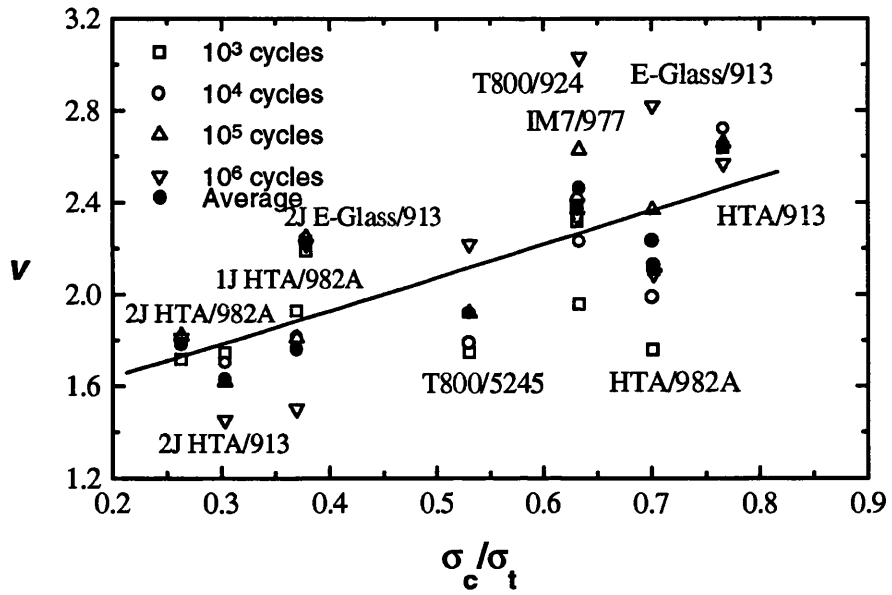

Figure 5-13. Dependence of constant-life model v parameter on the ratio of laminate compressive strength over tensile strength at different lives. The average value of v for each material is shown in solid symbol and the line is a linear curve fit through the average values.

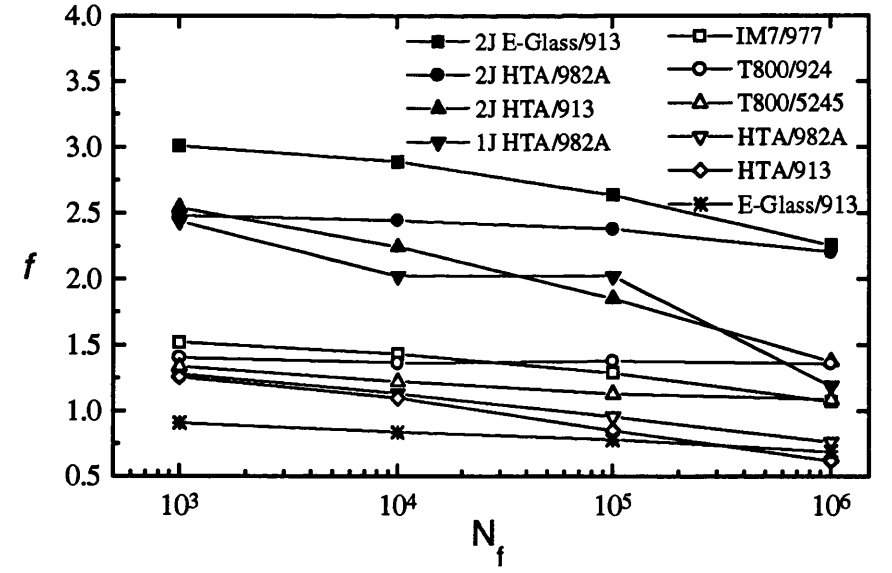

Figure 5-14. Dependence of constant-life model f parameter on life for $[(\pm 45, 0_2)_2]_S$ laminates in the virgin and damaged conditions.

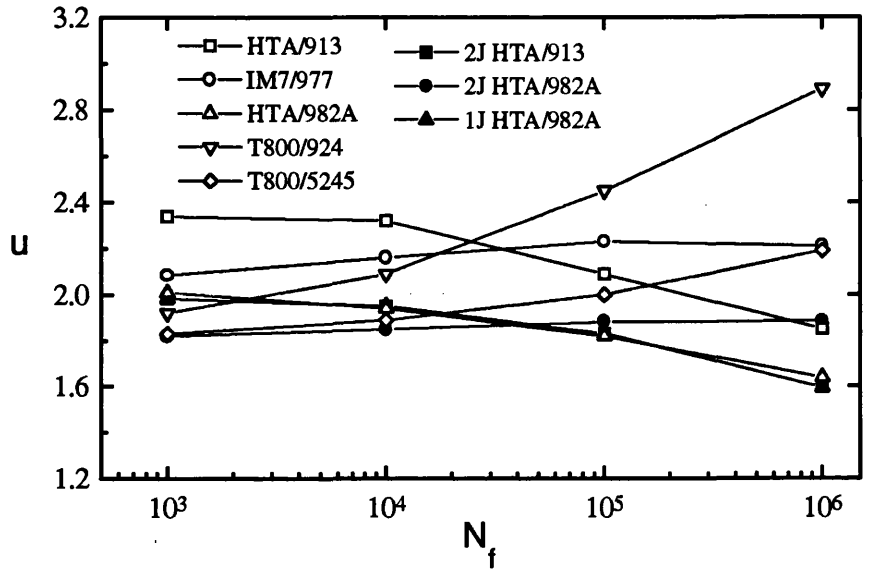

Figure 5-15. Dependence of constant-life model u parameter on life for $[(\pm 45, 0_2)_2]_S$ laminates in the virgin and damaged conditions.

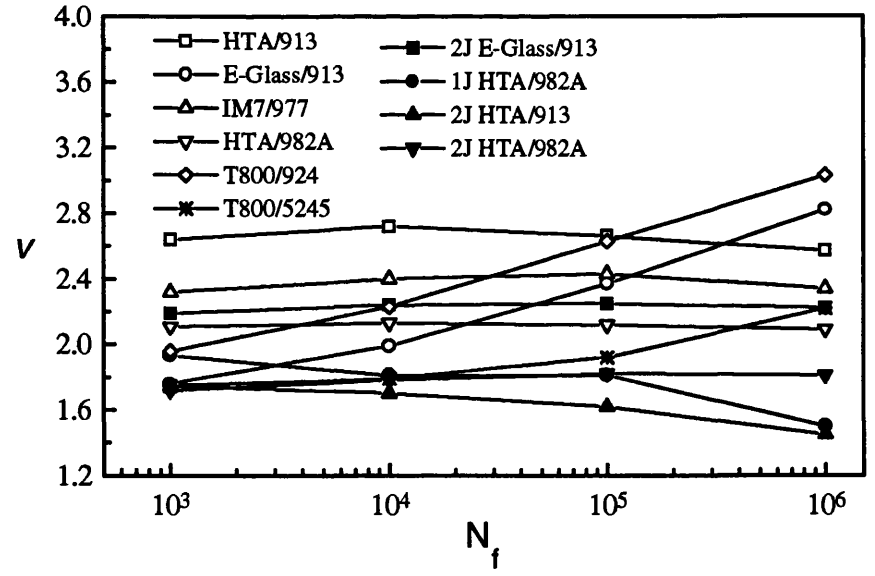

Figure 5-16. Dependence of constant-life model v parameter on life for $[(\pm 45, 0_2)_2]_S$ laminates in the virgin and damaged conditions.

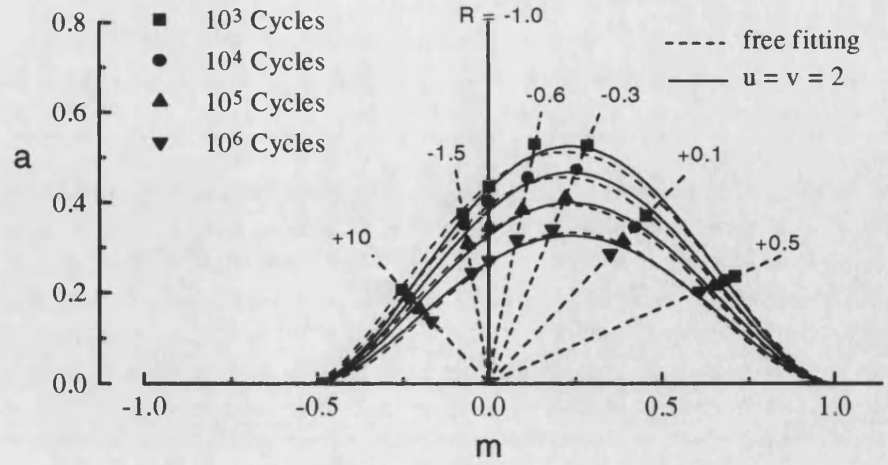

Figure 5-17. Constant-life plots for T800/5245. The dashed curve were obtained by free fitting all three parameters while the solid curves were obtained by the constant value of u and v equal to 2.

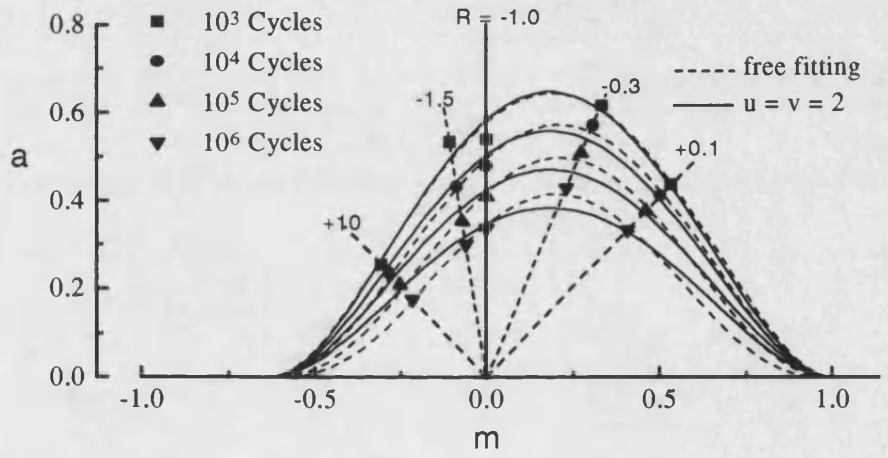

Figure 5-18. Constant-life plots for T800/924. The dashed curve were obtained by free fitting all three parameters while the solid curves were obtained by the constant value of u and v equal to 2.

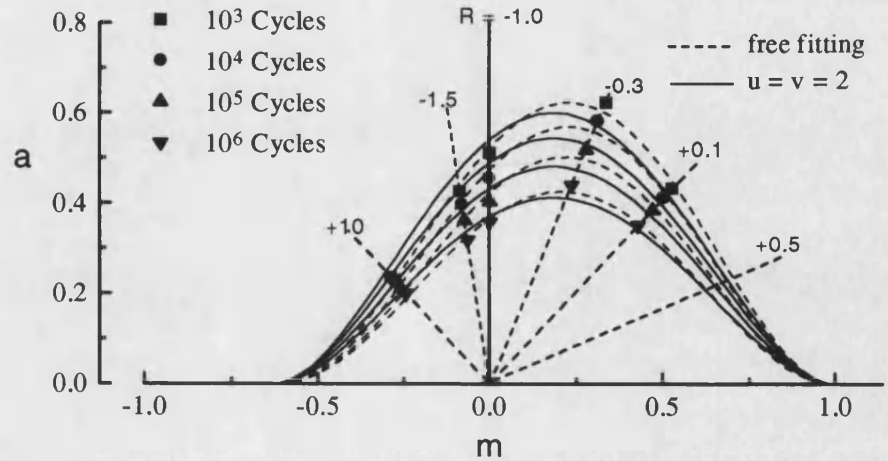

Figure 5-19. Constant-life plots for IM7/977. The dashed curve were obtained by free fitting all three parameters while the solid curves were obtained by the constant value of u and v equal to 2.

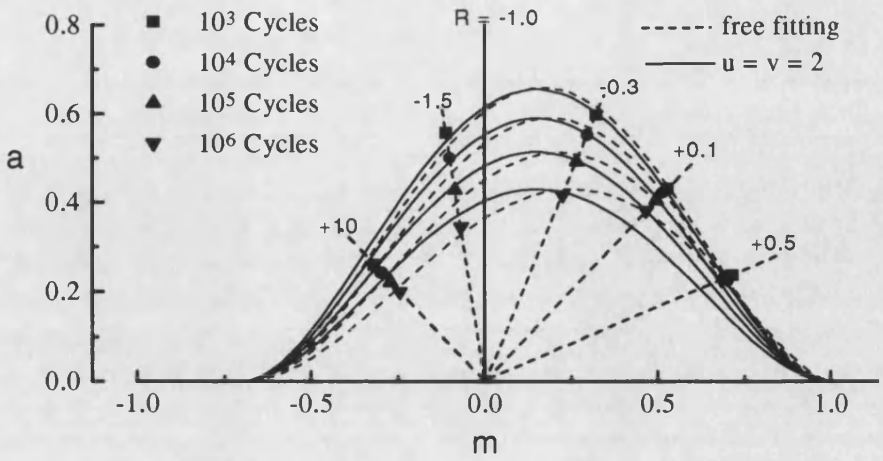

Figure 5-20. Constant-life plots for virgin HTA/982A. The dashed curve were obtained by free fitting all three parameters while the solid curves were obtained by the constant value of u and v equal to 2.

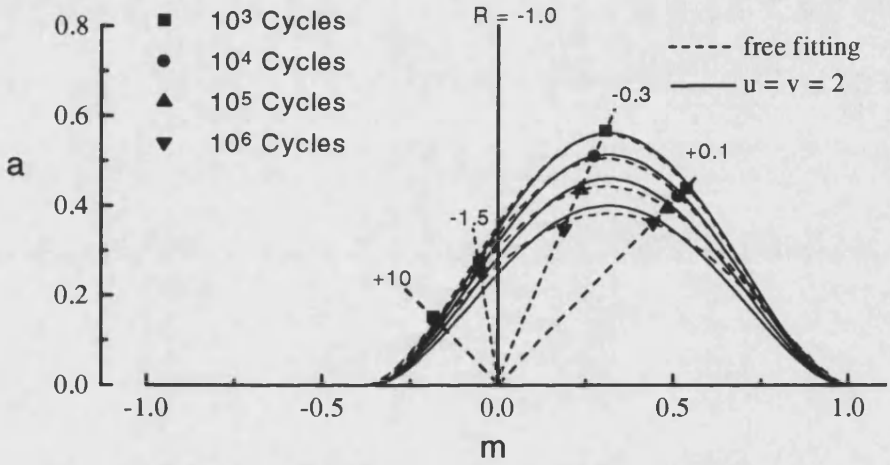

Figure 5-21 Constant-life plots for 1J impact-damaged HTA/982A. The dashed curve were obtained by free fitting all three parameters while the solid curves were obtained by the constant value of u and v equal to 2.

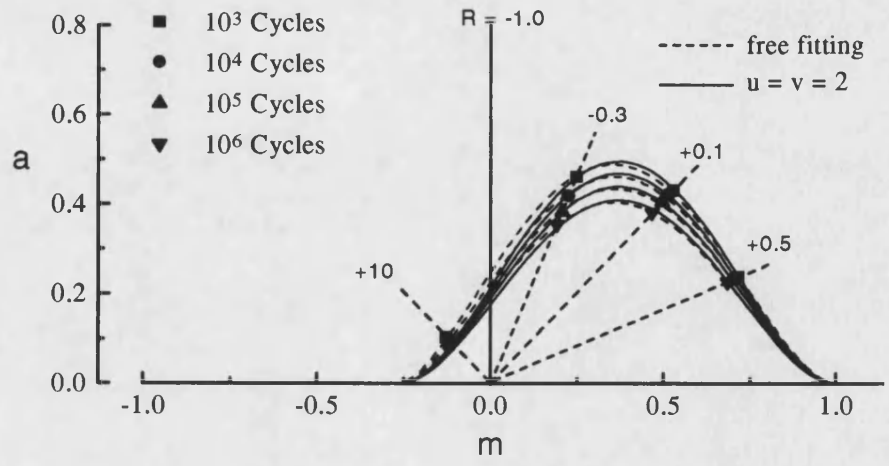

Figure 5-22. Constant-life plots for 2J impact-damaged HTA/982A. The dashed curve were obtained by free fitting all three parameters while the solid curves were obtained by the constant value of u and v equal to 2.

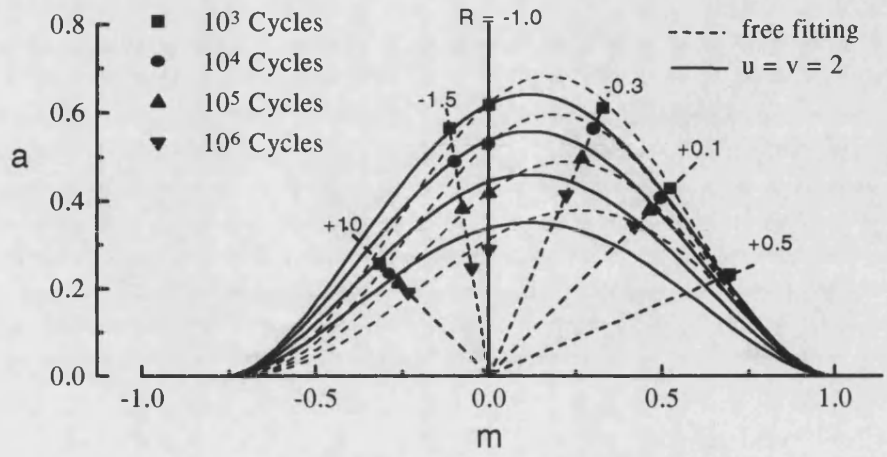

Figure 5-23. Constant-life plots for virgin HTA/913. The dashed curve were obtained by free fitting all three parameters while the solid curves were obtained by the constant value of u and v equal to 2.

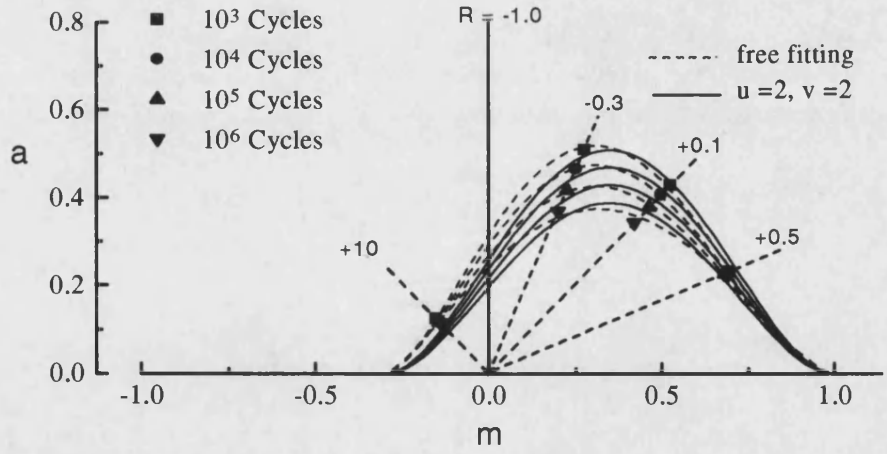

Figure 5-24. Constant-life plots for 2J impact-damaged HTA/913. The dashed curve were obtained by free fitting all three parameters while the solid curves were obtained by the constant value of u and v equal to 2.

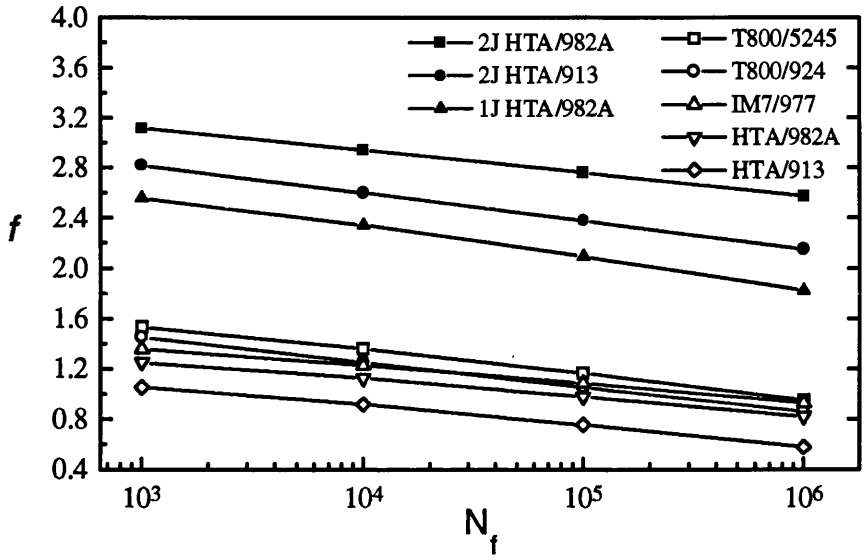

Figure 5-25. Variation of constant-life new f parameter on life for $[(\pm 45, 0_2)_2]_S$ laminates in the virgin and damaged conditions. These values were obtained while u and v were considered equal to 2.

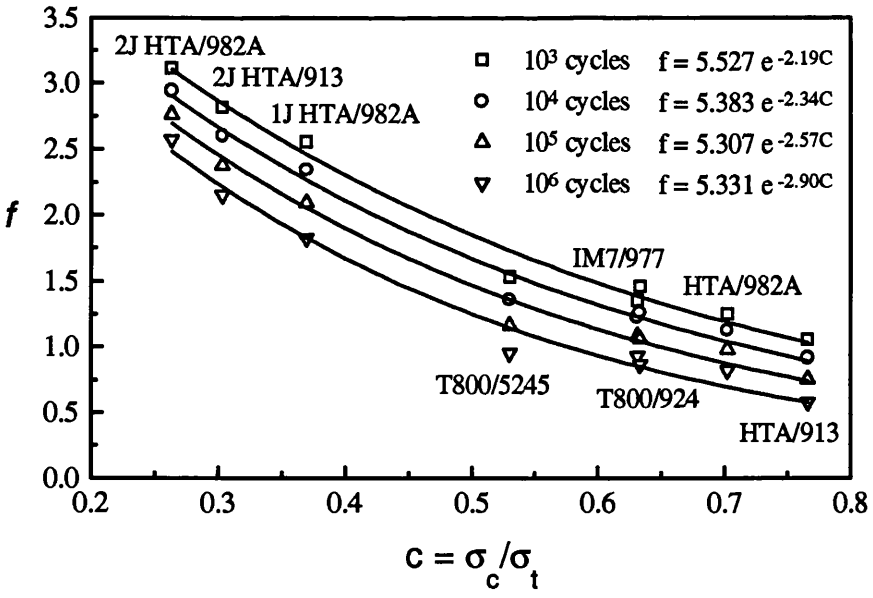

Figure 5-26. Dependence of constant-life new f parameter on c at four lives for $[(\pm 45, 0_2)_2]_S$ laminates in the virgin and damaged conditions. These values were obtained while u and v were considered equal to 2.

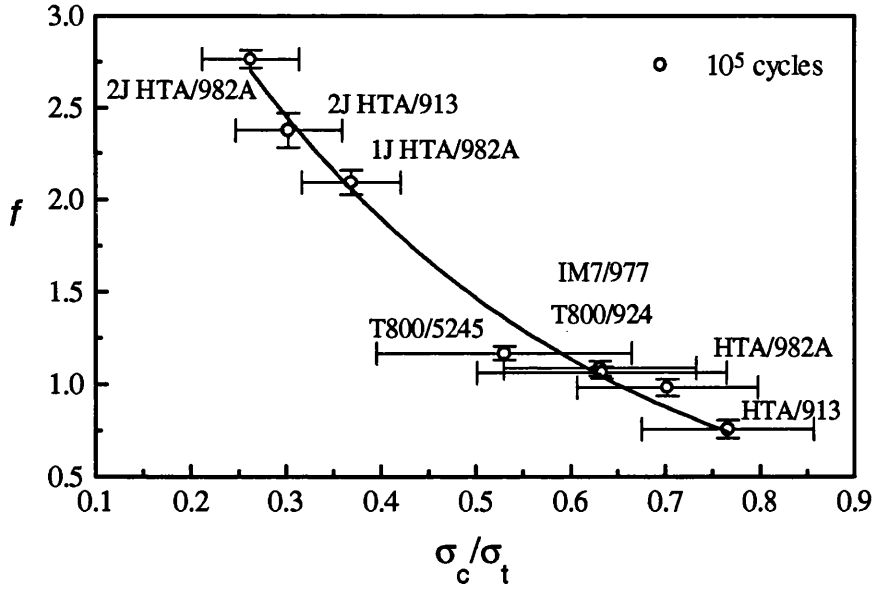

Figure 5-27. Dependence of constant-life new f parameter on c at 10^5 cycles for $[(\pm 45, 0_2)_2]_S$ laminates in the virgin and damaged conditions. These values were obtained while u and v were considered equal to 2. The vertical error bars are the average standard deviations for the fitted values of f for four lives, and the horizontal bars are obtained from the standard deviations for the measured tensile strengths and compressive strengths [$sdc = (sd\sigma_t + sd\sigma_c)^{1/2}$].

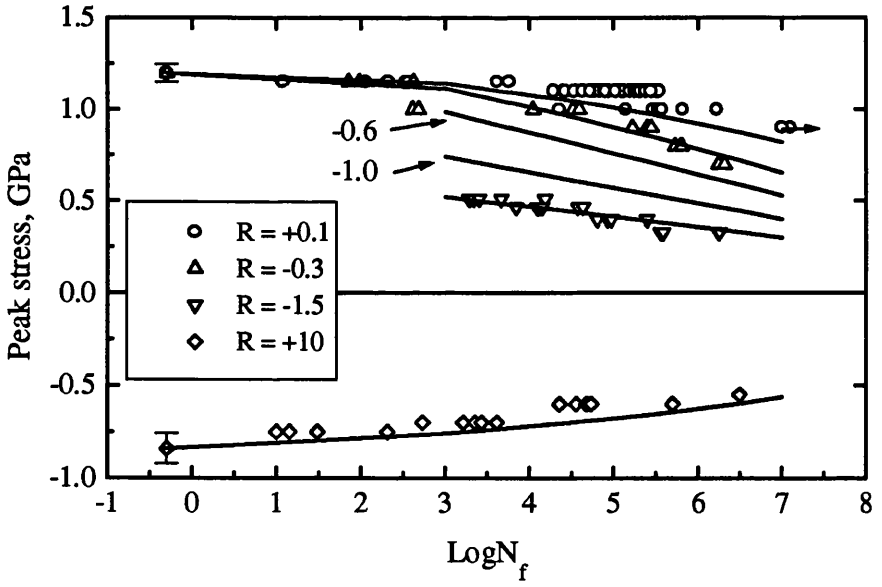

Figure 5-28. Stress/life data for the $[(\pm 45, 0_2)_2]_S$ HTA/982A CFRP laminate in the undamaged condition. The full lines are predicted curves by the modified constant-life model.

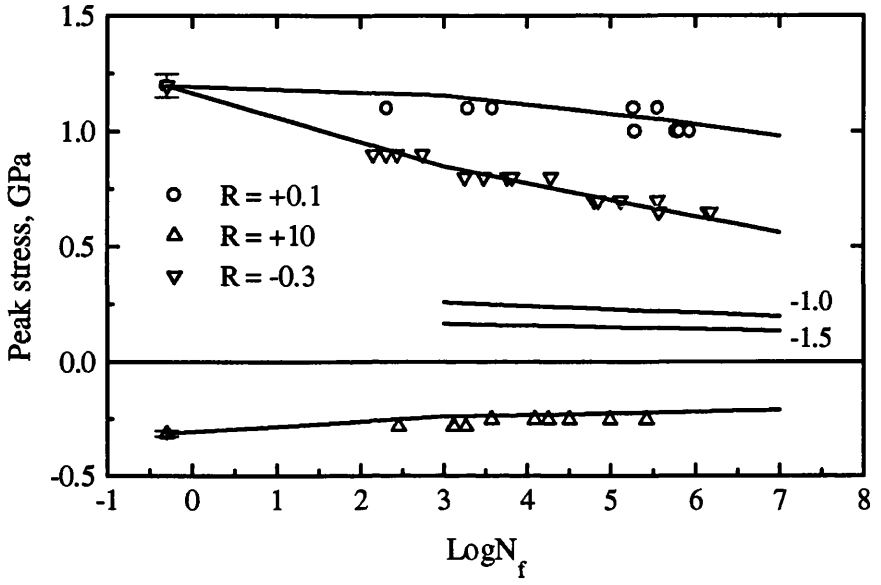

Figure 5-29. Stress/life data for the $[(\pm 45,0_2)_2]_S$ HTA/982A CFRP laminate after damage by a 2J impact event. The full lines are predicted curves by the modified constant-life model.

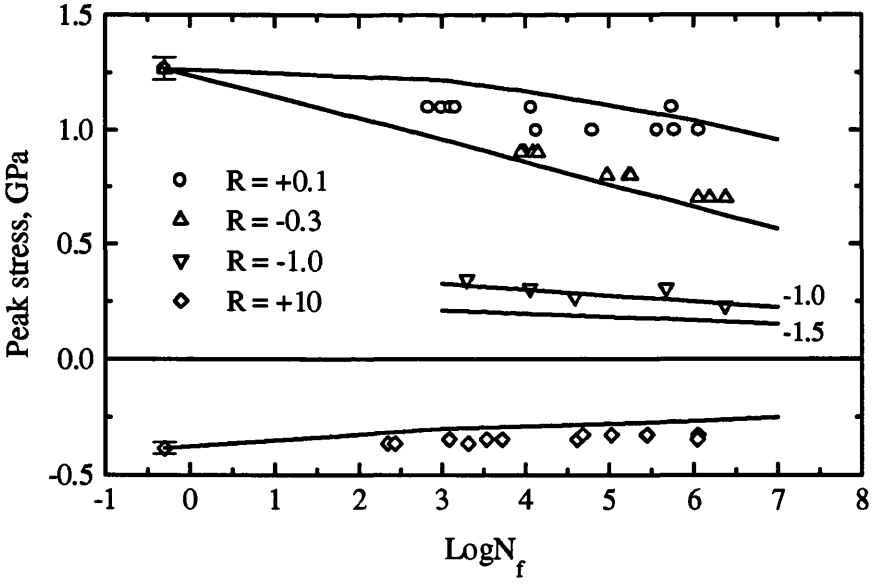

Figure 5-30. Stress/life data for the $[(\pm 45,0_2)_2]_S$ HTA/913 CFRP laminate after damage by a 2J impact event. The full lines are predicted curves by the modified constant-life model.

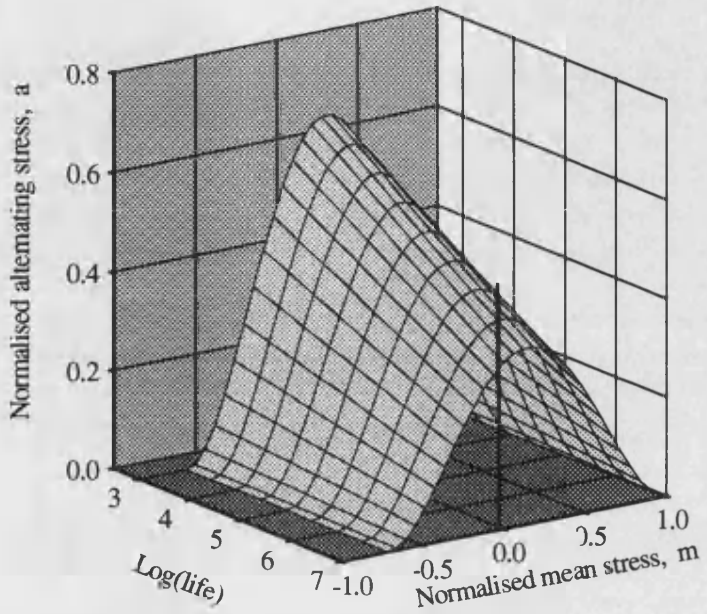

Figure 5-31. Three-dimensional surface plot of the a, m, logN_f constant-life relationship defined by the equation 5 for the $[(\pm 45,0_2)_2]_S$ HTA/982A laminate in the virgin condition.

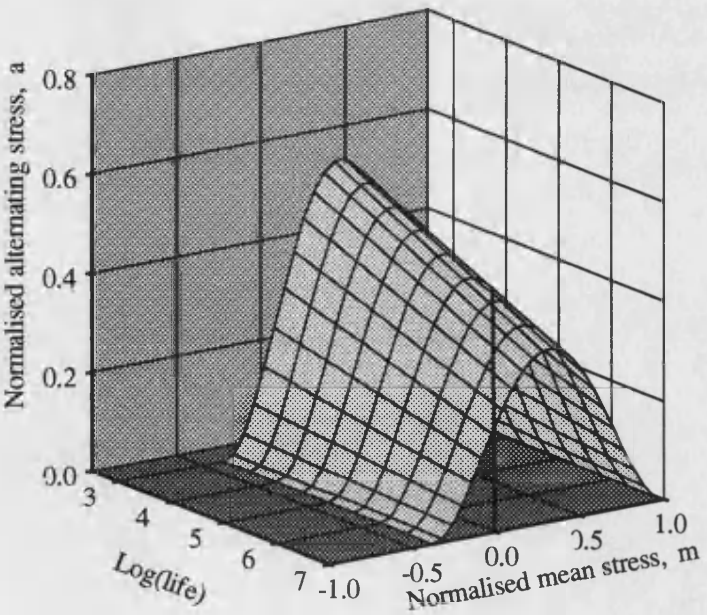

Figure 5-32. Three-dimensional surface plot of the a, m, logN_f constant-life relationship defined by the equation 5 for the $[(\pm 45,0_2)_2]_S$ HTA/982A laminate after a 1J impact event.

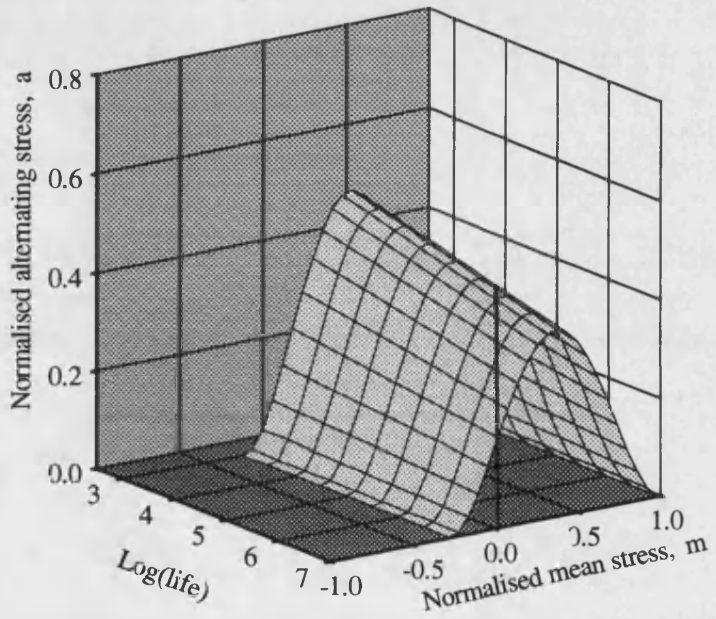

Figure 5-33. Three-dimensional surface plot of the a, m, logN_f constant-life relationship defined by the equation 5 for the $[(\pm 45,0_2)_2]_S$ HTA/982A laminate after a 2J impact event.

5.6 APPENDIX 1

Table A1. Spreadsheet for calculations of constant-life data from fatigue test results.

Virgin HTA/982A

Static Strength			Polynomial terms				Log	Fatigue Strengths			Derived Parameters		
σ_t	σ_c	R	a	b	c	d	N_f	σ_{max}	σ_{mean}	σ_{alt}	m	a	c
1.197	-0.840										1.000	0.000	
1.197	-0.840	0.5	1.1882	-0.016	0.00	0.00	3	1.1402	0.855	0.2851	0.7144	0.238	
1.197	-0.840	0.1	1.1916	-0.0145	0.0023	-8E-04	3	1.1471	0.631	0.5162	0.5271	0.431	-0.702
1.197	-0.840	-0.3	1.1957	0.0082	-0.013	0.000	3	1.1015	0.386	0.716	0.3221	0.598	
1.197	-0.840	-1.5	0.6279	-0.0129	-0.006	0.000	3	0.5343	-0.13	0.6679	-0.112	0.558	
1.197	-0.840	10	-0.822	0.0366	0.0019	0.00	3	-0.069	-0.38	0.3128	-0.319	0.261	
1.197	-0.840										-0.702	0.000	
1.197	-0.840										1.000	0.000	
1.197	-0.840	0.5	1.1882	-0.016	0.00	0.00	4	1.1242	0.843	0.2811	0.7044	0.235	
1.197	-0.840	0.1	1.1916	-0.0145	0.0023	-8E-04	4	1.1190	0.615	0.5036	0.5142	0.421	-0.702
1.197	-0.840	-0.3	1.1957	0.0082	-0.013	0.000	4	1.0173	0.356	0.6612	0.2975	0.552	
1.197	-0.840	-1.5	0.6279	-0.0129	-0.006	0.000	4	0.4787	-0.12	0.5984	-0.1	0.5	
1.197	-0.840	10	-0.822	0.0366	0.0019	0.00	4	-0.064	-0.35	0.2903	-0.296	0.243	
1.197	-0.840										-0.702	0.000	
1.197	-0.840										1.000	0.000	
1.197	-0.840	0.5	1.1882	-0.016	0.00	0.00	5	1.1082	0.831	0.2771	0.6944	0.231	
1.197	-0.840	0.1	1.1916	-0.0145	0.0023	-8E-04	5	1.0764	0.592	0.4844	0.4946	0.405	-0.702
1.197	-0.840	-0.3	1.1957	0.0082	-0.013	0.000	5	0.9067	0.317	0.5894	0.2651	0.492	
1.197	-0.840	-1.5	0.6279	-0.0129	-0.006	0.000	5	0.4109	-0.1	0.5136	-0.086	0.429	
1.197	-0.840	10	-0.822	0.0366	0.0019	0.00	5	-0.059	-0.33	0.2662	-0.272	0.222	
1.197	-0.840										-0.702	0.000	
1.197	-0.840										1.000	0.000	
1.197	-0.840	0.5	1.1882	-0.016	0.00	0.00	6	1.0922	0.819	0.2731	0.6843	0.228	
1.197	-0.840	0.1	1.1916	-0.0145	0.0023	-8E-04	6	1.0142	0.558	0.4564	0.466	0.381	-0.702
1.197	-0.840	-0.3	1.1957	0.0082	-0.013	0.000	6	0.7697	0.269	0.5003	0.2251	0.418	
1.197	-0.840	-1.5	0.6279	-0.0129	-0.006	0.000	6	0.3309	-0.08	0.4136	-0.069	0.346	
1.197	-0.840	10	-0.822	0.0366	0.0019	0.00	6	-0.053	-0.29	0.2403	-0.245	0.201	
1.197	-0.840										-0.702	0.000	

Table A1. Cont.

Virgin E-Glass/913

Static Strength			Polynomial terms				Log	Fatigue Strengths			Derived Parameters		
σ_t	σ_c	R	a	b	c	d	N_f	σ_{max}	σ_{mean}	σ_{alt}	m	a	c
0.86	0.603										1.000	0.000	
0.86	0.603	0.5	0.8387	-0.0752	0.0005	0.00	3	0.6176	0.4632	0.1544	0.5386	0.1795	
0.86	0.603	0.1	0.8306	-0.0849	0.00	0.00	3	0.5759	0.31675	0.25916	0.3683	0.3013	-0.701
0.86	0.603	-0.3	0.8359	-0.0833	-0.0023	0.00	3	0.5653	0.19786	0.36745	0.2301	0.4273	
0.86	0.603	-1.0	0.5786	-0.0558	0.000	0.00	3	0.4112	0	0.4112	0	0.4781	
0.86	0.603	10	-0.6006	-0.0167	0.009	0.00	3	-0.057	-0.3153	0.25799	-0.3666	0.3	
0.86	0.603										-0.7012	0.000	
0.86	0.603										1.000	0.000	
0.86	0.603	0.5	0.8387	-0.0752	0.0005	0.00	4	0.5459	0.40943	0.13648	0.4761	0.1587	
0.86	0.603	0.1	0.8306	-0.0849	0.00	0.00	4	0.491	0.27005	0.22095	0.3140	0.2569	
0.86	0.603	-0.3	0.8359	-0.0833	-0.0023	0.00	4	0.4659	0.16307	0.30284	0.1896	0.3521	-0.701
0.86	0.603	-1.0	0.5786	-0.0558	0.000	0.00	4	0.3554	0	0.3554	0	0.4133	
0.86	0.603	10	-0.6006	-0.0167	0.009	0.00	4	-0.053	-0.2914	0.23841	-0.3383	0.2772	
0.86	0.603										-0.7012	0.000	
0.86	0.603										1.000	0.000	
0.86	0.603	0.5	0.8387	-0.0752	0.0005	0.00	5	0.4752	0.3564	0.1188	0.4144	0.1381	
0.86	0.603	0.1	0.8306	-0.0849	0.00	0.00	5	0.4061	0.22336	0.18275	0.2597	0.2125	
0.86	0.603	-0.3	0.8359	-0.0833	-0.0023	0.00	5	0.3619	0.12667	0.23524	0.1473	0.2735	-0.701
0.86	0.603	-1.0	0.5786	-0.0558	0.000	0.00	5	0.2996	0	0.2996	0	0.3484	
0.86	0.603	10	-0.6006	-0.0167	0.009	0.00	5	-0.047	-0.258	0.2111	-0.3001	0.2455	
0.86	0.603										-0.7012	0.000	
0.86	0.603										1.000	0.000	
0.86	0.603	0.5	0.8387	-0.0752	0.0005	0.00	6	0.4055	0.30413	0.10138	0.3536	0.1179	
0.86	0.603	0.1	0.8306	-0.0849	0.00	0.00	6	0.3212	0.17666	0.14454	0.2054	0.1681	-0.701
0.86	0.603	-0.3	0.8359	-0.0833	-0.0023	0.00	6	0.2533	0.08866	0.16465	0.1031	0.1914	
0.86	0.603	-1.0	0.5786	-0.0558	0.000	0.00	6	0.2438	0	0.2438	0	0.2835	
0.86	0.603	10	-0.6006	-0.0167	0.009	0.00	6	-0.039	-0.2152	0.17604	-0.2502	0.2047	
0.86	0.603										-0.7012	0.000	

Table A1. Cont.

1J Impact-Damaged HTA/982A

Static Strength			Polynomial terms				Log	Fatigue Strengths			Derived Parameters		
σ_t	σ_c	R	a	b	c	d	N_f	σ_{max}	σ_{mean}	σ_{alt}	m	a	c
1.197	0.442										1.000	0.000	
1.197	0.442	0.1	1.2035	0.0179	-0.0097	0.00	3	1.1699	0.6434	0.5264	0.5375	0.4398	
1.197	0.442	-0.3	1.1958	-0.009	-0.0139	0.00	3	1.0434	0.3652	0.6782	0.3051	0.5665	-0.369
1.197	0.442	-1.5	0.2841	-0.007	0.000	0.00	3	0.2625	-0.0656	0.32812	-0.055	0.2741	
1.197	0.442	10	-0.431	0.0097	0.000	0.00	3	-0.0402	-0.2212	0.1809	-0.1847	0.1511	
1.197	0.442										-0.3693	0.000	
1.197	0.442										1.000	0.000	
1.197	0.442	0.1	1.204	0.0179	-0.0097	0.00	4	1.1199	0.6159	0.504	0.5145	0.4210	
1.197	0.442	-0.3	1.196	-0.009	-0.0139	0.00	4	0.937	0.3279	0.609	0.2739	0.5088	-0.369
1.197	0.442	-1.5	0.284	-0.007	0.000	0.00	4	0.2553	-0.0638	0.3191	-0.053	0.2666	
1.197	0.442	10	-0.431	0.0097	0.000	0.00	4	-0.0392	-0.2158	0.176	-0.180	0.1475	
1.197	0.442										-0.369	0.000	
1.197	0.442										1.000	0.000	
1.197	0.442	0.1	1.204	0.0179	-0.0097	0.00	5	1.0505	0.5777	0.4727	0.48268	0.3949	
1.197	0.442	-0.3	1.196	-0.009	-0.0139	0.00	5	0.8028	0.2809	0.5218	0.23473	0.4359	
1.197	0.442	-1.5	0.284	-0.007	0.000	0.00	5	0.2481	-0.0620	0.3101	-0.0518	0.2590	-0.369
1.197	0.442	10	-0.431	0.0097	0.000	0.00	5	-0.0383	-0.2105	0.1722	-0.1758	0.1438	
1.197	0.442										-0.3628	0.000	
1.197	0.442										1.000	0.000	
1.197	0.442	0.1	1.204	0.0179	-0.0097	0.00	6	0.9617	0.5289	0.43276	0.44188	0.36154	
1.197	0.442	-0.3	1.196	-0.009	-0.0139	0.00	6	0.6408	0.2243	0.4165	0.18736	0.3479	
1.197	0.442	-1.5	0.284	-0.007	0.000	0.00	6	0.2409	-0.0602	0.30112	-0.0503	0.2515	-0.369
1.197	0.442	10	-0.431	0.0097	0.000	0.00	6	-0.0373	-0.2052	0.1678	-0.1713	0.1402	
1.197	0.442										-0.3692	0.000	

Table A1. Cont.

2J Impact-Damaged HTA/982A

Static Strength			Polynomial terms				Log	Fatigue Strengths			Derived Parameters		
σ_t	σ_c	R	a	b	c	d	N_f	σ_{max}	σ_{mean}	σ_{alt}	m	a	c
1.197	0.315										1.000	0.000	
1.197	0.315	0.5	1.188	-0.016	0.000	0.00	3	1.140	0.855	0.285	0.714	0.238	
1.197	0.315	-0.3	1.159	-0.122	0.006	0.00	3	0.850	0.297	0.552	0.248	0.461	-0.263
1.197	0.315	10	-0.314	0.013	0.000	0.00	3	-0.028	-0.152	0.124	-0.127	0.104	
1.197	0.315										-0.263	0.000	
1.197	0.315										1.000	0.000	
1.197	0.315	0.5	1.188	-0.016	0.000	0.00	4	1.124	0.843	0.281	0.704	0.235	
1.197	0.315	-0.3	1.159	-0.122	0.006	0.00	4	0.772	0.270	0.502	0.226	0.419	-0.263
1.197	0.315	10	-0.314	0.013	0.000	0.00	4	-0.026	-0.145	0.119	-0.121	0.099	
1.197	0.315										-0.263	0.000	
1.197	0.315										1.000	0.000	
1.197	0.315	0.5	1.188	-0.016	0.000	0.00	5	1.108	0.831	0.277	0.694	0.231	
1.197	0.315	-0.3	1.159	-0.122	0.006	0.00	5	0.707	0.247	0.459	0.207	0.384	-0.263
1.197	0.315	10	-0.314	0.013	0.000	0.00	5	-0.025	-0.138	0.113	-0.115	0.094	
1.197	0.315										-0.263	0.000	
1.197	0.315										1.000	0.000	
1.197	0.315	0.5	1.188	-0.016	0.000	0.00	6	1.092	0.819	0.273	0.684	0.228	
1.197	0.315	-0.3	1.159	-0.122	0.006	0.00	6	0.654	0.229	0.425	0.191	0.355	-0.263
1.197	0.315	10	-0.314	0.013	0.000	0.00	6	-0.024	-0.131	0.107	-0.110	0.090	
1.197	0.315										-0.263	0.000	

Table A2. A MathCad program for constant-life calculations. *fatuv2c*

Constant Life Calculations for CFRP Fatigue
2J Impact-Damaged HTA/982A

Fatigue function: $a = f(n)(1 - m)^2(c + m)^2$

$a = \sigma_{alt}/\sigma_t \quad m = \sigma_m/\sigma_t$

$\sigma_{alt} = \frac{1}{2}\sigma_{max}(1 - R)$

$\sigma_m = \frac{1}{2}\sigma_{max}(1 + R)$

$R = \sigma_{min}/\sigma_{max}$

$\sigma_{alt} = \sigma_m(1-R)/(1+R)$

Material properties:

$\sigma_t := 1.197 \quad \sigma_c := 0.315$

$c := \frac{\sigma_c}{\sigma_t} \quad c = 0.263$

$f_3 := 5.527 \cdot e^{-2.19 \cdot c} \quad f_4 := 5.383 \cdot e^{-2.34 \cdot c} \quad f_5 := 5.307 \cdot e^{-2.57 \cdot c} \quad f_6 := 5.331 \cdot e^{-2.9 \cdot c}$

$f_3 = 3.106 \quad f_4 = 2.908 \quad f_5 = 2.699 \quad f_6 = 2.485$

Equation of f for different materials:

2J HTA/982A	$f = 3.66 - 0.181\ \text{Log}N_f$	T800/5245	$f = 2.13 - 0.193\ \text{Log}\ N_f$
2J HTA/913	$f = 3.49 - 0.223\ \text{Log}N_f$	T800/924	$f = 2.05 - 0.198\ \text{Log}\ N_f$
1J HTA/982A	$f = 3.31 - 0.245\ \text{Log}\ N_f$	IM7/977	$f = 1.79 - 0.142\ \text{Log}\ N_f$
		HTA/982	$f = 1.69 - 0.144\ \text{Log}\ N_f$
		HTA/913	$f = 1.55 - 0.160\ \text{Log}\ N_f$

2J Impact-damaged HTA/982A if $n = \text{log}N_f$ $f(n) := 3.66 - 0.181 \cdot n$

$f(3) = 3.117 \quad f(4) = 2.936 \quad f(5) = 2.755 \quad f(6) = 2.574$

1. Calculation of Constant-life plots for various lives ($n = \text{log}N_f$)

$X := 17 \quad i := 1..X \quad j := 1..X$ *.....setting up ranges*

$m_i := -0.4 + 0.08 \cdot i \quad n_j := 3 + 0.2 \cdot j$

$a(m,n) := f(n) \cdot \left[(1 - m)^2 \cdot (c + m)^2\right]$

$M_{(i,j)} := a\left(m_i, n_j\right)$

Plot of a (vertical scale) against m (left to right) for $\text{log}N_f$ values from 3 to 7 (front to back).

M = matrix of values of a for various m and n

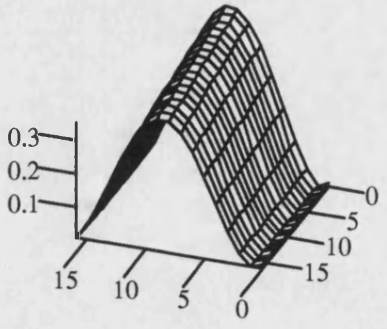

M

futur2c

2. Prediction of S/logN$_f$ curves from the Constant-life functions

For given R value, eg: $R := 0.1$

Solution of two simultaneous equations:

$a := 0.3$
$m := 0.3$ (guesses)

Given $a = f(n)\cdot(1 - m)^2\cdot(c + m)^2$

$$a = m\cdot\frac{(1 - R)}{(1 + R)}$$

$a(n) := \text{Find}(a, m)$

Values of a for a given R, for lives: $n := 3, 3.5 .. 7$ $\sigma_{max}(n) := \dfrac{2\cdot a(n)_1\cdot\sigma_t}{1 - R}$

WRITEPRN(data0_1) := $\sigma_{max}(n)$

(writes data for plotting)

$\sigma_{max}(n)$
1.153
1.135
1.116
1.096
1.075
1.053
1.03
1.005
0.979

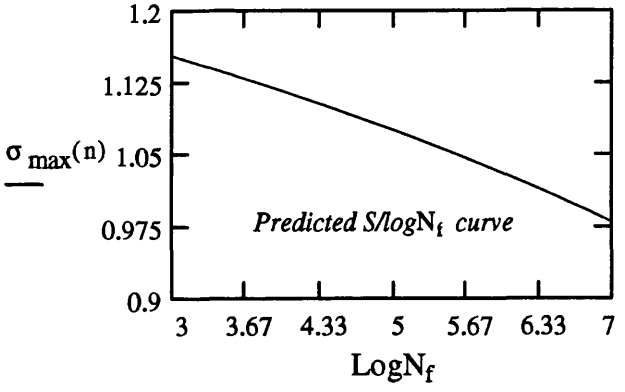

CHAPTER SIX:

CONCLUSIONS

CHAPTER SIX: CONCLUSIONS 132

6.1 CONCLUSIONS 133

6.2 FURTHER WORK 136

6.1 CONCLUSIONS

It has been the intention of this work to investigate the interaction between low-velocity impact damage and fatigue in fibre-reinforced plastics and to predict the fatigue response for virgin and impact-damaged materials by using a constant-life model. The impact response of two modern carbon-fibre/epoxy composites, namely HTA/982A and HTA/913, and a glass-fibre/epoxy laminate, E-Glass/913, and their fatigue behaviour in the virgin condition and after low-velocity impact at a wide range of stress ratios, R, were studied. The following conclusions can be drawn from this work:

1. The tensile and compressive strengths of the HTA/982A are 6% and 13%, respectively lower than those of the HTA/913, but its tensile modulus is 10% higher than that of the HTA/913.

2. Sectioning and ultrasonic C-scanning studies showed that the modes of failure under low-velocity impacts of 1-3J are matrix cracking and mainly delamination. Matrix cracks started at the edges of the impactor and inclined at approximately 45°. Only a 5J impact event caused fibre fractures in CFRP laminates.

3. Both ultrasonic C-scan and transient thermography were used successfully for the assessment of low-velocity impact damage. It seems that the resolution of C-scanning is higher than that of thermography. There are some differences between the results of C-scanning and thermography. This is due to the fact that the thermal contrast depends on the depths of the damage being imaged whilst the ultrasonic C-scan images are produced by the total attenuation caused by all the delaminations to the ultrasonic waves passing through the sample.

4. No delamination occurred in the region of the centre line of the impactor because of the low-shear stresses in this area.

5. The measurement of post-impact mechanical properties has shown that impact damage events at energies in the range 1-5J had little effect on the residual tensile strength although the compressive strength was markedly reduced. The mean compressive strength of CFRP composites was reduced by 64% after 3J

impact. In this respect, GRP is more damage tolerant than CFRP. After 5J impact incident energy, its compressive strength was reduced by 48%.

6. A semi-experimental model which is based upon bending stiffness mismatching were used to predict the residual compressive strength after impact. The predicted results are in good agreement with the experimental data for three investigated materials.

7. Fatigue test results of 20mm and 40mm wide samples showed that the width of sample has no significant effect on fatigue life. Although the wider samples showed less scatter of results and had higher values (for about half a decade) of mean and median life, the results of 40mm wide samples lie within the scatter bands of data for the 20mm wide samples.

8. The fatigue response of undamaged HTA/982A is similar to that of HTA/913. However, there is an indication that for R ratios other than –0.3, the slopes of the curves for HTA/913 are slightly steeper and hence the fatigue resistance of the older material is marginally poorer than that of the HTA/982A composite.

9. The fatigue resistance of the E-Glass/913 material is significantly poorer than that of the CFRP composites.

10. Fatigue testing of low-velocity impact-damaged materials showed that impact energies in the range 1-3J had no effect on the tensile fatigue behaviour at R = +0.1, although at high stress levels, *eg.* 90% of tensile strength, there was an indication of reduction of fatigue life, at lower stress levels no effect of prior impact-damage on the tensile fatigue behaviour could be observed.

11. In tension-compression cycling, the high-stress/low-cycle part of the S/N curve is affected significantly by prior impact-damage as a result of high value of compression component of stress, but under low-stress/high-cycle conditions damaged and undamaged materials have similar lives. In other words, as long as the compression component of stress is low, prior impact damage has no effect on the fatigue response of damaged materials. And as the compression

component of stress increases the slope of the S/N curve decreases, which indicates less sensitivity to fatigue.

12. In compression-compression cycling, R = +10, the S/N curves of impact-damaged materials are flat, almost horizontal, over a large range of cycles. In other words, the fatigue response of the damaged materials in compression is affected to the same proportion as the residual compressive strength, but their sensitivity to fatigue cycling is reduced.

13. The residual compressive strength of impact-damaged materials (not only reduces but also) improves during cycling.

14. The impact-damaged region does not grow in compression-compression cycling and its severity reduces during fatigue cycling. In tension-compression cycling, R = -0.3, however, clear evidence of damage propagation could be found and it appeared that the impact damage began to grow in the direction of 45° plies and interacted with fatigue-induced delamination originating at the free edges of specimen. This interaction reduces the fatigue life at high-stress level, but it has no effect on fatigue response under low-stress/high-cycles conditions.

15. Constant-life analysis of fatigue data showed that the constant-life model is valid for undamaged E-Glass/913. The appearance of the curves, however, is different from that of CFRP laminates, especially in that the right (predominantly tensile) wing of the curve is pulled downwards and the positions of the maxima in the constant-life curves are on the left hand side of R ratio -1.0, (negative m values) while in CFRP laminates the positions of the maxima in the constant-life curves are between the R ratios of -0.6 and -0.3.

16. The constant-life model remains valid for impact-damaged materials. The reduction in the compressive strength due to the prior impact damage is seen to result in a shift to the right of the left-hand tail of the curve, and the positions of the maxima in the constant-life curves are also shifted to the right.

17. Results showed that the virgin HTA/982A has the highest average value of alternating component of stress, $a_{max,}$ and hence the fatigue resistance over a

large range of cycles (10^3-10^6 cycles) of the older material, HTA/913 and also new modern CFRP laminates, *viz.* T800/5245, T800/924 and IM7/977, are poorer than that of the HTA/982A composite. GRP laminates showed the poorest performance of all as would be expected.

18. Result showed that the constant-life plots can be considered to be symmetric for the analysis of fatigue data and life prediction for CFRP laminates and can be represented by a one-parameter variable equation of the form:

$$a = f(1-m)^2(c+m)^2$$

19. The f parameter seems to be a linear function of loglife; $f = A - B\log N_f$.

20. It seems that there is an exponential relationship between f and the ratio of compressive strength over tensile strength, c, as: $f = Ae^{-Bc}$

21. There is a good agreement between predicted S/N curves with experimental stress/life data for CFRP laminates in the virgin condition and after low-velocity impact.

22. It seems that the modified constant-life model could be used successfully to predict a family of S/N curves or a three-dimensional surface plot of three parameters, a, m and log N_f, for both virgin and damaged CFRP laminates.

6.2 FURTHER WORK

As a part of the conclusion of this work, some further research is recommended as follows.

1. Investigation of the effect of low-velocity impacts, that are invisible to the naked eye and produce delamination and fibre fracture on mechanical properties and fatigue response.

2. Investigation of more effective non-destructive evaluation methods and efficient ways of evaluating the modes of failure in low-velocity impacts and of detecting active fatigue-induced damage more precisely.

In recent papers[2,3,4,5] Harris and co-workers have given descriptions of a constant-life model for fatigue-life prediction which appears to be applicable to a variety of different kinds of composite laminates. They have examined a wide range of composites with a view to assessing the potential usefulness of the technique and the level of confidence that a designer might have in using it to make preliminary predictions of life from limited data sets. They have discussed the fatigue response of four modern carbon-fibre-reinforced plastics (CFRP) materials, *viz.* T800/5245, T800/924, HTA/913, and IM7/977, all with a $[(\pm 45,0_2)_2]_S$ lay-up, after preliminary work in establishing the constant-life model for XAS-carbon/epoxy, Kevlar-49/epoxy, and hybrids of those two materials, in unidirectional lay-up[6,7,8]. They have shown that there is a general relationship between the alternating and mean components of stress of the form:

$$a = f(1 - m)^u(c + m)^v \quad \text{.....1)}$$

where a is the normalised alternating stress component, σ_{alt}/σ_t, m is the normalised mean stress component, σ_m/σ_t, and c is the normalised compression strength, σ_c/σ_t. The alternating component of stress, σ_{alt}, is equal to $\frac{1}{2}(\sigma_{max} - \sigma_{min})$, the mean stress, σ_m, is $\frac{1}{2}(\sigma_{max} + \sigma_{min})$, and σ_t and σ_c are the monotonic tensile and compressive strengths, respectively. From previous observations on these carbon-fibre composites, it appeared that f may be a function of the laminate tensile strength. The exponents u and v separately characterise the shapes of the right (predominantly tensile) and left (predominantly compressive) wings of a bell-shaped curve represented by equation 1, and allow for different degrees of asymmetry in the curve: f, u and v have all been found to be linear functions of loglife. The use of equation 1 to analyse stress/life data allows interpolation and a limited amount of extrapolation for the prediction, from only a modest data-base if necessary, of median fatigue lives representative of conditions (stress range and R ratio, defined as $\sigma_{min}/\sigma_{max}$) for which experimental data may not yet be available. Harris *et al* show[5], for example, that conservative prediction of a failure envelope covering a wide range of R ratios could be made for a 'new' CFRP material when the only data available for that material were the tensile and compression strengths and a stress/life curve for R = +0.1 defined by only five or six data points, provided some experience of other CFRP materials was available.

In this paper we discuss the interaction between the fatigue response of a composite and a prior state of damage caused by low-velocity impact, and we study the applicability of the constant-life model for predicting the lives of damaged laminates. We again start with a 'clean slate' by working with a material for which we have not previously reported fatigue results, another CFRP composite of $[(\pm 45,0_2)_2]_S$ lay-up, in the virgin and damaged states.

3. Investigation of the effect of lay-up sequence on fatigue behaviour of CFRP and GRP laminates and evaluation of the predictive capability of the modified constant-life equation for a wider range of composite structures.

4. Investigation of the statistical analysis of fatigue data in order to support the fatigue-life prediction models.

5. Preparation of software to predict the residual compressive strength after impact and to predict the stress/life data at desired R ratios for a new or an existing material.

REFERENCES

[1] Hull D, (1981), *An Introduction to Composite Materials*, Cambridge University Press, Cambridge, 1981.

[2] Harris B, (1986), *Engineering Composite Materials*, The Institute of Metals, London.

[3] Harris B, Dorey SE and Cook RG, (1988), *Strength and Toughness of Fibre Composites*, Composites Science and Technology, **31**, 121-141.

[4] Curtis PT, Gates J, Molyneux CG, (1993), *Impact Damage Growth in Carbon Fibre Composites*, Technical Report TR 93009, Franborough, Hants, UK.

[5] Curtis PT, (1987), *An Investigation of the Mechanical Properties of Improved Fibre Composite Materials*, J. Composite. Materials., **21**, P. 1118.

[6] Harris B, (1995), *Fatigue Behaviour of Polymer-Based Composites and Life Prediction Methods*, University of Bath, UK.

[7] Harris B, Gathercole N, Lee JA, Reiter H and Adam T, (1997), *Life Prediction for Constant-Stress Fatigue in Carbon-Fibre Composites,* Phil Trans Roy Soc (Lond), in press.

[8] Harris B, Gathercole N, Beheshty MH, Lee JA, Grimm B, Reiter H and Adam T, (1996), *Fatigue Damage Growth and Life Prediction for Carbon-Fibre Composites*, Final Report on Research Agreement Number CB/FRN/9/4-2112097, DRA, Franborough.

[9] Pavier MJ and Clarke MP, (1995), *Experimental Techniques for the Investigation of the Effect of Impacts Damage on Carbon-Fibre Composites*, Composite Science and Technology, **55**, 157-169.

[10] Cantwell WJ and Morton J, (1991), *The Impact Resistance of Composite Materials - a Review*, Composites, **22**, 5, 347-362.

[11] Reifsnider KL (editor), (1991), *Fatigue of composite Materials*, volume 4 of the series ***Composite Materials***, Series Editor RB Pipes, Elsevier Science Publishers B.V., Amsterdam.

[12] Chen AS and Harris B, (1993), *Fatigue-Induced Damage Mechanisms in Carbon Fibre Reinforced Plastic Composites*, Journal of Materials Science **28**, 2013-2027.

[13] Haque A, Krishnagopalan J and Jeelani S, (1993), *Fatigue Damage in Laminated Composites*, Journal of Reinforced Plastics and Composites, **12**, 1058-1069.

[14] Takemura K and Fujii T, (1994), *Fatigue Damage and Fracture of Carbon Fabric/Epoxy Composites under Tension-Tension Loading*, JSME International Journal, Series A, **37**, 472-480.

[15] Adam T, Dickson RF, Jones CJ, Reiter H, and Harris B, (1986), *A Power Law Fatigue Damage Model for Fibre-Reinforced Plastic Laminates*, Proc Inst. Mech. Eng. **200**, 155-166.

[16] Harris B, Reiter H, Adam T, Dickson RF and Fernando G, (1990), *Fatigue Behaviour of Carbon Fibre Reinforced Plastics*, Composites **21**, 232-242.

[17] Harris B, Chen AS, Coleman SL and Moore RJ, (1991), *Residual Strength and Toughness of Damaged Composites*, Journal of Materials Science **26**, 307-320.

[18] Stinchcomb WW and Bakis CE, (1991), *Fatigue of composite Materials Ch. 4*, Edited by Reifsnider KL, volume 4 of the series **Composite Materials**, Series Editor RB Pipes, Elsevier Science Publishers B.V., Amsterdam.

[19] Agarwall BD and Broutman LJ, (1990), *Analysis and Performance of Fibre Composites*, Second Edition, John Wiley and Sons, New York.

[20] Tsai GC, Doyle JF and Sun CT, (1987), Frequency Effects on the Fatigue Life and Damage of Graphite/ Epoxy Composites, J. Composite Materials, **21**, 2-13.

[21] Curtis DC, Moore DR, Slater B and Zahlan N, (1988), *Fatigue Testing of Multi-Angle Laminates of CF/PEEK*, Composites, **19**, November, 446-452.

[22] Adam T, Dickson RF, Fernando G, Harris B and Reiter H, (1987), *Fatigue Behaviour of Hybrid Composites*, Final Progress Report on MoD Agreement 2112/052 XR/MAT, University of Bath.

[23] Sims GD and Gladman DG, (1978), *Effect of Test Conditions on the Fatigue Strength of a Glass-Fabric Laminate: Part A- Frequency*, Plastics and Rubber: Materials and Applications, May 1978, 41-48.

[24] Harris B, (1994), *Fatigue of Glass-Fibre Composites*, in **Handbook of Polymer-Fibre Composites**, Ed. by FR Jones, Longman, Harlow, UK, 309-316.

[25] Jones CJ, Dickson RF, Adam T, Reiter H and Harris B, (1984), *The Environmental Fatigue Behaviour of Reinforced Plastics*, Proc. Royal Soc. London, **A396**, 315-338.

[26] Dickson RF, Jones CJ, Harris B, Leach DC and Moore DR, (1985), *The Environmental Fatigue Behaviour of Carbon Fibre Reinforced Polyether Ether Ketone*, J. Materials Science, **20**, 60-70.

[27] Sendeckyj GP, (1991), *Fatigue of Composite Materials Ch. 10*, Edited by Reifsnider KL, volume 4 of the series ***Composite Materials***, Series Editor RB Pipes, Elsevier Science Publishers B.V., Amsterdam.

[28] Lee LJ, Fu KE and Yang JN, (1996), *Prediction of Fatigue Damage and Life for Composite Laminates Under Service Loading Spectra*, Composites Science and Technology, **56**, 635-648.

[29] Adam T, Gathercole N, Reiter H, and Harris B, (1994), *Life Prediction for Fatigue of T800/5245 Carbon-Fibre Composites: II. Variable-Amplitude Loading*, Fatigue, **16**, 533-547.

[30] Harris B, Gathercole N, Reiter H and Adam T, (1997), *Fatigue of Carbon-Fibre Reinforced Plastics Under Block Loading Conditions*, Composites Part A, **28**, 4, 327-337.

[31] Harris B, Gathercole N, Lee JA, Almond DP, Adam T, and Reiter, (1996), *Fatigue-Life Prediction for Fibre-Reinforced Plastics*, in Proc. Seventh European Conference on Composites, ECCM7, London, Woodhead Publishing, Abington, UK, 69-74.

[32] Lee J, Harris B, Almond DP and Hammett F (1997), *Fibre-Composite Fatigue-Life Determination*, Composites Part A, **28**, 1,5-15.

[33] Gathercole N, Reiter H, Adam T and Harris B, (1994), *Life Prediction for Fatigue of T800/5245 Carbon-Fibre Composites: I Constant-Amplitude Loading*, Int J Fatigue, **16**, 523-532.

[34] Harris B, Gathercole N, Reiter H and Adam T, (1995), *Constant-Stress Fatigue Response and Life-Prediction for Carbon-Fibre Composites*, Proceeding of Duracosys 95, a research conference on the **Durability of Composite Systems** at the Free University of Brussels (VUB), (AA Balkema, Rotterdam, Netherlands) 63-73.

[35] Fernando G, Dickson RF, Adam T, Reiter H and Harris B, (1988), *Fatigue Behaviour of Hybrid Composites: Part 1 Carbon/Kevlar Hybrids*, J Materials Science, **23**, 3732-3743.

[36] Dickson RF, Fernando G, Adam T, Reiter H and Harris B, (1989), *Fatigue Behaviour of Hybrid Composites: Part 2 Carbon-Glass Hybrids,* J Materials Science, **24**, 227-233.

[37] Adam T, Fernando G, Dickson RF, Reiter H and Harris B, (1989), *Fatigue Life Prediction for Hybrid Composites*, Int. J Fatigue, **11**, 233-237.

[38] Richardson MOW and Wisheart MJ, (1996), *Review of Low-Velocity Impact Properties of Composite Materials*, Composites Part A, **27A**, 1123-11131.

[39] Hogg P, (1994), *Impact Resistance-Fibre Reinforced Polymers*, in **Handbook of Polymer-Fibre Composites**, edited by FR Jones, Longman, Harlow, UK, 334-340.

[40] Dorey G, (1994), *Impact Performance-CFRP Laminates*, in **Handbook of Polymer-Fibre Composites**, edited by FR Jones, Longman, Harlow, UK, 327-334.

[41] Boll DJ, Bascom WD, Weidner JC, and Murri WJ, (1986), *A Microscopy Study of Impact Damage of Epoxy-Matrix Carbon-Fibre Composites*, J Material Science, **21**, 2667-2677.

[42] Kinsey A, Saunders DEJ and Soutis C, (1995), *Post-Impact Compressive Behaviour of Low Temperature Curing Woven CFRP Laminates*, Composites, **26**, 661-667.

[43] Liu D, (1988), *Impact-Induced Delamination - A View of Bending Stiffness Mismatching*, Journal of Composite Materials, **22**, 674-691.

[44] Cantwell WJ, Curtis PT, and Morton J, (1984), *Impact and Subsequent Fatigue Damage Growth in Carbon Fibre Laminates*, Int. J Fatigue, **6**, 113-118.

[45] Hitchen SA, and Kemp RM, (1995), *The Effect of Stacking Sequence on Impact Damage in a Carbon Fibre/Epoxy Composite*, Composites, **26**, 207- 214.

[46] Choi HY and Chang FK, (1992), *A Model for Predicting Damage in Graphite/Epoxy Laminated Composites Resulting from Low-Velocity Point Impact*, Journal of Composite Materials, **26**, 14, 2134-2169.

[47] Edlund A, (1993), *Finite Element Modelling of Low-Velocity Impact Damage in Composite Laminates*, Proc. Of ICCM 9, Madrid July 1993, Volume. V, 334-341.

[48] Davies GAO, Zhou X, Zhou G and Watson S, (1994), *Numerical Modelling of Impact Damage*, Composites, **25**, 5, 342-350.

[49] Davies GAO and Zhang X, (1995), *Impact Damage Prediction in Carbon Composite Structures*, Int. J. Impact Engineering, **16**, 1, 149-170.

[50] Davies GAO, Zhou X and Hitchings D, (1996), *Impact damage and residual strengths of woven glass/polyester laminates*, Composites Part A, **27**, 12, 1147-1156.

[51] Guild FJ, Hogg PJ and Prichard JC, (1993), *A Model for the Reduction in Compression Strength of Continuous Fibre Composites after Impact Damage*, Composites, **24**, 4, 333-339.

[52] Caprino G, (1984), *Residual Strength Prediction of Impacted CFRP Laminates*, Journal of Composite Materials, **18**, 508-518.

[53] Papanicolaou GC and Stavropoulos D, (1995), *New Approach for Residual Compressive Strength Prediction of Impacted CFRP laminates*, Composites, **26**, 517-523.

[54] Soutis C and Fleck NA, (1990), *Static Compression Failure of Carbon Fibre T800/924C Composite Plate with a Single Hole*, Journal of Composite Materials, **24**, 536-558.

[55] Soutis C, Curtis PT and Fleck NA, (1993), *Compressive Failure of Notched Carbon Fibre Composites,* Proc. Royal Society London A, **440**, 241-256.

[56] Soutis C, (1994), *Damage Tolerance of Open-Hole CFRP Laminates Loading in Compression*, Composites Engineering, **4**, 3, 317-327.

[57] Soutis C and Fleck NA, (1991), *Failure Prediction Technique for Compression Loaded Carbon Fibre-Epoxy Laminate with Open Holes*, Journal of Composite Materials, **25**, 1476- 1498.

[58] Soutis C and Curtis PT, (1996), *Prediction of the Post-Impact Compressive Strength of CFRP Laminated Composites*, Composites Science and Technology, **56**, 677-684.

[59] Stellbrink, KKU, (1982), *Influence of Low-Velocity Impact on the Fatigue Behaviour of CFRP-Laminates*, Fatigue and Creep of Composite Materials, Ch.36, 319-327.

[60] Cantwell W, Curtis P and Morton J, (1983), *Post-Impact Fatigue Performance of Carbon Fibre Laminates with Non-Woven and Mixed-Woven Layers*, Composites **14**, 301-305.

[61] Aoki R, and Heyduck J, (1990), *An Experimental Study of Impact-Damaged Panels Under Compression Fatigue Loading*, in Developments in the Sc. and Tech. of Composite Materials, Ed. Fuller J. *et al*, Ch.15, 633-642.

[62] Ramkumar RL, (1983), *Effect of Low-Velocity Impact Damage on the Fatigue Behaviour of Graphite/Epoxy Laminates*, in Long-Term Behaviour of Composites, ASTM STP 813, ED. O'Brien TK, American Society for Testing and Materials, Philadelphia, 116-135.

[63] Clark G, and Van Blaricum TJ, (1987), *Load Spectrum Modification Effects on Fatigue of Impact-Damaged Carbon Fibre Composite Coupons*, Composites, **18**, 243-251.

[64] Jones R, Williams JF, and Tay TE, (1987), *Is Fatigue Testing of Impact Damaged Laminates Necessary?*, Composite Structures, **8**, 1-12.

[65] Ong CL, Sheu MF, Liou YY, and Hsiao TJ, (1991), *The Study of the Fatigue Characteristics of Composite after Impact*, 36th International SAMPE Symposium, April 15-18, pp. 912-923.

[66] Griffin CF, and Becht GJ, (1991), *Fatigue Behaviour of Impact Damaged BMI and Thermoplastic Graphite Composites*, 36th International SAMPE Symposium April 15-18, pp. 2197-2209.

[67] Clark G, and Saunders DS, (1991), *Morphology of Impact Damage Growth by Fatigue in Carbon Fibre Composite Laminates*, Materials Forum, **15**, 333-342.

[68] Chen AS, (1991), *The Effect of Fatigue-Induced Damage on the Mechanical Properties of CFRP Composites*, PhD Thesis, University of Bath, UK.

[69] Harris B, Reiter H, Gathercole N, Adam T, Chen AS, (1992), *Fatigue Life Prediction for Composite Materials under Variable Loading Conditions*, Final Technical Report on Agreement Number D/ER1/9/4/2112/RAE(F), Ministry of Defence Procurement Executive.

[70] Curtis, PT (ED.), (1988), ***CRAG Test Methods for the Measurement of Engineering Properties of Fibre-Reinforced Plastics Composites***, RAE, (Farnborough), Technical Report TR 88012, Procurement Executive, Ministry of Defence, Farnborough, Hants.

[71] Halmshaw R, (1991), *Non-Destructive Testing*, Second Edition, Edward Arnold, London.

[72] Summerscales J, (1990), *NDT of Advanced Composites, an overview of the possibilities*, British Journal of NDT, 32, 11, P568-577.

[73] Gros XE, (1995), *Review of NDT Techniques for Detection of Low Energy Impacts in Carbon Reinforcements*, SAMPE Journal, 31, 2, P2934.

[74] Hamzah AR, (1996), *The Application of Transient Thermography to Defect Detection*, Ph.D. Thesis, University of Bath, UK.

[75] Moghisi M, (1985), *Ultrasonic and Acoustic Emission Studies of Plasma Sprayed Coatings*, Ph.D. Thesis, University of Bath, UK.

[76] Krenchel H, (1964), **Fibre Reinforcement,** (Akademisk Forlag, Copenhagen , Denmark).

[77] Cantwell WJ and Morton J, (1989), *Geometrical Effects in the Low-Velocity Impact Response of CFRP*, Composite Structures, **12**, 39-59.

[78] Hong S and Liu D, (1989), *On the Relationship Between Impact Energy and Delamination Area*, Experimental Mechanics, June, 115-120.

[79] Soutis C, (1991), *Measurement of the Static Compressive Strength of Carbon Fibre-Epoxy Laminates*, Composite Science and Technology, **42**, 373-392.

[80] Bishop SM, and Morton J, (1982), *The Fatigue Properties of Notched CFRP*, ICAF (Toulouse, France).

PUBLISHED PAPERS

[1] Beheshty MH and Harris B, (1997), *Fatigue Life Prediction for Impact-Damaged Carbon-Fibre Composites,* Submitted to the Journal of Composite Science and Technology (Dec. 1996).

[2] Beheshty MH and Harris B, (1997), *Post-Impact Fatigue Behaviour of CFRP and the Growth of Low-Velocity Impact Damage During Cycling,* Proceedings of International Conference of Fatigue of Composites, Paris, 3-5 June, 1997, 355-362.

[3] Beheshty MH and Harris B, (1997), *Fatigue Behaviour of Carbon-Fibre-Reinforced Plastics After Low-Velocity Impact,* Forth National and Second International Seminar of Polymer Science and Technology, Tehran, Iran, 3-5 November, 1997.

FATIGUE LIFE PREDICTION FOR IMPACT-DAMAGED CARBON-FIBRE COMPOSITES

MH Beheshty and B Harris

School of Materials Science, University of Bath, Bath BA2 7AY

Abstract: *Following earlier work on the development of a life-prediction method for four types of carbon-fibre composites subjected to constant-stress fatigue, we have now attempted to assess the validity of the method for composites which have sustained damage from low-velocity impacts. This part of the work has been carried out on a fifth CFRP composite, HTA/982A, having the same structure, a* $[(\pm 45,0_2)_2]_S$ *lay-up, as those previously investigated. Replicate stress/life data were obtained at four stress ratios (R) of +0.1, -0.3, -1.5 and +10 on virgin samples and on samples damaged by a falling-weight delivering 1J of energy. The constant-life model is shown to be valid for the undamaged laminate and is also able to account for the effects of the impact damage in reducing the compression strength and consequent compressive fatigue response of the material.*

1. INTRODUCTION

Although the fatigue behaviour of composites in general and of carbon-fibre composites in particular has long been a subject of serious study, it is still by no means possible to make safe predictions for any given group of these materials for which the fatigue response has not previously been extensively investigated. Furthermore, while fibre composites are finding increasing application in aerospace structures as a consequence of their high specific stiffness and strength, these materials are also highly sensitive to impact by foreign bodies[1]. Low-velocity impact damage is inevitable. It may be caused during manufacture, by careless handling, for example, or in service, by hailstones, bird strike, *etc.* It may also occur during maintenance, perhaps by accidentally dropped tools. The influences of this kind of damage on the fatigue life and reliability of the affected structure are not well recognised and, in consequence, the prediction of fatigue life for impact-damaged materials is still far from satisfactory.

Fatigue experiments are expensive of time and resources. When a newly developed composite material is being considered for a given application, fatigue data are ideally required at an early stage of the design process and yet, in general, a detailed fatigue profile is rarely available until late in the development of project. And post-impact fatigue behaviour, even for a material of which the fatigue response has been extensively studied, is still unlikely to be understood. Conservative predictions of the lives of damaged composites cannot therefore be made with certainty.

2. MATERIALS AND TESTING PROCEDURES

2.1 Experimental material

The material used in this paper is the carbon-fibre composite HTA/982A manufactured by ICI Fiberite. It consists of the high-strength, standard-modulus, continuous Tenax HTA 12k carbon fibre in Fiberite 982A, a modified epoxy resin with good hot-wet characteristics and a cure temperature of 120°C, coded Fiberite HyE 3982AH. This material, which was supplied by Fiberite (Europe) in zero-bleed prepreg form, is thus a representative of the older-established variety of carbon-fibre composites, similar in many respects to the more familiar T300 composites, and it affords a direct comparison with the Ciba-Geigy HTA/913 material that we have studied previously.

The main 16-ply lay-up sequence of $[(\pm 45,0_2)_2]_S$ was selected to represent a structure of importance to the aerospace industry. All of the composites were laid up by hand and hot-pressed, following the manufacturer's recommendations (90 minutes at 120°C and 630kPa) as 300mm by 450mm plates. After curing, the hot-pressed laminates had a nominal thickness of 2 mm. Straight-sided test samples were cut to dimensions of 200mm long by 20mm or 40mm wide on a water-cooled circular saw with a diamond wheel. The 20mm wide samples were used for establishing the fatigue behaviour of the undamaged material, as in previous studies carried out by this group, while the 40mm-wide samples were used for impact and post-impact fatigue tests. The cut edges of the samples were lightly polished and, after abrasion of the end surfaces, end tabs of 1.5mm thick soft aluminium were glued on with Ciba Geigy Redux 403 epoxy-resin paste. The adhesive was cured in a dry oven at 40°C for 24hr. The central gauge sections of the test samples were 100mm long. Direct measurements of the fibre volume fraction gave a mean value of 0.53 (*cf.* the value of 0.6 that would have been expected from the 'notional' resin content of the prepreg). A similar value (0.54) was also obtained for the comparator material, HTA/913, although only the notional value of 0.6 was reported in our previous papers relating to this and other carbon-fibre-reinforced plastics.

2.2 Testing procedures

The measurements of monotonic tensile properties on the 20mm wide samples were carried out in a universal Instron Model 1195 machine at a cross-head speed of 2mm/min. Compression tests on virgin samples and post-impact compression tests were carried out in a 100kN servo-hydraulic Instron Model 1342 testing machine at a fixed loading rate of 20 kN/min, anti-buckling fixtures of the kind described by Curtis[9] being used to support the coupons during compression loading so as to prevent macro-buckling. The monotonic tensile

tests on 40mm wide samples were carried out under load control in a 200kN servo-hydraulic Mayes test machine model DH 200, again at a rate of 20kN/min.

Fatigue tests were carried out in 100kN servo-hydraulic Instron series 1300 machines under load control. Post-impact fatigue tests at a stress ratio, R, of +0.1 were carried out, also under load control, in the 200kN Mayes machine, and anti-buckling fixtures were again used for compression-compression or tension-compression fatigue tests. All fatigue tests were run at frequencies between 2.5 and 8 Hz with constant-amplitude sine-wave loading, under ambient laboratory conditions.

Impact damage was introduced into the test samples by means of a purpose-built, falling-weight test instrument with a 12.7mm diameter hemispherical tup, based on BS 2782 part 3 method 353A. The mass of the impacter was 0.248kg for 1J and 2J impacts, the impact energy being varied by changing the drop height. Impact events at 3J and 5J were made from a constant height of 1m by changing the mass of the impacter. During the impact event the specimen was clamped between two steel rings of internal diameter 30mm and the impact head was captured on rebound after impact to prevent secondary strikes.

3. Experimental Results

3.1 Laminate mechanical properties

The basic mechanical properties of the experimental laminates are given in Table 1.

Table 1.Monotonic mechanical properties of experimental laminates (standard deviations in brackets).

Material	V_f	Tensile modulus, GPa	Tensile strength, GPa	Tensile failure strain, %	Compression strength, GPa	Ratio of compression strength to tensile strength
HTA/982A	0.54	80.1(8.5)	1.20(0.05)	1.50(0.12)	0.84(0.08)	0.70
HTA/913	0.53	69.8 (4.4)	1.27 (0.05)	1.73 (0.10)	0.97 (0.08)	0.77

Since the fibre types and fibre contents are nominally identical in these two laminates, the differences between the laminate properties shown in this table must reflect either the effects of the different matrix resins or differences in the processing procedures (or the two together). But since no detailed information for the 982A resin is available, no useful comparison of the matrices can be made. The HTA/913 laminate was autoclaved rather than hot-pressed, for 60 minutes at 120°C, slightly less than the pressing time for the HTA/982A, but the resulting fibre content is only marginally lower, as shown in Table 1. For a laminate of $[(\pm 45,0_2)_2]_S$ construction, the Krenchel factor[10], η ($= \Sigma a_n \cos^4\theta$), has the value 0.625. Thus for a

laminate with V_f = 0.54 of HTA fibres of Young's modulus E_f = 238GPa (manufacturer's data) and an epoxy resin of modulus E_m = 2GPa, the expected laminate stiffness should be about 81GPa, close to the experimental value given in Table 1. The small difference in V_f and quite large changes in resin properties, either intrinsic or as a result of processing differences, will have almost no effect on this calculation, and it is difficult, therefore, to see why the experimental stiffness of the HTA/913 composite should be as low as 70GPa unless there were some fibre alignment problem not previously detected.

Processing and/or interfacial characteristics are likely to be responsible for the fact that the two strengths of the HTA/913 laminate are both somewhat greater than those of the HTA/982A. The compression strength of the HTA/982A is also rather lower relative to the material's tensile strength than that of the HTA/913.

3.2 Post-impact mechanical properties

The effects of impact on the monotonic tensile and compression strengths of the HTA/982A laminate are shown in Figure 1. It can be seen that despite visible signs of major surface and sub-surface damage at the higher energy levels, the tensile strength is not affected up to impact energy levels of 3J and is only slightly reduced by a 5J impact. By contrast, the compression strength is markedly affected, even by a 1J impact, the effects of which are almost undetectable by eye. The mean compression strength was reduced by 45% and 64% after 1J and 3J incident energy, respectively. It can be concluded that the impact-induced damage is mainly delamination (as revealed by C-scanning, Figure 2) because delamination reduces the shear and compression strengths but has little effect on tensile strength, whereas broken fibres have more effect on tensile strength. It is interesting that the scatter of residual compressive strengths at each level of impact energy is significantly less than that for the residual tensile strengths. For a typical CFRP with $[0,90,0,\pm45,0]_S$ lay-up it was shown by Dorey[11] that delaminations occurred at incident energies between 1 and 3J and reduced the compressive strength by 50% but had little effect on tensile strength. At incident energies above 3J, fibres were broken and this reduced the tensile strength. Figure 2 shows that even a 1J impact event produced significant delamination.

3.2 Fatigue stress/life curves

Replicate stress/life data were obtained for the virgin HTA/982A laminate at four stress ratios of +0.1, –0.3, –1.5 and +10 and the results are shown in Figure 3. The diagram shows the actual data points and the fitted curves are third-order or second-order polynomials fitted to full data sets. The overall appearance of the curves is similar to those previously reported for the other laminates mentioned above and the dashed curves in this figure are median-

stress/loglife curves for the comparator HTA/913 laminate taken from reference 5. It can be seen that for the most part these curves lie within the scatter bands of data for the HTA/982A, although there is an indication that for R ratios other than –0.3, the slopes of the curves for HTA/913 are slightly steeper and hence the fatigue resistance of the older material is marginally poorer than that of the HTA/982A composite.

Comparable fatigue data for the HTA/982A material with prior damage from a 1J low-velocity impact are shown in Figure 4, together with the curves fitted to the data for the virgin material from Figure 3. It appears that a 1J impact has had no effect on the tensile fatigue behaviour at R = +0.1, presumably because the tensile strength is itself unaffected by this level of damage. At R = –1.5 and +10, on the other hand, the $\sigma/\log N_f$ curves are markedly affected. It can be seen that the slopes have been considerably reduced, roughly in the same proportion as the compression strength itself has fallen, and the relatively straight lines through the failure points are now very flat, almost horizontal. At R = –0.3, however, which is a tension-compression mode in which the compression component of stress is low, the $\sigma/\log N_f$ curve has also shifted downward but to a less marked extent than those for R = –1.5 and R = +10. The flatness of these last two curves suggests that although the intrinsic compression strength of the laminate has been materially diminished by the small amount of prior damage the relative sensitivity to subsequent fatigue is less at these two R ratios than in the virgin material. By contrast, during cycling in the mainly tensile –0.3 régime, the $\sigma/\log N_f$ curve is slightly steeper than that for the undamaged material, suggesting increased sensitivity to fatigue.

One possible explanation for the marked reductions in the slopes of the $\sigma/\log N_f$ curves for high-compression R ratios may be found in the results of a series of experiments to determine the residual strength after cycling of the damaged laminate. It is a common feature of the fatigue behaviour of fibre composites that the residual strength of the material falls as a consequence of cycling. Examples may be found in references 12 and 13, among many others. It is this behaviour which forms the basis of the familiar 'wear-out' model of fatigue failure. By contrast, the effect of the impact damage in the HTA/982A in impairing the load-bearing ability of the laminate appears to be reduced when the damage laminate is cycled in repeated compression, as illustrated in Figure 5. The 5% or so increase in the compression strength after 10^6 cycles is well-defined and could reasonably explain why the $\sigma/\log N_f$ curve for R = +10 is very flat and why many of the individual fatigue experiments become run-outs.

4. DISCUSSION

4.1 Pooling of fatigue data

In earlier papers[2,5], following the lead of Whitney[14], we have used the method of normalising and pooling fatigue data as a step towards more reliable life prediction. This procedure makes use of the assumption that the fatigue lives follow a type III asymptote (Weibull) distribution and that the shape parameter of the distribution for the pooled data is the same as that for a subset of data for any replicate group of constant-stress fatigue tests. Design allowables for smaller subsets can therefore be predicted with greater confidence because the value of the shape parameter, *m*, is fixed by the characteristics of the larger population. Much of this earlier work is in agreement that the value of *m* for such a pooled distribution will be of the order of unity, but sufficiently greater than unity to ensure that the distribution has not degenerated to an exponential function with no minimum life.

The analysis is carried out by normalising each replicate data set with respect to the median life, $m(N_f)$, at the operative fatigue stress and then pooling all normalised data, for all stresses and all R values. The pooled data are then ranked (we use the mean-rank method, which gives the plotting position as $i/(N + 1)$, our choice of which we defend in reference 5) and plotted as shown in Figure 6. The distribution for the undamaged material is similar to those of other CFRP laminates described in reference 5, but the effect of the prior impact damage is to change the shapes of both tails of the distribution. As the inset in Figure 6 shows, the central parts of the two distributions overlap substantially, but there are both more longer-life failures and more shorter-life failures when the material has prior damage, reflecting the very flat $\sigma/\log N_f$ curves for tests at high-compression R ratios. The Weibull parameters for these curves were obtained, as described in reference 5, by a Levenberg-Marquardt non-linear least-squares routine in the Microcal Origin software, and the characteristics of the HTA/982A laminate in the damaged and undamaged state can be compared in Table 2 with those of the other CFRP laminates that we have studied. The standard errors of these fits were all of the order of 0.002. The values of the location parameter, *a*, are all close to zero, as would be expected since the distributions are necessarily bounded at zero, and the *b* values are all approximately unity, as expected for a normalised distribution. The value of the shape parameter, *m*, for the HTA/982A laminate is again within the range of values previously obtained, and the average value for all of our undamaged laminates is 1.39, with a coefficient of variation of about 17% . The consistency of this parameter, and its similarity to the value obtained by Whitney[14] in his analysis of a quite different CFRP, suggests that median or extreme-value life predictions based on such an average value could be made quite confidently from relatively small fatigue data bases.

The prior damage, though, appears to have the effect of placing this approach in jeopardy, since the flattening of the $\sigma/\log N_f$ curves for R = -1.5 and +10, in raising the left-hand tail of the distribution and lowering its right-hand tail results in a much lower value of the Weibull shape parameter. The value of m = 0.98 shown in Table 2 (and an even lower value of 0.6 given by a maximum likelihood estimate) indicate distributions with no minimum life, such as the exponential distribution, for which m = 1. Clearly, the analytical techniques that we are using are insufficiently sensitive, when the slope of the $\sigma/\log N_f$ curve is very flat, to distinguish between a peaked distribution and a smoothly falling distribution. We could improve the situation somewhat by ignoring the very long normalised lives for the damaged material. These are up to five times greater than the longest values in the distributions of the undamaged materials, and they can be ignored since, for extreme-value or median life predictions, it is only necessary to ensure a good fit to the left-hand tail of the distribution, as pointed out by Castillo[15]. But even censoring of the longer-life data is unlikely to raise the value of m beyond unity.

Table 2. Distribution parameters for pooled fatigue lives for several CFRP laminates.

Laminate	Number of values	a	b	m
T800/5245	164	0.09	1.24	1.25
T800/924	90	0.03	0.94	1.49
IM7/977	93	0.05	1.23	1.41
HTA/913	88	0.10	1.17	1.71
HTA/982A (virgin)	113	0.20	1.11	1.10
HTA/982A (damaged)	63	0.17	1.30	0.74

4.2 Constant-life analysis for the undamaged laminate

The procedure for carrying out the constant-life analysis has been described in detail elsewhere[3,4,5]. Following this procedure, we first plot conventional stress/median-life fatigue curves for each experimental R ratio, and from these plots, the coefficients of fitted polynomial curves are extracted for the purpose of interpolation. The coefficients are then inserted into a spread sheet set up to calculate pairs of co-ordinates (m,a) for constant-life plots as given by equation 1. These (m,a) data pairs were then plotted, together with the normalised tensile and compressive strengths, to construct constant-life curves for given lives, e.g. 10^3, 10^4, 10^5, and 10^6 cycles, the curves being produced by non-linear regression fits to the data points by Microcal *Origin* software. Note that the choice of lives for this purpose must depend on the spread of data. In our previous papers we have used only 10^4, 10^5, and 10^6 cycles, but better predictions can be obtained, provided there is a sufficiently wide spread of lives at different R ratios, if the shortest life chosen is somewhat nearer to the left-hand axis of the $\sigma/\log N_f$ curve than 10^4 cycles. A constant-life plot showing the (m,a) data pairs for the four R ratios studied at the four lives referred to above, together with the extreme data pairs

representing the monotonic tensile and compression strengths, is shown in Figure 7. The curves were fitted through the data sets by means of non-linear least-squares routine referred to earlier, and the values of the parameters *f*, *u* and *v* returned by the programme, together with the associated standard errors for the fit, are shown in Figure 8. It can be seen that all three parameters decrease with increasing life, *u* and *f* at approximately the same rates, while *v* is much less strongly dependent on loglife. The relationships represented in the figure are:

$$f = 1.92 - 0.18.\log N_f$$

$$u = 2.61 - 0.12.\log N_f \quad \ldots\ldots 2)$$

$$v = 2.42 - 0.04.\log N_f$$

In previous papers we have noted that an average value of *f* could be used as a fixed parameter for further curve fitting to obtain new relationships for the life dependence of *u* and *v* without significantly reducing the goodness of fit, and from the results for different laminates it appeared that the value of *f* was in fact related to the laminate tensile strength, σ_t. If the constant-life curves for 10^4, 10^5 and 10^6 cycles in Figure 7 are treated in the same way, then the correlation is extended to include HTA/982A, as shown in Figure 9. Although this linear plot is given by the relationship:

$$f = 2.42.\sigma_t - 2.06 \quad \ldots\ldots 3)$$

with a correlation coefficient of 0.977, it seems likely that a more realistic function for prediction purposes may be a parabolic relationship, passing through the origin, of the form:

$$f = 0.54\,\sigma_t^{2.6} \quad \ldots\ldots 4)$$

When the value of *f* is fixed and the curves of the type shown in Figure 7 are refitted to find new values of *u* and *v*, these exponents are found to be increasing linear functions of $\log N_f$ instead of the decreasing functions shown in Figure 8, and the slopes of these lines were shown in reference 5 to be linked in a qualitative manner to the nature of the composite. For the four laminates discussed in that paper, the slopes of the lines of *u* vs. $\log N_f$ and *v* vs. $\log N_f$ were all similar for the three composites that were reinforced with the intermediate-modulus T800 and IM7/977 fibres, whereas they were markedly higher for the composite with the high-strength HTA fibres. When the latest results for the HTA/982A composite are considered in the same context, there is an interesting new feature which is shown in Table 3.

Table 3. Slopes of the lines u,v = A + B.logN_f *for five* $[(\pm 45,0_2)_2]_S$ *CFRP laminates*

Material	exponent	Slope B	exponent	Slope B
T800/5245	u	0.327	v	0.365
T800/924	u	0.398	v	0.396
IM7/977	u	0.333	v	0.256
HTA/982A	u	0.280	v	0.400
mean of above four (cv)	***u***	***0.335 (15%)***	***v***	***0.354 (19%)***
HTA/913	u	0.588	v	0.867

We note that although there are small differences in the values of u and v among the first four materials listed, and there are also small differences between the values of the two exponents for a particular laminate, reflecting the asymmetries of the constant-life curves, the results are more notable for their similarities than for their differences. There is in fact a remarkable degree of uniformity of behaviour between these four materials — note the relatively small coefficients of variation within the group of four, particularly gratifying since the fatigue response of the new HTA/982A laminate has only here been characterised at four R ratios, rather than the five used for all of the other materials. It is all the more obvious, then, that the behaviour of the HTA/913 laminate is different. But our conclusion must also now be changed, since the distinguishing feature of the laminate must be the resin rather than the fibre, as we had previously concluded, since the homogeneous group now includes both intermediate-modulus and high-strength fibres, but only modern modified resins.

4.3 Life prediction for the undamaged laminate

The next stage of the constant-life analysis is to use the information contained in Figure 8 (or the equivalent information in equations 2) to solve the pair of simultaneous equations which describe the entire stress/R-ratio/life surface of the material. These equations, as presented in reference 5 and elsewhere, are:

$$a = f(\log N_f).(1-m)^{u(\log N_f)}(c+m)^{v(\log N_f)} \qquad \text{.....5)}$$
$$a = m\left(\frac{1-R}{1+R)}\right)$$

The first of these is the constant-life equation, equation 1, modified to include information about the life-dependence of the parameters f(logN_f) u(logN_f) and v(logN_f), as established from Figure 8. The second is derived from the conventional definition of the stress ratio, R. Solution of these two equations is easily carried out with a package like MathSoft which will graph or tabulate σ/logN_f curves for a chosen range of R values. The output can be in one of two forms, depending on requirements, a three-dimensional constant-life surface plot, showing the full variation of (a,m,logN_f), or a family of σ/logN_f curves at desired R ratios. An example of this analysis, for the HTA/982A laminate, is shown in Figure 10, which includes the

original stress/life data for the four R ratios +0.1, –0.3, –1.5 and +10, the back-predicted curves for the same R ratios, and predicted curves for R ratios –0.6 and -1 for which no data have been obtained. The agreement between the data points and the predicted curves is good, as would be expected. These predicted curves for R = +0.1 –0.3 and +10 are somewhat better than those that we have obtained previously because the range of life dependence for f, u and v has here been extended to include 10^3 cycles instead of being restricted to the range 10^4 to 10^6 cycles. This considerably improves the ability of the method to predict the shape of the $\sigma/\log N_f$ curve over the first three decades.

4.4. Constant-life analysis for the damaged laminate

Constant-life plots for the HTA/982A laminate after incurring damage by a 1J low-velocity impact event are shown in Figure 11. The four curves for 10^3, 10^4, 10^5 and 10^6 cycles have been fitted by allowing the three parameters f, u and v freedom to take any values, but because of the closeness of the four points for R = +0.1, it was necessary to force the curve for 10^6 cycles to remain close to the other three in order to avoid an unacceptable shape for this curve.

A more useful and direct comparison between the damaged and undamaged laminates can be made by plotting the families of constant-life curves for the two conditions on a single plot, as in Figure 12. In this case, we have reverted to the earlier method of fixing an average value of f for the three lives in question and refitting the data sets by allowing only the values of u and v to vary. The overall shape of the constant-life plot is apparently unchanged by the prior damage, and the constant-life equation, equation 1, remains a valid descriptor of the constant-life surface. The reduction in the compression strength that we have already discussed is seen to result in a shift to the right of the left-hand tail of the curve, and the flattening of the $\sigma/\log N_f$ curve for R = +10 shown in Figure 4 causes a squeezing together of the three points lying on the line for R = 10. The positions of the maxima in the constant-life curves are also shifted to the right. The values of the fitting parameters, f, u and v for the damaged composite are shown, together with those for the virgin material, in Figure 13. The values of the three parameters are much closer together in the damaged material, reflecting the changes in shape of the constant-life curves, and all three lines showing the life-dependence of the parameters fall close together within a space more or less bounded by the lines for f and u for the undamaged laminate. An unexpected aspect of these results, however, is the fact that the f values for the damaged laminate are much higher than those for the virgin material, and do not fit the pattern of relationship with the laminate tensile strength that has so far covered the behaviour of all CFRP $[(\pm 45,0_2)_2]_S$ laminates so far tested in the course of this work. This is perhaps not surprising if we reflect that the area enclosed within the constant-life curves for the damaged material is markedly reduced as a consequence of the effect of the damage on the

laminate compression strength. But an important consequence of this is that, although the constant-life model appears to work just as well with damaged as with undamaged material, a simple knowledge of the fatigue response of an undamaged laminate (the f, u and v parameters), together with the results of measurements of the compression strength after impact (CAI), could not be used to predict the fatigue response of that damaged laminate without the need for further fatigue data. Attempts to fit constant-life curves to the data points for the damaged laminate shown in Figure 11 by fixing the value of the f parameter at 0.87, as indicated by the relationship in Figure 9, is simply not feasible. This suggests that other relationships between material properties and the constant-life model parameters should be sought.

5. CONCLUSIONS

1. In this paper we describe preliminary attempts to predict the fatigue life of an impact-damaged CFRP laminate by the use of a constant-life model that has been developed over a number of years for virgin CFRP composites of a wide range of composites.

2. Measurement of post-impact mechanical properties has shown that impact damage in the range 1-5J had little effect on the residual tensile strength although the compression strength was markedly reduced.

3. The constant-life model was used successfully to predict the fatigue response of undamaged HTA/982A from only four experimental $\sigma/\log N_f$ curves.

4. The constant-life model also appears to provide a valid descriptor of the fatigue response of the laminate after it had sustained damage from a 1J low-velocity impact event. The left-hand (predominantly compression) quadrant of the constant-life diagram is substantially modified by the impact damage, through its effect in reducing the compression strength of the material, but the curve in the right-hand is much less unaffected. It can be concluded that the constant-life model remains valid and can be used for prediction of fatigue-life for impact-damaged materials.

5. The relationship between the constant-life parameter, f, and the laminate tensile strength has previously been shown to provide a means of establishing an approximate set of $\sigma/\log N_f$ curves for a new material from a very limited fatigue data base. When the

laminate has sustained damage which affects the compression strength and not the tensile strength, however, this relationship is no longer valid.

6. ACKNOWLEDGEMENTS

MH Beheshty would like to acknowledge the financial support of the Ministry of Culture and Higher Education of Iran during his study at the University of Bath. This work builds substantially on a series of research programmes on the fatigue behaviour of carbon-fibre composites carried out at Bath with funding from the DRA (Farnborough).

7. REFERENCES.

1. Cantwell WJ, Curtis PT and Morton J, (1984), *Impact and subsequent fatigue damage growth in carbon fibre laminates*, Int J Fatigue, **6**, 113-118.
2. Gathercole N, Reiter H, Adam T and Harris B, (1994), *Life prediction for fatigue of T800/5245 carbon-fibre composites: I Constant-amplitude loading*, Int J Fatigue, **16**, 523-532.
3. Harris B, Gathercole N, Reiter H and Adam T, (1995), *Constant-stress fatigue response and life-prediction for carbon-fibre composites*, Proceeding of Duracosys 95, a research conference on the ***Durability of Composite Systems*** at the Free University of Brussels (VUB), (AA Balkema, Rotterdam, Netherlands) 63-73.
4. Harris B, Gathercole N, Lee JA, Almond DP, Adam T, and Reiter, (1996), *Fatigue-life prediction for fibre-reinforced plastics*, in Proc. Seventh European Conference on Composites, ECCM7, London, (Woodhead Publishing, Abington, UK), 69-74.
5. Harris B, Gathercole N, Lee JA, Reiter H and Adam T, (1997), *Life prediction for constant-stress fatigue in carbon-fibre composites*, Phil Trans Roy Soc (Lond), in press.
6. Adam T, Dickson RF, Jones CJ, Reiter H, and Harris B, (1986), *A power-law fatigue damage model for fibre-reinforced plastic laminates*, Proc Inst. Mech. Engrs, **200**, 155-166.
7. Fernando G, Dickson RF, Adam T, Reiter H and Harris B, (1988), *Fatigue behaviour of hybrid composites: I Carbon/Kevlar hybrids*, J Mater Sci, **23**, 3732-3743.
8. Adam T, Fernando G, Dickson RF, Reiter H and Harris B, (1989), *Fatigue life prediction for hybrid composites*, Int. J Fatigue, **11**, 233-237.
9. Curtis, PT (ed.), (1988), ***CRAG Test Methods for the Measurement of Engineering Properties of Fibre-Reinforced Plastics Composites***, RAE, (Farnborough), Technical Report TR 88012, (Procurement Executive, Ministry of Defence, Farnborough, Hants, UK).
10. Krenchel H, 1964, ***Fibre Reinforcement***, (Akademisk Forlag, Copenhagen Denmark).
11. Dorey G, (1994), *Impact performance – CFRP laminates*, in ***Handbook of Polymer-Fibre Composites***, edited by FR Jones, (Longman, Harlow, UK), 327-334.
12. Jones CJ, Dickson RF, Adam T, Reiter H, Harris B, 1984, Proc Roy Soc Lond, **A396**, 315-338.
13. Chen AS, Harris B, 1993, J Mater Sci, **28**, 2013-2027.
14. Whitney JM, 1981, ***Fatigue of Fibrous Composite Materials STP 723***, (American Society for Testing and Materials, Philadelphia USA), 133-151.
15. Castillo E, 1988, ***Extreme Value Theory In Engineering***, (Academic Press, Boston/London).

ILLUSTRATIONS

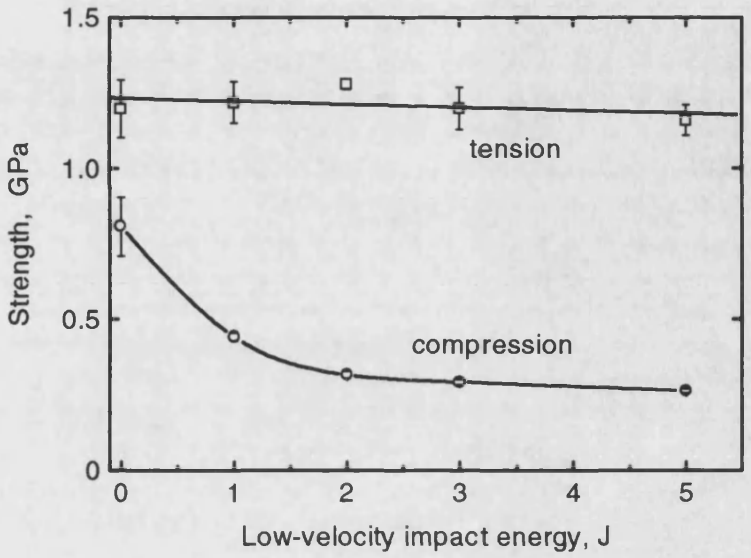

Figure 1. Effect of low-velocity impact damage on the residual tensile and compression strengths of $[(\pm 45,0_2)_2]_S$ *HTA/982A CFRP laminate. The impacts were made on samples with unsupported back faces.*

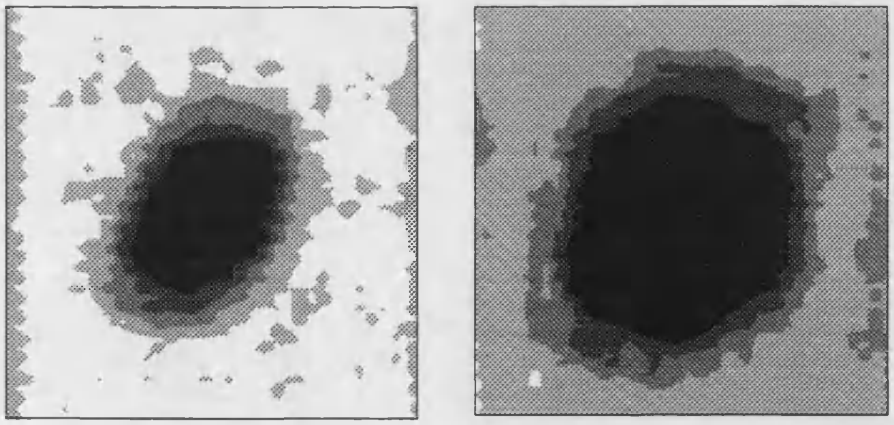

a) 1J impact b) 2J impact

Figure 2. Ultrasonic c-scans of $[(\pm 45,0_2)_2]_S$ *HTA/982A samples impacted at two different energy levels (Scan area was 40mm by 40mm).*

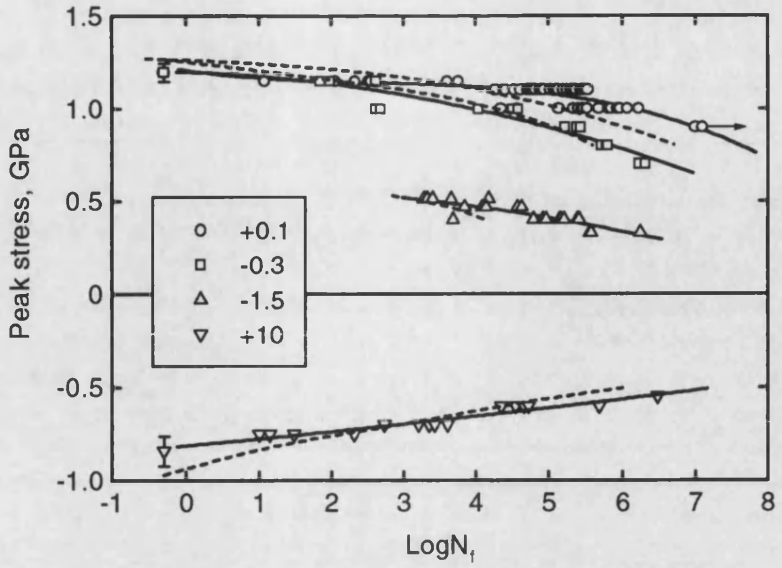

Figure 3. $\sigma/\log N_f$ *curves for HTA/982A CFRP laminate of* $[(\pm 45,0_2)_2]_S$ *lay-up in the undamaged condition. The full curves are fitted polynomial curves of order two or three and the dashed curves represent median-stress/life curves for HTA/913 laminate, taken from reference 5.*

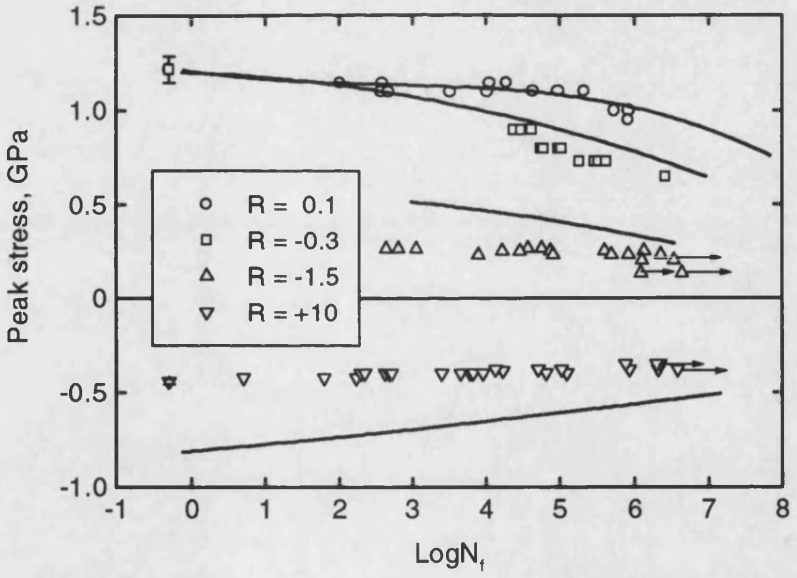

Figure 4. $\sigma/\log N_f$ *curves for HTA/982A CFRP laminate of* $[(\pm 45,0_2)_2]_S$ *lay-up after damage by a low-velocity impact of 1J. The full lines are polynomial curves fitted to the data for the virgin laminate.*

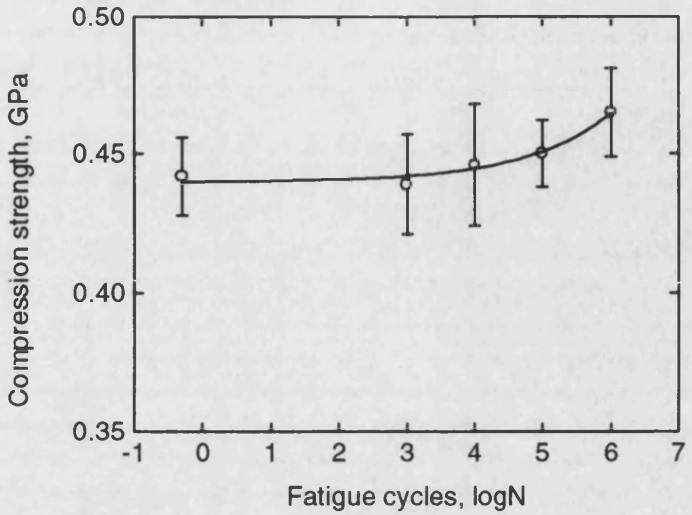

Figure 5. Residual compression strength after fatigue cycling of samples of HTA/982A $[(\pm 45,0_2)_2]_S$ *laminate with prior damage by a low-velocity impact of 1J. The cycling was at R = +10, at a peak stress (compressive) of 0.35GPa (79% of the residual compression strength).*

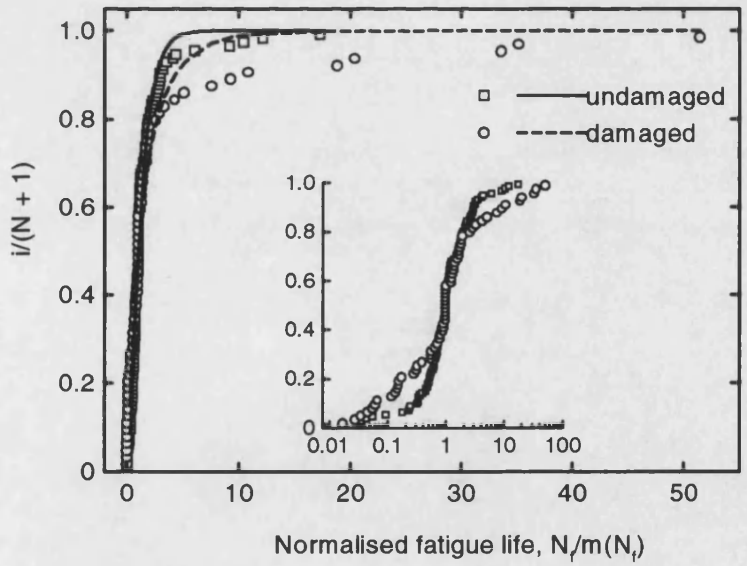

Figure 6. Three-parameter Weibull plots of normalised fatigue lives for HTA/982A $[(\pm 45,0_2)_2]_S$ *laminate in the virgin condition and after a low-velocity impact damage of 1J. The fatigue lives are normalised with respect to the median life,* $m(N_f)$*, for each individual data set (stress, R). The inset shows the abscissa on a log scale to accentuate the differences between the distributions.*

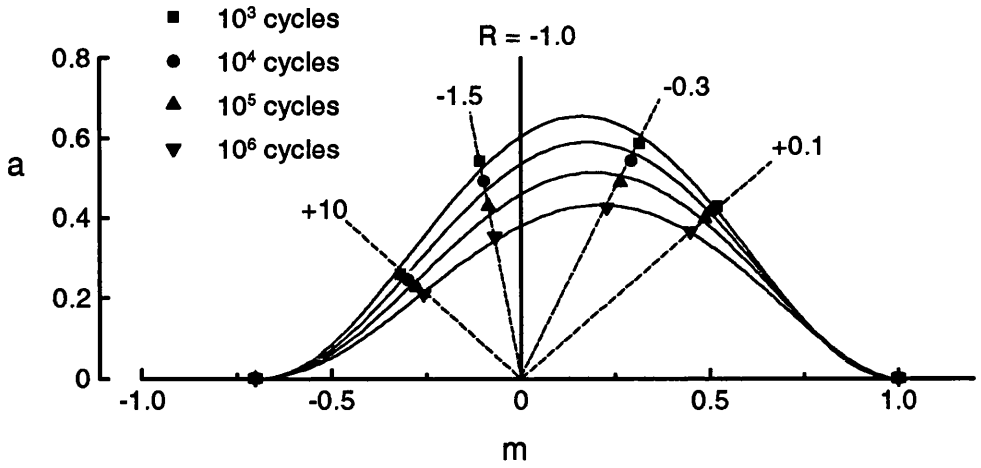

Figure 7. Constant-life plots for HTA/982A $[(\pm 45,0_2)_2]_S$ *laminate in the undamaged condition. The curves are obtained by freely fitting all three parameters.*

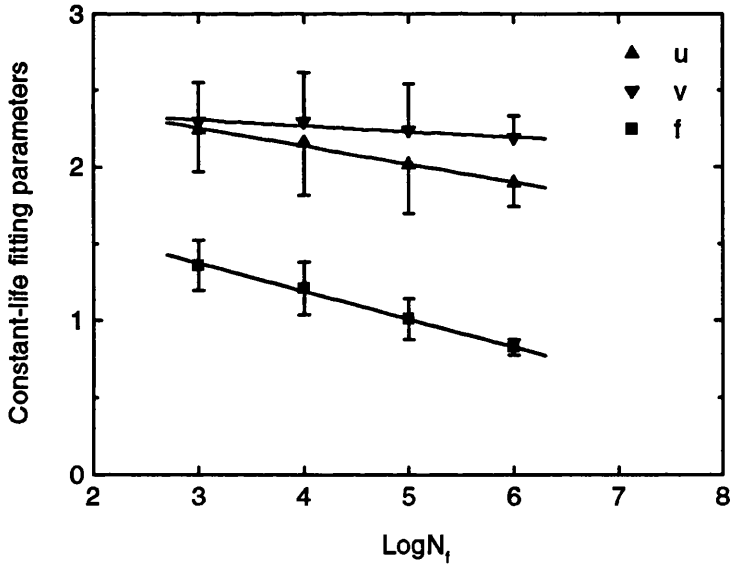

Figure 8. Dependence of the constant-life fitting parameters, f, u and v, on life for HTA/982A $[(\pm 45,0_2)_2]_S$ *laminate in the undamaged condition.*

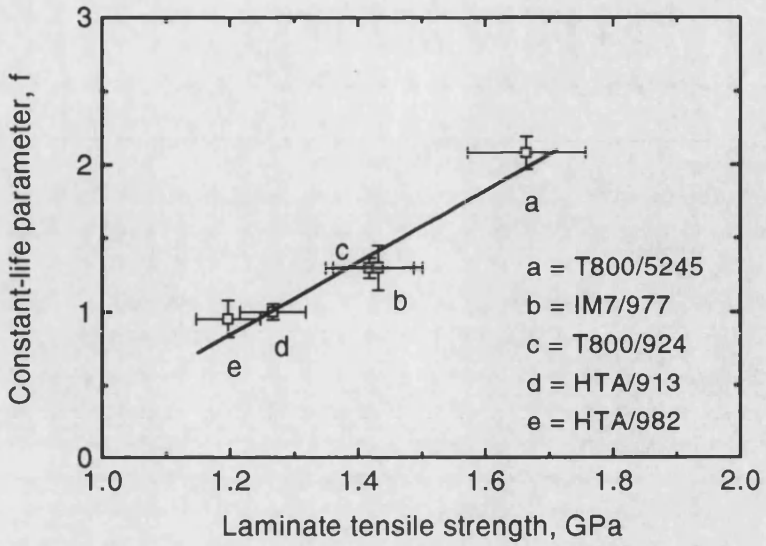

Figure 9. Dependence of constant-life model f parameter on laminate tensile strength. The vertical error bars are standard deviations for the fitted values of f, and the horizontal bars are standard deviations for the measured tensile strengths. The plotted f values are the means of the values obtained by curve fitting to obtain constant-life curves for 10^4, 10^5 and 10^6 cycles.

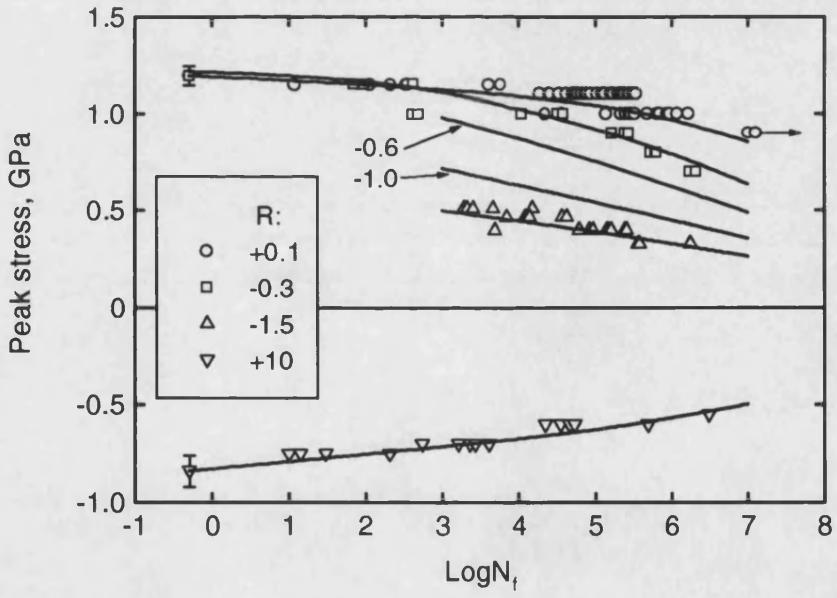

Figure 10. Stress/life data for the $[(\pm 45,0_2)_2]_S$ HTA/982A CFRP laminate in the undamaged condition. The full curves are curves predicted by the constant-life model.

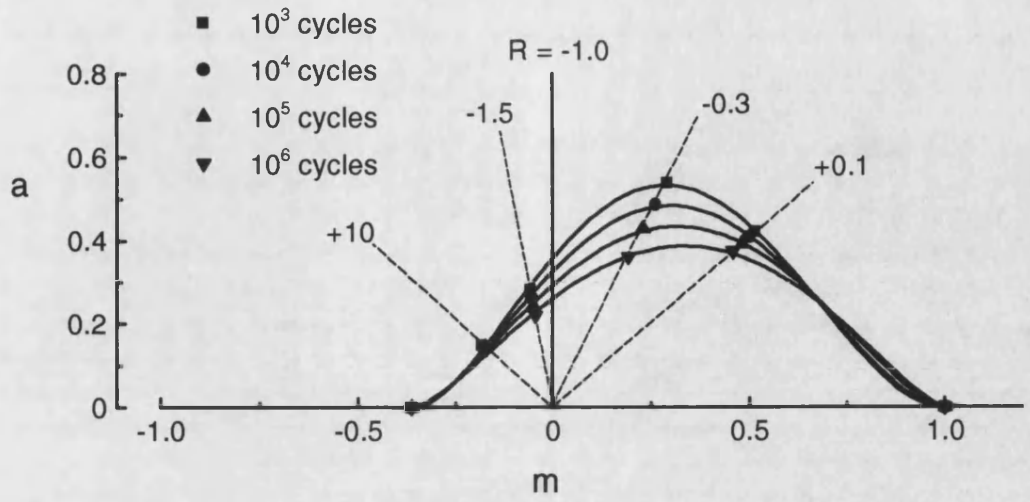

Figure 11. Constant-life plots for HTA/982A $[(\pm 45,0_2)_2]_S$ laminate following prior damage by a 1J impact. The curve for 10^6 cycles has been artificially forced to remain close to the other three curves above R = 0.1

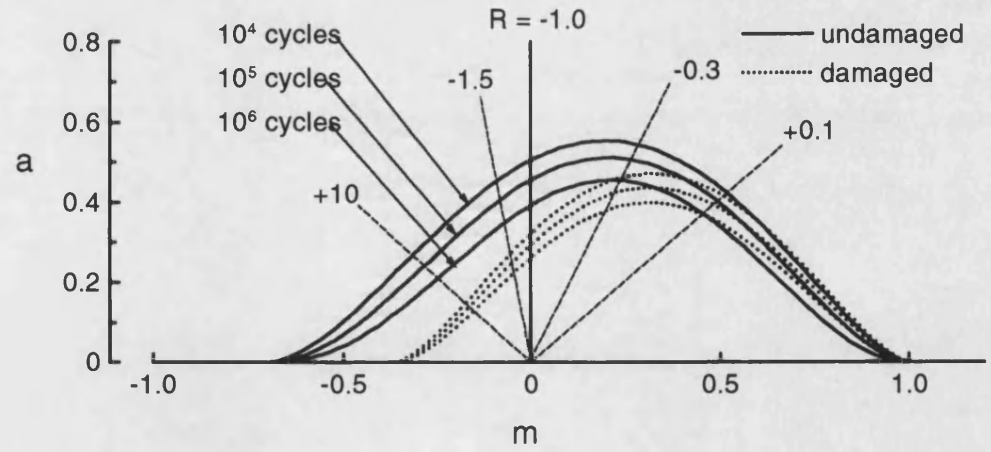

Figure 12. Constant-life curves for HTA/982A $[(\pm 45,0_2)_2]_S$ laminate in the virgin condition and after prior impact with a low-velocity impact of 1J. The two sets of curves lie in the same sequence as that indicated on the graph. The curve fits have been made by fixing an average value of f for the three lives indicted.

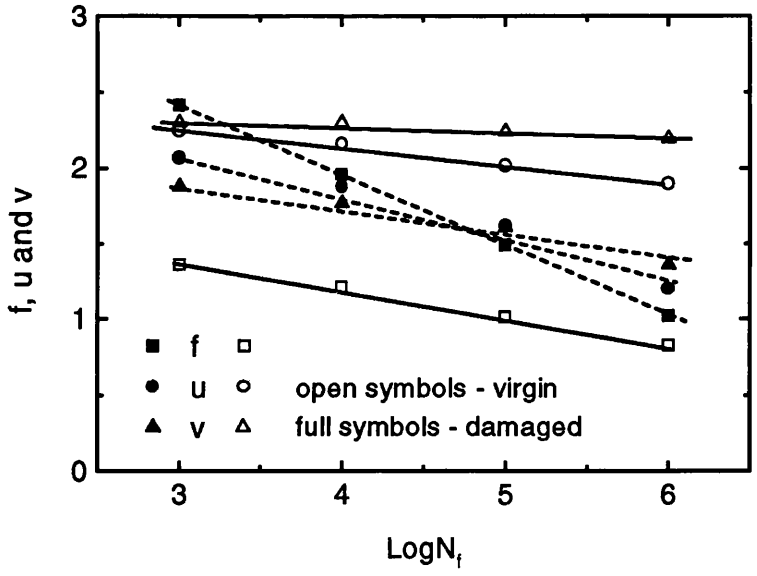

Figure 13. Variation of the constant-life fitting parameters, f, u and v, with life for HTA/982A [(± 45,0_2)$_2$]$_S$ *laminate in the virgin condition and after damage by a 1J low-velocity impact. The values of f, u and v were obtained by free fitting of all three parameters.*

POST-IMPACT FATIGUE BEHAVIOUR OF CFRP AND THE GROWTH OF LOW-VELOCITY IMPACT DAMAGE DURING FATIGUE

MH BEHESHTY and B HARRIS

School of Materials Science, University of Bath, Bath BA2 7AY, UK.

Abstract: The fatigue response of an HTA/982A $[(\pm 45,0_2)_2]_S$ carbon-fibre/epoxy laminate in the virgin condition and after low-velocity impact-damage has been investigated in order to study the effect of prior impact damage on the fatigue behaviour. Replicate stress/life data were obtained at four stress ratios on the sound material and after impacts of 1J and 2J. Results showed that impact events with energies of 1J and 2J had no effect on the tensile fatigue behaviour at R = +0.1, probably because the tensile strength is unaffected by this level of damage. At R = – 1.5 and +10, on the other hand, the $\sigma/\log N_f$ curves are markedly affected their slopes being considerably reduced, roughly in the same proportion to the reduction in compression strength. The extent of impact damage was determined by ultrasonic C-scanning.

1. Introduction

In a series of papers[1,2,3,4] Harris and co-workers have given descriptions of a constant-life model for fatigue-life prediction which appears to be applicable to a variety of different kinds of composite laminates. A wide range of composites has been studied with a view to assessing the potential usefulness of the model and the likely level of confidence in using it to make preliminary predictions of life from limited data sets. They have shown that there is a general relationship between the alternating and mean components of stress of the form:

$$a = f(1 - m)^u(c + m)^v \qquad 1)$$

where a is the normalised alternating stress component, σ_{alt}/σ_t, m is the normalised mean stress component, σ_m/σ_t, and c is the normalised compression strength, σ_c/σ_t. The alternating component of stress, σ_{alt}, is equal to $\frac{1}{2}(\sigma_{max} - \sigma_{min})$, the mean stress, σ_m, is $\frac{1}{2}(\sigma_{max} + \sigma_{min})$, and σ_t and σ_c are the monotonic tensile and compressive strengths, respectively. f appears to be a function of the laminate strength characteristics, while the exponents u and v characterise the shapes of the right (predominantly tensile) and left (predominantly compressive) wings of the bell-shaped curve represented by equation 1 and allow for asymmetry in the curve. The parameters f, u and v have all been found to be linear functions of loglife.

One of the major factors limiting the design of fibre composite structures is their relative weakness under impact. These structures are highly sensitive to impact by foreign bodies[5]. and low-velocity impact damage is inevitable. It may be caused during manufacture, by careless handling, or in service, by hailstones, bird strike, *etc.* It may also occur during maintenance. The influences of this kind of damage on the

fatigue life and reliability of the affected structure are not well recognised. And post-impact fatigue behaviour, even for a material of which the fatigue response has been extensively studied, is still unlikely to be understood.

In this paper we discuss the interaction between the fatigue response of a composite and a prior state of damage caused by low-velocity impact, and we intend to study the applicability of the constant-life model described above for predicting the lives of damaged laminates.

2. Experimental material

The material used in this work is the HTA/982A carbon-fibre composite from ICI Fiberite, and the 16-ply lay-up sequence of $[(\pm 45,0_2)_2]_S$ was selected to represent a structure of interest to the aerospace industry. The composites were laid up by hand and hot-pressed for 90 minutes at 120°C and 630kPa to make 300mm by 450mm plates of nominal thickness 2 mm. Straight-sided test samples were cut to dimensions of 200mm long by 20mm or 40mm wide on a water-cooled circular saw with a diamond wheel. The 20mm-wide samples were used for establishing the fatigue behaviour of the undamaged material and the 40mm-wide samples were used for impact and post-impact fatigue tests. The cut edges of the samples were lightly polished and end tabs aluminium were glued on to leave a central gauge section of 100mm. Direct measurements of the fibre volume fraction gave a mean value of 0.53.

3. Testing procedures

The measurements of monotonic tensile properties on the 20mm wide samples were carried out in an Instron 1195 machine at a cross-head speed of 2mm/min. Compression tests on virgin samples and post-impact compression tests were carried out in a 100kN servo-hydraulic Instron Model 1342 machine at a fixed loading rate of 20 kN/min with anti-buckling fixtures of the kind described by Curtis[6]. The monotonic tensile tests on 40mm wide samples were carried out under load control in a 200kN servo-hydraulic Mayes DH 200 machine, again at a rate of 20kN/min.

Fatigue tests were carried out in 100kN servo-hydraulic Instron series 1300 machines under load control. Post-impact fatigue tests at a stress ratio, R, of +0.1 were carried out, also under load control, in the 200kN Mayes machine. All fatigue tests were run at frequencies between 2.5 and 8 Hz with constant-amplitude sine-wave loading, under ambient laboratory conditions.

Impact damage was introduced into the test samples by means of a purpose-built, falling-weight test instrument, based on BS 2782, with a 12.7mm diameter hemispherical tup. The mass of the impacter was 0.248kg for 1J and 2J impacts, the impact energy being varied by changing the drop height. During the impact event the specimen was clamped between two steel rings of internal diameter 30mm and the impact head was captured on rebound after impact to prevent secondary strikes. The extent of the damage caused by impact events and the development of this damage during subsequent fatigue cycling were assessed by means of ultrasonic C-scanning.

4. Results and discussion

4.1 Mechanical properties

The tensile and compression strengths of the laminate before and after impact are shown in Table 1. It can be seen that impacts of 1J and 2J have no effect on the tensile strength of the material, but the compression strength, as is normal with composite materials of this kind, is seriously reduced. For example, nearly 50% of the original compression strength is lost after impact at only 1J, even though at this energy level there is no visible sign of damage on either face of the laminate. The lack of effect on the tensile strength may be due to the fact that the nature of impact damage is mainly delamination and matrix cracking as it was revealed by sectioning. The overall delamination area within the material, as determined from c-scans, is nevertheless substantial, as the table shows.

Table 1. Strengths of $[(\pm 45,0_2)_2]_S$ HTA/982 laminate, before and after impact: 40mm wide samples (standard deviations in brackets).

Impact energy, J	Tensile strength, GPa	Compression strength, GPa	Percentage loss in compression strength	Overall delamination area, mm^2
0	1.23 (0.095)	0.81 (0.098)	0	0
1	1.22 (0.068)	0.44 (0.014)	45	175
2	1.28 (0.003)	0.32 (0.012)	61	342

4.2 Fatigue behaviour

The fatigue response of the laminate is shown in the form of conventional stress/life plots at four different R ratios in Figure 1.

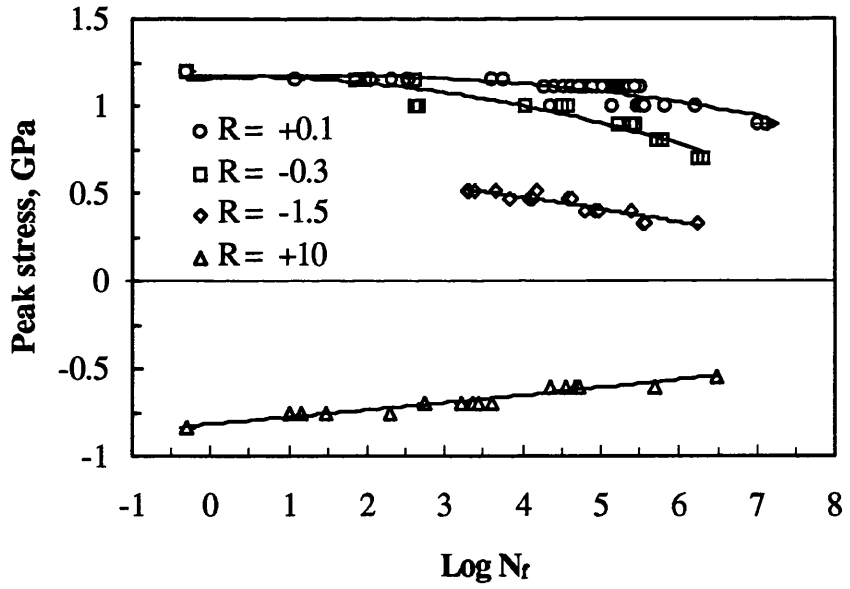

Figure 1. Stress/life data for the $[(\pm 45,0_2)_2]_S$ HTA/982A laminate at R ratios, $\sigma_{min}/\sigma_{max}$, of +0.1, -0.3, -1.5 and +10. The lines are best-fit polynomial curves through the individual data sets for each R ratio.

These results are typical of those normally obtained for this kind of CFRP laminate, and are similar to those for a comparable HTA/913 material discussed by Harris *et*

al[4]. The effects of 1J and 2J impacts on the subsequent fatigue response are shown in Figure 2 and Figure 3. In each of these figures, the individual $\sigma/\log N_f$ data points are plotted together with the curves for the undamaged material in Figure 1. It can be seen that the impact damage does not affect the fatigue response in a purely tensile cycling mode (R = +0.1), but the deviation of the stress/life points for the damaged material from the undamaged polynomial curves increases as the proportion of compression stress in the fatigue cycle increases. This deviation is also greater at 2J impact energy than at 1J, as would be expected. It is interesting to note that the scatter for the fatigue-life data obtained from the damaged samples is no greater than, and perhaps even less than, that obtained from the undamaged material.

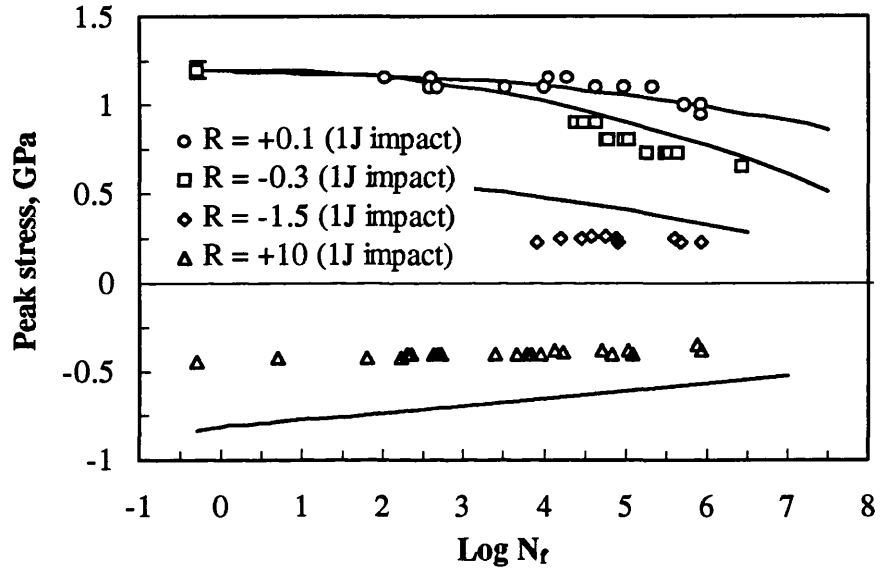

Figure 2. Stress/life data for the $[(\pm 45,0_2)_2]_S$ *HTA/982A laminate at R ratios of +0.1, -0.3, -1.5 and +10 after low-velocity impact of 1J*

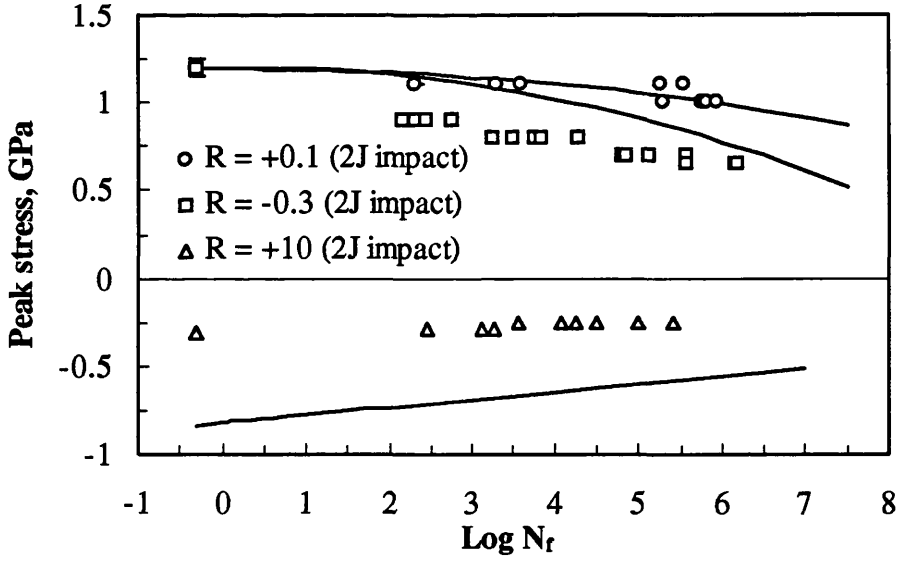

Figure 3. Stress/life data for the $[(\pm 45,0_2)_2]_S$ *HTA/982A laminate at R ratios of +0.1, -0.3, and +10 after low-velocity impact of 2J.*

The stress/life curves for the damaged laminates in repeated compression cycling (R = +10) are extremely flat, despite the high loss in compressive load-bearing ability resulting from the impact. This suggests not only that the type of damage caused by the impact does not grow during subsequent fatigue cycling, but also that the effect of that damage may be reduced to some extent by the compressive fatigue loading. This suggestion is supported to some extent by the results in Figure 4 which shows the change in residual compression strength with repeated-compression cycling (R = +10) of a sample that had previously been impacted at 1J. This kind of increase in post-impact residual properties in non-woven and mixed woven laminates was also mentioned by Cantwell *et al*[5,7] who reported that cycling led to improvements in static strength of up to 30% in non-woven and up to 40% in mixed woven composites. The reason for this improvement is not clear, although it could be associated with a notch blunting mechanism similar to that noted by Bishop and Morton[8] during tests on notched laminates.

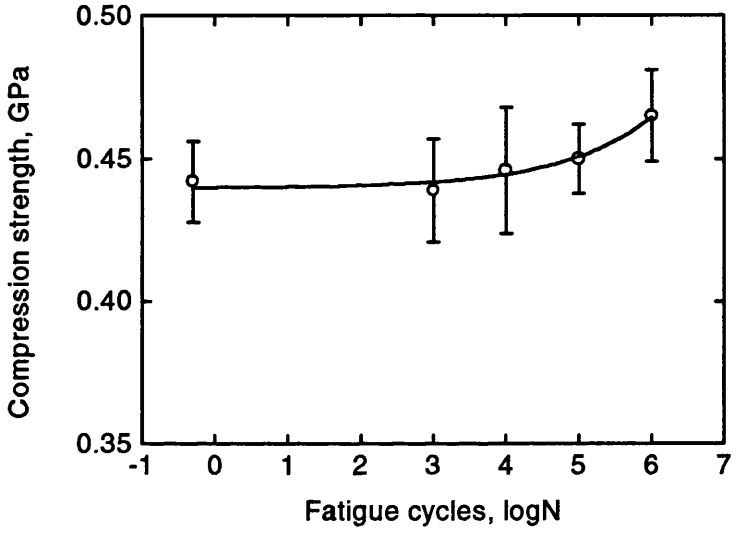

Figure 4. Residual compression strength after fatigue cycling of samples of $[(\pm 45,0_2)_2]_S$ *HTA/982A laminate with prior damage by a low-velocity impact of 1J. The cycling was at R = +10, at a peak stress (compressive) of 0.35GPa (79% of the residual compression strength).*

A direct comparison of the effects of different levels of impact energy may be seen from Figure 5 which is a plot of the median stress/life data at R = –0.3 for the virgin laminate and the laminate damaged by impacts of 1J and 2J. The curves in this figure are again polynomials (this form of curve-fit is chosen simply for convenience: it is not intended to suggest that there is any mechanistic argument for such a fit).

For R = –0.3, the cycle is dominated by the tensile component of stress, and as we have seen, the tensile properties are unaffected by the impact damage. Nevertheless, even the relatively small compression component at this R ratio is sufficiently great to interact with the impact damage to cause a marked and progressive change in the position of the $\sigma/\log N_f$ curve. It can be seen from Figure 5 that at low stress levels (*eg.* 0.7GPa, 57% of the monotonic tensile strength) undamaged and damaged laminates had similar lives. At low stress levels and an R ratio of –0.3, the compressive component of stress is not significant. And although for a peak stress of 0.7GPa, for instance, the minimum stress, –0.21GPa, is about 66% of the compression strength of a sample with 2J impact damage this still has no effect on the

fatigue life of the material. It can be concluded, therefore, that as long as the nature of the impact damage is matrix cracking and delamination, it has no effect on pure tension and tension-dominated tension-compression cycling.

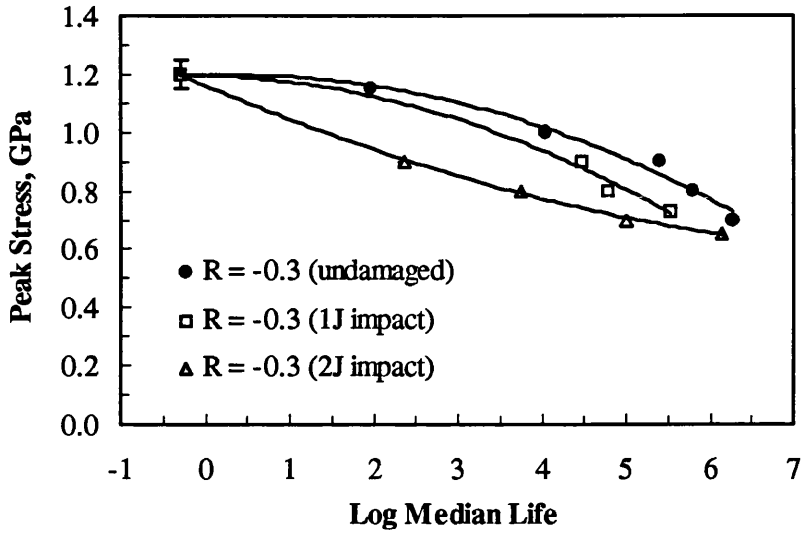

Figure 5. Median stress/loglife curves for $[(\pm 45,0_2)_2]_S$ *HTA/982A laminate at R = –0.3, showing the effect of low-velocity impact damage.*

4.3 Damage development

Information on the changes in the size of the damaged region during fatigue cycling was obtained by ultrasonic C-scanning. Figure 6 shows an example of the results obtained by this technique. The sample in question has been subjected to an impact event of 1J and subsequently cycled in repeated compression (R = +10) at a peak stress level of –0.38GPa (*ie.* 86% of the residual compression strength after the impact. The median life under these conditions is 78,000 cycles, and the illustrations show that after 10,000, 25,000 and 60,000 cycles there have been no significant changes in the size of the delaminated zone. This observation is in accord with the comments made earlier on the stress/life and residual strength results.

By contrast, a similar sequence of images for a sample cycled at R = –0.3 shows clear evidence of a growth in the size of the delaminated region.

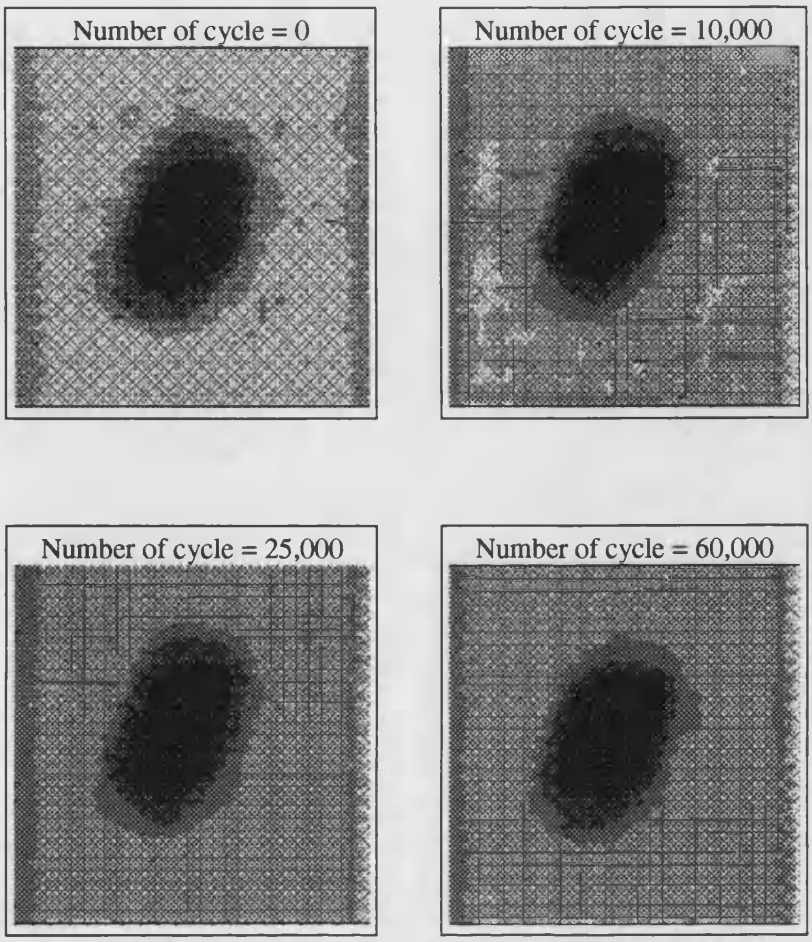

Figure 6. Ultrasonic C-scan images from samples impacted at 1J and subsequently fatigue cycled at R = +10 and a peak stress of –0.38GPa (scan area was 42mm by 40mm).

5. Conclusions

This paper reports the results of an investigation of the fatigue behaviour of a $[(\pm 45,0_2)_2]_S$ HTA/982A carbon-fibre/epoxy laminate in the virgin condition and after low-velocity impacts of 1J and 2J.

Impact events of 1J and 2J had no effect on the tensile strength of the material, although the compression strength was seriously reduced. The lack of effect on the tensile strength may be due to the fact that the nature of impact damage was mainly delamination and matrix cracking, as revealed by sectioning. Although there was no visible sign of damage on either back or front faces of the laminates after a 1J impact, the event produced substantial delamination, as revealed by ultrasonic C-scanning.

Results showed that 1J and 2J impacts had no effect on the tensile fatigue behaviour at R = +0.1, probably because the tensile strength is unaffected by this level of damage. At R = –1.5 and +10, on the other hand, the $\sigma/\log N_f$ curves are markedly affected. At R = –0.3 the cycle is dominated by the tensile component of stress, but even the relatively small compression component at this R ratio significantly changed the position of the $\sigma/\log N_f$ curve, although at low stress levels, undamaged and damaged laminates had similar lives at this R ratio. It can therefore be concluded that

provided the nature of impact damage is restricted to matrix cracking and delamination, it has no effect on pure tension and tension-dominated tension-compression cycling.

C-scanning of interrupted fatigue tests at R = +10 showed that no damage propagation occurred until just before failure of the specimen. At R = –0.3, however, clear evidence of damage propagation could be found by C-scanning and it appeared that the impact damage began to grow in the direction of 45° plies and interacted with fatigue-induced delamination originating at the free edges of specimen.

A preliminary attempt has been made to predict the fatigue life of an impact-damaged CFRP laminate by the use of a constant-life model. This has proved reasonably successful, and the results will be published elsewhere.

6. Acknowledgements

MH Beheshty would like to acknowledge the financial support of the Ministry of Culture and Higher Education of Iran during his study at the University of Bath. This work builds substantially on a series of research programmes on the fatigue behaviour of carbon-fibre composites carried out at Bath with funding from the DRA (Farnborough).

7. References

1. Gathercole N, Reiter H, Adam T and Harris B, (1994), *Life prediction for fatigue of T800/5245 carbon-fibre composites: I Constant-amplitude loading*, Int J Fatigue, **16**, 523-532.
2. Harris B, Gathercole N, Reiter H and Adam T, (1995), *Constant-stress fatigue response and life-prediction for carbon-fibre composites'*, Proceeding of Duracosys 95, a research conference on the ***Durability of Composite Systems*** at the Free University of Brussels (VUB), (AA Balkema, Rotterdam, Netherlands) 63-73.
3. Harris B, Gathercole N, Lee JA, Almond DP, Adam T, and Reiter, (1996), *Fatigue-life prediction for fibre-reinforced plastics*, in Proc. Seventh European Conference on Composites, ECCM7, London, (Woodhead Publishing, Abington, UK, 69-74.
4. Harris B, Gathercole N, Lee JA, Reiter H and Adam T, (1997), *Life prediction for constant-stress fatigue in carbon-fibre composites,* Phil Trans Roy Soc (Lond), in press.
5. Cantwell WJ, Curtis PT and Morton J, (1984), *Impact and subsequent fatigue damage growth in carbon fibre laminates*, Int. J Fatigue, **6**, 113-118.
6. Curtis, PT (ed.), (1988), ***CRAG Test Methods for the Measurement of Engineering Properties of Fibre-Reinforced Plastics Composites***, RAE, (Farnborough), Technical Report TR 88012, (Procurement Executive, Ministry of Defence, Farnborough, Hants, UK).
7. Cantwell W, Curtis P and Morton J, (1983), *Post-Impact Fatigue Performance of Carbon Fibre Laminates with Non-Woven and Mixed-Woven Layers*, Composites, **14**, 301-305.
8. Bishop SM, and Morton J, (1982), *The fatigue properties of notched CFRP*, ICAF (Toulouse, France).

FATIGUE BEHAVIOUR OF CARBON-FIBRE-REINFORCED PLASTICS AFTER LOW-VELOCITY IMPACT

MH BEHESHTY and B HARRIS
Department of Materials Science and Engineering,
University of Bath, Bath BA2 7AY, UK.

Abstract

This paper describes the fatigue response of two carbon-fibre/epoxy laminates of $[(\pm 45,0_2)_2]_S$ construction, viz. HTA/982A and HTA/913, after low-velocity impact in order to study the effect of prior impact damage on fatigue behaviour of polymer composite materials. Replicate stress/life data were obtained at different stress ratios on the materials after impacts of 1J and 2J. Results showed that impact events with energies of 1J and 2J had no effect on the tensile fatigue behaviour at R = +0.1, probably because the tensile strength is unaffected by this level of damage. In tension-compression and compression-compression cycling, on the other hand, the $\sigma/\log N_f$ curves are markedly affected, their slopes being considerably reduced, particularly in pure compression, roughly in the same proportion as the reduction in compressive strength. But results indicate that under low-stress/high-cycle conditions the virgin and damaged materials will have similar lives.

1. INTRODUCTION

Composite materials such as carbon-Kevlar- and glass-fibre-reinforced plastics offer significant benefits, among which we may include improved stiffness-to-weight ratio and toughness as the most important among the group of mechanical properties. In appropriate cases, they also present a reduction in overall cost as the main commercially important factor. For load-bearing applications where variable stresses are present, fatigue is a factor that must be taken into consideration. Although in the aerospace application of composite materials at current design strains, it is assumed[1] that fatigue is not a problem, newer tougher materials are now available that will hopefully permit increases in design strains. Fatigue behaviour could therefor become an important design issue.

One of the major factors limiting the design of fibre composite structures is their relative weakness under impact[2]. These structures suffer from localised impact loading[3] and may contain barely visible impact damage (BVID) which severely reduces the structural integrity of the component[4].Low-velocity impact damage, such as that imparted by a dropped tool or runway debris, is also inevitable and often undetectable by the naked eye. As a result, in recent years many research programs have been undertaken in an attempt better to understand the impact response of

composite materials[3,4]. While it is true that fatigue studies have been carried out on these materials since they first began to be studied as serious engineering materials, and also that in recent years there has been work on the fatigue response of impact-damaged materials[5,6,7,8], their behaviour under wide range of loading conditions to include from pure tension to pure compression cycling has not been extensively studied. The influences of low-velocity impact damage on the fatigue life and reliability of the affected structure are not well recognised. Moreover, post-impact fatigue behaviour, even for a material of which the fatigue response has been extensively studied, is still unlikely to be understood.

In a previous paper[9] we discussed the fatigue response of an HTA/982A carbon-fibre/epoxy laminate in the virgin condition and after low-velocity impacts of 1J and 2J and the growth of low-velocity impact damage during fatigue. Now, we discuss the fatigue response of an HTA/913 $[(\pm 45,0_2)_2]_S$ CFRP laminate after a low-velocity impact of 2J and tension-tension cycling of 3J impact-damaged HTA/982A and HTA/913 laminates.

2. EXPERIMENTAL MATERIALS

The materials studied in this work are the HTA/982A and HTA/913 carbon-fibre/epoxy composites from ICI Fiberite (Europe) and Ciba-Geigy (UK), respectively and the 16-ply lay-up sequence of $[(\pm 45,0_2)_2]_S$ was used to represent a structure of interest to the aerospace industry. The composites were laid up by hand and cured according to the manufacturers' procedures at 120°C. The cured plates had a nominal thickness of 2mm. Straight-sided test samples were cut to dimensions of 200mm long by 20mm or 40mm wide on a water-cooled circular saw with a diamond wheel. The 20mm-wide samples were used for establishing the fatigue behaviour of the undamaged material and the 40mm-wide samples were used for impact and post-impact fatigue tests. The cut edges of the samples were lightly polished and end tabs of aluminium were glued on to leave a central gauge section of 100mm. Direct measurements of the fibre volume fraction gave a mean value of 0.54. and 0.53 for HTA/982A and HTA/913, respectively.

3. TESTING PROCEDURES

The measurements of monotonic tensile properties on the 20mm wide samples were carried out in an Instron 1195 machine at a cross-head speed of 2mm/min. Compression tests on virgin samples and post-impact compression tests were carried out in a 100kN servo-hydraulic Instron Model 1342 machine at a fixed loading rate of 20 kN/min with anti-buckling fixtures of the kind described by Curtis[10]. The monotonic tensile tests on 40mm wide samples were carried out under load control in a 200kN servo-hydraulic Mayes DH 200 machine, again at a rate of 20kN/min.

Fatigue tests were carried out in 100kN servo-hydraulic Instron series 1300 machines under load control. Post-impact fatigue tests at a stress ratio, R, of +0.1 were carried out, also under load control, in the 200kN Mayes machine. All fatigue tests were run at frequencies between 2.5 and 8 Hz with constant-amplitude sine-wave loading, under ambient laboratory conditions.

Impact damage was introduced into the test samples by means of a purpose-built, falling-weight test instrument, based on BS 2782, with a 12.7mm diameter hemispherical tup. The mass of the impacter was 0.248kg for 1J and 2J impacts, the impact energy being varied by changing the drop height. During the impact event the specimen was clamped between two steel rings of internal diameter 30mm and the impact head was captured on rebound after impact to prevent secondary strikes. The extent of the damage caused by impact events was assessed by means of 5MHz ultrasonic C-scanning.

4. RESULTS AND DISCUSSION

4.1. Mechanical Properties

The tensile and compression strengths of the laminates before and after impact are shown in Table 1. Since the fibre types and fibre contents are nominally identical in these two laminates the differences between the properties shown in this table must reflect either the effects of the different matrix resins or differences in the processing procedures (or the two together). But since no detailed information for the 982A resin is available, no useful comparison of the matrices can be made. It can be seen that impacts of 1J and 2J have no effect on the tensile strength of the materials, but the compressive strengths, as is normal with composite materials of this kind, are seriously reduced. For example, nearly 50% of the original compressive strength is lost after impact at only 1J, even though at this energy level there is no visible sign of damage on either face of the laminate.

Table 1. Monotonic mechanical properties of experimental laminates, 40mm wide samples. (standard deviations in brackets).

Impact energy, J	HTA/982A		HTA/913	
	Tensile strength, GPa	Compressive strength, GPa	Tensile strength, GPa	Compressive strength, GPa
0	1.2 (0.095)	0.81 (0.098)	1.2 (0.01)	0.97 (0.075)
1	1.2 (0.068)	0.44 (0.014)	-	0.514 (0.015)
2	1.2 (0.003)	0.32 (0.012)	1.1(0.01)	0.384 (0.024)

It can be seen from Figure 1 that the mean compressive strength was reduced by 45% and 64% after 1J and 3J incident energy, respectively and the two CFRP laminates showed similar behaviour. It is interesting that although their initial compressive strengths are quite different (0.84GPa for HTA/982A in comparison to 0.97GPa for HTA/913), and their resins are also different, the percentage losses in

their compressive strengths after impact are similar. It can be concluded that the impact-induced damage is mainly delamination (as revealed by C-scanning, Figure 2) because delamination reduces the shear and compressive strengths but has little effect on tensile strength, whereas broken fibres have more effect on tensile strength. The lack of effect on the tensile strength may be due to the fact that the nature of impact damage is mainly delamination and matrix cracking, as can be seen from Figure 3 which shows the damage map of a sample of HTA/982A impacted at 2J and sectioned through the centre of impact-damaged zone in longitudinal direction relative to the fibres.

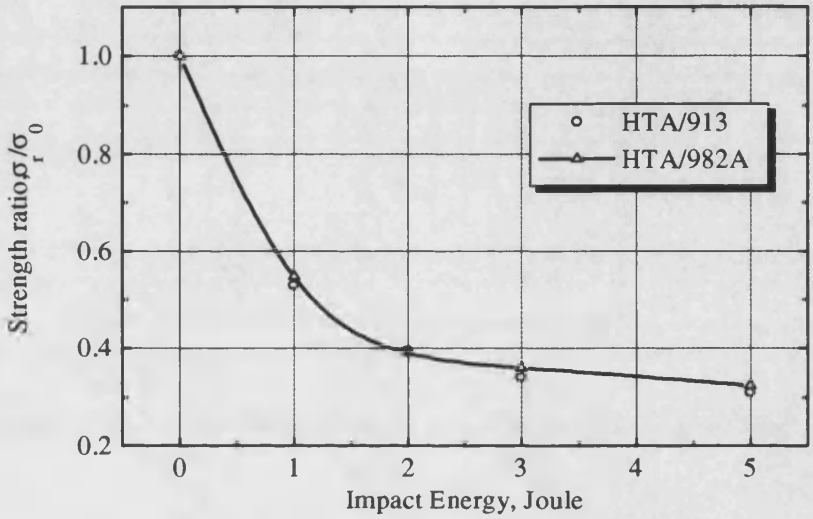

Figure 1. Effect of low-velocity impact damage on the residual compressive strength of HTA/913 and HTA/982A CFRP laminates. The impacts were made on samples with unsupported back face.

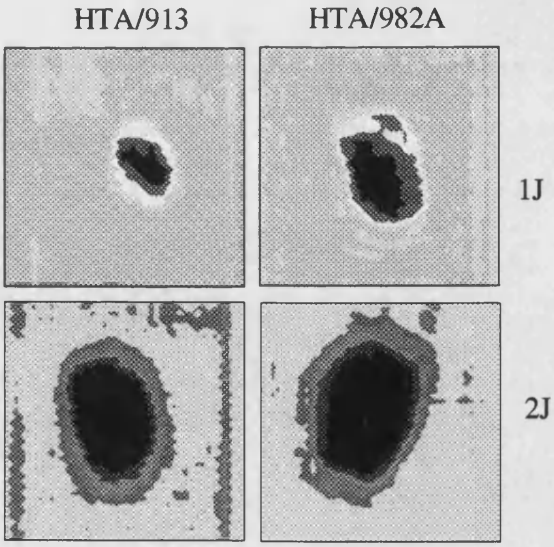

Figure 2. Ultrasonic C-scan images from samples of HTA/913 and HTA/982A impacted at 1J and 2J. Scan area was 42mm by 42mm.

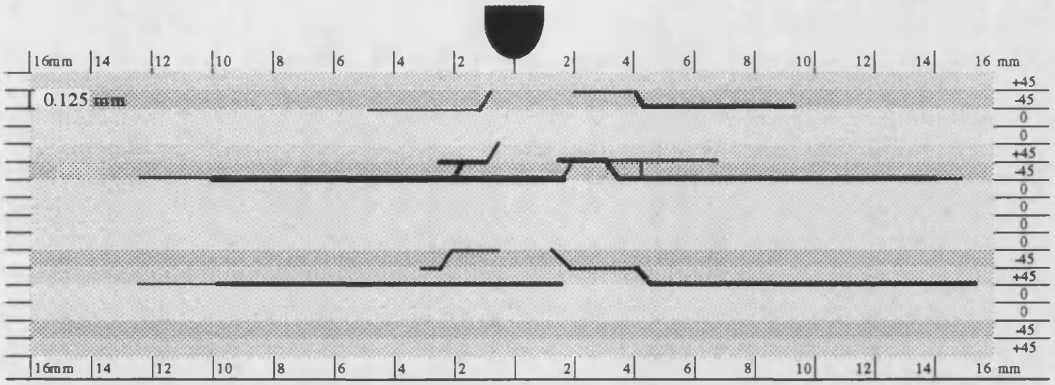

Figure 3. The damage map of a sample of HTA/982A after a 2J impact event.

4.2. Fatigue Response

Replicate stress/life data were obtained at four stress ratios of +0.1, -0.3, -1.0 and +10 for HTA/913 laminate after a 2J impact and the results are shown in Figure 4. In this figure the individual $\sigma/\log N_f$ data points are plotted together with the curves fitted to the data for the virgin material taken from reference 11. The overall appearance of the curve is similar to those which we have previously reported for impact-damaged HTA/982A[9]. It appears that a 2J impact has had no effect on the tensile fatigue behaviour at R = +0.1, presumably because the tensile strength is itself unaffected by this level of damage.

At R = –1.0 and +10, however, the $\sigma/\log N_f$ curves are markedly affected. It can be seen that the slopes have been considerably reduced, roughly in the same proportion as the reduction in compressive strength, and the relatively straight lines through the failure points are now very flat, almost horizontal. It can be seen that a slight reduction in the magnitude of applied peak compressive stress, for example 5%, can lead to a hundred-fold difference in fatigue life. On the other hand, the considerable scatter of data indicates the large order of magnitude of differences in fatigue lives at a constant stress level. This kind of flat S/N curves over a large range of cycles generated from experimental data of impact-damaged materials has been mentioned in the literature[12], but has not been explained. It may be due to the fact that after an impact event the severity of delamination in the damaged zone in each interface is not equal, as revealed by sectioning. In some parts of the damaged zone, very thick delaminations are observed. This kind of severe delamination causes catastrophic failure in a monotonic compression test, but cycling makes it uniform or closes the open delamination and hence reduces the severity of the delamination and results in an increase in post-impact fatigue compressive strengths. This phenomenon, therefore, increases the fatigue life and leads to a flat S/N curve.

At R = –0.3 which is a tension-compression mode in which the compression component of stress is low, the $\sigma/\log N_f$ curve has also shifted downward but to a less marked extent than those for R = –1.0 and R = +10. The flatness of these last two

curves suggests that although the intrinsic compressive strength of the laminate has been materially diminished by the small amount of prior damage the relative sensitivity to subsequent fatigue is less at these two R ratios than in the virgin material. By contrast, during cycling in the mainly tensile –0.3 régime, the $\sigma/\log N_f$ curve is slightly steeper than that for the undamaged material, suggesting increased sensitivity to fatigue.

It is worthwhile indicating that it is not true to say impact-induced matrix cracking and delamination have no effect on pure tension cycling for all stress levels. Table 2 shows the original fatigue life data for $[(\pm 45,0_2)_2]_S$ HTA/982A laminate at a stress ratio of R = +0.1 for two stress levels, in the virgin condition and after damage by 1J and 2J low-velocity impacts. To make a reasonable comparison (omitting the size effect) the data for virgin condition are from 40mm wide samples. In this table σ_{max} and σ_t are peak stress and monotonic tensile strength, respectively. It can be seen that at σ_{max} = 1.0GPa which is equal to 83% of σ_t, undamaged and damaged materials behaved alike and the stress/life data for damaged materials are in the scatter band of data for undamaged materials, but at σ_{max} = 1.1GPa which is equal to 91% of σ_t the fatigue lives are shifted to the lower lives. In other words, impact-induced damage accelerates the process of accumulation of fatigue damage. This may be due to the high applied strain tolerated by the material at high peak stress. From the design point of view since the design strains are not considered so high, this reduction of fatigue lives for damaged materials is not of great importance.

Table 2. Fatigue life data for $[(\pm 45,0_2)_2]_S$ HTA/982A laminate at a stress ratio of R = +0.1 for two stress levels, in the virgin condition and after damage by 1J and 2J low-velocity impacts.

Sample Number	σ_{max} = 1.1GPa, 91% of σ_t			σ_{max} = 1.0GPa, 83% of σ_t		
	Virgin*	1J impact	2J impact	Virgin*	1J impact	2J impact
1	61,177	470	204	216,068	384,320	196,900
2	107,101	3,307	1,920	253,454	543,000	584,240
3	159,687	10,446	1,950	282,724	843,220	596,640
4	227,577	44,259	3,760	483,602		642,380
5	236,081	95,321	185,830	864,000	-	853,940
6	-	212,986	351,200	940,648	-	-
Mean life	158,325	61,131	71,807	506,749	590,320	574,820
Median life	159,687	27,352	1,950	383,163	543,00	596,640

* For 40mm sample wide.

The stress/life data for 3J impact-damaged HTA/913 and HTA/982A at R = +0.1 at peak stress of 1.0GPa are shown in Table 3. Ultrasonic C-scanning studies showed that 3J impact events produced large-scale delamination in these materials, 473mm^2 and 592mm^2 in HTA/913 and HTA/982A, respectively. Sectioning also showed that the mode of impact damage after 3J is mainly delamination and matrix cracking. Despite these huge prior damages, there was no significant change in their tension cycling response after 3J impact event at a peak stress of 1.0GPa. Because of the enormous scatter of fatigue test results it is difficult to say whether or not the prior

impact damage affected fatigue life. But it can be said that as long as the nature of the impact damage is matrix cracking and delamination, it has no effect on pure tension cycling of FRP at rather low applied peak stresses.

It is worthwhile indicating that attempts have been made to predict the fatigue life of an impact-damaged CFRP laminate by the use of a constant-life model. This has proved reasonably successful, as can be seen for instance from Figure 5, and the results will be published elsewhere.

Table 3. Fatigue life data for HTA/982A and HTA/913 laminates at R = +0.1 and peak stress of 1.0GPa, in the virgin condition and after damage by a 3J low-velocity impact.

Sample Number	HTA/982A		HTA/913	
	Virgin [a]	3J impact	Virgin [b]	3J impact
1	216,068	80,930	449,997	471,070
2	253,454	85,190	456,028	783,070
3	282,724	156,380	469,462	1,847,320
4	483,602	966,760	604,625	3,181,490+ [c]
5	864,000	-	700,277	-
6	940,648	-	-	-
Mean life	506,749	322,315	536,078	1,033,820
Median life	383,163	120,785	469,462	783,070

a) For 40mm sample wide.
b) For 20mm sample wide
c) Test interrupted due to the high number of cycle.

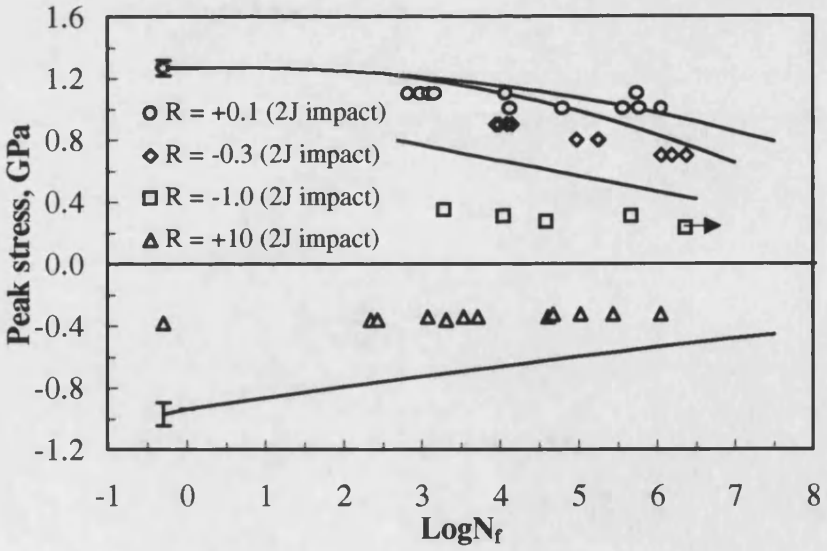

Figure 4. σ/logN$_f$ curves for HTA/913 CFRP laminate of [(±45,0$_2$)$_2$]$_S$ lay-up after damage by a low-velocity impact of 2J. The full lines are polynomial curves fitted to the data for the virgin laminate.

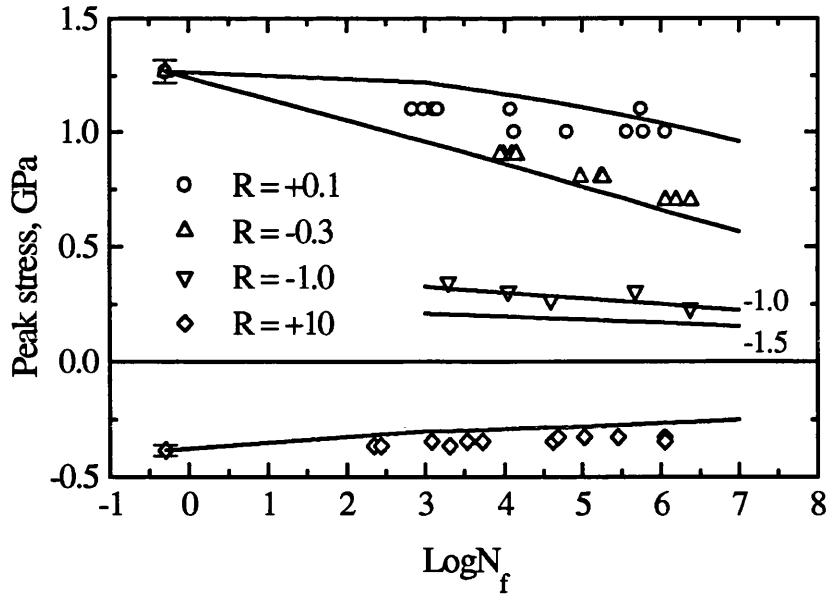

Figure 5. Stress/life data for the [(±45,0$_2$)$_2$]$_S$ HTA/913 CFRP laminate after damage by a 2J impact event. The full curves are predicted results and symbols are experimental values.

5. CONCLUSION

This paper reports the results of an investigation of the fatigue behaviour of HTA/982A and HTA/913 [(±45,0$_2$)$_2$]$_S$ carbon-fibre/epoxy laminates after low-velocity impacts.

Low-velocity impact damage events at energies in the range 1-3J had no effect on the residual tensile strength although the compressive strength was markedly affected. Ultrasonic C-scanning and sectioning studies showed that the modes of failure are matrix cracking and mainly delamination. The effects of this kinds of impact damage on fatigue behaviour of two CFRP laminates can be summarised as follows:

Tension-tension cycling: This type of prior impact damage has no effect on pure tension cycling particularly at low-stress levels.

Tension-compression cycling: Results showed that the high-stress/low-cycle part of the S/N curve is affected significantly, but under low-stress/high-cycle conditions damaged and undamaged materials have similar lives. In other words, as long as the compression component of stress is low, prior impact damage has no effect on the fatigue response of damaged materials. And as the compression component of stress increases the slope of the S/N curve decreases, which indicates less sensitivity to fatigue.

Compression-compression cycling: In pure compression, the S/N curves are flat, almost horizontal, over a large range of cycles. The fatigue resistance of the material is affected in the same proportion as the residual compressive strength.

6. ACKNOWLEDGEMENTS

MH Beheshty would like to acknowledge the financial support of the Ministry of Culture and Higher Education of Iran during his study at the University of Bath. This work builds substantially on a series of research programmes on the fatigue behaviour of carbon-fibre composites carried out at Bath with funding from the DRA (Farnborough).

7. REFERENCES

[1] Curtis PT, Gates J, Molyneux CG, (1993), *Impact Damage Growth in Carbon Fibre Composites*, Technical Report TR 93009, Franborough, Hants, UK.

[2] Soutis C and Curtis PT, (1996), *Prediction of Post-Impact Compressive Strength of CFRP Laminated Composites*, Composite Science and Technology, **56**, 677-684.

[3] Cantwell WJ and Morton J, (1991), *The Impact Resistance of Composite Materials - a Review*, Composites, 22, 5, 347-362.

[4] Richardson MOW and Wisheart MJ, (1996), *Review of Low-Velocity Impact Properties of Composite Materials*, Composites Part A, 27A, 1123-11131.

[5] Stellbrink, kku, (1982), *Influence of Low-Velocity Impact on the Fatigue Behaviour of CFRP-Laminates*, Fatigue and Creep of Composite Materials, Ch.36, 319-327.

[6] Cantwell W, Curtis P and Morton J, (1983), *Post-Impact Fatigue Performance of Carbon Fibre Laminates with Non-Woven and Mixed-Woven Layers, Composites*, 14, 3, 301-305.

[7] Ramkumar, RL, (1983), *Effect of Low-Velocity Impact Damage on the Fatigue Behaviour of Graphite/Epoxy Laminates*, Long-term Behaviour of Composites, ASTM STP 813, T.K. O'Brien, Ed., American Society for Testing and Materials, Philadelphia, 116-135

[8] Clark G, and Saunders DS, (1991), *Morphology of Impact Damage Growth by Fatigue in Carbon Fibre Composite Laminates*, Materials Forum, 15, 333-342.

[9] Beheshty MH and Harris B, (1997), *Post-Impact Fatigue Behaviour of CFRP and the Growth of Low-velocity Impact Damage During Fatigue*, International Conference of Fatigue of Composites, Paris 3-5 June 1997.

[10] Curtis, PT (ed.), (1988), ***CRAG Test Methods for the Measurement of Engineering Properties of Fibre-Reinforced Plastics Composites***, RAE, (Farnborough), Technical Report TR 88012, (Procurement Executive, Ministry of Defence, Farnborough, Hants, UK).

[11] Harris B, Gathercole N, Lee JA, Reiter H and Adam T, (1997), *Life prediction for constant-stress fatigue in carbon-fibre composites*, Phil Trans Roy Soc (Lond), in press.

[12] Jones R, Williams JF and Tay TE, (1987), *Is Fatigue Testing of Impact Damaged Laminates Necessary?*, Composite Structures, 8, 1-12.